UC Davis
UC Davis Electronic Theses and Dissertations

Title

Structural Control on the Viscoelastic Behavior and Shear Relaxation in Chalcogenide Glass-Forming Liquids

Permalink

https://escholarship.org/uc/item/6kt7h318

Author

Yuan, Bing

Publication Date

2022

Peer reviewed|Thesis/dissertation

Structural Control on the Viscoelastic Behavior and Shear Relaxation in
Chalcogenide Glass-Forming Liquids

By

BING YUAN
DISSERTATION

Submitted in partial satisfaction of the requirements for the degree of

DOCTOR OF PHILOSOPHY

in

Materials Science and Engineering

in the

OFFICE OF GRADUATE STUDIES

of the

UNIVERSITY OF CALIFORNIA

DAVIS

Approved:

_____

Sabyasachi Sen, Chair

_____

Yayoi Takamura

_____

Ricardo H. R. Castro

Committee in Charge

2022

Structural Control on the Viscoelastic Behavior and Shear Relaxation in Chalcogenide Glass-Forming Liquids

Abstract

Chalcogenide glasses are an important class of materials that consist of sulfides, selenides or tellurides of group IV and/or V elements, namely Ge, As, P and Si with minor concentrations of other elements such as Ga, Sb, In. Because of their infrared transparency that can be tuned by changing chemistry and can be actively altered by exposure to band gap irradiation, chalcogenide glasses find use in passive and active optical devices. Chalcogenide glass infrared lenses have found applications in the auto industry and in night vision security systems for both civil and military use. Infrared transmission in several key wavelength windows has enabled their use as optical fibers, lasers and fiber-amplifiers for telecommunication and as infrared laser power delivery systems for medical applications. Moreover, their large optical nonlinearity and high refractive index make them attractive candidate materials for all-optical switches in optical circuits. Finally, in thin film form, chalcogenide phase-change materials are of extraordinary technological importance in rewritable non-volatile memory storage applications (e.g., CD, DVD and Blu-Ray). A complete knowledge of the atomic structure of any material is of key importance in understanding and formulating accurate predictive models for its properties. Besides structure, the dynamical processes associated with structural relaxation and annealing near the glass transition controls the technological utility of inorganic glasses.

In this dissertation Raman and one- and two- dimensional multi-nuclear (^{31}P, ^{77}Se, ^{125}Te) nuclear magnetic resonance (NMR) spectroscopic techniques are utilized to elucidate the compositional evolution of the atomic structure at the short- and intermediate- range and chemical

order in a series of binary selenide glass-forming systems, namely: S_xSe_{100-x}, $Se_{100-x}I_x$, Te_xSe_{100-x}, and P_xSe_{100-x}. These spectroscopic results yield a rather detailed picture of the compositional evolution of the atomic structure of these glasses, where the constituent structural moieties range from 0-dimensional molecules to 1-dimensional linear chains all the way to a 3-dimensional network. The corresponding physical properties such as the glass transition temperature and the molar volume are shown to be intimately linked to and consistent with the compositional evolution of the atomic structure in each system.

On the other hand, the shear-mechanical response of all compositions in the supercooled liquid state are investigated via a combination of small-amplitude oscillatory and steady shear parallel plate rheometry to build an atomic-scale understanding of the frequency dependent viscoelasticity and structural relaxation processes. These results reveal the mechanistic connection between the structure including its connectivity and dimensionality and the shear relaxation processes, such as the rapid segmental chain motion associated with polymeric chains, the slow bond scission/renewal dynamics caused by interconversions between the structural moieties and the strong secondary bonding interactions, as well as the fast rotational motion and cooperative dynamics resulted from molecules. Depending on the structural moieties presented in a liquid, one or more shear relaxation processes may exist and contribute to the viscous flow. In addition, the shear-mechanical response evolves systematically with the structural transformation of these liquids as a function of composition within each system. When taken together, these results enable us to establish fundamental connections between the "microscopic" and the "macroscopic" aspects of viscoelasticity and relaxational phenomena in chalcogenide glass-forming liquids and to develop robust predictive atomistic models of structure-dynamics-relaxation for all studied systems.

Table of Contents

List of Figures

List of Tables

Chapter 1

Introduction

With its unmatched versatility in technological capabilities, it is not an overstatement to say that glass has shaped and advanced the human civilization in more ways than any other class of material. From windows and containers to lenses in telescopes and microscopes, innovative developments in glass science and technology have been key enablers of civilization throughout history.[1–6] This strong societal impact of glass continues in the modern times in the form of various photonic applications such as optical fibers for long-distance telecommunication, and damage-resistant liquid crystal display (LCD) panels for electronic devices, which have transformed the ways we live and communicate in the modern world.[1,5,7–11] The functionality of glass has been harnessed in many other areas as well, e.g., bioactive glasses are used today in healthcare and complex oxide glasses are the material of choice for radioactive waste encapsulation, to name a few.[12–15] Therefore, it is only appropriate that the United Nations has declared 2022 as the International Year of Glass.

Glasses are traditionally formed by cooling from a melt below its melting point. If the cooling rate is sufficiently high then crystallization can be avoided, and a dynamically equilibrated supercooled liquid is obtained. Further lowering temperature results in a drastic increase in liquid viscosity, which decreases the diffusivity of the constituent atoms, and at some point, the viscosity becomes too high for the supercooled liquid to reach the state of equilibrium through atomic motion and structural rearrangement in the timescale of observation. Consequently, the liquid is said to "freeze" into a non-crystalline solid — a glass. This kinetic transition is termed the glass transition that occurs at a temperature T_g, which depends on the cooling rate. Figure 1-1 illustrates the change in volume with temperature during this liquid-to-glass transition.[16]

Chalcogenide glasses are an important class of materials that are sulfides, selenides or tellurides, mainly of Ge, As, P and Si that have found wide-ranging applications in the areas of
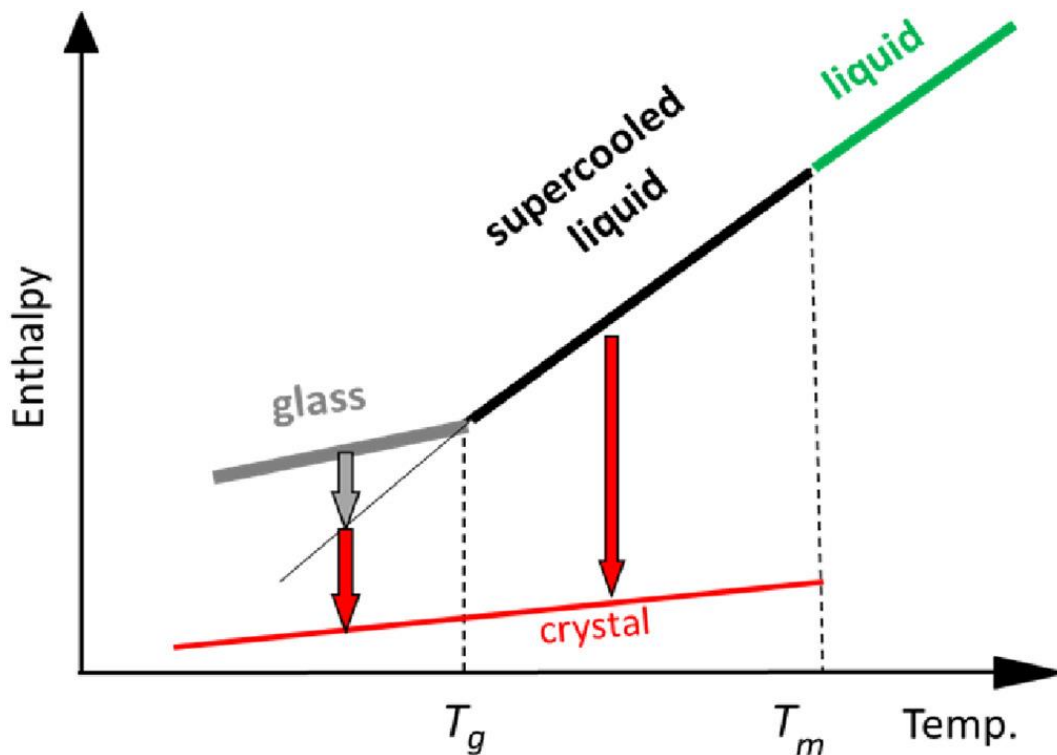
Figure 1-1 Schematic representation of the enthalpy as a function of temperature of a glass-forming liquid. The liquid upon cooling below its melting point T_m undergoes either a phase transition (red line) and enters the thermodynamically stable crystal regime or goes through glass transition (and black and grey line) and enters supercooled liquid regime and subsequently the glassy state through the dynamic glass transition at the glass transition temperature T_g. Vertical dashed lines denote T_m and T_g, respectively. Figure is taken from [16].

infrared photonics, telecommunication, optical memory storage, photovoltaics and environmental remote sensing (Fig. 1-2).[17–24] The remarkable compositional flexibility of chalcogenides in the form of continuous alloying allows for excellent tuning of their electronic, thermal-mechanical, optical and other properties. The structural peculiarities such as the formation of homopolar bonds, molecular and other low-dimensional topological units and violation of chemical order are of key importance in controlling the physical properties of these materials.[25–33]
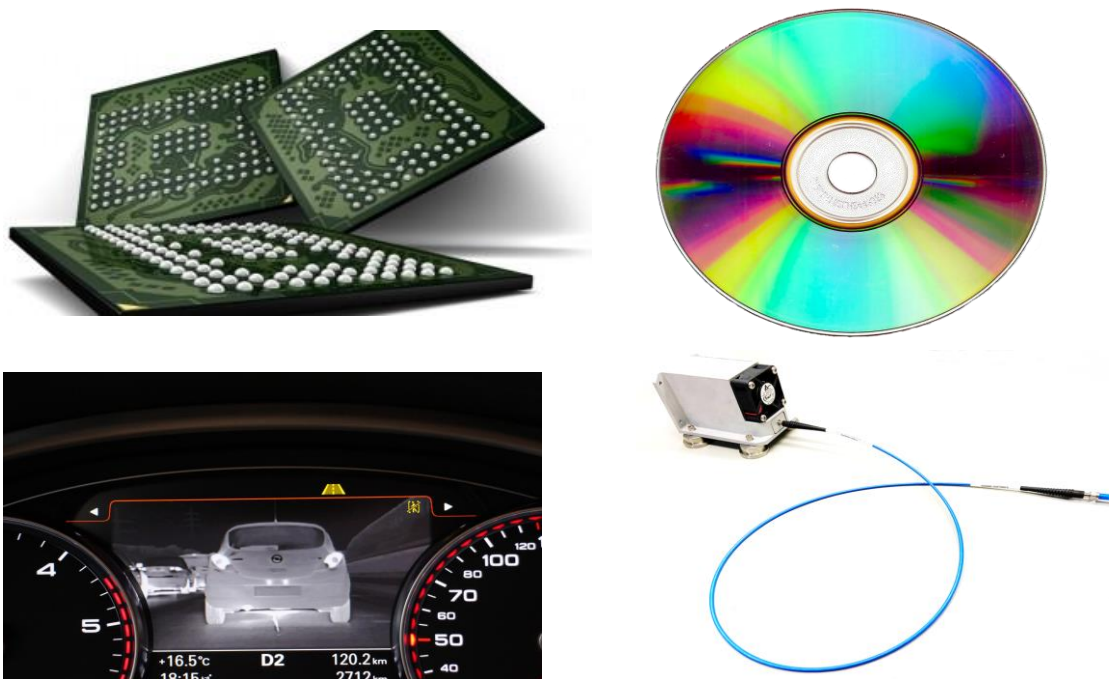
Figure 1-2 Applications of chalcogenide-based glasses. Top left: phase change memory. Top right: CD-RW. Bottom left: Automobile night vision. Bottom right: IR Fiber.

However, besides structure, accelerating the design of functional glasses to address the grand challenges faced by our society today requires fundamental knowledge of the dynamical processes and their mechanistic connection to various relaxation phenomena in the parent melts or supercooled liquids from which these glasses are derived, which are of crucial importance in all stages of industrial glass production. More specifically, the multitude of relaxational modes and their interrelationships in supercooled glass-forming liquids are intimately linked to their viability for various processing techniques and are of key significance in controlling the corresponding processing parameters.[34,35]

This dissertation focuses on the application of a uniquely powerful combination of state-of-the-art rheological, calorimetric, and Raman and multi-nuclear NMR spectroscopic measurements to build a comprehensive atomistic understanding of the structural and

compositional evolution of the dynamical processes and their mechanistic relationships to shear relaxation in supercooled chalcogenide liquids. The nature of the structural moieties and the resulting dimensionality and connectivity of the network (e.g., isolated vs. associated molecules, 1-D chains, 2-D sheets, or 3-D polyhedral networks) are shown to be intimately linked to the structural relaxation and viscous flow.[36–38] Such understanding will facilitate the optimization
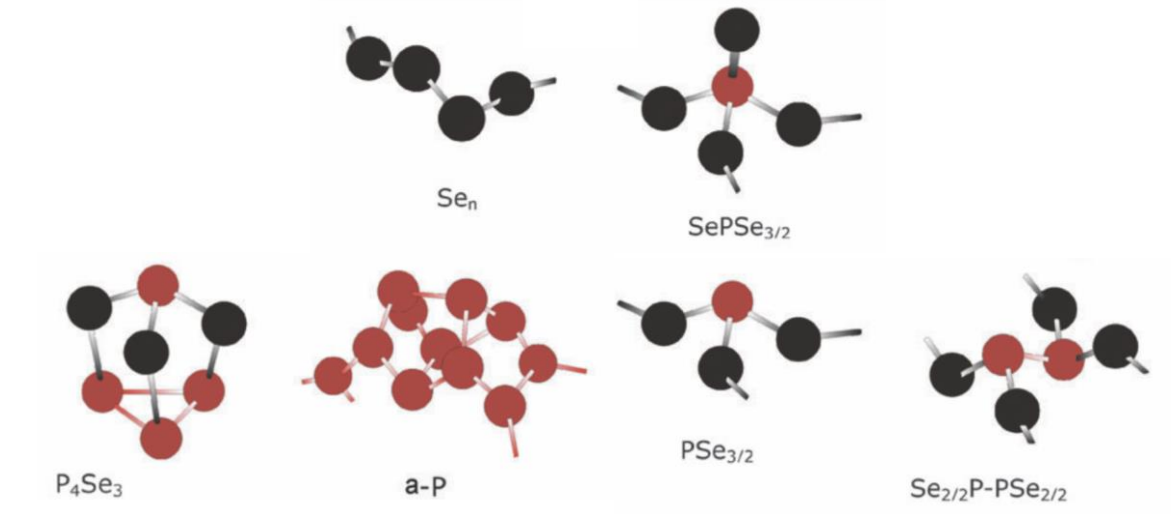
Figure 1-3 Various building blocks or structural moieties characteristic of P-Se glasses. Se and P atoms are shown in black and red, respectively. Figure is taken from [33].

of the composition, and of the methods and parameters for the processing of chalcogenide glasses, thereby enabling their application in a wide range of modern technologies. Vitreous Se consists practically exclusively of two-fold Se atoms forming 1-D linear polymeric chains and is an excellent glass former that has been extensively studies in the literature. The structural dimensionality of these chains remains unchanged with the addition of iodine or tellurium. However, iodine serves as a chain terminator, which results in the shortening of the chain length, while tellurium exhibits very different chemistry, which significantly alters the physical properties of the glass. On the other hand, addition of sulfur prefers the formation

of eight-membered ring molecules, thus reducing the structural dimensionality. Finally, initial addition of phosphorus results in three- and four-coordinated P-Se polyhedra, which crosslink the Se chains and increases the degree of connectivity. In contrast, increasing the P content results in Van der Waals bonded molecular environments, which drastically lowers the structural connectivity. Keeping these attributes in mind, four binary glass-forming systems, $S_x Se_{100-x}$ ($0 \leq x \leq 90$), $Se_{100-x}I_x$ ($0 \leq x \leq 3$), $Te_x Se_{100-x}$ ($0 \leq x \leq 35$), and $P_x Se_{100-x}$ ($0 \leq x \leq 70$), are chosen for the present studies as the structural moieties in these four systems systematically evolve from 1-D linear chains in pure Se to 0-D molecules on one end and all the way to 3-D networks on the other end. An example of the structural moieties in binary P-Se system is shown in Figure 1-3.[33]

The structural investigation of all four families of binary chalcogenide glasses is carried out using a combination of Raman and [77]Se, [125]Te and [31]P Nuclear Magnetic Resonance (NMR) spectroscopic techniques and the results are presented in Chapters 2a, 3, 4a and 5a. While Raman spectroscopy provides qualitative structural information based on the frequency shift of incident light due to inelastic scattering from interatomic stretching and bending vibrations, NMR spectroscopy is an element-specific technique that detects transitions between nuclear spin energy levels that allows for the identification and quantitation of local bonding environments of various nuclides in a material.[39–44] NMR spectroscopy can provide element specific information not only on the short-range order in terms of the average coordination environment in the form of the isotropic chemical shift δ_{iso} but also on the intermediate range structural characteristics, including an understanding of the connectivity between the various structural moieties, as well as the average symmetry and conformation of these moieties.[45] Besides the δ_{iso} of a nuclide, which is characteristic of its coordination environment and can be typically obtained from a magic-angle-

spinning (MAS) NMR experiment, the chemical shift anisotropy (CSA) carries important complementary information related to the symmetry of the local electronic environment of a nuclide and, in combination with δ_{iso}, can often be useful in deciphering the intermediate-range order in glass structure beyond the nearest-neighbor length scale. Chemical shift is a second rank tensor and a determination of the full tensor in the form of CSA provides information on the conformational geometry of the coordination polyhedra. The inhomogeneous broadening of the NMR spectra from the structural disorder (i.e., distribution of bond angles and bond lengths) in glasses, in combination with the low sensitivity and low natural abundance of nuclides such as ^{77}Se and ^{125}Te makes the NMR study of chalcogenide glasses incredibly challenging. Therefore, besides the typical one-dimensional magic-angle-spinning (MAS) NMR experiments, a novel high-resolution two-dimensional (2D) NMR technique, namely, magic-angle-turning phase adjusted spinning sideband (MATPASS) NMR is implemented to alleviate these problems.[46–49] The MATPASS technique can separate the CSA from the isotropic chemical shift, resulting in
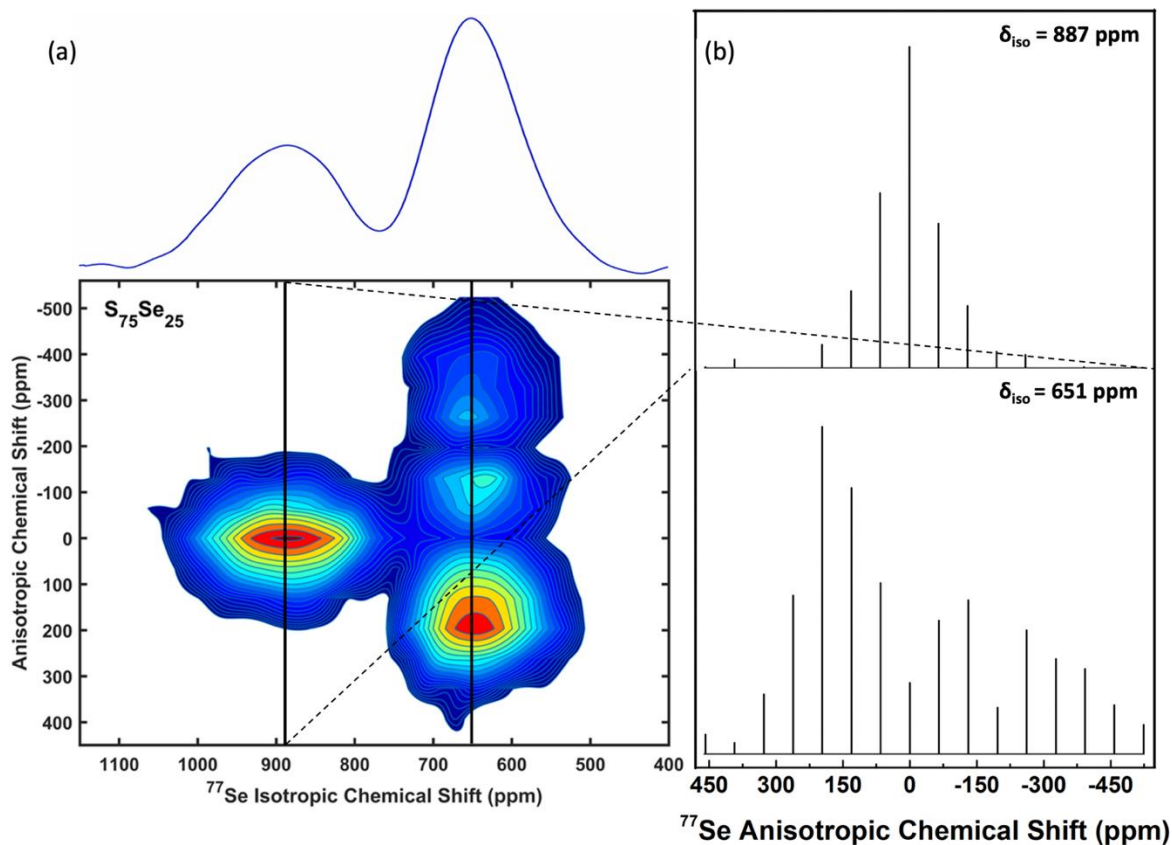
Figure 1-4 2D ^{77}Se MATPASS/CPMG NMR spectrum of $S_{75}Se_{25}$ glass with (a) the total isotropic projection along isotropic dimension and (b) the anisotropic ^{77}Se NMR spinning sideband intensities taken at δ_{iso} = 887 and 651 ppm. Figure is taken from [50].

increased spectral resolution in the isotopic dimension, while preserving the information contained in the CSA along the anisotropic dimension (Fig. 1-4).[50] This separation of isotropic and anisotropic chemical shift interactions results in an isotropic NMR spectrum corresponding to a high-resolution MAS spectrum at infinite spinning speed, i.e., free of any CSA-related broadening. Furthermore, the application of the Carr-purcell Meiboom-Gill (CPMG) echo train acquisition of the MATPASS data can reduce the data collection time significantly.[48,51] A consideration of CSA in combination with isotropic shift provides unequivocal identification of structural units, and the structural models are proposed for each studied system. These MATPASS NMR experiments were carried out at relatively high magnetic fields (~ 20 T) using the facilities at the National High Magnetic Field Laboratory in Tallahassee, Florida.

As noted above, the processing of glasses from their parent supercooled liquids depends critically on the rheological behavior of the latter. The frequency ω dependence of the shear mechanical response, including the storage and loss shear moduli (G′ and G″, respectively) and viscosity h, of glass-forming liquids shed light on the atomistic details of the relaxation processes associated with the glass transition and related relaxation phenomena. Chapters 2b, 3, 4b and 5b and c in this dissertation presents results of our investigation on the influence of the compositional evolution of structural network on the shear mechanical response and the modes of structural relaxation of supercooled liquids in all four binary systems S_xSe_{100-x}, $Se_{100-x}I_x$, Te_xSe_{100-x}, and P_xSe_{100-x}.

The shear viscosity is one of the most important transport properties which changes drastically with temperature and can be expressed as $\eta(T) = \eta_0 \exp\left[E(T)/RT\right]$, where $E(T)$ is the activation energy of the viscous flow and R is the ideal gas constant. The temperature dependence of the viscosity curve could vary from a nearly-Arrhenius behavior with a single activation energy that is practically independent of temperature, all the way to a strongly non-Arrhenius behavior, where the activation energy increases rapidly with decreasing temperature. Angell has shown that, if η is expressed as a function of T_g/T, i.e., temperature scaled by the glass transition temperature T_g, then a useful classification scheme emerges as a function of the parameter m, which is termed "fragility index" and is defined as:[52]

$$m = \left.\frac{d\log_{10}\eta}{d(T_g/T)}\right|_{T=T_g} \tag{1-1}$$

The glass-forming liquids with increasingly non-Arrhenius behavior of η are then characterized by progressively increasing values of *m*. Glass-forming liquids with low and high values of *m* were denoted by Angell as "strong" and "fragile", respectively (Fig. 1-5).[53] Viscosity measurements are carried out for all four binary systems using steady shear parallel plate rheometry. On the other hand, the viscous flow is also closely related to structural relaxation
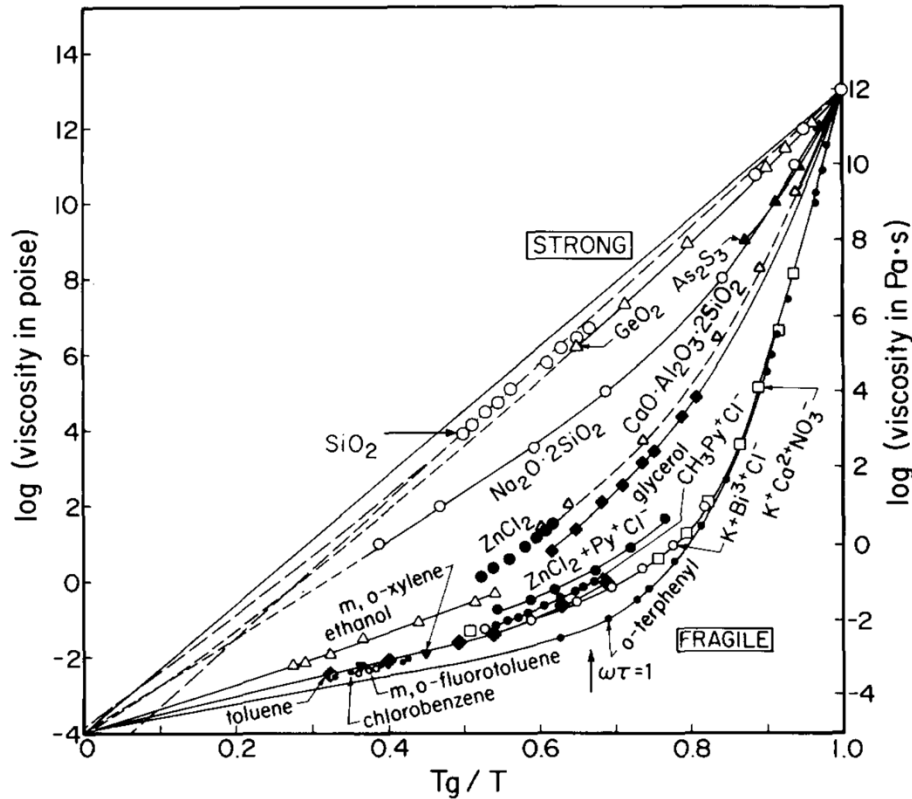
Figure 1-5 Viscosity of a collection of glass-forming liquids as a function of T_g/T where T_g is defined as a temperature where viscosity is 10^{12} Pa·s. Note the "strong-fragile" classification scheme. Strong (fragile) liquids are characterized by activation energy of viscous flow that is weakly (strongly) dependent on temperature. Figure is taken from [53].

process, which is probed through the frequency dependence of the shear-mechanical response via small amplitude oscillatory shear (SAOS) measurements. These experiments are also performed with parallel plate rheometers, which consist of an oscillatory upper plate and a stationary lower plate as shown in Figure 1-6. In a typical experiment, the sample is sandwiched in between the two plates with a disc-like geometry and a sinusoidal strain is applied through the upper plate over

a range of frequencies on the sample while the resultant stress response is monitored through a transducer (Fig. 1-6). The viscoelastic behaviors of the studied glass-forming liquids are characterized by the storage modulus G' and loss modulus G'' which corresponds to the elastic (solid-like) and viscous (fluid-like) contributions to the measured stress response, respectively. When the probing frequency is high, the stress response of the liquid will be dominated by the elastic behavior with G' > G''. Conversely, viscous behavior will be the predominant contribution with G'' > G'. Moreover, the corresponding characteristic shear relaxation time can be easily obtained as the reciprocal of the frequency at G' = G'' (Fig. 1-6). It is important to note that the probing frequency window of a typical parallel plate rheometer is about 10^{-2} to 10^{3} rad/s, therefore only a portion of the whole G' and G'' spectrum is revealed within the observation window at each acquisition temperature. In turn, a sequential observation of the viscoelastic spectrum in a wide frequency range can be obtained by consecutively changing the probing temperature and the experimental master curve can be constructed use time-temperature superposition (TTS). The resultant master curve may contain one or more structural relaxation processes indicated by the number of G'-G'' crossovers. By obtaining the corresponding timescale distribution and activation energies of the observed relaxation processes and simulating the master curves using appropriate

Figure 1-6 From left to right: picture of the Anton Paar MCR 92 rheometer with parallel-plate and Peltier heater setup, sample geometry in a shearing experiment with parallel-plate setup, typical G' and G'' spectrum as a function of oscillatory frequency.

models, these structural relaxation processes can be assigned to different atomistic mechanisms in the selected four Se-containing systems. The structural and rheological data are then combined to establish robust atomistic models of structural control on the dynamics and relaxation phenomena in these binary chalcogenide glass-forming systems.

The contents of each of these chapters have been published as separate journal articles as follows: Chapter 2a in the *Journal of Physical Chemistry B*, Chapter 2b in the *Journal of Chemical Physics*, Chapter 3 in the *Journal of Non-Crystalline Solids*, Chapter 4a and 4b in the *Journal of Non-Crystalline Solids*, Chapter 5a in the *Journal of Physical Chemistry B*, Chapter 5b in the *Journal of Non-Crystalline Solids*, and Chapter 5c in the *Journal of Chemical Physics*.

Reference

[1]   D.L. Morse, J.W. Evenson, Welcome to the Glass Age, Int. J. Appl. Glas. Sci. 7 (2016) 409–412.

[2]   M. Bolt, Glass: The eye of science, Int. J. Appl. Glas. Sci. 8 (2017) 4–22.

[3]   J.C. Mauro, Decoding the glass genome, Curr. Opin. Solid State Mater. Sci. 22 (2018) 58–64.

[4]   J.C. Mauro, E.D. Zanotto, Two Centuries of Glass Research: Historical Trends, Current Status, and Grand Challenges for the Future, Int. J. Appl. Glas. Sci. 5 (2014) 313–327.

[5]   H. Rawson, Glasses and Their Applications, Royal Institute of Metals, London, 1991.

[6]   L. Wondraczek, J.C. Mauro, Advancing glasses through fundamental research, J. Eur. Ceram. Soc. 29 (2009) 1227–1234.

[7]   R.D. Maurer, Glass fibers for optical amplification, Proc. IEEE. 61 (1973) 452–462.

[8]   R.D. Maurer, P.C. Schultz, Fused silica optical waveguide, 3659915, 1972.

[9]   P.L. Bocko, M.H. Mitchell, AMLCD glass substrates- foundations for high-tech displays, Glas. Res. 12 (2002) 26–29.

[10]   P.L. Bocko, G.R. Trott, Glass for the future: Displays and semiconductors, IEEE Symp. VLSI Circuits, Dig. Tech. Pap. 2 (2013) 86–89.

[11]   D.M. Moffatt, Glass substrates for flat panel displays, MRS Bull. (1996) 31–34.

[12]   A.R. Boccaccini, D.S. Brauer, L. Hupa, Bioactive glasses: fundamentals, technology and applications, Royal Society of Chemistry, 2016.

[13]   E. Boccardi, F.E. Ciraldo, A.R. Boccaccini, Bioactive glass-ceramic scaffolds: Processing and properties, MRS Bull. 42 (2017) 226–232.

[14]   I.W. Donald, Immobilisation of radioactive and non-radioactive wastes in glass-based systems: an overview, Glas. Technol. 48 (2007) 155–163.

[15]   J.S. McCloy, A. Goel, Glass-ceramics for nuclear-waste immobilization, MRS Bull. 42 (2017) 233–238.

[16]   E.D. Zanotto, J.C. Mauro, The glassy state of matter: Its definition and ultimate fate, J. Non. Cryst. Solids. 471 (2017) 490–495.

[17]   L. Calvez, Chalcogenide glasses and glass-ceramics: Transparent materials in the infrared for dual applications, Comptes Rendus Phys. 18 (2017) 314–322.

[18]   J.M. Harbold, F.Ö. Ilday, F.W. Wise, J.S. Sanghera, V.Q. Nguyen, L.B. Shaw, I.D. Aggarwal, Highly nonlinear As–S–Se glasses for all-optical switching, Opt. Lett. 27 (2002) 119.

[19]   C. Quémard, F. Smektala, V. Couderc, A. Barthélémy, J. Lucas, Chalcogenide glasses with high non linear optical properties for telecommunications, J. Phys. Chem. Solids. 62 (2001) 1435–1440.

[20]   B. Bureau, X.H. Zhang, F. Smektala, J.L. Adam, J. Troles, H.L. Ma, C. Boussard-Plèdel, J. Lucas, P. Lucas, D. Le Coq, M. R. Riley, J. H. Simmons, Recent advances in chalcogenide glasses, J. Non. Cryst. Solids. 345&346 (2004) 276–283.

[21]   A. Zakery, S.R. Elliott, Optical properties and applications of chalcogenide glasses: a review, J. Non. Cryst. Solids. 330 (2003) 1–12.

[22]   P.A. Vermeulen, J. Momand, B.J. Kooi, Reversible amorphous-crystalline phase changes in a wide range of $Se_{1-x}Te_x$ alloys studied using ultrafast differential scanning calorimetry, J. Chem. Phys. 141 (2014) 024502.

[23]   M. Wuttig, N. Yamada, Phase-change materials for rewriteable data storage, Nat. Mater. 6 (2007) 824.

[24]   J.S. Sanghera, I.D. Aggarwal, Active and passive chalcogenide glass optical fibers for IR applications: A review, J. Non. Cryst. Solids. 256&257 (1999) 6–16.

[25]   A.W. Mao, B.G. Aitken, R.E. Youngman, D.C. Kaseman, S. Sen, Structure of glasses in the pseudobinary system Ga_2Se_3-$GeSe_2$: Violation of chemical order and 8-N coordination rule, J. Phys. Chem. B. 117 (2013) 16594–16601.

[26]   B. Bureau, J. Troles, M. LeFloch, F. Smektala, G. Silly, J. Lucas, Solid state ^{77}Se NMR investigations on arsenic-selenium glasses and crystals, Solid State Sci. 5 (2003) 219–224.

[27]   G. Yang, Y. Gueguen, J.C. Sangleboeuf, T. Rouxel, C. Boussard-Plédel, J. Troles, P. Lucas, B. Bureau, Physical properties of the Ge_xSe_{1-x} glasses in the 0<x<0.42 range in correlation with their structure, J. Non. Cryst. Solids. 377 (2013) 54–59.

[28] D.C. Kaseman, I. Hung, Z. Gan, B. Aitken, S. Currie, S. Sen, Structural and topological control on physical properties of arsenic selenide glasses, J. Phys. Chem. B. 118 (2014) 2284–2293.

[29] T. Wang, O. Gulbiten, R. Wang, Z. Yang, A. Smith, B. Luther-Davies, P. Lucas, Relative contribution of stoichiometry and mean coordination to the fragility of Ge-As-Se glass forming liquids, J. Phys. Chem. B. 118 (2014) 1436–1442.

[30] D.C. Kaseman, I. Hung, Z. Gan, S. Sen, Observation of a continuous random network structure in Ge_xSe_{100-x} glasses: Results from high-resolution ^{77}Se MATPASS/CPMG NMR spectroscopy, J. Phys. Chem. B. 117 (2013) 949–954.

[31] D.C. Kaseman, K.M. Oliveira, T. Palazzo, S. Sen, Selenium chain length distribution in Ge_xSe_{100-x} glasses: Insights from ^{77}Se NMR spectroscopy and quantum chemical calculations, J. Phys. Chem. B. 120 (2016) 4513–4521.

[32] G. Yang, B. Bureau, T. Rouxel, Y. Gueguen, O. Gulbiten, C. Roiland, E. Soignard, J.L. Yarger, J. Troles, J.C. Sangleboeuf, P. Lucas, Correlation between structure and physical properties of chalcogenide glasses in the As_xSe_{1-x} system, Phys. Rev. B. 82 (2010) 195206.

[33] A. Bytchkov, F. Fayon, D. Massiot, L. Hennet, D.L. Price, ^{31}P solid-state NMR studies of the short-range order in phosphorus-selenium glasses, Phys. Chem. Chem. Phys. 12 (2010) 1535–1542.

[34] B.G. Aitken, S.C. Currie, B.C. Monahan, L. Wu, E.W. Coonan, Chalcogenide glass for low viscosity extrusion and injection molding, 1 (2006) United States Patent.

[35] Q. Zheng, J.C. Mauro, Viscosity of glass-forming systems, J. Am. Ceram. Soc. 100 (2017) 6–25.

[36] C.M. Roland, Viscoleastic Behavior of Rubbery Materials, Oxford University Press, Oxford, 2011.

[37] J.D. Ferry, Viscoelastic properties of polymers, John Wiley & Sons, 1980.

[38] M. Doi, S.F. Edwards, The Theory of Polymer Dynamics, Oxford University Press, Oxford, 1986.

[39] E. Fukushima, S.B. Roeder, Experimental Pulse NMR: A Nuts and Bolts Approach, CRC Press, 2018.

[40] M.J. Duer, Solid State NMR Spectroscopy: Principles and Applications, John wiley & sons, 2008.

[41] H. Eckert, Structural Characterization of Noncrystalline Solids and Glasses Using Solid State NMR, Prog. Nucl. Magn. Reson. Spectrosc. 24 (1992) 159–293.

[42] R.E. Youngman, S.T. Haubrich, J.W. Zwanziger, M.T. Janicke, B.F. Chmelka, Short- and intermediate-range structural ordering in glassy boron oxide, Science (80-.). 269 (1995) 1416–1420.

[43] F. Fayon, C. Bessada, J.P. Coutures, D. Massiot, High-resolution double-quantum ^{31}P MAS NMR study of the intermediate-range order in crystalline and glass lead phosphates, Inorg. Chem. 38 (1999) 5212–5218.

[44] C.T.G. Knight, R.J. Kirkpatrick, E. Oldfield, The connectivity of silicon sites in silicate glasses, as determined by two-dimensional ^{29}Si nuclear magnetic resonance spectroscopy, J. Non. Cryst. Solids. 116 (1990) 140–144.

[45] D.L. Sidebottom, Fragility of network-forming glasses: a universal dependence on the topological connectivity, Phys. Rev. E. 92 (2015) 062804.

[46] Z. Gan, R.R. Ernst, An improved 2D magic-angle-turning pulse sequence for the measurement of chemical-shift anisotropy, J. Magn. Reson. - Ser. A. 123 (1996) 140–143.

[47] O.N. Antzutkin, S.C. Shekar, M.H. Levitt, Two-Dimensional Sideband Separation in Magic-Angle-Spinning NMR, J. Magn. Reson. Ser. A. 115 (1995) 7–19.

[48] I. Hung, T. Edwards, S. Sen, Z. Gan, MATPASS/CPMG: A sensitivity enhanced magic-angle spinning sideband separation experiment for disordered solids, J. Magn. Reson. 221 (2012) 103–109.

[49] D.C. Kaseman, I. Hung, K. Lee, K. Kovnir, Z. Gan, B. Aitken, S. Sen, Tellurium speciation, connectivity, and chemical order in As_xTe_{100-x} glasses: Results from two-dimensional ^{125}Te NMR spectroscopy, J. Phys. Chem. B. 119 (2015) 2081–2088.

[50] B. Yuan, W. Zhu, I. Hung, Z. Gan, B. Aitken, S. Sen, Structure and Chemical Order in S-Se Binary Glasses, J. Phys. Chem. B. 122 (2018) 12219–12226.

[51] H.Y. Carr, E.M. Purcell, Effects of diffusion on free precession in nuclear magnetic resonance experiments, Phys. Rev. 94 (1954) 630–638.

[52] C.A. Angell, Relaxation in Liquid, Polymers and Plastic Crystal-Strong/Fragile Patterns

and Problems, J. Non. Cryst. Solids. 131–133 (1991) 13–31.

[53]   C.A. Angell, Strong and fragile liquids, Relaxations Complex Syst. (1985) 3–11.

Chapter 2a

Structure and Chemical Order in S-Se Binary Glasses

2a.1 Abstract

The compositional evolution of the structure and chemical order in binary S_xSe_{100-x} glasses $(0 \leq x \leq 90)$ is investigated using a combination of high-resolution 2D ^{77}Se isotropic-anisotropic correlation NMR and Raman spectroscopy. The results indicate that the structure of S-Se glasses consist of two types of topological elements, namely polymeric $[Se,S]_n$ chains and eight-membered Se_yS_{8-y} rings $(0 \leq y \leq 8)$. The relative concentration of Se atoms monotonically decreases in the chain elements and concomitantly increases in the ring elements with increasing S concentration. Moreover, the Se speciation results are consistent with an average heterocyclic ring composition of Se_1S_7 at low S content ($\leq$40 at.% S), while the composition shifts to $Se_{1.5}S_{6.5}$ at higher S content ($\geq$60 at.% S), indicating increasing incorporation of multiple Se atoms in each ring element. The Raman spectra suggest that -Se-Se- association is favored, when more than one Se atoms is incorporated in chains and rings. As in their elemental forms, the S and Se atoms retain their preference of forming rings and chains in binary S_xSe_{100-x} glasses, which predicts a linear compositional variation in the relative fractions of these topological elements. This structural evolution is consistent with the corresponding variation in the T_g and molar volume, both of which exhibit a linear decrease with increasing S concentration.

2a.2 Introduction

Chalcogenide glasses consist of one or more of the chalcogen elements S, Se and Te and constitute an important class of optical materials that has received great attention for a wide range of applications in photonics, non-volatile memories and remote sensing.[1–3] The elemental chalcogens, i.e., S, Se and Te are also glass-formers by themselves and their structure-property relations have been extensively investigated. The most stable form of S is its orthorhombic polymorph (α-S) which transforms to the monoclinic form (β-S) at 95.6 $^{\circ}$C and the latter undergoes melting at 119 $^{\circ}$C.[4] The structural building blocks in both α-S and β-S polymorphs are eight-membered S_8 rings. The structure of glassy S obtained from quenching the melt also consists predominantly of these S_8 ring molecules. Molten sulfur is characterized by a rather unique property known as living polymerization, which corresponds to a reversible transformation between S_8 ring molecules and $[S]_n$ chains at 159 $^{\circ}$C.[5,6] The transformation of S_8 rings to $[S]_n$ chains results in a relatively sudden rise in viscosity with increasing temperature beyond the transition point.[7] Consequently this transition renders the chain : ring ratio in glassy sulfur dependent on the cooling rate of the melt.[8] Se is chemically similar to S as the former can also exist in crystalline structures which are made of Se_8 rings, namely the monoclinic polymorphs α-Se and β-Se. However, the most stable and commonly occurring polymorph of Se has a trigonal crystal structure consisting of covalently bonded parallel helical $[Se]_n$ chains.[9] Although the structure of glassy Se remained controversial in the past regarding its ring vs. chain content, recent two-dimensional (2D) ^{77}Se nuclear magnetic resonance (NMR) spectroscopic studies have conclusively demonstrated that the structure of glassy Se essentially consists solely of $[Se]_n$ chains.[10] The element Te crystallizes in a hexagonal structure with spiral $[Te]_n$ chain elements, which is analogous to trigonal Se. However, compared to Se, the shorter second neighbor

interaction distance in crystalline Te leads to quasi-metallic behavior[4,11]. This enhanced metallic character results in an extremely poor glass-forming ability for Te, compared to that for S and Se. Similar to glassy selenium, the structure of amorphous Te is also comprised of disordered $[Te]_n$ chains, but with significantly weaker interchain interaction.[12]

Structural studies have also been extended in the past to binary chalcogen systems. In particular, several excellent studies were reported on the structure of binary Se-Te glasses. It may be noted here that Se and Te can form a continuous solid solution where Se and Te atoms are believed to form composite chains in the crystal structure.[13] In a more recent study of Se-Te glasses, Bureau *et al.* used ^{77}Se NMR to demonstrate a random distribution of Se and Te atoms in the chain elements, with some preference for heteropolar bonding.[14] Tverjanovich *et al.* used a combination of Raman spectroscopy and density functional theory-based calculations of the vibrational spectra to confirm this structural model of Se-Te glasses.[15]

Unlike the Se-Te system, where the size and the bonding preferences of the two elements are similar, S and Te constitute a binary system where the elements are quite different in size and electronegativity. Whereas Te prefers to form $[Te]_n$ chains, S prefers to form S_8 rings. As a consequence of these differences between S and Te and of the metallic nature of Te itself, the formation of homogeneous binary S-Te glasses is rather challenging, although a previous study claimed to have been able to obtain glasses over a limited composition range (20-50% Te) by splat quenching.[16]

The structural evolution in the S-Se binary system, on the other hand, has been studied primarily in the crystalline and molten states and on quenched products dissolved in CS_2, using X-ray diffraction, Raman and ^{77}Se NMR spectroscopy.[17–20] Unfortunately, the structural disorder in the S_xSe_{100-x} crystals did not allow for the determination of atom positions via diffraction

measurements.[21] The spectroscopic studies of crystalline and molten S_xSe_{100-x} indicated the presence of a mixture of Se_yS_{8-y} ring molecules, with S_7Se being the predominant molecular species at low Se concentration (≤ 25 at.% Se), while the concentration of S_6Se_2 molecules became comparable to the latter at ~ 40 at.% Se.[19,20] Moreover, it was suggested that the Se atoms prefer to form Se-Se linkages in the S_6Se_2 molecules.[19,21] Additionally, ^{77}Se NMR of molten S_xSe_{100-x} indicated that a significant fraction of Se and S atoms take part in polymeric structural moieties in the form of $[Se,S]_n$ chains. However, to the best of our knowledge, no systematic structural study of glasses in this system has been reported in the literature to date.

In the present study, we report the results of a structural investigation of binary S_xSe_{100-x} glasses with $0 \leq x \leq 90$, using Raman spectroscopy and high-resolution 2D magic-angle-turning phase adjusted spinning sideband (MATPASS) ^{77}Se NMR spectroscopy.[22] The 2D ^{77}Se MATPASS NMR spectra allow for the identification and quantitation of different Se environments in glasses with high accuracy, based on the separation of isotropic and anisotropic chemical shift in two different dimensions and the correlation between them. The compositional evolution of the chain and molecular topological elements thus obtained is used to build a structural model of these glasses that is shown to be consistent with their thermophysical properties, namely molar volume and glass transition temperature T_g.

2a.3 Experimental Methods

2a.3.1 Sample Preparation

Binary S_xSe_{100-x} glasses with $x = 0$, 10, 30, 45, 60, 75 and 90 were synthesized in $7 - 15$ g batches using the conventional melt quench method. Elemental sulfur and selenium (Alfa Aesar, 99.999%) were mixed together in stoichiometric ratios and subsequently flame sealed in evacuated

(10^{-4} Torr) quartz ampoules. The fused ampoules were placed in a rocking furnace, slowly heated to 673 K over 8 hours and subsequently held at this temperature and rocked for 48 hours. The melts were then quenched by dipping the ampoules in water.

2a.3.2 2D ^{77}Se MATPASS/CPMG NMR Spectroscopy

The 2D ^{77}Se MATPASS NMR spectra for all glasses were acquired at the National High Magnetic Field Laboratory using a 63 mm bore 18.8 T magnet equipped with a Bruker Avance III HD console operating at the resonance frequency of 152.7 MHz for [77]Se. Glass samples were crushed and packed into 3.2 mm ZrO_2 rotors and were spun at 10 kHz. Samples with high S content (S ≥ 45 at.%) are soft and malleable at ambient temperature and therefore, were blended with small pieces of dry ice, to crush into powder. All ^{77}Se NMR data were collected at 263 K, to avoid heating of these glass samples above their T_g during magic-angle-spinning (MAS). The pulse sequence used a series of five MAT π-pulses (4.0 μs) with incremented inter-pulse delays according to the timings detailed by Hung *et al*.[22] The method of States *et al*.[23] for hypercomplex data acquisition was applied to of the Car-Purcell-Meiboom-Gill (CPMG) pulse phase and the receiver phase. Acquisition consisted of 16 hypercomplex t_1 increments each with 24 transients and 90 s recycle delay. A total of 30 CPMG echoes were co-added for S/N improvement before the processing of 2D spectra. All spectra were externally referenced by recording the [17]O signal of natural abundance H_2O and then using the appropriate frequency ratio reported in the IUPAC recommendations.[24]

The [77]Se chemical shift anisotropy (CSA) tensors reported here follow the Haeberlen convention[25] defined as:

$$|\delta_{zz} - \delta_{iso}| \geq |\delta_{xx} - \delta_{iso}| \geq |\delta_{yy} - \delta_{iso}|,$$

$$\delta_{iso} = \frac{1}{3}(\delta_{zz} + \delta_{xx} + \delta_{yy}),$$

$$\Delta = \delta_{zz} - \delta_{iso},$$

$$\eta = \frac{\delta_{yy} - \delta_{xx}}{\Delta},$$

where δ_{xx}, δ_{yy}, and δ_{zz} are the principle components of the chemical shift tensor and δ_{iso} is the isotropic chemical shift. The magnitude of the CSA is Δ, and its asymmetry is denoted as η.

2a.3.3 Density and T_g measurement

The density of S_xSe_{100-x} glasses was measured using a Micromeritics Accupyc II gas expansion pycnometer under a helium environment of 6N purity. Each measurement was carried out on ~ 2.0 g of sample loaded into a 1 cm^3 cup. Density values reported in this study are averages of 10 consecutive measurements at room temperature. The glass transition temperature T_g of the S_xSe_{100-x} glasses was measured using a Mettler-Toledo DSC1 differential scanning calorimeter. Approximately 15 mg glass was loaded in a hermetically sealed 40 µL aluminum crucible and scans were performed at 10 °C/min under a flowing nitrogen environment. T_g was determined to within ± 2 °C as the onset of the glass transition.

2a.3.4 Raman spectroscopy

The Raman spectra of all glasses were collected in backscattering geometry with a resolution of 1 cm^{-1}, using a Renishaw 1000 Raman Microscope System equipped with a diode laser operating at a wavelength of 785 nm. Backscattered light was detected using a charge-coupled device cooled at 200 K.

2a.4 Results and Discussion

2a.4.1 Physical properties

The T_g, density and molar volume of all S_xSe_{100-x} glasses are listed in Table 2a-1 and the compositional variation is displayed in Fig. 2a-1. These results are in good agreement with the

previously reported values in the literature.[26–29] Both T_g and molar volume of these glasses decrease approximately linearly with increasing S content (Fig. 2a-1). This trend in molar volume for S_xSe_{100-x} glasses is reflected in a similar trend in the crystalline state, as exemplified by orthorhombic sulfur and trigonal selenium with molar volumes of 15.50 cm^3/mol and 16.45 cm^3/mol, respectively.[30,31] It is now well established in the literature that, while the structure of amorphous S is predominantly comprised of S_8 molecular rings, that of amorphous Se consists practically exclusively of polymeric $[Se]_n$ chains, with chain lengths on the order of ~ 200 atoms.[8,10,32] Therefore, if S and Se maintain their preference in binary S_xSe_{100-x} glasses to form, respectively, rings and chains, then progressive addition of S to Se should result in a concomitant replacement of polymeric chains with ring molecules. Such compositional variation of the atomic structure is expected to result in a progressive weakening of the chain-chain interaction as they get interspersed with weakly bonded molecules and, thus, is consistent with the observed linear decrease in T_g and in the atomic packing efficiency of S_xSe_{100-x} glasses with increasing S content (Fig. 2a-1).

Table 2a-1 Glass transition temperature T_g, density, and molar volume of S_xSe_{100-x} glasses.

Composition	T_g (± 2.0 ºC)	Density (± 0.002 g/cm^3)	Molar volume (cm^3/mol)
Se	38.8	4.270	18.49± 0.01
$S_{10}Se_{90}$	30.5	4.063	18.28 ± 0.01
$S_{30}Se_{70}$	20.7	3.612	17.97 ± 0.01
$S_{45}Se_{55}$	14.4	3.275	17.67 ± 0.01
$S_{60}Se_{40}$	4.0	2.916	17.43 ± 0.02
$S_{75}Se_{25}$	−7.1	2.548	17.19 ± 0.03
$S_{90}Se_{10}$	−18.5	----	----

(a)
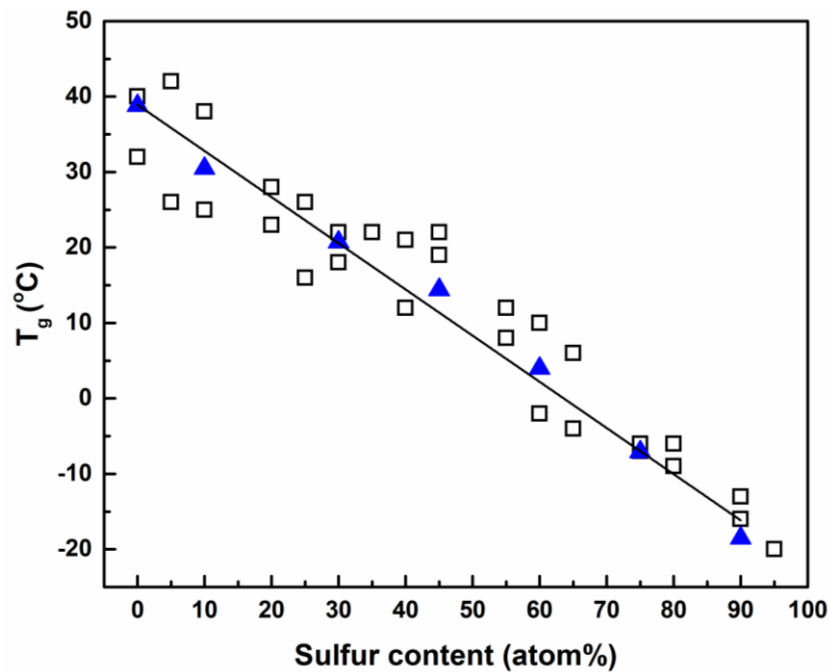
(b)
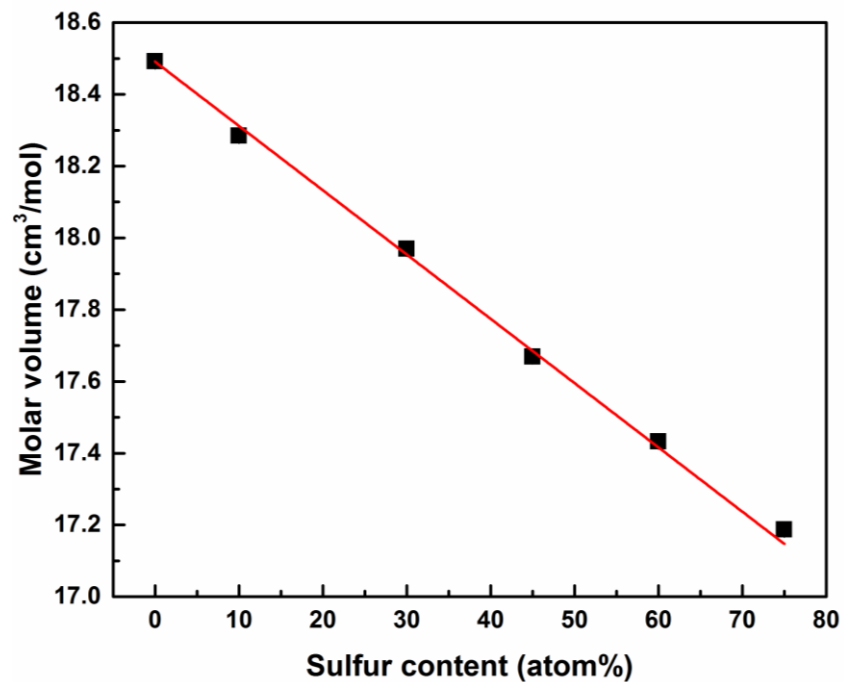
Figure 2a-1 (a) T_g values of binary S_xSe_{100-x} glasses obtained in the present study (filled triangles) and values reported in the literature[26–29] (open squares). (b) molar volume of binary S_xSe_{100-x} glasses determined in the present study. Straight lines through the data points in (a) and (b) represent linear least squares fits to the data collected in this study.

2a.4.2 ^{77}Se NMR

Typical examples of ^{77}Se 2D MATPASS/CPMG NMR spectra of S_xSe_{100-x} glasses are shown in Fig. 2a-2. The 2D MATPASS experiment separates spinning sidebands along the anisotropic dimension and projects the isotropic spectra to the other dimension as if the spinning speed is infinitely fast (Fig. 2a-2a). The ^{77}Se isotropic NMR spectrum of glassy Se displays a single broad resonance centered at ~ 850 ppm that corresponds to the -Se-**Se**-Se- environment in $[Se]_n$ chains, consistent with previous literature reports (Fig. 2a-2b).[10,33] Addition of S to Se results in the shift of the peak position of this resonance to ~ 880-900 ppm and in the appearance of a second well-resolved resonance in the isotropic ^{77}Se NMR spectra that is centered at δ_{iso} ~ 640-660 ppm (Fig. 2a-2b). This second resonance increases monotonically in relative intensity with progressive increase in S content (Fig. 2a-2b). The shift of the amorphous Se resonance to higher ppm (higher frequency) values upon addition of sulfur is indicative of the effect of incorporation of S atoms into the $[Se]_n$ chains. It was shown in a previous ^{77}Se NMR study of S_xSe_{100-x} melts by Chivers *et al.* that progressive replacement of Se nearest neighbors by S in $[Se]_n$ chains, i.e., the formation of -Se-**Se**-S- and -S-**Se**-S- linkages, results in the shift of the corresponding [77]Se resonance to higher frequencies.[20] Moreover, Chivers *et al.* also demonstrated that the [77]Se δ_{iso} for the Se sites in Se_yS_{8-y} ring molecules ranges between 600 and 730 ppm in S_xSe_{100-x} melts. This assignment is consistent with the range of 530 to 670 ppm recently reported for -Se-**Se**-Se- sites in Se_8 rings in the crystalline monoclinic allotrope α-Se.[10]

Further insight into the structural assignment of these [77]Se resonances in the isotropic NMR spectra of S_xSe_{100-x} glasses can be gained by considering the corresponding chemical shift tensor parameters Δ and η, which can be obtained from simulation of the corresponding spinning sideband spikelet pattern in the anisotropic dimension (Fig. 2a-3).[34] The simulation of the anisotropic

(a)
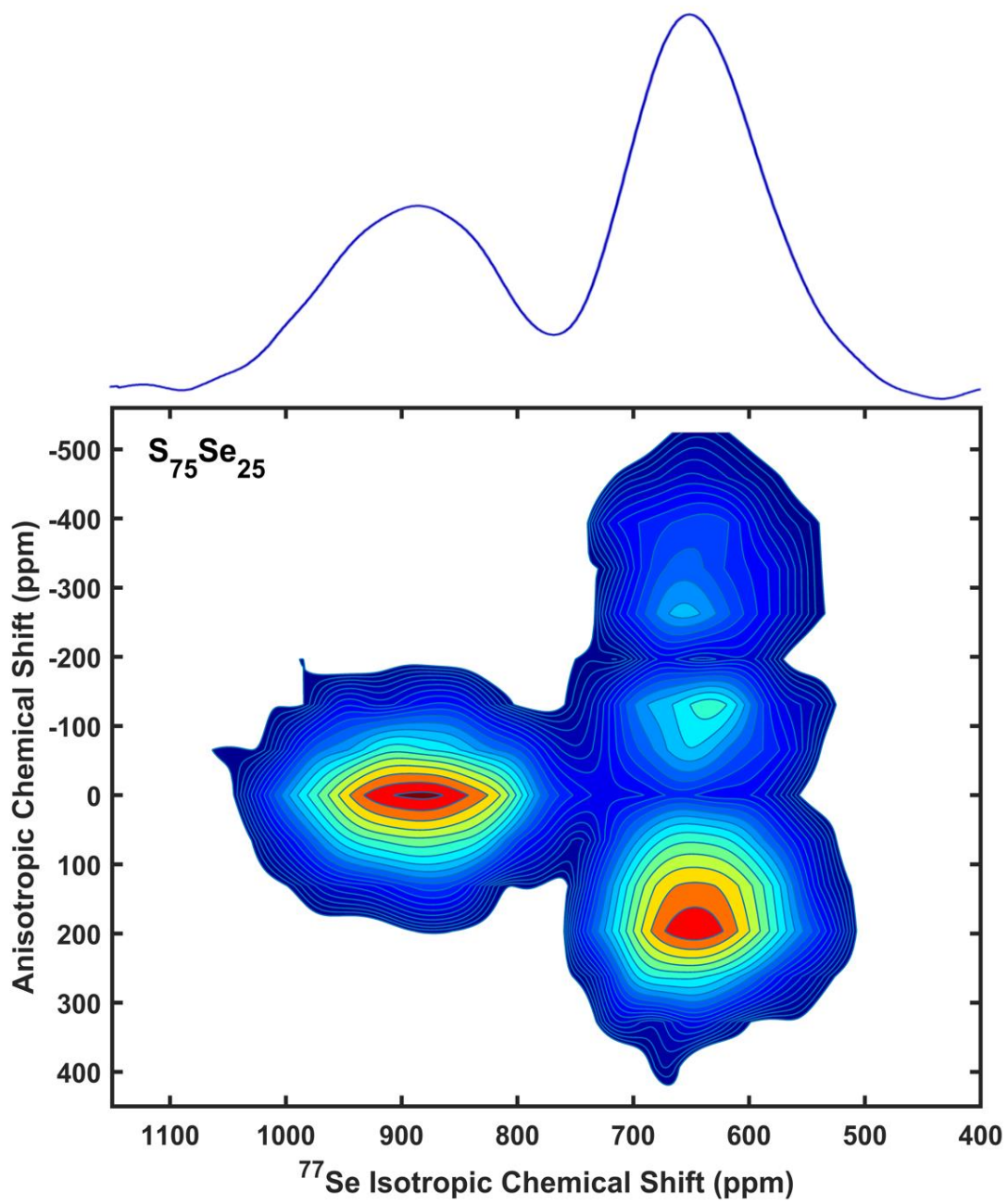
(b)
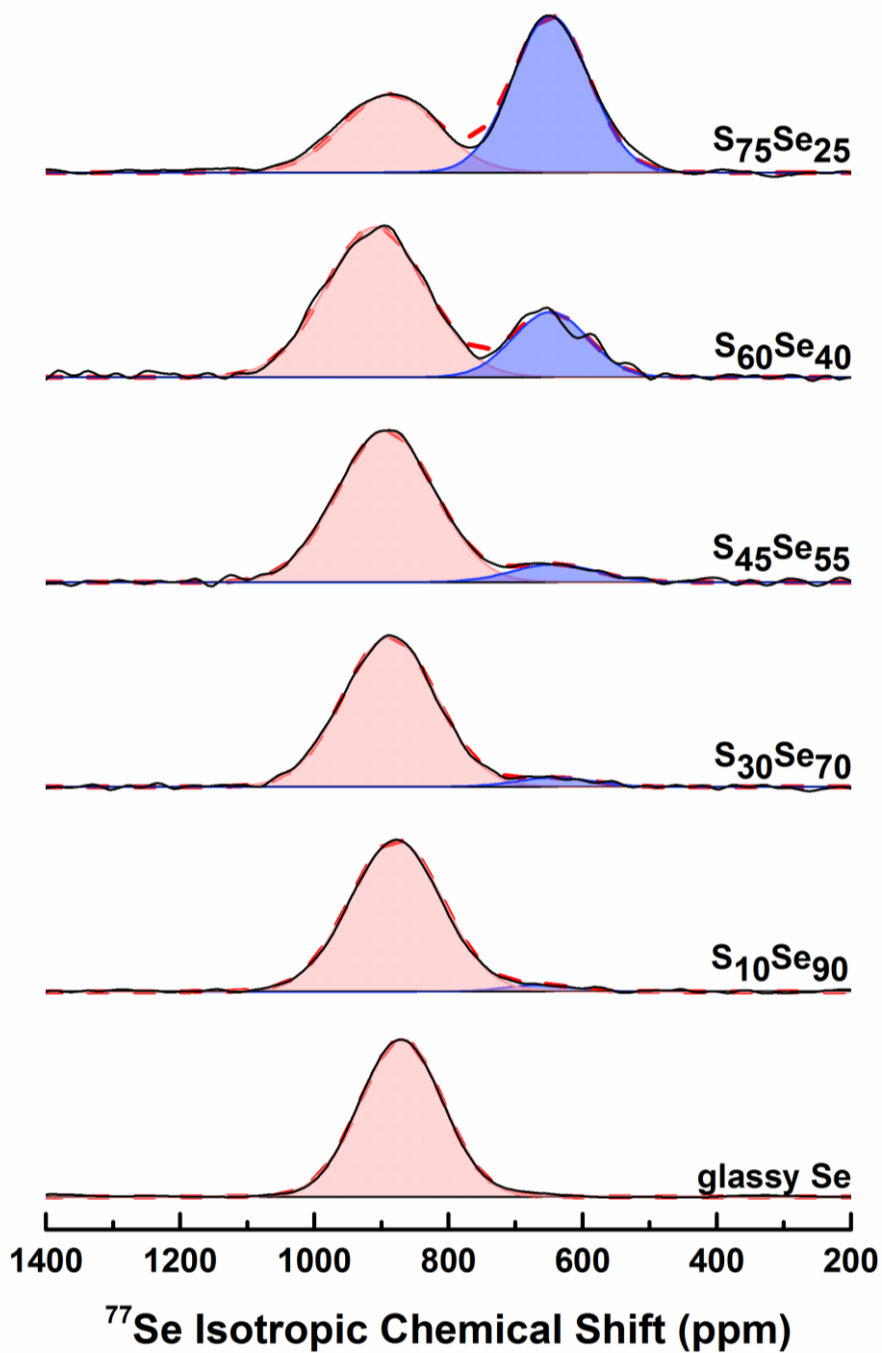
Figure 2a-2 ^{77}Se NMR spectra of S_xSe_{100-x} glasses: (a) Representative 2D ^{77}Se MATPASS/CPMG NMR spectrum of $S_{75}Se_{25}$ glass with total projection along isotropic dimension (solid blue line). (b) Experimental (solid black line) and simulated (red dashed line) ^{77}Se isotropic NMR spectra of S_xSe_{100-x} glasses with compositions denoted alongside the spectra. Gaussian simulation components are shown in pink and blue.

slices at and around $\delta_{iso} \sim 850$ ppm results in average values of $\Delta \approx -153$ ppm and $\eta \approx 0.80$. These

Δ and η values are completely consistent with those reported for the -Se-**Se**-Se- environment in

$[Se]_n$ chains in amorphous Se.[35] On the other hand, the simulation of slices at and around $\delta_{iso} \sim$

650 ppm yields a rather different average Δ and η of ≈ -500 ppm and ≈ 0.15, respectively (Fig. 2a-

4). These Δ and η values are quite comparable with those (Δ ranging between -430 and -450 ppm

and η ranging between 0.2 and 0.4) recently reported for -Se-**Se**-Se- sites in Se$_8$ rings in α-Se.[10]

Taken together, the δ_{iso}, Δ and η values for the two [77]Se resonances in the isotropic NMR spectra

of S_xSe_{100-x} glasses in Fig. 2a-2b suggest that the replacement of nearest neighbor Se with S in

Se_yS_{8-y} rings and $[Se]_n$ chains has a relatively minor effect on the anisotropy parameters Δ and η.

In order to test this hypothesis, *ab initio* calculations of the [77]Se chemical shift tensor parameters

for such Se environments in Se_yS_{8-y} ring molecules were carried out using the gauge-including

projector augmented wave (GIPAW) method.[36]   The -S-**Se**-S- environments were obtained by

replacing the S2 site with Se and the -Se-**Se**-S- environments were obtained by simultaneously

replacing the S2 and the S3 sites with Se in the S_8 molecules in crystalline orthorhombic sulfur.[37]

These structures were then optimized, by allowing the atomic coordinates to vary, using density

functional theory as implemented in the code CASTEP (Biovia Inc.) within the generalized

gradient approximation (GGA) and with the PBE (Perdew-Burke-Ernzerhof) exchange-correlation

functional.[38,39]   Forces less than ~ 30 meV Å^{-1} were observed at the end of the optimization

process. The [77]Se chemical shift calculations were carried out on these optimized structures using

the code CASTEP-NMR within the GGA and with an energy cutoff of 600 eV.[36]   Ultra-soft

pseudopotentials were used to describe core-valence interactions. The Brillouin zone was sampled

using the Monkhorst-Pack scheme and a $4\times4\times4$ k-point grid. The isotropic chemical shift δ_{iso} was

obtained from isotropic shielding σ_{iso} using the relationship: $\delta_{iso} = - (\sigma_{iso} - \sigma_{ref})$ where σ_{ref} is the

isotropic shielding of a reference material. The *trigonal* allotrope of Se was used as a reference and the calculated ^{77}Se σ_{iso} of 784 ppm is equated to the experimental δ_{iso} value of 795 ppm for the single Se site in this allotrope. Marple *et al.* have shown in previous studies that such calculations
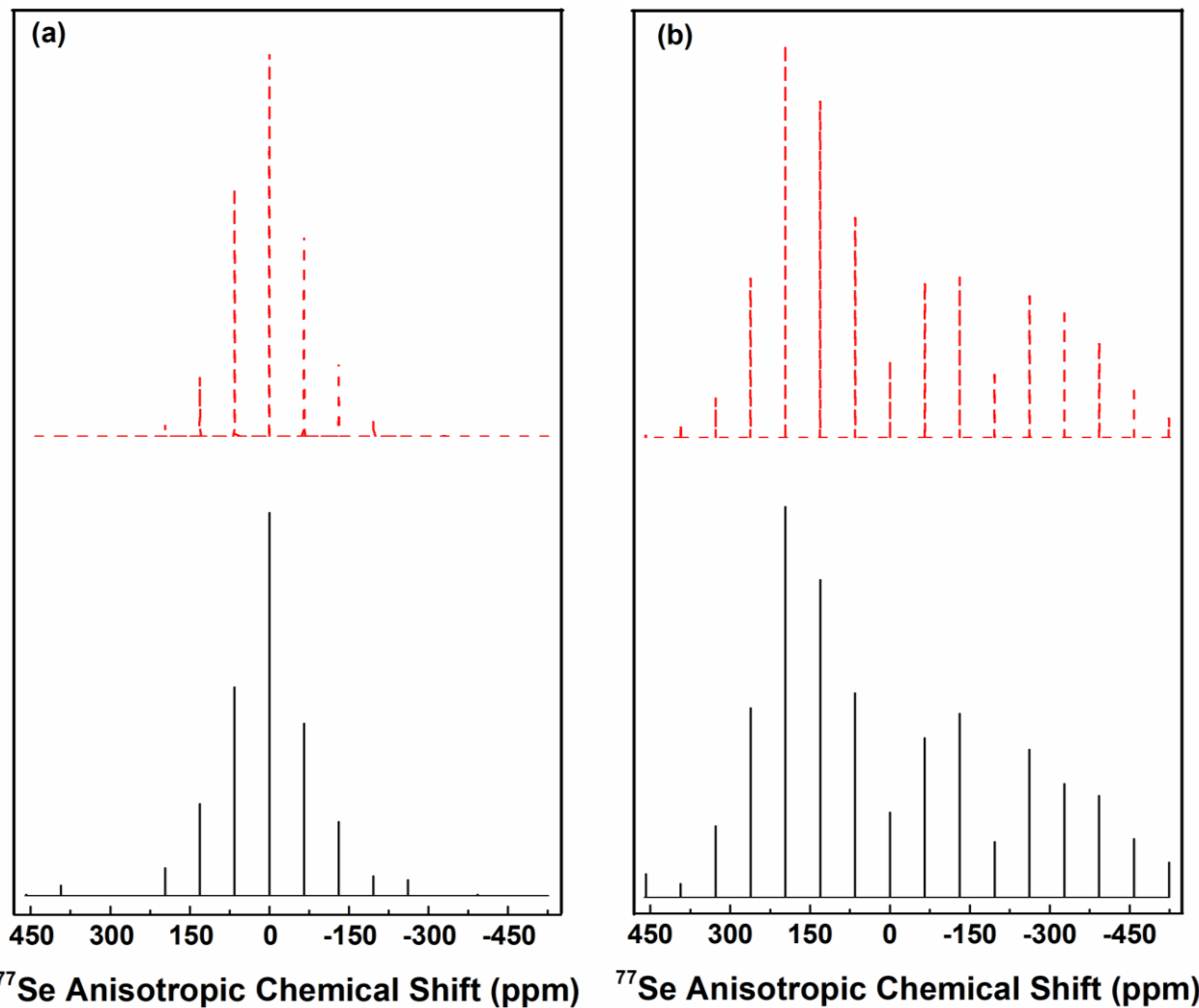
Figure 2a-3 Comparison of experimental (bottom) and simulated (top) anisotropic ^{77}Se NMR spinning sideband intensities of $S_{75}Se_{25}$ glass taken at (a) $\delta_{iso} = 887$ ppm, and (b) $\delta_{iso} = 651$ ppm.

yield fairly accurate estimates of the ^{77}Se δ_{iso} and Δ in the chain (trigonal) and ring (monoclinic) allotropes of Se, except the calculated value of Δ needs to be scaled down by a factor of two.[10] The present calculations yield comparable values of ^{77}Se δ_{iso} (550 to 570 ppm), Δ (−430 ppm) and η (0.15 to 0.30) for the -Se-**Se**-S- and -S-**Se**-S- environments in Se_yS_{8-y} rings, and these parameters

are also similar to those characteristic of the -Se-**Se**-Se- environments in Se_8 rings in α-Se, as noted above. Therefore, the [77]Se resonance at $\delta_{iso} \sim$ 640-660 ppm may correspond to any one or all of these ring environments.
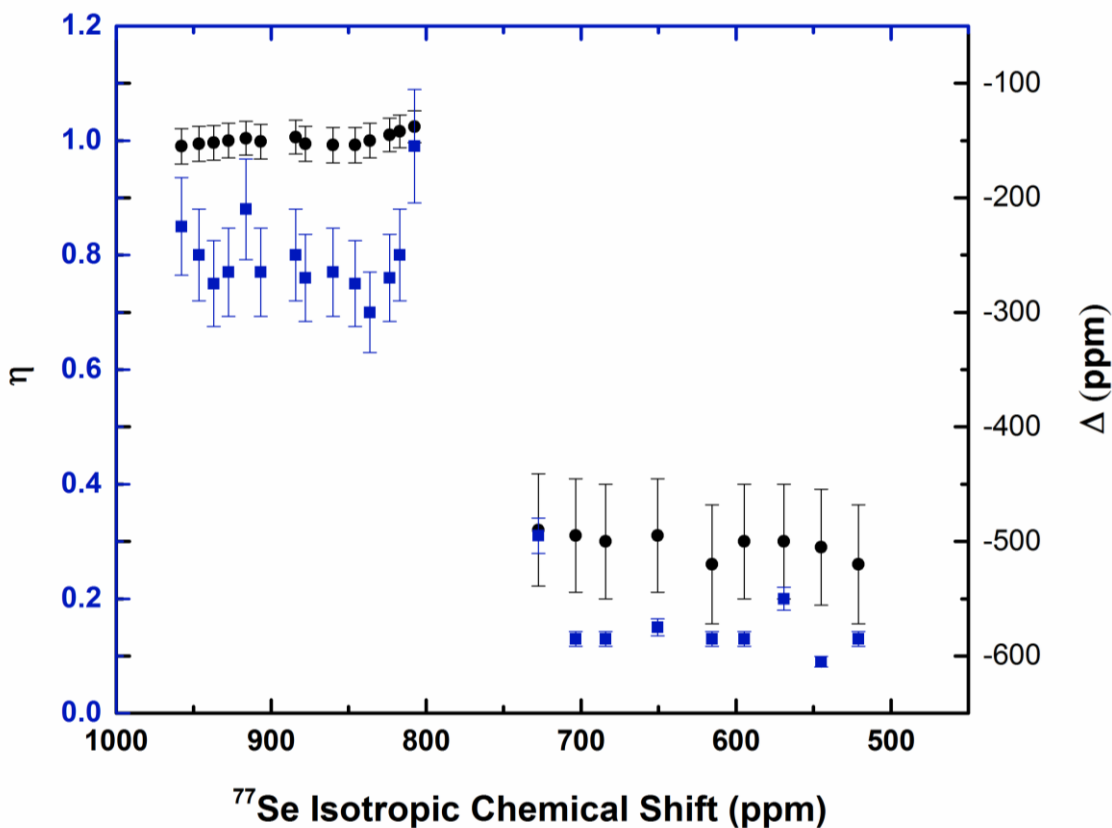
Figure 2a-4 Representative [77]Se chemical shift tensor parameters $\varDelta$ (black circle) and η (blue square) as a function of isotropic chemical shift, shown here for $S_{75}Se_{25}$ glass.

Additional constraints on the average stoichiometry of the Se_yS_{8-y} rings in these glasses can be imposed from the simulation of these ^{77}Se isotropic NMR spectral line shapes in Fig. 2a-2b with two components to yield the relative fractions of the Se atoms in chain and in ring environments from the peak integrals. The compositional evolution of the ratio of these two Se environments is shown in Fig 2a-5, which indicates that, for compositions near pure Se, most of the Se atoms reside in a chain environment. On the other hand, for glasses with composition near pure S, the majority of the Se atoms are found in a ring environment, attesting to the strong

preference of S atoms to form S_8 rings. It is therefore reasonable to propose a structural model where in a glass of composition S_xSe_{100-x}, there are $x/8$ eight-membered rings per formula unit, and on an average each such ring can accommodate y Se atoms, i.e., these are Se_yS_{8-y} rings. This model is equivalent to the substitution of y S atoms in each of the $x/8$ S_8 rings with y Se atoms. The substituted S atoms are incorporated into $[Se,S]_n$ chains. In this scenario, in one formula unit of the S_xSe_{100-x} glass there are $(x*y/8)$ Se atoms in rings and $[(100-x)-(x*y/8)]$ Se atoms in chains. The ring $vs.$ chain Se speciation predictions of this structural model for $y = 1$ and $y = 1.5$ are compared with the experimentally observed Se speciation data in Fig. 2a-6. It is clear from Fig. 2a-5 that the model prediction for $y = 1$ agrees rather well with the experimental Se speciation for S concentrations of up to 40 at.%. However, at higher S concentrations of $\geq$60 at.%, the experimental speciation is closer to the model prediction for $y = 1.5$. Therefore, the chain vs. ring speciation data for Se, as obtained from ^{77}Se NMR, are consistent with an average heterocyclic ring composition of Se_1S_7 for glasses with up to 40 at.% S. Further addition of S promotes increasing incorporation of Se atoms in Se_yS_{8-y} rings, such that the average ring composition becomes $Se_{1.5}S_{6.5}$ for glasses with $\geq$60 at.% S. It is to be noted that an average ring composition of Se_1S_7 does not preclude the presence of Se_2S_6 rings since some of these eight-membered rings may be homocyclic, i.e., S_8 rings, and a coexistence of S_8, Se_1S_7 and Se_2S_6 rings may be entropically favored in a glass. However, the Se ring speciation in glasses, as obtained in this study from ^{77}Se NMR, shows a trend that is opposite of that previously reported in S_xSe_{100-x} melts by Chivers $et\ al.$[20] Those authors suggested that the concentration of the Se_2S_6 rings increases with increasing Se concentration, with the relative abundances of the Se_1S_7 and the Se_2S_6 rings becoming comparable at ~ 40 at.% Se.[20] On the other hand, the Se ring speciation in S_xSe_{100-x} glasses, as obtained in the present study, shows that the average ring composition is Se_1S_7 at low

S (high Se) concentration and it becomes $Se_{1.5}S_{6.5}$, thus suggesting an increased fraction of Se_2S_6 rings, and possibly rings with even higher Se content (e.g., Se_3S_5, Se_4S_4) in glasses with ≤40 at.% Se. As discussed below, the Raman spectroscopic results are consistent with this structural model.
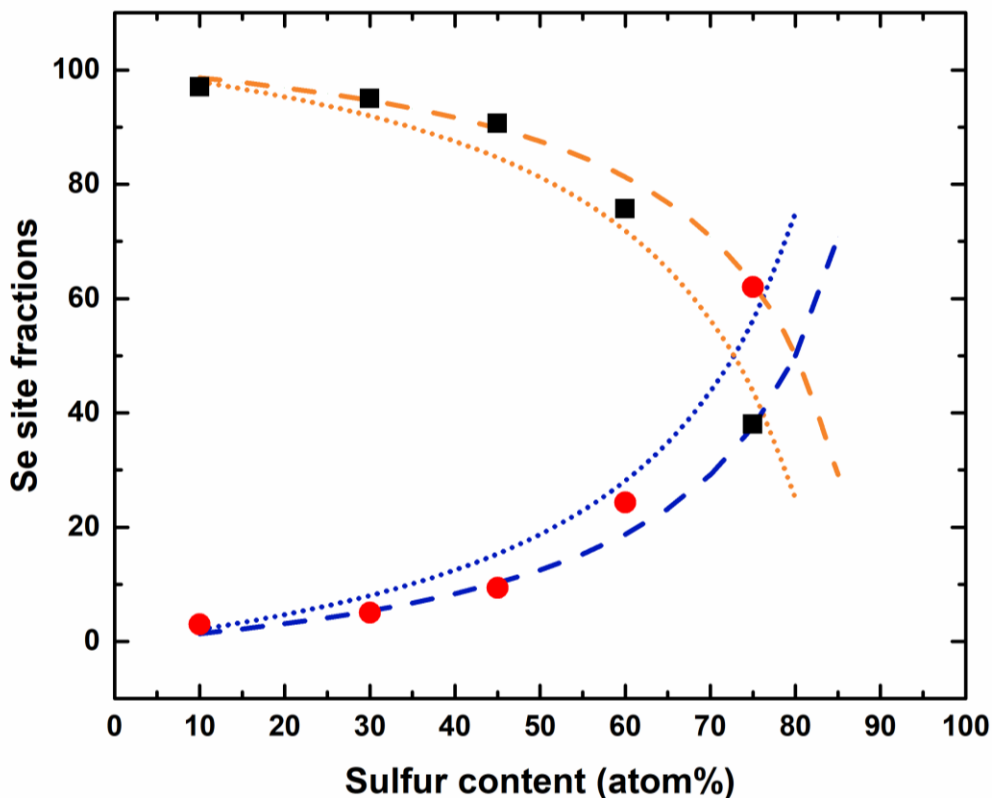
Figure 2a-5 Compositional variation of Se site fractions in chains (squares) and rings (circles), obtained from simulations of ^{77}Se isotropic NMR spectra. Dashed (dotted) orange and blue lines are Se site fractions in chains and rings, respectively, expected from the structural model proposed in this study, for an average ring composition of Se_1S_7 ($Se_{1.5}S_{6.5}$). See text for details.

2a.4.3 Raman spectroscopy

The Raman spectra of the binary S_xSe_{100-x} glasses are shown in Fig. 2a-6. All spectra contain a relatively strong band centered near ~ 250 to 260 cm^{-1} that can be readily assigned to the symmetric Se-Se bond-stretching mode in $[Se]_n$ chains.[40] The incorporation of S in these $[Se]_n$ chains is presumably reflected in the progressive shift of the frequency of this band from 251 cm^{-1} to 261 cm^{-1}, with increasing S concentration (Fig. 2a-6). This result is also corroborated by the

fact that the ^{77}Se NMR spectra of all glasses contain the resonance corresponding to the $[Se,S]_n$ chains (Fig. 2a-2b). The relatively narrow and strong vibrational bands located at ~ 150 and 216 cm^{-1} in the Raman spectra of the high sulfur containing glasses are characteristic of S_8 rings typical of crystalline S, and correspond to the anti-symmetric and symmetric bending modes (Fig. 2a-6).[8,21] These vibrational bands are accompanied by another strong and narrow band near 202 cm^{-1} in the glass spectra in Fig. 2a-6. Additionally, two more bands in the spectral region between 160–190 cm^{-1} appear in the Raman spectrum of the $S_{60}Se_{40}$ glass and become clearly resolved near 163 and 175 cm^{-1}, in the spectrum of the $S_{75}Se_{25}$ glass (see Fig. 2a-6, inset). The frequencies of these three bands at 202, 175 and 163 cm^{-1} agree well with those predicted, respectively, for the bending of Se_1S_7, Se_2S_6 and Se_3S_5 rings, by Ward in a previous Raman spectroscopic study of S_xSe_{100-x} crystals and melts.[17] These predictions are based on the model proposed by Ward, which assumed a linear scaling of the ring bending frequency with the average force constant and with the inverse square root of the molecular weight of the ring, where the average force constant was further assumed to vary linearly with the degree of substitution of S with Se in the Se_yS_{8-y} ring.[17] This structural assignment of these vibrational bands and their relative intensities in Fig. 2a-6 clearly suggest the predominance of the Se_1S_7 rings among the Se-substituted Se_yS_{8-y} ring environments in S_xSe_{100-x} glasses. Moreover, the appearance of Se_2S_6 and Se_3S_5 rings in glasses with the highest S contents suggests increasing incorporation of multiple Se atoms in the Se_yS_{8-y} rings. These results are qualitatively consistent with the scenario of the evolution of the average Se_yS_{8-y} ring composition in S_xSe_{100-x} glasses, as obtained from the ^{77}Se NMR results discussed above.
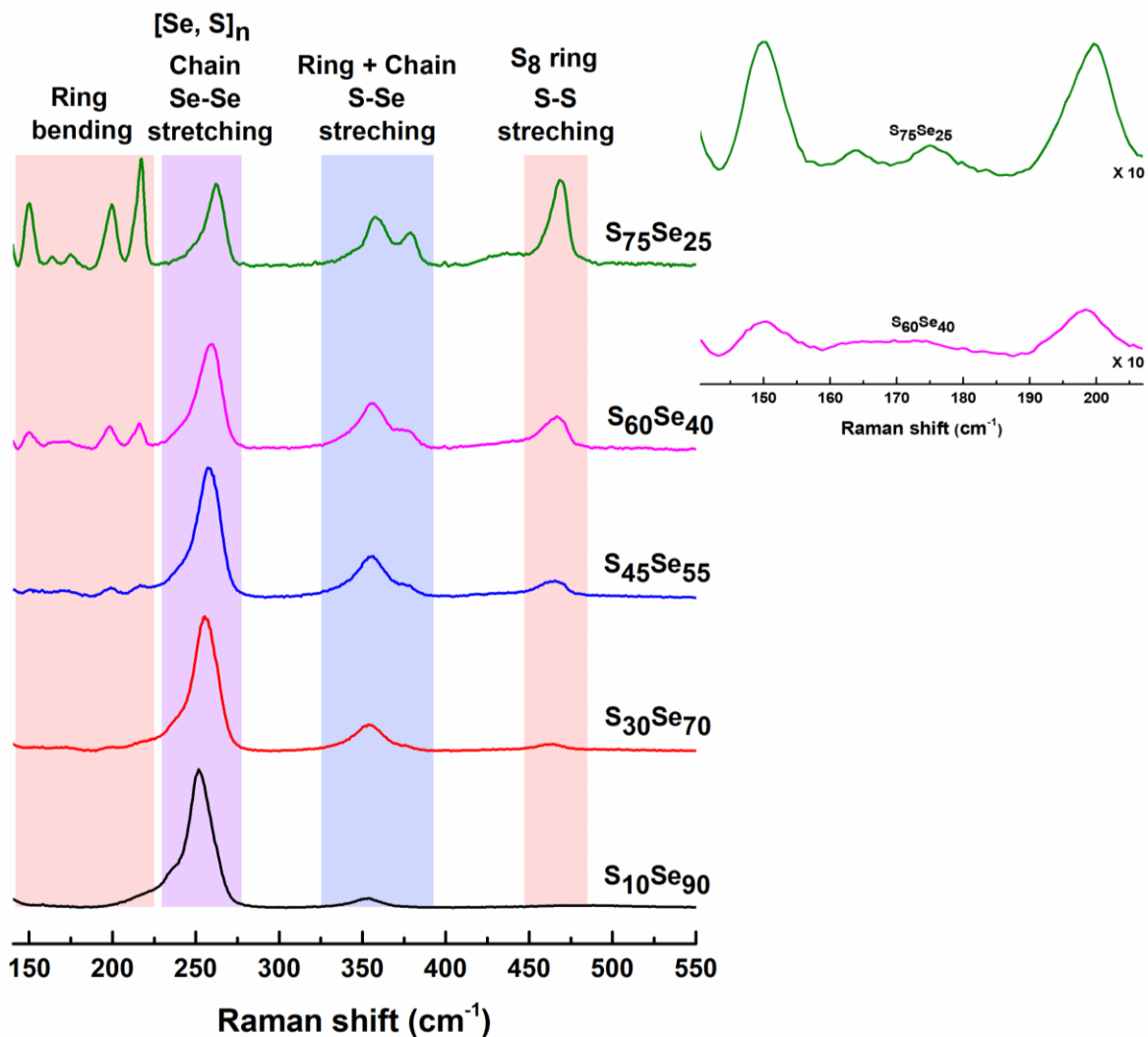
Figure 2a-6 Unpolarized Raman spectra of S_xSe_{100-x} glasses. Inset to the right shows a magnified (10x) view of the ring bending modes in $S_{60}Se_{40}$ (bottom) and $S_{75}Se_{25}$ (top) glasses.

It is apparent from the Raman spectra in Fig. 2a-6 that increasing S content also results in a concomitant increase in the intensity of the band near 468 cm^{-1}, corresponding to the symmetric S-S bond-stretching mode for the S_8 rings.[8] In addition, two more bands centered at ~ 360 cm^{-1} and 379 cm^{-1} with a weak band present as a shoulder near 340 cm^{-1} display a similar behavior of increasing intensity with S content (Fig. 2a-6). Previous Raman spectroscopic studies of S_xSe_{100-x} crystals have assigned these bands to S-Se stretches as these frequencies are intermediate between the S-S stretching near 470 cm^{-1} and Se-Se stretches near 260 cm^{-1}.[17,18] As such, the presence

of these bands directly implies mixing between S and Se in the chain and ring elements in the structure.

In general, the Raman bands in the 340 - 380 cm^{-1} region in these materials are believed to represent two types of S-Se stretching modes: (i) strongly coupled S-Se stretches in -S-Se-S- linkages are manifested as vibrational bands near ~ 340 and 380 cm^{-1} while (ii) isolated S-Se stretches in -S-Se-Se-S- moieties appear as a band near ~ 360 cm^{-1}.[18,41,42]   It is noteworthy that previous studies of binary S-Se crystals concluded that both coupled and isolated S-Se stretching bands are from Se$_y$S$_{8-y}$ ring molecules with adjacent Se atoms in -S-Se-Se-S- moieties being the preferred bonding scenario if more than one Se atoms are present in these rings.[19,21] As shown in Fig. 2a-6, the intensity of the vibrational bands in the 340 - 380 cm^{-1} region is increasing significantly with increasing sulfur content. This observation indicates that a significant fraction of Se atoms is incorporated into the Se$_y$S$_{8-y}$ ring structures as -S-Se-S- and -S-Se-Se-S- linkages, when sufficient sulfur is present in the system. Moreover, both Se$_1$S$_7$ and Se$_2$S$_6$ type rings may coexist in the structure. These conclusions are completely consistent with the structural model proposed above, on the basis of the ^{77}Se NMR spectroscopic results. Finally, it may be noted that the band near 360 cm^{-1}, corresponding to S-Se stretches in -S-Se-Se-S- moieties has a noticeable presence even in the Raman spectra of glasses with low sulfur concentration (S $\leq$ 30 at.%) that have rather weak or no signature of the vibrational bands corresponding to the Se$_y$S$_{8-y}$ rings (Fig. 2a-6). This result suggests that all of the -S-Se-Se-S- moieties corresponding to the 360 cm^{-1} band may not belong to the Se$_y$S$_{8-y}$ ring elements in the structure, but a significant fraction likely belongs to the [Se,S]$_n$ chain elements.

2a.5 Conclusion

The structure of S_xSe_{100-x} glasses consists of copolymeric $[S,Se]_n$ chains and heterocyclic S_ySe_{8-y} rings. Se and S atoms show strong preference to form the chain and the ring elements, respectively, which prevents a random or homogeneous mixing between these two elements. The compositional variation of the chain vs. ring speciation of Se atoms is consistent with an average ring composition of Se_1S_7 in glasses with ≤ 40 at.% S. Further increase in S content results in the incorporation of more Se atoms in the ring elements, resulting in an average ring composition of $Se_{1.5}S_{6.5}$. It is, however, not the peculiar chemical order between S and Se but the total chain vs. ring content in the structure that controls both the packing and the mobility of the constituent structural units. As the total chain content increases with increasing Se concentration in these glasses, the stronger interaction between the chain elements compared to rings, results in less efficient atomic packing and lower mobility, which are manifested in the decreasing molar volume and increasing T_g, respectively.

Acknowledgement

References

[1] A. Zakery, S.R. Elliott, Optical properties and applications of chalcogenide glasses: a review, J. Non. Cryst. Solids. 330 (2003) 1–12.

[2] B. Bureau, X.H. Zhang, F. Smektala, J.L. Adam, J. Troles, H.L. Ma, C. Boussard-Plèdel, J. Lucas, P. Lucas, D. Le Coq, M. R. Riley, J. H. Simmons, Recent advances in chalcogenide glasses, J. Non. Cryst. Solids. 345&346 (2004) 276–283.

[3] L. Calvez, Chalcogenide glasses and glass-ceramics: Transparent materials in the infrared for dual applications, Comptes Rendus Phys. 18 (2017) 314–322.

[4] M. Popescu, Non-Crystalline Chalcogenides, Kluwer Academic Publishers, 2002.

[5] S.C. Greer, Reversible Polymerizations and Aggregations, Annu. Rev. Phys. Chem. 53 (2002) 173–200.

[6] S.C. Greer, "Living" polymers, Adv. Chem. Phys. 94 (1996) 261.

[7] G.O. Sofekun, E. Evoy, K.L. Lesage, N. Chou, R.A. Marriott, the Rheology of Liquid Elemental Sulfur Across the λ-Transition, J. Rheol. (N. Y. N. Y). 62 (2018) 469–476.

[8] A.G. Kalampounias, K.S. Andrikopoulos, S.N. Yannopoulos, Probing the sulfur polymerization transition in situ Raman spectroscopy, J. Chem. Phys. 118 (2003) 8460–8467.

[9] G. Lucovsky, A. Mooradian, W. Taylor, G.B. Wright, R.C. Keezer, Identification of the fundamental vibrational modes of trigonal, α-monoclinic and amorphous selenium, Solid State Commun. 5 (1967) 113–117.

[10] M. Marple, J. Badger, I. Hung, Z. Gan, K. Kovnir, S. Sen, Structure of Amorphous Selenium by 2D ^{77}Se NMR Spectroscopy: An End to the Dilemma of Chain versus Ring, Angew. Chemie. 129 (2017) 9909–9913.

[11] B. Bureau, S. Danto, H.L. Ma, C. Boussard-Plédel, X.H. Zhang, J. Lucas, Tellurium based glasses: A ruthless glass to crystal competition, Solid State Sci. 10 (2008) 427–433.

[12] M.H. Brodsky, R.J. Gambino, J.E. Smith, Y. Yacoby, The Raman Spectrum of Amorphous Tellurium, Phys. Status Solidi. 52 (1972) 609–614.

[13] E. Grison, Studies on tellurium-selenium alloys, J. Chem. Phys. 19 (1951) 1109–1113.

[14] B. Bureau, C. Boussard-plèdel, M. Lefloch, J. Troles, J. Lucas, D. Rennes, D. Beaulieu, Selenium-Tellurium Sequences in Binary Glasses as Depicted by ^{77}Se and ^{125}Te NMR, J. Phys. Chem. B. 109 (2005) 6130–6135.

[15] A. Tverjanovich, A. Cuisset, D. Fontanari, E. Bychkov, Structure of Se-Te glasses by Raman spectroscopy and DFT modeling, J. Am. Ceram. Soc. 101 (2018) 5188–5197.

[16] D. Jecu, J. Jaklovszky, A. Trutia, I. Apostol, M. Dinescu, I.N. Mihailescu, G. Aldica, M. Popescu, N. Vlahovici, S. Zamfira, E. Indrea, Preparation, Structure and Optical Properties of Glasses in the Systems Selenium-Sulfur and Tellurium-Sulfur, J. Non. Cryst. Solids. 90 (1987) 319–322.

[17] A.T. Ward, Raman Spectroscopy of Sulfur, Sulfur-Selenium, and Sulfur-Arsenic Mixtures, J. Phys. Chem. 72 (1968) 4133–4139.

[18] R. Laitinen, R. Steudel, Vibrational Spectroscopic Investigations of S_nSe_{n-8} Molecules, J. Mol. Struct. 68 (1980) 19–32.

[19] R.S. Laitinen, T.A. Pakkanen, ^{77}Se NMR spectroscopic characterization of selenium sulfide ring molecules Se_nS_{8-n}, Inorg. Chem. 26 (1987) 2598–2603.

[20] T. Chivers, R. Laitinen, K. Schmidt, Se NMR spectroscopic study of the molecular composition of sulfur-selenium melts, Can. J. Chem. 70 (1992) 719–725.

[21] R. Steudel, R. Laitinen, Cyclic Selenium Sulfides, in: Inorg. Ring Syst., Springer, Berlin, Heidelberg, 1982: pp. 177–197.

[22] I. Hung, T. Edwards, S. Sen, Z. Gan, MATPASS/CPMG: A sensitivity enhanced magic-angle spinning sideband separation experiment for disordered solids, J. Magn. Reson. 221 (2012) 103–109.

[23] D.J. States, R.A. Haberkorn, D.J. Ruben, A 2D Nuclear Overhauser Experiment with pure absorption phase in four quadrants, J. Magn. Reson. 48 (1982) 286–292.

[24] R.K. Harris, E.D. Becker, S.M. Cabral De Menezes, R. Goodfellow, P. Granger, NMR nomenclature: Nuclear spin properties and conventions for chemical shifts (IUPAC recommendations 2001), Pure Appl. Chem. 73 (2001) 1795–1818.

[25] U. Haeberlen, High Resolution NMR in Solids Selective Averaging: Supplement 1 Advances in Magnetic Resonance, Elsevier, 2012.

[26] P.I. Buler, E.A. Kuleshov, L.G. Protasova, Molar Volume of Glasses in the Se-S System, Fiz. i Khimiya Stekla. 10 (1984) 628–630.

[27] L.G. Protasova, E.A. Kuleshov, P.I. Buler, S.G. Vlasova, Thermal Expansion and the Glass-Formation Temperature of Glasses in the Se-S System, Fiz. i Khimiya Stekla. 12 (1986) 168–171.

[28] P.I. Buler, L.G. Protasova, I.G. Shaposhnikova, Thermal Capacity of Glasses of the System Se-S in the Temperature Interval 173-333K, Fiz. i Khimiya Stekla. 12 (1986) 544–548.

[29] R. Svoboda, J. Málek, Kinetic fragility of Se-based binary chalcogenide glasses, J. Non. Cryst. Solids. 419 (2015) 39–44.

[30] S.C. Abrahams, The crystal and molecular structure of orthorhombic sulfur, Acta Crystallogr. 8 (1955) 661–671.

[31] K. Vedam, D.L. Miller, R. Roy, Elastic Constants of Selenium in the Hexagonal and Glassy Phases, J. Appl. Phys. 37 (1966) 3432–3434.

[32] W. Zhu, M. Lockhart, B. Aitken, S. Sen, Dynamical rigidity transition in the viscoelastic properties of chalcogenide glass-forming liquids, J. Non. Cryst. Solids. (2018).

[33] B. Bureau, J. Troles, M. Le Floch, F. Smektala, J. Lucas, Medium range order studied in

selenide glasses by ^{77}Se NMR, J. Non. Cryst. Solids. 326&327 (2003) 58–63.

[34] D. Massiot, F. Fayon, M. Capron, I. King, S. Le Calvé, B. Alonso, J.O. Durand, B. Bujoli, Z. Gan, G. Hoatson, Modelling one- and two-dimensional solid-state NMR spectra, Magn. Reson. Chem. 40 (2002) 70–76.

[35] D.C. Kaseman, I. Hung, Z. Gan, S. Sen, Observation of a Continuous Random Network Structure in Ge_xSe_{100-x} Glasses: Results from High-Resolution ^{77}Se MATPASS/CPMG NMR Spectroscopy, J. Phys. Chem. B. 117 (2013) 949–954.

[36] C. Bonhomme, C. Gervais, F. Babonneau, C. Coelho, F. Pourpoint, T. Azaïs, S.E. Ashbrook, J.M. Griffin, J.R. Yates, F. Mauri, C.J. Pickard, First-principles calculation of NMR parameters using the gauge including projector augmented wave method: A chemists point of view, Chem. Rev. 112 (2012) 5733–5779.

[37] B.E. Warren, J.T. Burwell, The Structure of Rhombic Sulphur, J. Chem. Phys. 3 (1935) 6–8.

[38] S.J. Clark, M.D. Segall, C.J. Pickard, P.J. Hasnip, M.I.J. Probert, K. Refson, M.C. Payne, First principles methods using CASTEP, Zeitschrift Für Krist. 220 (2005) 567–570.

[39] J.P. Perdew, K. Burke, M. Ernzerhof, Generalized gradient approximation made simple, Phys. Rev. Lett. 77 (1996) 3865–3868.

[40] S.N. Yannopoulos, K.S. Andrikopoulos, Raman scattering study on structural and dynamical features of noncrystalline selenium, J. Chem. Phys. 121 (2004) 4747–4758.

[41] R. Laitinen, L. Ninisto, R. Steudel, Structural Studies on the Sulfur-Selenium Binary Systerm, Acta Chem. Scand. 33 (1979) 737–747.

[42] R. Laitinen, T. Pakkanen, A Theoretical Investigation of the Sulfur-Selenium Bond, J. Mol. Struct. 91 (1983) 337–352.

Chapter 2b

Is the λ-transition in Liquid Sulfur a Fragile-to-Strong Transition?

2b.1 Abstract

The abrupt and large increase in the viscosity of liquid sulfur above the λ-transition temperature T_λ corresponds to a reversible structural transformation in the form of a ring-to-chain polymerization reaction. The mechanistic connection between this structural transformation and viscosity is investigated by studying the compositional dependence of the shear relaxation behavior of supercooled $S_x Se_{100-x}$ liquids, as their structural evolution mimics that of liquid sulfur across the λ-transition. The results of steady and oscillatory shear parallel-plate rheometry indicate that the viscosity of these liquids is controlled by the S/Se – S/Se bond scission/renewal dynamics and the timescale of these dynamics rapidly increases as the relative concentrations of rings and chains in the structure become comparable. The coexistence of these two types of topological units in these liquids lowers the conformational entropy of the chain elements due to steric hindrance from the ring elements, resulting in a rapid drop in the fragility as S is added to Se. The same topological effect resulting from the ring-to-chain transformation in liquid S renders the highly fragile molecular liquid below T_λ, a strong polymerized liquid above T_λ. Therefore, it is argued that the λ-transition of liquid S corresponds to a fragile-to-strong liquid-liquid transition.

43

2b.2 Introduction

The existence and nature of liquid-liquid transitions in glass-forming liquids and their possible continuation into the glassy state are highly debated issues in condensed-matter science. [1–5] It is reasonable to expect that such a transition would have a signature in the temperature dependence of the shear viscosity η of glass-forming liquids. The functional form of $\eta(T)$ could vary from a nearly-Arrhenius behavior with a single activation energy that is practically independent of temperature, all the way to a strongly non-Arrhenius behavior, where the activation energy increases rapidly with decreasing temperature. Angell has shown that, if η is expressed as a function of T_g/T, i.e., temperature scaled by the glass transition temperature T_g, then a useful classification scheme emerges as a function of the parameter m, which is termed "fragility index" and is defined as[6]:

$$m = \frac{dlog_{10}\eta}{d(T_g/T)}\Big|_{T=T_g} \tag{1}$$

The glass-forming liquids with increasingly non-Arrhenius behavior of η are then characterized by progressively increasing values of m. Glass-forming liquids with low and high values of m were denoted by Angell as "strong" and "fragile", respectively. [6] Although m is defined according to Eq. 1 at $T \approx T_g$, the temperature dependence of the viscosity of a glass-forming liquid over the entire range of supercooling can be related to its fragility index. This situation is possibly most directly evident in the MYEGA (Mauro-Yue-Ellison-Gupta-Allan) equation[7] that describes $\eta(T)$ well for a large variety of glass-forming liquids over a wide range of temperatures, and can be written as:

$$\log_{10}\eta(T) = \log_{10}\eta_\infty + \left(\log_{10}\eta_{T_g} - \log_{10}\eta_\infty\right)\frac{T_g}{T}exp\left[\left(\frac{m}{\log_{10}\eta_{T_g}-\log_{10}\eta_\infty} - 1\right)\left(\frac{T_g}{T} - 1\right)\right] \tag{2}$$

In Eq. 2 $log_{10} \eta_{T_g}$ and $log_{10}\eta_\infty$ correspond to the logarithm of shear viscosity at T_g and at infinite temperature, respectively, and the latter quantity is used as a fit parameter in practice. It is clear from Eq. 2 that $\eta(T)$ of a glass-forming liquid over the entire range of supercooling is expected to be characterized by a single value of *m*. However, a series of studies in recent years on a variety of metallic, chalcogenide and halide glass-forming liquids have reported a violation of this behavior where $\eta(T)$ is characterized by a low value of *m,* i.e., the liquid is strong at low temperatures near T_g, while the high-temperature viscosity (typically $\eta < 1$ Pa.s) is characteristic of that of a fragile liquid with high *m*. [8–12] The strength of the fragile-to-strong (FST) has been expressed in terms of the ratio *F* of the high- and low- temperature fragilities, which typically ranges between $2 \leq F \leq 8$, with metallic liquids being characterized by some of the highest *F* values. [8] This FST was hypothesized to signify an underlying liquid-liquid structural transition, although the atomistic nature of this transition has remained unclear. Moreover, a recent experimental study has suggested that the existence of the FST, at least in some glass-forming liquids, may be an artifact of the inaccuracies associated with the viscosity measurement technique employed at high temperature and with the derivation of the fragility index from calorimetric methods near T_g.[12]

In contrast with these glass-forming liquids, elemental sulfur presents a unique case of a well-characterized structural transition. Sulfur above its melting point at 119 °C is a molecular liquid that predominantly contains S_8 rings and is characterized by viscosities on the order of 10^{-2} Pa.s.[13] The structure of this equilibrium liquid abruptly changes across $T_\lambda \approx 159$ °C, where the rings open up into diradicals and polymerize to form S_n chains.[14] This ring-to-chain transformation, being completely reversible, is an example of "living polymerization" and has been termed in the literature as the λ-transition, as the corresponding jump in the heat capacity C_p

shows a cusp-like behavior across this transition.[15] Among several other properties that display

a sharp change across the λ-transition, the viscosity of liquid sulfur abruptly increases by nearly

five orders of magnitude (Fig. 2b-1) from ~ 0.05 Pa.s at 160 °C to ~ 930 Pa.s at 187 °C.[13,16]

Further increase in temperature results in a lowering of viscosity (Fig. 2b-1). The thermo-

reversible nature of the ring-to-chain transformation process in liquid sulfur and the temperature

dependence of the ring:chain ratio above the λ-transition have been studied in detail by

Yannopoulos and coworkers using *in situ* high-temperature Raman spectroscopy.[17] Their

results indicated a monotonic increase in the S_n polymeric chain fraction in the liquid with

increasing temperature at least up to 300 °C, although the rate of the ring-to-chain conversion

continuously decreases with temperature. Hence, the sudden upward jump in viscosity across

T_λ can indeed be ascribed to the polymerization reaction.

However, the determination of the fragility index *m* of liquid sulfur above and below the

λ-transition from relaxation time measurements has been claimed to be problematic in the recent

past, due to the presence of multiple relaxation mechanisms and their unknown contributions to

viscosity.[14] Directly using the viscosity data for molecular liquid sulfur below the λ-

transition[13] and a glass transition temperature T_g ranging between –23 and –30 °C, where the

viscosity is ~ 10^{12} Pa.s, yields *m* ~ 149 ±3 below T_λ (Fig. 2b-1). On the other hand, the viscosity

data of the polymerized liquid above T_λ are consistent with those reported [16,18] for the

supercooled liquid obtained from reheating glassy S, quenched from a temperature well above

T_λ to preserve the polymeric structure (Fig. 2b-1). When taken together, these viscosity data yield

m ~ 35 ±3 for the polymerized liquid. As such, these results indicate an FST with increasing

temperature for liquid sulfur.   However, considering the presence of multiple relaxation

mechanisms in liquid S, the validity of such a simplistic treatment of the temperature dependence of viscosity remains questionable.
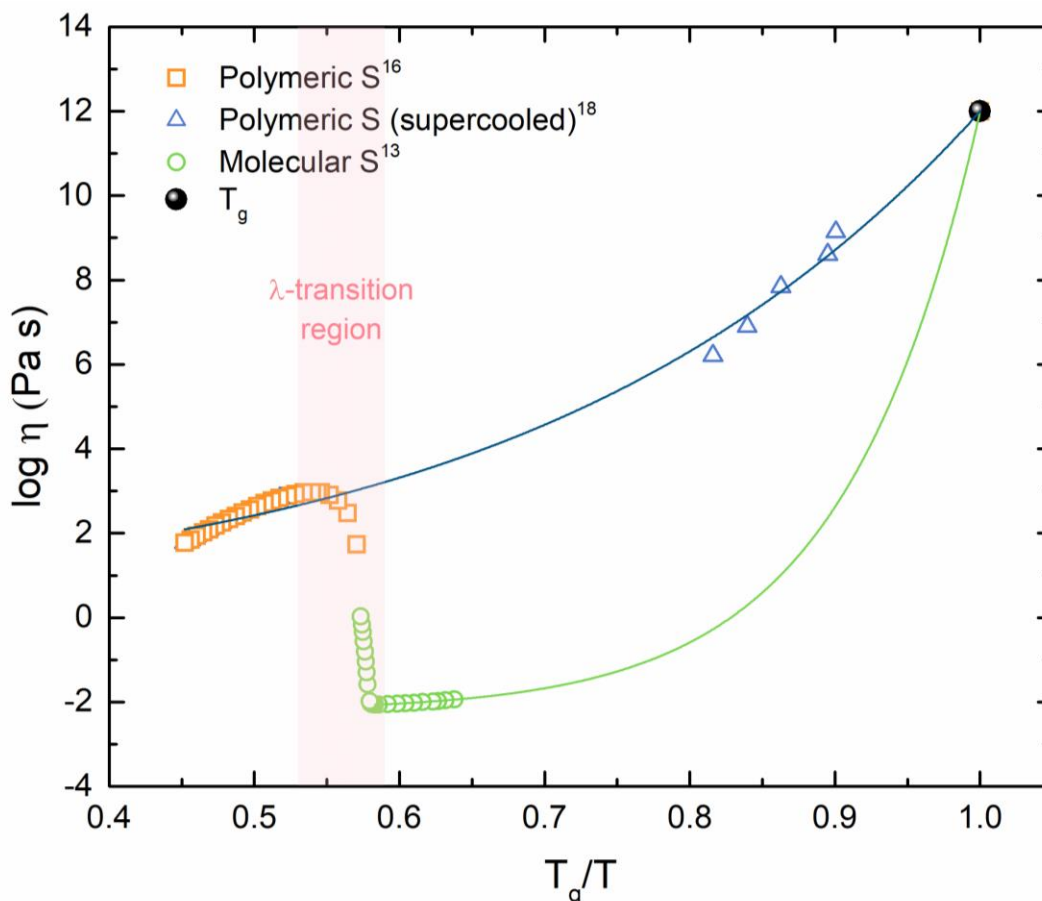
Figure 2b-1 Viscosity of molecular (circles) and polymeric (squares) liquid sulfur across the λ–transition as a function of T_g/T.[13,16] Viscosity of polymeric liquid S in its supercooled state is shown with triangles.[18] Viscosity at T_g is taken to be 10^{12} Pa.s. Lines through the data are fits of the MYEGA equation.

Elemental selenium, as another member of chalcogen family, shares chemical similarities with sulfur, yet exhibits very different properties as a glass-forming liquid. Amorphous and liquid selenium consist practically solely of polymeric Se_n chains and therefore, do not display the ring-to-chain transformation that is characteristic of sulfur with increasing temperature.[19] The fragility of selenium is also known be relatively high with the most reliable estimates of *m* varying between ~70 and 80.[20,21]

47

In a previous Raman and [77]Se Nuclear Magnetic Resonance (NMR) study of the S-Se binary system it was shown that the addition of selenium stabilizes the glassy state and T_g linearly increases with increasing selenium concentration.[22] Moreover, both S and Se retain their preferences of forming rings and chains as in their elemental forms, respectively, although heterocyclic Se_yS_{8-y} rings ($0 \leq y \leq 8$) and $[S, Se]_n$ chains are also formed. Therefore, the S-Se binary liquids display an increasing chain:ring ratio with increasing Se content and thus mimic the topological transformation of molten sulfur above the λ-transition. Here we report the results of detailed steady and small-amplitude-oscillatory shear rheometric measurements of the viscoelastic relaxation behavior of binary S_xSe_{100-x} liquids ($10 \leq x \leq 75$). These results provide important clarification of the atomistic aspects of viscous flow and relaxation in these liquids and confirm that the λ-transition of liquid sulfur indeed corresponds to an FST.

2b.3 Experimental Methods

Binary S_xSe_{100-x} glasses with $x = 10$, 30, 45, 60 and 75 were prepared from mixtures of constituent elements (99.999% purity) that were taken in evacuated silica ampoules and melted at 400°C for 24 hours. The melts were subsequently quenched by dipping the ampoule in water. Details of the synthesis, thermophysical and structural characterization of these glasses are reported in Chapter 2a.[22] The rheological measurements reported in the present study were carried out within the linear viscoelastic regime using an Anton Paar MCR 92 parallel plate rheometer equipped with a Peltier heater, under a constant flow of nitrogen gas. Viscosity measurements on these supercooled S_xSe_{100-x} liquids were carried out under steady shear condition, using a 25 mm diameter upper plate and a stationary lower plate, on samples with a disc-like geometry with ~ 0.8 mm thickness. At each temperature, the Newtonian viscosity was measured

at several shear rates $\dot{\gamma}$ ranging between 1 s^{-1} and 100 s^{-1} and the average viscosity was reported. The small-amplitude-oscillatory-shear (SAOS) rheometry measurements were carried out using 8 mm diameter plates and the sample thickness was ~ 1.2 mm. At each temperature the samples were held for 5 minutes to attain thermal equilibrium, followed by the application of oscillatory strain with angular frequency ω varying between 0.01 and 600 rad/s, and concomitantly the torque was measured to obtain the storage and loss moduli G′ and G″ as a function of ω.

2b.4 Results and Discussion

The shear viscosity of the supercooled S_xSe_{100-x} liquids is shown in Fig. 2b-2 as a function of scaled temperature T_g/T. The fits of the MYEGA equation (Eq. 2) to these viscosity data are also shown in Fig. 2b-2. The compositional variation of the corresponding m values obtained from these fits is shown in Fig. 2b-3, and compared with the m for Se as reported in the literature[20,21] and with the abovementioned m values for molecular and polymerized liquid S. It is clear from Fig. 2b-3 that pure chain and ring environments corresponding to Se and molecular S liquids, respectively, exhibit super-Arrhenius behavior with large m values. On the other hand, the binary S-Se liquids are characterized by lower m, compared to either pure Se or molecular S; m decreases with the initial addition of either S to Se or vice versa, which suggests that the coexistence of chain and ring elements in these liquids results in a rapid decrease in fragility and m reaches a minimum value of ~ 37 in binary $S_{75}Se_{25}$ liquid (Fig. 2b-3). This trend also resembles the variation of m for liquid S itself, which has the highest fragility in the molecular state and the lowest fragility in the polymerized state above the λ-transition (Fig. 2b-3), where the liquid is characterized by the coexistence of comparable fractions of S_8 rings and S_n chains.[17,23] Sidebottom has pointed out in a series of recent studies the importance of structural connectivity

on the fragility of a wide variety of inorganic glass-forming liquids.[24,25] It may be noted in this regard that the average short-range connectivity of all S_xSe_{100-x} liquids is identical as the coordination number of both S and Se is 2. Therefore, the intermediate-range connectivity and steric effects should be taken into account to explain the remarkable compositional variation of m in these liquids. Further insight into this problem can be obtained from the rheometric measurements of the viscoelastic relaxation processes and timescales in these liquids.
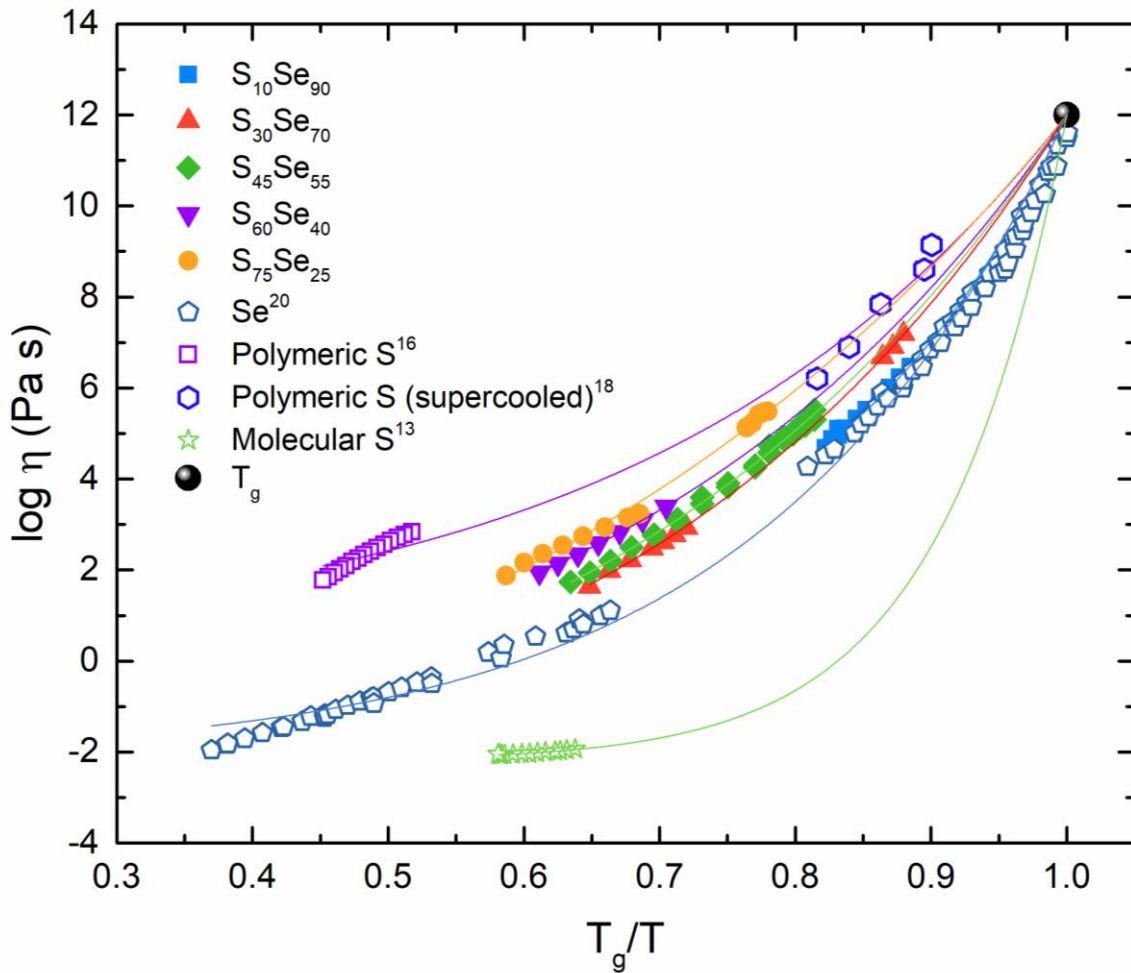
Figure 2b-2 Viscosity of binary S_xSe_{100-x} liquids measured in the present study. Viscosity data of Se are from[20] and of S are from Fig. 2b-1. Viscosity at T_g for all compositions is taken to be 10^{12} Pa.s. Lines through the data are fits of the MYEGA equation.
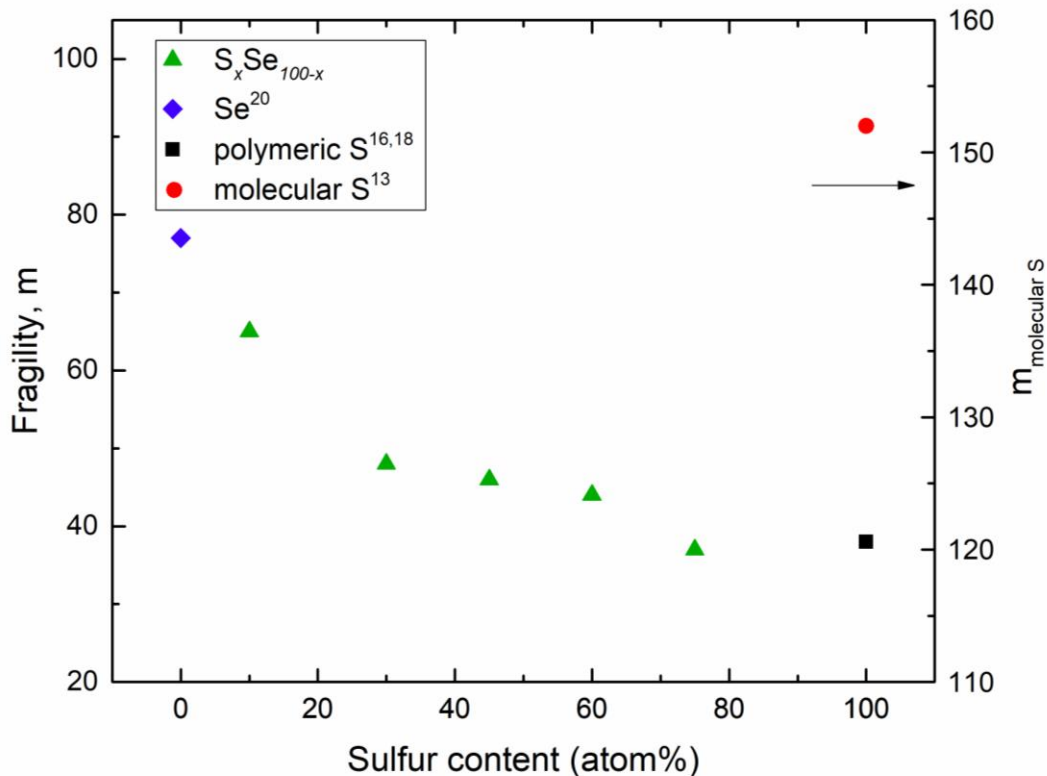
Figure 2b-3 Compositional dependence of fragility of S_xSe_{100-x} liquids as obtained from the fits of the MYEGA equation in Fig. 2b-2.

Figure 2b-4 shows the master curves of G′(ω) and G″(ω) for the binary S_xSe_{100-x} liquids obtained using time-temperature superposition of the SAOS rheometry data. All master curves display two G′– G″ crossovers corresponding to the existence of two separate relaxation processes. Previous studies have reported similar observations on both elemental S and Se liquids; in our earlier rheological investigation of supercooled Se, a slow Debye-like and a fast relaxation process were respectively attributed to Se-Se bond scission/renewal dynamics and segmental Se chain motion.[26] It is clear from Fig. 2b-4 that the slow relaxation process corresponding to the low-frequency G′– G″ crossover is temporally decoupled from the fast process corresponding to the high-frequency G′–G″ crossover by several orders of magnitude. The difference $\Delta\tau$ between the fast and the slow relaxation timescales τ_f and τ_s , respectively, increases with increasing sulfur content (Fig. 2b-4). The temperature dependence of τ_f and τ_s for all binary S_xSe_{100-x} liquids is

shown in Figure 2b-5 as a function of T_g/T and is compared with that for supercooled Se. It is evident from Fig. 2b-5 that the timescale and its temperature dependence for the fast process of segmental chain dynamics for all liquids are quite similar. In contrast to τ_f, and similar to viscosity shown in Fig. 2b-2, τ_s monotonically increases with increasing sulfur content at identical T_g/T. This behavior is consistent with the observation made in a recent study by Zhu *et al.* that the viscosity of supercooled Se is controlled by the slow process.[26] Here this observation is shown to also hold true for a binary liquid of composition $S_{45}Se_{55}$ (Fig. 2b-6). The relative contribution of the slow and fast processes towards viscosity η can be estimated using the Maxwell equation: $\eta = G\tau$, where τ is the timescale of the process and G is the corresponding shear modulus. The shear moduli G_s and G_f for the fast and slow processes, respectively, can be obtained from the plateau values of $G'(\omega)$ on the high-frequency side of the corresponding $G' - G''$ crossovers in Fig. 2b-4. The viscosity contributions $G_s\tau_s$ and $G_f\tau_f$ from the slow and the fast processes, respectively, are compared to the experimentally measured viscosity in Fig. 2b-6. This comparison immediately indicates that $\eta \approx G_s\tau_s$, while the contribution of $G_f\tau_f$ to viscosity is negligible.
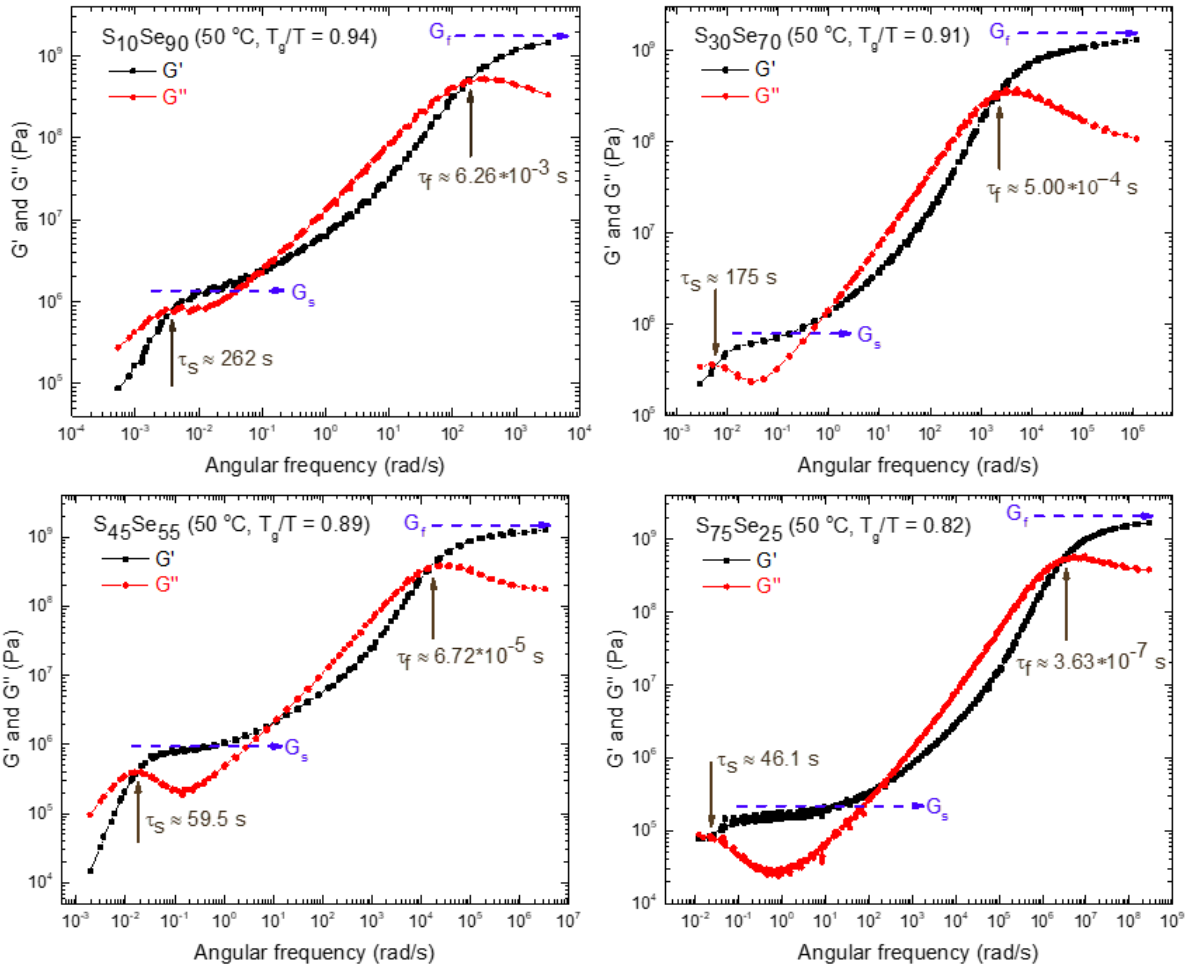
Figure 2b-4 Master curves of storage modulus G' (square) and loss modulus G" (circle) of supercooled binary S_xSe_{100-x} liquids. The TTS reference temperature is listed alongside each composition. Locations of G'- G" crossovers associated with the relaxation times τ_f and τ_s for the fast and slow processes, respectively, are marked by vertical arrows and the respective values of τ_f and τ_s at the TTS reference temperature are listed alongside. Corresponding shear moduli G_f and G_s are marked by horizontal dashed lines.

The corresponding activation energies for τ_f and τ_s, respectively, are ~ 230 to 280 kJ/mol and ~ 130 to 170 kJ/mol (Fig. 2b-5). The latter activation energy is indeed similar to the energy required for S/Se – S/Se bond scission.[26–28] Assuming that the addition of S to Se should not affect the average chain length in the structure, intuitively one may expect that the fast segmental
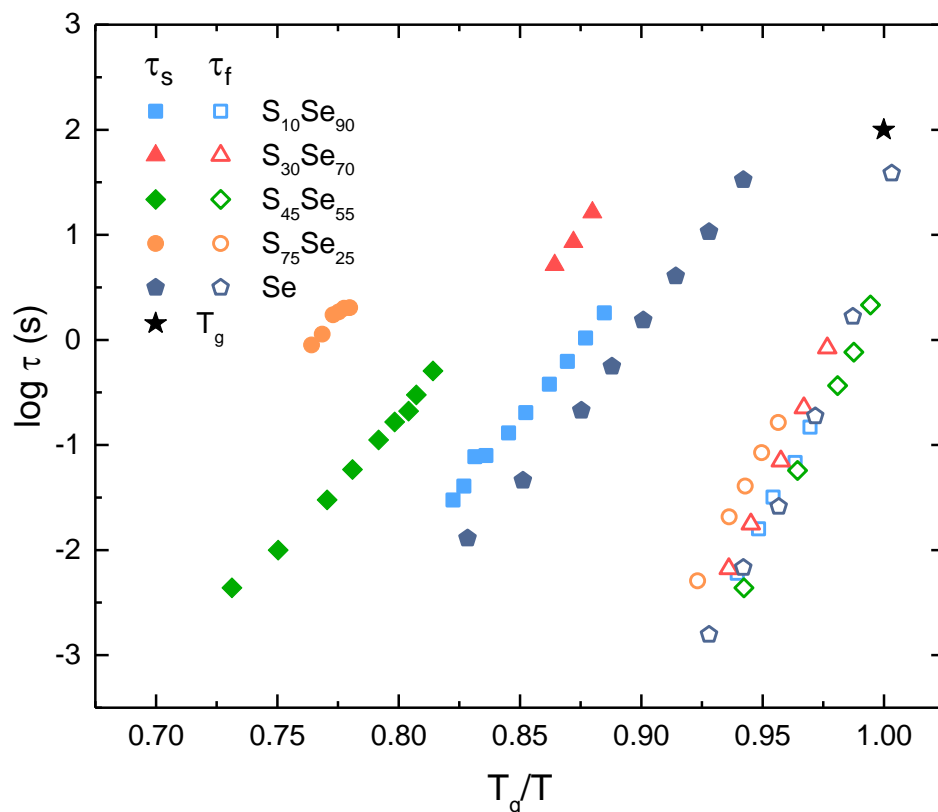
Figure 2b-5 Temperature dependence of τ_f (open symbols) and τ_s (filled symbols) shown as a function of T_g/T for supercooled binary S_xSe_{100-x} liquids.

motion of the chain elements would be relatively unaffected by the appearance of heterocyclic Se_yS_{8-y} rings. This expectation is corroborated by the observation of a weak compositional dependence of τ_f for the S_xSe_{100-x} liquids (Fig. 2b-5). On the other hand, τ_s may increase significantly due to the coexistence of ring and chain elements in the structure, if the latter results in a steric hindrance towards achieving proper orientational configuration of the structural moieties corresponding to the formation of the transition-state activated complexes for the $S/Se-S/Se$ bond scission/renewal process. We hypothesize that this lowering of the chain conformational entropy in the presence of rings is responsible for the lower fragility of the binary S_xSe_{100-x} liquids (Fig. 2b-3). A similar situation is encountered in liquid S (Figs. 2b-1,2) as an increasing fraction of the rings open and polymerize into chains with increasing temperature above T_λ. Therefore, the abrupt

increase in the viscosity of liquid S across the λ-transition is consistent with an FST. However, it may be noted here that this transition in liquid S is characterized by a non-monotonic temperature dependence of viscosity and the fragility of the liquid decreases with increasing temperature across the transition. In contrast, the reported FST in other glass-forming liquids is associated with a monotonic decrease in viscosity and an increase in the fragility across the transition, with increasing temperature.
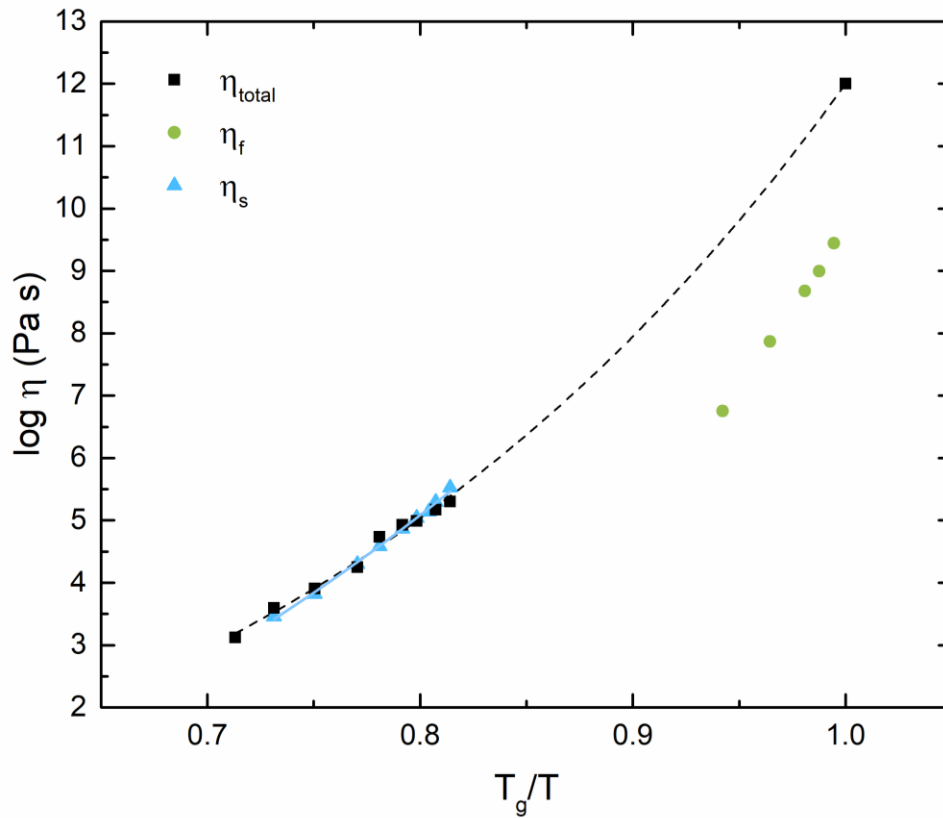
Figure 2b-6 Viscosity contributions from the slow process $\eta_s = G_s\tau_s$ (triangles) and from the fast process $\eta_f = G_f\tau_f$ (circles) for supercooled $S_{45}Se_{55}$ liquid. Experimentally measured viscosity (squares) for this liquid and the corresponding MYEGA fit (dashed line) are shown for comparison. Viscosity at T_g is taken to be 10^{12} Pa.s.

2b.5 Conclusion

In summary, the systematic compositional evolution of the viscoelastic relaxation behavior of supercooled S_xSe_{100-x} liquids indicates that the timescale of the S/Se – S/Se bond scission/renewal dynamics rapidly increases with S concentration as the relative concentrations of rings and chains in the structure become comparable. This observation suggests a lowering of conformational entropy of the chain elements due to steric hindrance from the ring elements that slows down the orientational rearrangement of structural moieties required for the bond scission/renewal process. This dynamical process, being responsible for viscous flow, renders the S_xSe_{100-x} liquids progressively less fragile with increasing S concentration. When taken together, these results indicate that the λ-transition in liquid S is also a fragile-to-strong transition.

References

[1]   P.F. McMillan, M. Wilson, M.C. Wilding, D. Daisenberger, M. Mezouar, G. Neville Greaves, Polyamorphism and liquid–liquid phase transitions: challenges for experiment and theory, J. Phys. Condens. Matter. 19 (2007) 415101.

[2]   G. Zhao, Y.J. Yu, X.M. Tan, Nature of the first-order liquid-liquid phase transition in supercooled silicon, J. Chem. Phys. 143 (2015) 54508.

[3]   S. Woutersen, B. Ensing, M. Hilbers, Z. Zhao, C. Austen Angell, A liquid-liquid transition in supercooled aqueous solution related to the HDA-LDA transition, Science (80-.). 359 (2018) 1127–1131.

[4]   I. Saika-voivod, P.H. Poole, F. Sciortino, Fragile-to-Strong transition and polyamorphism in the energy landscape of liquid silica, Nature. 412 (2001) 514.

[5]   J.H.E. Cartwright, A.G. Checa, J.D. Gale, D. Gebauer, C.I. Sainz-Díaz, Calcium carbonate polyamorphism and its role in biomineralization: How many amorphous calcium carbonates are there?, Angew. Chemie - Int. Ed. 51 (2012) 11960–11970.

[6]   C.A. Angell, Relaxation in Liquid, Polymers and Plastic Crystal-Strong/Fragile Patterns and Problems, J. Non. Cryst. Solids. 131–133 (1991) 13–31.

[7]   J.C. Mauro, Y. Yue, A.J. Ellison, P.K. Gupta, D.C. Allan, Viscosity of glass-forming liquids, Proc. Natl. Acad. Sci. 106 (2009) 19780–19784.

[8]   C. Zhang, L. Hu, Y. Yue, J.C. Mauro, Fragile-to-strong transition in metallic glass-forming liquids, J. Chem. Phys. 133 (2010) 14508.

[9]   P. Lucas, G.J. Coleman, M. Venkateswara Rao, A.N. Edwards, C. Devaadithya, S. Wei, A.Q. Alsayoud, B.G. Potter, K. Muralidharan, P.A. Deymier, Structure of $ZnCl_2$ Melt. Part II: Fragile-to-Strong Transition in a Tetrahedral Liquid, J. Phys. Chem. B. 121 (2017) 11210–11218.

[10]   J. Orava, H. Weber, I. Kaban, A.L. Greer, Viscosity of liquid Ag-In-Sb-Te: Evidence of a fragile-to-strong crossover, J. Chem. Phys. 144 (2016) 194503.

[11]   S. Stølen, T. Grande, H.B. Johnsen, Fragility transition in $GeSe_2$-Se liquids, Phys. Chem. Chem. Phys. 4 (2002) 3396–3399.

[12]   W. Zhu, M.A.T. Marple, M.J. Lockhart, B.G. Aitken, S. Sen, An experimental critique on the existence of fragile-to-strong transition in glass-forming liquids, J. Non. Cryst. Solids. 495 (2018) 102–106.

[13]   J. Ruiz-Garcia, E.M. Anderson, S.C. Greer, Shear viscosity of liquid sulfur near the polymerization temperature, J. Phys. Chem. 93 (1989) 6980–6983.

[14]   B. Ruta, G. Monaco, V.M. Giordano, F. Scarponi, D. Fioretto, G. Ruocco, K.S. Andrikopoulos, S.N. Yannopoulos, Nonergodicity factor, fragility, and elastic properties of polymeric glassy sulfur, J. Phys. Chem. B. 115 (2011) 14052–14063.

[15]   E.D. West, The Heat Capacity of Sulfur from 25 to 450°, the Heats and Temperatures of

Transition and Fusion, J. Am. Chem. Soc. 81 (1959) 29–37.

[16] G.O. Sofekun, E. Evoy, K.L. Lesage, N. Chou, R.A. Marriott, the Rheology of Liquid Elemental Sulfur Across the λ-Transition, J. Rheol. (N. Y. N. Y). 62 (2018) 469–476.

[17] A.G. Kalampounias, K.S. Andrikopoulos, S.N. Yannopoulos, Probing the sulfur polymerization transition in situ Raman spectroscopy, J. Chem. Phys. 118 (2003) 8460–8467.

[18] A. Eisenberg, L.A. Teter, Relaxation mechanisms in polymeric sulfur, J. Phys. Chem. 71 (1967) 2332–2340.

[19] M. Marple, J. Badger, I. Hung, Z. Gan, K. Kovnir, S. Sen, Structure of Amorphous Selenium by 2D ^{77}Se NMR Spectroscopy: An End to the Dilemma of Chain versus Ring, Angew. Chemie. 129 (2017) 9909–9913.

[20] P. Koštál, J. Málek, Viscosity of selenium melt, J. Non. Cryst. Solids. 356 (2010) 2803–2806.

[21] P. Koštál, J. Málek, Viscosity of Se-Te glass-forming system, Pure Appl. Chem. 87 (2015) 239–247.

[22] B. Yuan, W. Zhu, I. Hung, Z. Gan, B. Aitken, S. Sen, Structure and Chemical Order in S-Se Binary Glasses, J. Phys. Chem. B. 122 (2018) 12219–12226.

[23] A. V. Tobolsky, A. Eisenberg, Equilibrium Polymerization of Sulfur, J. Am. Chem. Soc. 81 (1959) 780–782.

[24] D.L. Sidebottom, Fragility of network-forming glasses: a universal dependence on the topological connectivity, Phys. Rev. E. 92 (2015) 062804.

[25] D.L. Sidebottom, S.E. Schnell, Role of intermediate-range order in predicting the fragility of network-forming liquids near the rigidity transition, Phys. Rev. B. 87 (2013) 054202.

[26] W. Zhu, B.G. Aitken, S. Sen, Observation of a dynamical crossover in the shear relaxation processes in supercooled selenium near the glass transition, J. Chem. Phys. 150 (2019) 094502.

[27] V.Q. Nguyen, J.S. Sanghera, I.K. Lloyd, I.D. Aggarwal, D. Gershon, Room temperature dielectric properties of the $As_{40}S_{(60-x)}Se_x$ glass system, J. Non. Cryst. Solids. 276 (2000) 151–158.

[28] R. Steudel, Roperties of Sulfur-Sulfur Bonds, Angew. Chemie Int. Ed. English. 14 (1975) 665–720.

Chapter 3

Structure and Rheology of Se-I Glasses and Supercooled Liquids

3.1 Abstract

The structural evolution and shear relaxation behavior of binary $Se_{100-x}I_x$ $(0 \leq x \leq 3)$ glasses and supercooled liquids are investigated using Raman spectroscopy and parallel plate rheometry, respectively. The spectroscopic results indicate cleavage and termination of Se polymeric chains by I atoms via the formation of Se-I bonds, leading to shortening of the average chain length with progressive addition of I atoms. Moreover, at I contents of $\geq 2\%$, a fraction of the I atoms forms I_2 dimers. The results from rheometry demonstrate that the structural relaxation rates associated with the fast segmental chain motion and the slow bond scission/renewal dynamics in $Se_{100-x}I_x$ liquids increase upon addition of I, with the shortening of the chain length. The increased configurational degrees of freedom of shorter selenium chains leads to a decrease in the isothermal viscosity, T_g and the packing efficiency and an increase in fragility in liquids with higher I content.

3.2 Introduction

Amorphous chalcogenides have been studied extensively in the past because of their optical transparency in the infrared range. Selenium is one of the chalcogens known for its excellent glass forming ability in its elemental form and its stability against crystallization. It is now well established in literature that the structure of vitreous Se consists practically exclusively of twofold coordinated Se atoms forming polymeric chains [1]. The average coordination number $<r> = 2$ of vitreous Se is conventionally taken to signify the lowest limit of nearest-neighbor structural connectivity in chalcogenide glasses. However, the introduction of halogens (X= Cl, Br, I) is known to result in the scission of intrachain Se-Se linkages and the formation of terminal Se-X bonds [2] through the following reaction:

$$-Se–Se–Se–Se– + X–X \leftrightarrow –Se–Se–X + X–Se–Se–$$
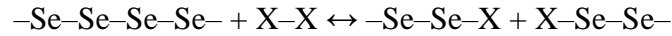
Previous studies based on extended x-ray absorption fine structure spectroscopy and neutron scattering of binary Se-I melts have indicated that such a mode of incorporation of I atoms into Se chains is limited and at high I content (~ 80%) a large fraction of the I atoms form I_2 dimers. This observation was ascribed to the fact that the Se–I and I–I bonds are characterized by comparable bond strength [3]. On the other hand, previous studies of binary Se-I melts also showed that the decrease in Se chain length with increasing I content would result in a concomitant lowering of viscosity [2-4].

Recent studies of the shear relaxation behavior of supercooled Se demonstrated the existence of two relaxation processes, namely the slow bond scission/renewal dynamics and the fast segmental chain motion [5,6]. The slow process was shown to be closely related to shear relaxation and viscous flow, while the fast relaxation process remains temporally decoupled from

shear relaxation until the temperature closely approached glass transition from above. This scenario remains unchanged upon addition of cross-linkers such as Ge or As, as long as the average length of the selenium chain segments in between the crosslinking points remains longer than three to five Se atoms. As the network connectivity increases beyond this point with further addition of Ge or As, the segmental chain motion cannot be sustained and the fast process disappears [7]. Although binary Se-I melts have been studied in the past, the relationship between the structure and the rheological behavior of supercooled Se-I liquids, including the effect of shortening of the Se chains via their termination with halogen atoms on the shear relaxation behavior, remains unknown to date. Here we report the results of the first systematic Raman spectroscopic study of the structure of binary $Se_{100-x}I_x$ ($0 \leq x \leq 3$) glasses, as well as a rheological study of the shear relaxation behavior of select supercooled Se-I liquids. The correlations between the composition-dependent structural evolution and viscosity, molar volume and glass transition temperature are discussed.

3.3 Experimental Methods

3.3.1 Glass synthesis and physical characterization

Binary $Se_{100-x}I_x$ glasses with $x = 0.5$, 1, 1.5, 2, and 3 were synthesized in 10 ~12 g batches using the conventional melt-quench method. Mixtures of elemental Se (Alfa Aesar, 99.999%) and I_2 (Sigma-Aldrich, $\geq$99%) were loaded in quartz ampoules (8 mm inner diameter) that were subsequently evacuated (10^{-4} Torr) and flame-sealed. The bottom of the ampoules containing the batched iodine was submerged in liquid nitrogen during flame sealing in order to avoid iodine sublimation. The ampoules were then loaded into a rocking furnace, slowly heated to 673 K over

8 hours and held at this temperature for 12 hours to ensure melt homogeneity. The melts were subsequently quenched by dipping the ampoules in water.

The density of Se$_{100-x}$I$_x$ glasses was measured using a Micrometritic Accupyc II gas expansion pycnometer under helium (6N purity) environment. For each measurement, approximately 1.0 g of glass sample was loaded into a 1 cm^3 cup. The reported densities in this study are averages of 10 consecutive measurements at room temperature.

The glass transition temperature T_g was measured using a Mettler-Toledo DSC1 differential scanning calorimeter. Approximately 20 mg powdered glass sample was loaded into a hermetically sealed 40 μL aluminum crucible. Scans were performed with a heating rate of 10 K/min under a continuously flowing of nitrogen environment. T_g was determined to within ± 1 K as the onset of the glass transition. The activation energy of the glass transition and, hence, of structural relaxation was determined from the cooling and heating rate q dependence of the DSC profile of the glass transition. In particular, the samples were first heated to 338 K, which is well above T_g, and then cooled to 273 K, which is well below T_g, at a specific cooling rate q and subsequently held at that temperature for 5 min, followed by an upscan at the same rate back to 338 K and the fictive temperature T_f was taken to be ~ T_g [8,9].

3.3.2 Raman Spectroscopy

The Raman spectra of all glasses were collected in backscattered geometry using a Brucker RFS 100/S Fourier-transform Raman spectrometer equipped with a Nd:YAG laser operating at a wavelength of 1064 nm. Each Raman spectrum was collected using a laser power level of 30 mW, and is an average of 64 scans taken with 2 cm^{-1} resolution.

3.3.3 Parallel Plate Rheometry

The small amplitude oscillatory shear (SAOS) rheological measurements reported in the present study were carried out on an Anton-Paar MCR92 parallel plate rheometer equipped with a Peltier heater under a constant flow of nitrogen gas. All measured samples were first heated above their softening point, then trimmed into a disc geometry with ~1 mm thickness that was sandwiched between the 8 mm oscillating upper plate and the stationary lower plate. For each measurement, an oscillatory strain within the linear viscoelastic range of the material with angular frequency ω varying between 1 and 600 rad/s was applied and the induced torque was measured simultaneously to obtain the storage and the loss moduli G' and G'' as a function of probing frequency. Multiple measurements were carried out at various temperatures for each composition and master curves of $G'(\omega)$ and $G''(\omega)$ were constructed using time-temperature superposition (TTS). It may be noted here that TTS is only approximately obeyed by these liquids. The viscosity master curves were then calculated from the relation $\eta(\omega) = \frac{\sqrt{G'^2 + G''^2}}{\omega}$. Details of the experimental setup and procedure can be found in a previous publication [10]. Additionally, Newtonian viscosity measurements on the supercooled $Se_{97}I_3$ liquid were carried out under steady shear condition, using a 25 mm diameter upper plate and a stationary lower plate, on a sample with a disc-like geometry with ~ 0.8 mm thickness. Although the duration of each measurement is only a few minutes, the $Se_{97}I_3$ supercooled liquid is susceptible to iodine loss and surface crystallization. Therefore, fresh samples were used for rheological measurements at each temperature to avoid thermal cycling and each measurement was repeated on multiple samples to ensure reproducibility and estimate experimental error. The physical appearance of the samples was checked immediately after the end of each measurement, which indicated the lack of any discernible surface crystallization.

3.4 Results and Discussion

3.4.1 Physical properties

The density and molar volume of these $Se_{100-x}I_x$ glasses are listed in Table 3-1. The molar volume of these glasses increases monotonically with increasing iodine concentration (Fig. 3-1a). When considering the effect of introducing I atoms, which exhibit similar atomic size but significantly heavier molar mass than Se atoms, it is intuitive that the density would increase with increasing I content. On the other hand, the I atoms are monovalent and act as Se chain terminators so that the average chain length is expected to decrease with addition of I. Therefore, the increase in molar volume with increasing I concentration suggests a decreasing efficiency in the packing of the selenium chains in the structure as the average length of these chains progressively shortens. This hypothesis suggests a scenario where long chains are more likely to exhibit chain folding and entanglement and therefore, a more efficient packing compared to short chains. Moreover, by the same token, the shortening of Se chains would lead to a less rigid structure that is capable of undergoing more rapid structural relaxation, which would result in a lowering of T_g with increasing addition of I. Such a trend is indeed observed experimentally for these $Se_{100-x}I_x$ glasses, where T_g decreases nearly linearly in a monotonic fashion with increasing x. (Fig. 3-1b).

Table 3-1 Density and molar volume of $Se_{100-x}I_x$ glasses.

Composition	Density (g/cm^3)	Molar volume (cm^3/mol)
Se	4.270 ± 0.001	18.49 ± 0.01
$Se_{99.5}I_{0.5}$	4.277 ± 0.006	18.52 ± 0.02
$Se_{99}I_1$	4.277 ± 0.003	18.58 ± 0.01
$Se_{98.5}I_{1.5}$	4.283 ± 0.009	18.61 ± 0.04
$Se_{98}I_2$	4.283 ± 0.004	18.66 ± 0.02
$Se_{97}I_3$	4.287 ± 0.006	18.76 ± 0.03
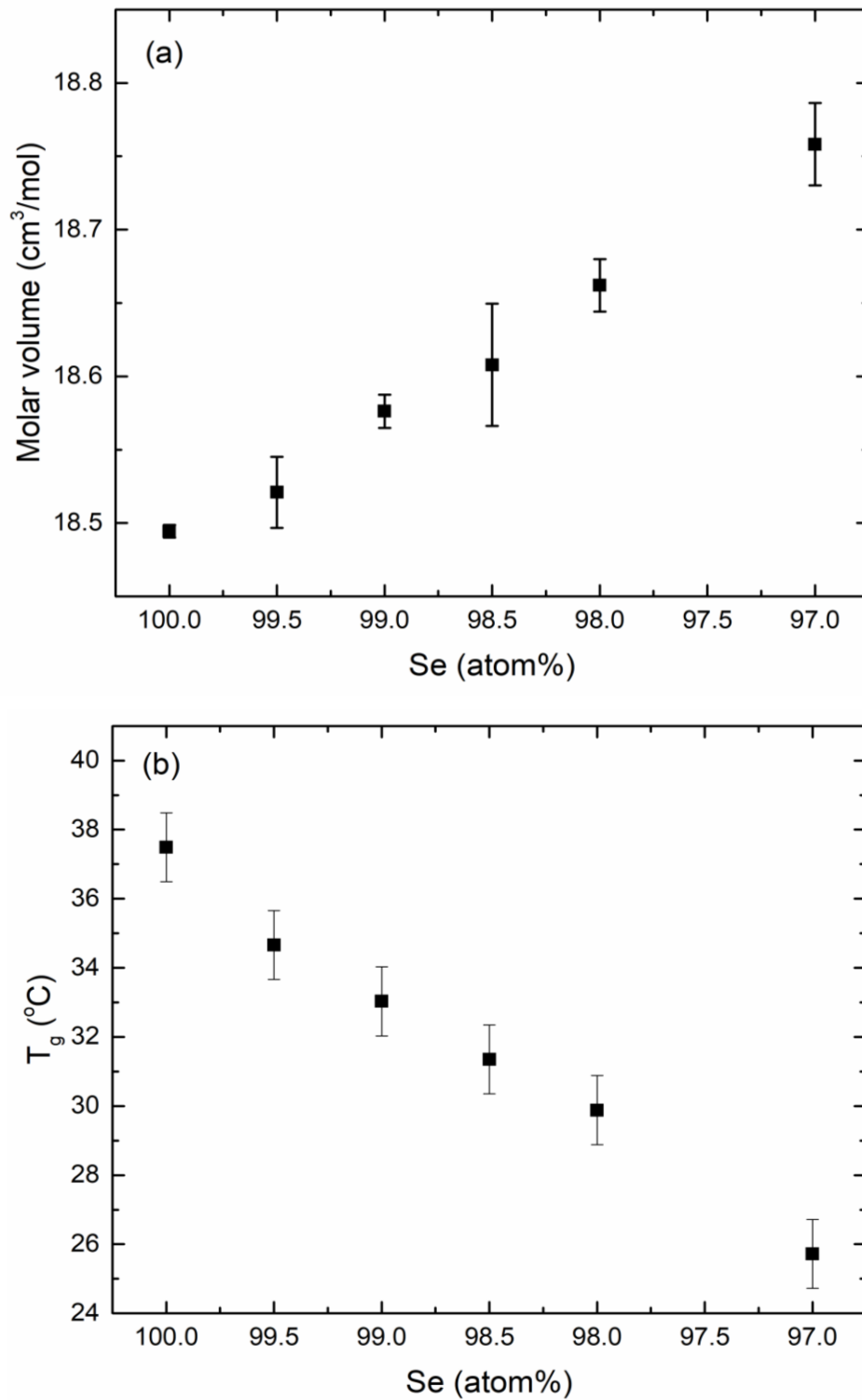
Figure 3-1 (a) Molar volume and (b) glass transition temperature T_g of binary $Se_{100-x}I_x$ glasses.

3.4.2 Structure by Raman Spectroscopy

The Raman spectra of all Se$_{100-x}$I$_x$ glasses are shown in Fig. 3-2. The three major high-frequency bands in the 150-300 cm^{-1} range can be assigned to I–I (~172 cm^{-1}), Se–I (~210 cm^{-1}), and Se–Se (~250 cm^{-1}) stretching modes [11,12]. The bending modes are located in the 50-150 cm^{-1} range. The Se–Se stretching band is the most intense, which indicates the abundance of the Se chains in glasses. The intensity of the Se–I stretching band increases monotonically with increasing I content, which is consistent with the increasing concentration of the terminal Se–I bonds and corresponding shortening of the average Se chain length. This observation is in agreement with the thermophysical property trends discussed above. On the other hand, the I–I stretching band starts to appear at relatively high I concentration (I $\geq$ 2%) and increases in intensity with addition of I. This finding suggests that, beyond a threshold of ~ 2% I, not all I atoms are incorporated in Se chains and a fraction of these atoms form I$_2$ dimers. This propensity for I to form both Se-I and I-I bonds is consistent with the fact that Se and I exhibit similar electronegativity, which suggests similar bond strength for Se–Se and I–I bonds. Moreover, previous studies of Se-I melts reported interchange of Se–I and I–I linkages and the formation of I$_2$ molecules in the molten state [3].

3.4.3 Viscosity, shear relaxation and fragility

The frequency dependence of $G'(\omega)$ and $G''(\omega)$ at various temperatures and the corresponding master curves for pure Se and Se$_{97}$I$_3$ supercooled liquids obtained from the TTS of the SAOS rheometry data are shown in Fig. 3-3. The two relaxation processes corresponding to the low- and high- frequency crossovers between $G'(\omega)$ and $G''(\omega)$ in pure Se were shown in
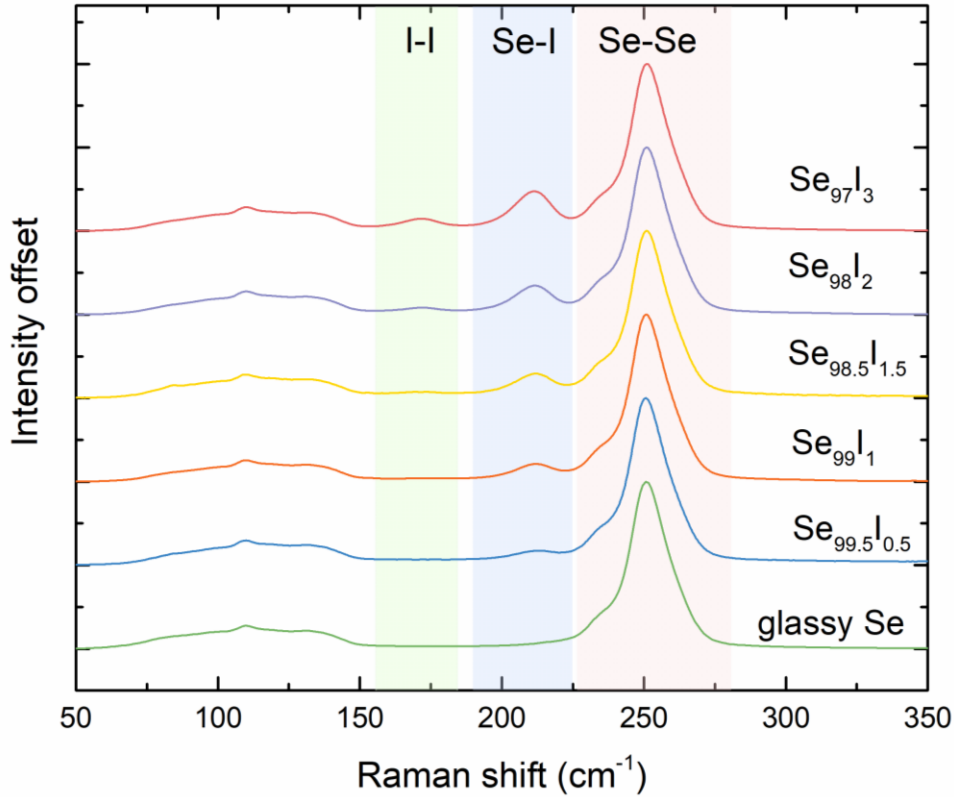
Figure 3-2 Unpolarized Raman spectra of $Se_{100-x}I_x$ glasses. All spectra are normalized with respect to the most intense peak at ~ 250 cm^{-1}.

previous studies to represent, respectively, the slow Se-Se bond scission/renewal process and the fast segmental chain motion [5]. Correspondingly the viscosity $\eta(\omega)$ displays two onsets of frequency dependence. In contrast with Se, the $Se_{97}I_3$ supercooled liquid displays a clear high-frequency G'(ω)-G"(ω) crossover. However, in the low-frequency terminal region G'(ω) and G"(ω) display only a kink due to the changes in the relative strength and degree of temporal coupling between the two relaxation processes. Nevertheless, the two-step onset of the frequency dependence of $\eta(\omega)$ remains clear. Such behavior was ascribed in previous studies to the terminal modes in short-chain polymers [13]. Therefore, similar to pure Se, two relaxation processes also exist in the $Se_{97}I_3$ supercooled liquids. The similarity in the activation energy E_a of the fast and the slow processes (Fig. 3-4), estimated from the temperature dependence of the corresponding relaxation times for the two liquids (~337 ± 23 kJ/mol and ~179 ± 5 kJ/mol, respectively, for Se

and ~308 ± 10 kJ/mol and ~145 ± 8 kJ/mol, respectively, for Se$_{97}$I$_3$) is a further corroboration of this hypothesis [5,14,15].
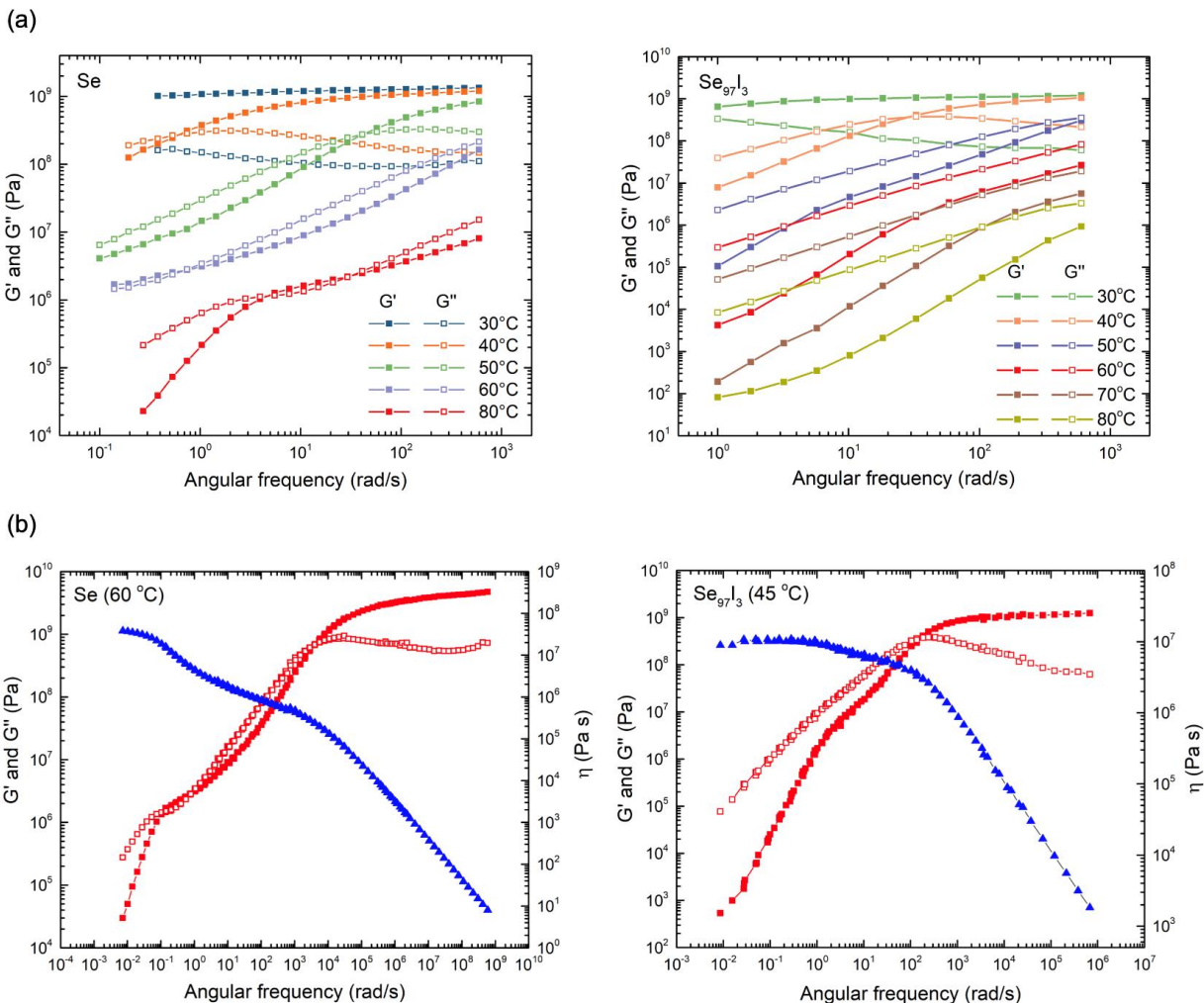
Figure 3-3 (a) Temperature dependence of G′(ω) and G"(ω) of (left panel) pure Se [5] and (right panel) Se$_{97}$I$_3$ liquids. (b) Master curves of frequency dependence of G′ (filled red squares) and G″ (open red squares), and viscosity η (filled blue triangles) of (left panel) pure Se [5] and (right panel) Se$_{97}$I$_3$ liquids. The reference temperature for TTS is listed alongside the composition in each panel. Experimental errors in G′(ω) and G"(ω) are within the size of the symbols.

However, and more importantly, a comparison of the relaxation timescales between the two liquids shows that, compared to Se, the Se$_{97}$I$_3$ liquid has faster and more similar timescales for both processes (Fig. 3-4). It is tempting to hypothesize that further shortening in the selenium chain length at higher I concentration would lead to an eventual collapse of the two processes into a
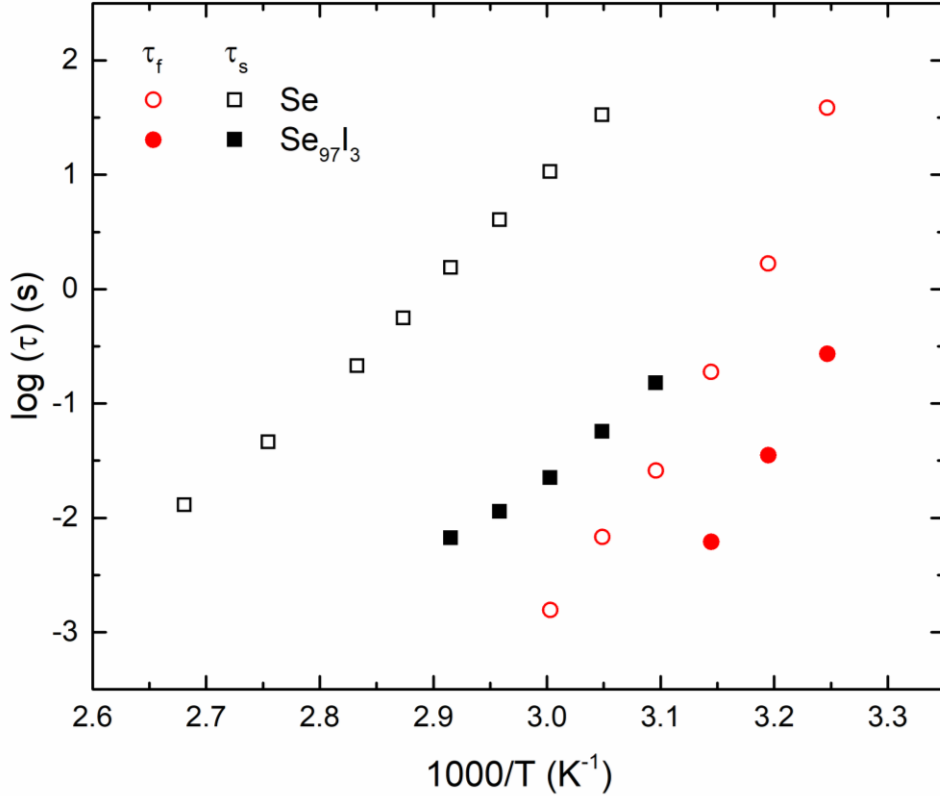
Figure 3-4 Temperature dependence of τ_s (squares) and τ_f (circles) for supercooled Se (open symbols) [5] and $Se_{97}I_3$ liquids (solid symbols).

single relaxation process. According to the Maxwell relation, viscosity can be estimated as $\eta = (G_f - G_s)\tau_f + G_s\tau_s \approx G_f\tau_f + G_s\tau_s$, where the G and τ are the plateau shear moduli and relaxation time, and where the subscripts f and s correspond to the fast and slow processes, respectively. Since both shear moduli are found to have insignificant temperature dependence in the $Se_{97}I_3$ liquid, the temperature dependence of viscosity should be reflected in that of the relaxation times. Therefore, the results shown in Fig. 3-4 suggest a decrease in viscosity of $Se_{100-x}I_x$ liquids with progressive addition of I. This expectation is in agreement with the experimental viscosity data obtained in this study for the $Se_{97}I_3$ liquid using steady shear measurements (Fig. 3-5). Therefore, when taken together, these results indicate that the viscosity and the timescale of shear relaxation processes both decrease with the shortening of Se chain length as intuitively expected, since shorter chains

should have more degrees of freedom and thus faster structural rearrangement compared to longer chains.
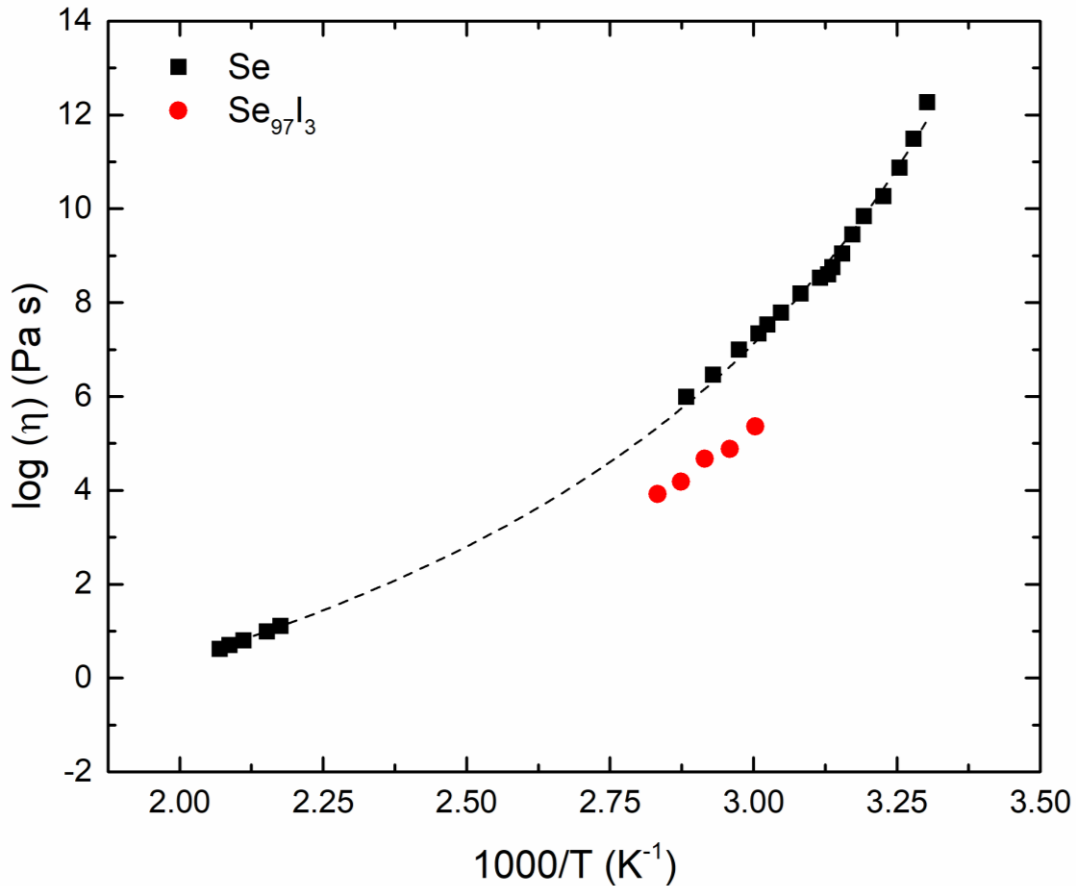
Figure 3-5 Temperature dependence of viscosity of pure Se (filled squares) [19] and Se$_{97}$I$_3$ (solid circles) liquids. The dashed line is a guide to eye.

The Rouse model for flow in chain polymers predicts that for unentangled chain polymer melts the viscosity η is linearly proportional to the chain length N [16]. Assuming the chain length in supercooled Se liquid is on the order of ~230 atoms, the Se$_{97}$I$_3$ glass should have an average minimum chain length of ~67 atoms (with 65 Se atoms and two terminal I atoms) if all I atoms participate in selenium chain termination via formation of Se-I bonds [17]. The viscosity of Se and Se$_{97}$I$_3$ at ~333 K is approximately 2.19×10^7 Pa.s and 2.32×10^5 Pa.s, respectively (Fig. 3-5). Therefore, it is clear that the $\eta \sim N$ relation is not satisfied for these two liquids, which suggests the likelihood of significant chain entanglement in supercooled Se liquid. Finally, the effect of

addition of I and shortening of the selenium chain length is investigated in this study by comparing the heating and cooling rate dependence of the activation energy of the glass transition of supercooled Se and $Se_{98}I_2$ liquids. This activation energy E_a for a supercooled liquid at T ~ T_g is related in the literature to its "fragility index" m, which is defined as: $m = \frac{d\log_{10}\eta}{dT_g/T}\Big|_{T=T_g}$ and can be obtained using the Wang-Velikov-Angell (WVA) method which relates m to E_a via the expression:

$m = E_a/(ln10\ RT_g)$, where R is the ideal gas constant and E_a/R is the slope of the $\ln(1/q)$ vs $1/T_f$ curve (Fig. 3-6) [8,9,18]. The $Se_{98}I_2$ composition was chosen for this experiment instead of $Se_{97}I_3$ as the latter is significantly more susceptible to iodine loss and surface crystallization during the DSC experiments, which could last for several hours at the slowest cooling/heating rates. It is clear from Fig. 3-6 that $\ln(1/q)$ for both liquids is not linearly proportional to $1/T_f$ as the E_a is dependent on temperature. Therefore, the slope is taken at the slowest cooling (or heating) rate of 0.2 K/min in this study to ensure that the calculated value of m for pure Se is consistent with the m determined directly from the viscosity data available in the literature at T ~ T_g [19]. This method yields m ~ 81 for pure Se, while m ~ 89 for the $Se_{98}I_2$ liquid. This small but significant increase in fragility with addition of I further indicates that the formation of short selenium chains results in a higher degree of motional freedom and consequently in a larger temperature dependence of the configurational entropy of the chains [20].
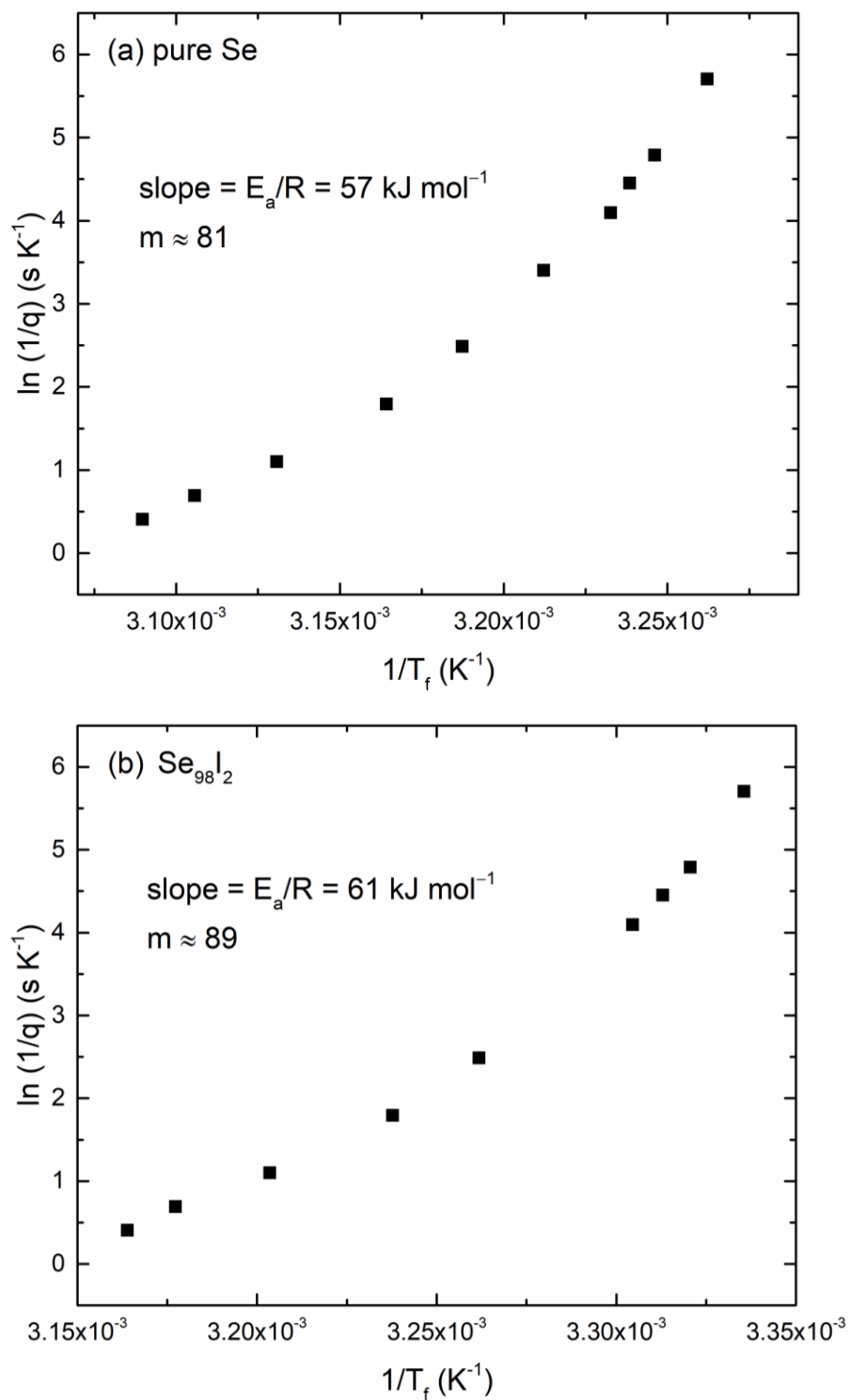
Figure 3-6 ln($1/q$) vs $1/T_f$ for (a) pure Se and (b) Se$_{98}$I$_2$ supercooled liquids. All experimental errors are within the size of the symbols.

3.5 Conclusions

When incorporated into amorphous Se, halogens such as I, being monovalent, act as chain terminators. Therefore, progressive addition of I into Se results in the cleavage of Se-Se bonds and the formation of Se-I bonds, which leads to the shortening of Se chains and, consequently, a decrease in isothermal viscosity and T_g as well as an increase in molar volume and fragility. The characteristic timescales for the bond scission/renewal and the fast segmental chain motion associated with structural relaxation become faster and more similar with decreasing chain length. Furthermore, the scaling of isothermal viscosity with chain length indicates the likelihood of significant chain entanglement in supercooled selenium liquid.

Acknowledgement

References

[1]   M. Marple, J. Badger, I. Hung, Z. Gan, K. Kovnir, S. Sen, Structure of Amorphous Selenium by 2D ^{77}Se NMR Spectroscopy: An End to the Dilemma of Chain versus Ring, Angew. Chemie. 129 (2017) 9909–9913.

[2]   J.C. Perron, J. Rabit, J.F. Rialland, Impurity dependence of the viscosity of liquid selenium, Philos. Mag. B Phys. Condens. Matter; Stat. Mech. Electron. Opt. Magn. Prop. 46 (1982) 321–330.

[3]   K. Maruyama, Y. Kawakita, M. Yao, H. Endo, M. Misawa, Intra- and Intermolecular Correlations in Liquid Selenium-Halogen Systems, J. Phys. Soc. Japan. 60 (1991) 3032–3044.

[4]   V.H. Krebs, W. Morsch, Molekelgröße des amorphen schwarzen Selens, Z Anorg Allg Chem. 263 (1950) 305–309.

[5]   W. Zhu, B.G. Aitken, S. Sen, Observation of a dynamical crossover in the shear relaxation processes in supercooled selenium near the glass transition, J. Chem. Phys. 150 (2019) 094502.

[6]   W. Zhu, I. Hung, Z. Gan, B. Aitken, S. Sen, Dynamical process related to viscous flow in a supercooled arsenic selenide glassforming liquid: Results from high-temperature ^{77}Se NMR Spectroscopy, J. Non. Cryst. Solids. 526 (2019) 119698.

[7]   S. Sen, Y. Xia, W. Zhu, M. Lockhart, B. Aitken, Nature of the floppy-to-rigid transition in chalcogenide glass-forming liquids, J. Chem. Phys. 150 (2019) 144509.

[8]   S. Wei, P. Lucas, C. Austen Angell, Phase Change Alloy Viscosities Down to T_g using Adam-Gibbs-Equation Fittings to Excess Entropy Data: A Fragile-to-Strong Transition, J. Appl. Phys. 118 (2015) 034903.

[9]   Y. Yue, R. Von der Ohe, S.L. Jensen, Fictive temperature, cooling rate, and viscosity of glasses, J. Chem. Phys. 120 (2004) 8053–8059.

[10]   S. Sen, W. Zhu, B.G. Aitken, Behavior of a supercooled chalcogenide liquid in the non-Newtonian regime under steady vs. oscillatory shear, J. Chem. Phys. 147 (2017) 034503.

[11]   T. Kume, T. Hiraoka, Y. Ohya, S. Sasaki, H. Shimizu, Soft phonon in the Incommensurate Phases of Bromine and Iodine studied by Raman scattering, Jt. 20th AIRAPT 43rd EHPRG Int. Conf. High Press. Sci. Technol. (2005).

[12]   S.N. Yannopoulos, K.S. Andrikopoulos, Raman scattering study on structural and dynamical features of noncrystalline selenium, J. Chem. Phys. 121 (2004) 4747–4758.

[13]   C. Gainaru, R. Figuli, T. Hecksher, B. Jakobsen, J.C. Dyre, M. Wilhelm, R. Böhmer, Shear-Modulus Investigations of Monohydroxy Alcohols: Evidence for a Short-Chain-Polymer Rheological Response, Phys. Rev. Lett. 112 (2014) 098301.

[14]   T. Cottrell, The strengths of chemical bonds, Academic Press, 1958.

[15]   B. Yuan, B. Aitken, S. Sen, Is the λ-transition in liquid sulfur a fragile-to-strong transition?, J. Chem. Phys. 151 (2019) 041105.

[16] J.D. Ferry, Viscoelastic properties of polymers, John Wiley & Sons, 1980.

[17] K.M. Bernatz, I. Echeverría, S.L. Simon, D.J. Plazek, Characterization of the molecular structure of amorphous selenium using recoverable creep compliance measurements, J. Non. Cryst. Solids. 307–310 (2002) 790–801.

[18] L.M. Wang, V. Velikov, C.A. Angell, Direct determination of kinetic fragility indices of glassforming liquids by differential scanning calorimetry: Kinetic versus thermodynamic fragilities, J. Chem. Phys. 117 (2002) 10184–10192.

[19] P. Koštál, J. Málek, Viscosity of selenium melt, J. Non. Cryst. Solids. 356 (2010) 2803–2806.

[20] G. Adam, J.H. Gibbs, On the temperature dependence of cooperative relaxation properties in glass-forming liquids, J. Chem. Phys. 43 (1965) 139–146.

Chapter 4a

Chemical Order in Binary Se-Te Glasses: Results from High-Resolution 2D ^{77}Se and ^{125}Te MATPASS NMR Spectroscopy

4a.1 Abstract

The structure of binary Te_xSe_{100-x} ($0 \leq x \leq 35$) glasses is studied using high-resolution two-dimensional magic-angle-turning phase-adjusted spinning sidebands (2D MATPASS) [77]Se and [125]Te nuclear magnetic resonance (NMR) spectroscopy. The ^{77}Se ([125]Te) isotropic NMR spectra are consistent with the presence of three different kinds of Se (Te) sites, which correspond to Se–**Se (Te)**–Se, Te–**Se (Te)**–Se, and Te–**Se (Te)**–Te environments. The compositional variation of the relative fractions of the three Se sites indicates that the Se and Te atoms are randomly distributed to form $[Se, Te]_n$ copolymer chains. The ^{77}Se and [125]Te NMR isotropic chemical shifts for Se and Te atoms in isostructural environments are found to display a linear correlation. The systematic compositional variation of the CSA of Se–**Se**–Se sites can be related to the appearance of Te atoms as next-nearest neighbors of Se atoms in the $[Se, Te]_n$ chains.

4a.2 Introduction

Complex amorphous tellurides in the Ge-Sb-Te and related systems have found important technological applications in the areas of phase change memory and infrared photonics [1–3]. Recent studies have shown that Te_xSe_{100-x} binary alloys can serve as a model system for the investigation of phenomena such as semiconductor-to-metal and reversible amorphous-to-crystalline transitions, which are relevant to phase-change memory applications [1]. Therefore, it is essential to study the structure of glasses in this system in order to understand the nature of these phase transitions for future applications.

Se and Te are isoelectronic and the structure of the stable crystalline polymorphs of both elements consists of polymeric $[Se]_n$ or $[Te]_n$ helical chains, where Se and Te atoms are twofold coordinated [4,5]. However, these two elements behave quite differently in their glass-forming tendencies. Se can be readily vitrified upon quenching of the parent melt, while Te can only be vitrified as thin films and readily crystallizes upon supercooling the melt in bulk. This difference between Se and Te limits the composition range for bulk glass formation in the Te_xSe_{100-x} system to $x \leq 50$ [6,7]. The structure of Te_xSe_{100-x} glasses have been studied in the past using a wide variety of techniques [8–10]. Although the atom rearrangement in these copolymer chains has been scrutinized using varies experimental techniques, no consensus has been reached yet. Itoh used a combination of neutron and X-ray diffraction and reverse Monte Carlo modeling and proposed a structural model for the $Te_{40}Se_{60}$ glass where Se and Te atoms are alternately connected with the presence of some $[Se]_n$ fractions and Te-Te dimers in $[Se, Te]_n$ chains [8]. On the other hand, a recent Raman spectroscopic study suggested that the Se and Te atoms are randomly distributed in the copolymeric $[Se, Te]_n$ chains with some preference for heteropolar bonding [9]. This structural model is similar to that originally proposed by Bureau *et al.* [10] on the basis of a [77]Se magic-angle

spinning (MAS) nuclear magnetic resonance (NMR) spectroscopic study. These authors reported the composition dependent variation of the relative fraction of different Se environments as obtained from the simulation of the ^{77}Se MAS NMR spectral line shapes. However, the experimental conditions utilized by these authors ([77]Se resonance frequency of 57.3 MHz and spinning speed of 15 kHz) precluded complete separation of spinning sidebands from isotropic peaks due to the relatively large chemical shift anisotropy (CSA) and chemical shift distribution for [77]Se that are characteristic of the constituent Se environments. These authors also reported the [125]Te MAS NMR spectra of these glasses, although the CSA and chemical shift distribution related line broadening was found to be too large for [125]Te to retrieve any information regarding Te speciation [10].

^{77}Se and [125]Te NMR spectroscopy remain challenging in chalcogenide glasses due to the low natural abundance of these nuclides (~7% each), their long spin-lattice relaxation times, large CSA and chemical shift range, which are particularly problematic for [125]Te. These issues result in lengthy data collection and broad and unresolved NMR spectra. Some of these problems can be alleviated effectively via the implementation of the two-dimensional magic-angle turning phase-adjusted spinning sidebands (2D MATPASS) NMR technique. The MATPASS technique can separate the CSA from the isotropic chemical shift, resulting in increased spectral resolution in the isotropic dimension, while preserving the information contained in the CSA along the anisotropic dimension [11]. This separation of isotropic and anisotropic chemical shift interactions results in an isotropic NMR spectrum corresponding to a high-resolution MAS spectrum at infinite spinning speed, i.e., free of any CSA-related broadening. Moreover, a consideration of CSA in combination with isotropic shift can often provide unequivocal identification of structural units. The isotropic vs. anisotropic separation experiment allows the use of high magnetic fields for increased

sensitivity and resolution without requiring faster spinning with small sample volume rotors. Finally, the application of the Carr-Purcell Meiboom-Gill (CPMG) echo train acquisition of the MATPASS data can reduce the data collection time significantly [11]. In this chapter, I report the results of a combined high-resolution ^{77}Se and ^{125}Te 2D MATPASS/CPMG NMR spectroscopic study of the structure and chemical order in binary Te_xSe_{100-x} glasses with $0 \leq x \leq 35$. The compositional evolution of the relative fractions of different Se and Te environments as obtained from the corresponding isotropic NMR spectra provides unique information on the bonding preference of Se and Te atoms in these glasses. Additionally, the CSA of the Se sites, as obtained from the anisotropic spectra, reveals the effect of the replacement of Se next-nearest neighbors with Te.

4a.3 Experimental

4a.3.1 Sample synthesis and physical characterization

Binary Te_xSe_{100-x} glasses with $x = 0, 10, 20, 25, 30, 35$ were synthesized in ~14 g batches from mixtures of constituent elements (Alfa Aesar, 99.999%) that were taken in evacuated fused quartz ampoules and melted at 873 K for 12 hours. The melts were then quenched by dipping the ampoules in ice-water. Chemical analysis of all glasses was carried out using an electron microprobe (Cameca SE-100) equipped with wavelength dispersive spectrometers. The compositions of all glasses were found to be within ±0.5 at% of nominal and they were chemically homogeneous at the micron-scale.

The density of these Te_xSe_{100-x} glasses was measured using a Micrometritic Accupyc II gas expansion pycnometer under helium (6N purity) environment. For each measurement,

approximately 1.0 g of glass sample was loaded into a 1 cm^3 cup. The reported densities in this study are averages of 10 consecutive measurements at room temperature.

4a.3.2 NMR spectroscopy

The 2D ^{77}Se and ^{125}Te MATPASS/CPMG NMR spectra for all glasses were acquired at the National High Magnetic Field Laboratory using a 31 mm bore 19.6 T magnet equipped with a Bruker Avance NEO console operating at the resonance frequency of 158.7 MHz and 262.3 MHz for ^{77}Se and ^{125}Te, respectively. Glass samples were crushed and packed into 3.2 mm ZrO$_2$ rotors and were spun at 10 kHz.

The MAT/CPMG pulse sequence [11] was used for ^{77}Se with $\pi/2$ and π pulses of 3.0 and 6.0 μs, respectively. The method of States *et al.* [12] for hypercomplex data acquisition was applied to the CPMG pulse phase and the receiver phase. The 2D acquisition consisted of 16 hypercomplex t_1 increments each with 36 transients, 81 CPMG echoes per transient and 75 s recycle delay, for a total experimental duration of 24 hours per spectrum. For ^{125}Te, the projection version of the pulse sequence, *pj*MAT/CPMG, [13] was used for covering the wider ^{125}Te frequency range with all pulses set to 2.7 μs. The 2D acquisition consisted of 16 hypercomplex t_1 increments spanning only half a rotor period ($-\tau_r/4$ to $+\tau_r/4$), each with 360 transients, 13 CPMG echoes per transient and 30 s recycle delay, for a total experimental duration of 96 hours per spectrum. The 2D MAT spectra were sheared to an isotropic/anisotropic representation in the direct/indirect dimensions during processing, as detailed in Ref. [11]. The isotropic and anisotropic line shapes were simulated using DMFit [14]. ^{77}Se and ^{125}Te NMR spectra were externally referenced by recording the ^{17}O signal of natural abundance H$_2$O and using the appropriate frequency ratios reported in the IUPAC recommendations [15]. The chemical shift anisotropy (CSA) tensors reported here are defined using the Haeberlen convention[16] as:

$$|\delta_{zz} - \delta_{\mathrm{iso}}| \geq |\delta_{xx} - \delta_{\mathrm{iso}}| \geq |\delta_{yy} - \delta_{\mathrm{iso}}|,$$

$$\delta_{\mathrm{iso}} = \tfrac{1}{3}(\delta_{zz} + \delta_{xx} + \delta_{yy}),$$

$$\Delta = \delta_{zz} - \delta_{\mathrm{iso}},$$

$$\eta = \frac{\delta_{yy} - \delta_{xx}}{\Delta},$$

where δ_{xx}, δ_{yy}, and δ_{zz} are the principle components of the chemical shift tensor and δ_{iso} is the isotropic chemical shift. The magnitude of the CSA is Δ, and the asymmetry of the CSA is denoted by η.

4a.4 Results and Discussion

^{77}Se isotropic NMR spectra of the Te_xSe_{100-x} ($x = 0$ - 35) glasses are shown in Fig. 4a-1. The ^{77}Se NMR spectrum of glassy Se shows a single symmetric broad peak with $\delta_{\mathrm{iso}} \sim 870$ ppm, which can be unambiguously assigned to a Se–**Se**–Se environment [17,18]. The initial addition of Te gives rise to a new Se environment, which appears as a shoulder centered near $\delta_{\mathrm{iso}} \sim 750$ ppm. Progressive increase in the Te content results in an increase in the intensity of this shoulder as well as the appearance of a low-frequency tail centered near $\delta_{\mathrm{iso}} \sim 600$ ppm, which becomes prominent in Te-rich compositions ($x \geqslant 30$). These two isotropic [77]Se resonances can be assigned on the basis of a previous study by Bureau *et al.* [10] to Se–**Se**–Te and Te–**Se**–Te environments, respectively. Accordingly, the ^{77}Se isotropic NMR spectra were fitted with three Gaussian peaks to obtain the composition-dependent variation of the relative fractions for the three Se environments (Fig. 4a-1). The intensity, position and width of these peaks corresponding to the best fits are listed in Table 4a-1. The δ_{iso} for these Se environments display a nearly linear shift to lower frequency by ~ 100 ppm with the replacement of each Se nearest neighbor by a Te atom (Table 4a-1). This trend and the absolute values of [77]Se δ_{iso} are in qualitative agreement with those

Figure 4a-1 Experimental (black solid lines) and simulated (red dashed lines) ^{77}Se isotropic NMR spectra for Te$_x$Se$_{100-x}$ glasses. Individual simulation components for Se–**Se**–Se, Se–**Se**–Te and Te–**Se**–Te sites are denoted in blue, green and pink, respectively.

Table 4a-1 Simulation parameters for ^{77}Se isotropic NMR line shapes.

Glass composition	Se	Te$_{10}$Se$_{90}$	Te$_{20}$Se$_{80}$	Te$_{25}$Se$_{75}$	Te$_{30}$Se$_{70}$	Te$_{35}$Se$_{65}$
Se–**Se**–Se						
δ_{iso} (±10 ppm)	869	878	882	876	844	826
peak width (±10 ppm)	145	145	150	154	170	165
relative fraction (±5%)	100	81	65	56	48	39
Te–**Se**–Se						
δ_{iso} (±10 ppm)		778	777	755	720	700
peak width (±10 ppm)		170	180	185	178	170
relative fraction (±5%)		19	30	37	43	49
Te–**Se**–Te						
δ_{iso} (±10 ppm)			680	694	590	570
peak width (±10 ppm)			185	183	185	177
relative fraction (±5%)			5	7	9	12

reported in previous ^{77}Se MAS NMR studies of binary Se-Te and ternary Ge-Se-Te glasses as well as with the density functional theory based calculations of ^{77}Se NMR δ_{iso} of these Se environments in short Se-Te chain segments terminated by H atoms [10,19]. This trend was attributed in a previous study [19] to the increased shielding at the central Se site as the more electronegative Se atom pulls the large electron cloud from the nearest neighbor Te atoms towards itself. The relative area fractions of these three peaks yield the compositional evolution of the relative fractions of the Se–**Se**–Se, Se–**Se**–Te and Te–**Se**–Te Se environments (Table 4a-1). This variation is shown in Fig. 4a-2 and is compared to two different structural models, namely the chain crossing model and the random distribution model, to elucidate the bonding preference between Se and Te atoms in these glasses.

The chain crossing model assumes a perfectly homogeneous distribution of the Te atoms in the [Se,Te]$_n$ copolymeric chains such that the Te atoms are all separated by equal distance. On the other hand, the random distribution model assumes a random spatial distribution of Te atoms in the [Se,Te]$_n$ copolymeric chains such that there is no preference between the formation of heteropolar and homopolar bonds for either Se or Te [10]. It is clear from Fig. 4a-2 that the Se site speciation in these Te$_x$Se$_{100-x}$ glasses shows remarkable agreement with that expected from the random distribution model, which suggests an equal preference for Se (Te) atoms to form Se–Se (Te-Te) and Se–Te bonds. This result is in qualitative agreement with previous Raman and ^{77}Se MAS NMR spectroscopic studies that suggest a nearly random distribution of Se and Te atoms in the structure of these glasses [9,10]. However, it may be noted that these previous studies indicated some preference for heteropolar bonding, while the Se speciation results obtained in the present study suggest a perfectly random distribution within experimental error.
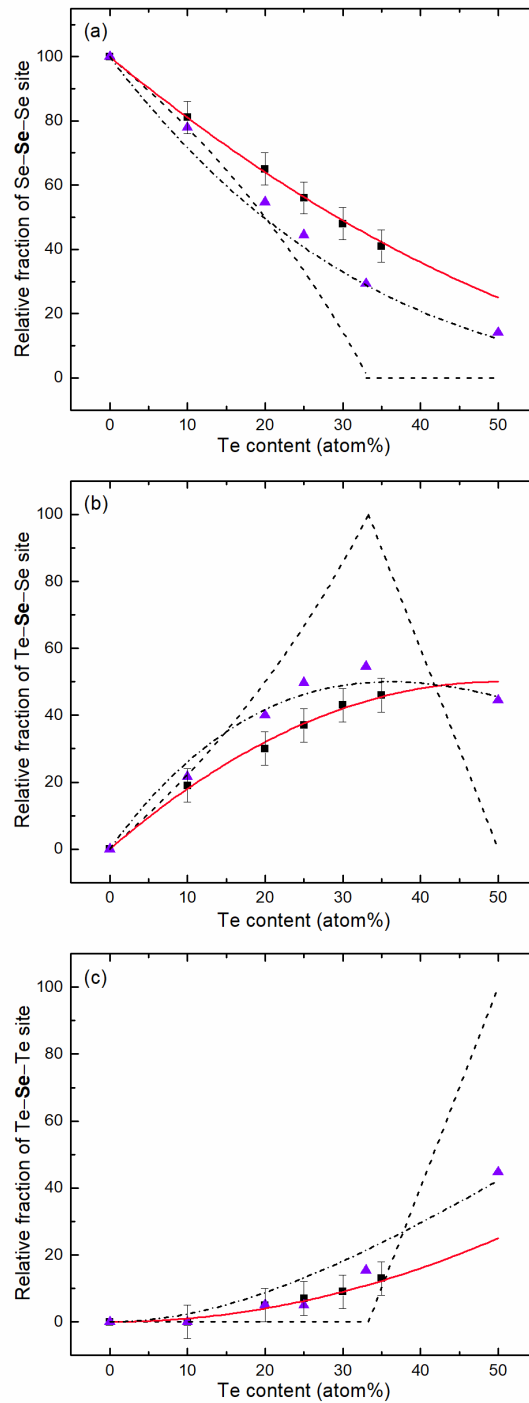
Figure 4a-2 Compositional variation of (a) Se–**Se**–Se, (b) Se–**Se**–Te and (c) Te–**Se**–Te site fractions obtained from simulations of ^{77}Se isotropic NMR spectra (black squares). Literature values from a previous ^{77}Se MAS NMR spectroscopic study (purple triangles) [10], chain crossing model (dashed black line), random distribution model (solid red line), and partially random distribution model with some preference for heteropolar bonding as reported in [10] (dashed dotted black line). Solid triangles are data from [10] as determined from ^{77}Se MAS NMR spectra.

86

The ^{125}Te isotropic NMR spectra of Te$_x$Se$_{100-x}$ glasses with $25 \leq x \leq 35$ are shown in Fig. 4a-3. The short T_2 relaxation time of ^{125}Te makes it practically impossible to obtain ^{125}Te MATPASS NMR spectra of glasses with $x \leq 25$. It is clear that compared to the ^{77}Se isotropic NMR spectra in Fig. 4a-1 the ^{125}Te spectral line shapes display poorer resolution and signal:noise ratio as the latter is severely broadened by the large chemical shift distribution that is characteristic of the ^{125}Te nuclide. However, similar to Se, one expects the Te atoms to be present in three different environments, namely Se–**Te**–Se, Te–**Te**–Se, and Te–**Te**–Te, consistent with the observation that none of the ^{125}Te isotropic NMR line shapes can be fitted well with a single Gaussian peak. Although attempts at simulation of these line shapes with three peaks corresponding to the three Te environments did not lead to unique solutions, the peak positions appear to be invariably located near $\delta_{iso} \sim$ 1100, 1300 and 1500 ppm. Previous ^{125}Te *pj*MATPASS/CPMG NMR studies of As-Te glasses suggest that the lowest frequency peak near 1100 ppm corresponds to the Te–**Te**–Te environment [13]. Consequently, the ^{125}Te δ_{iso} at $\sim$ 1300 and 1500 ppm can be assigned to the Te–**Te**–Se and Se–**Te**–Se environments (Fig. 4a-3). An example of such a fit is shown in Fig. 4a-3 where the relative areas of the three peaks were constrained to remain close to the expected random distribution. Despite the lower signal:noise ratio relative to the ^{77}Se spectra, the compositional evolution of the ^{125}Te isotropic NMR spectral line shapes is thus consistent with a random distribution of Te atoms in the glass structure. It is interesting to note here that the ^{77}Se and ^{125}Te δ_{iso} for the isostructural nearest-neighbor environments of Se and Te atoms are approximately linearly correlated according to the relation: $\delta_{iso}(^{125}\text{Te})_{ppm} = 1.75* \delta_{iso}(^{77}\text{Se})_{ppm}$. Such linear relationships were also reported in previous NMR studies of organoselenium and organotellurium compounds as well as of polychalcogenide anions [20].
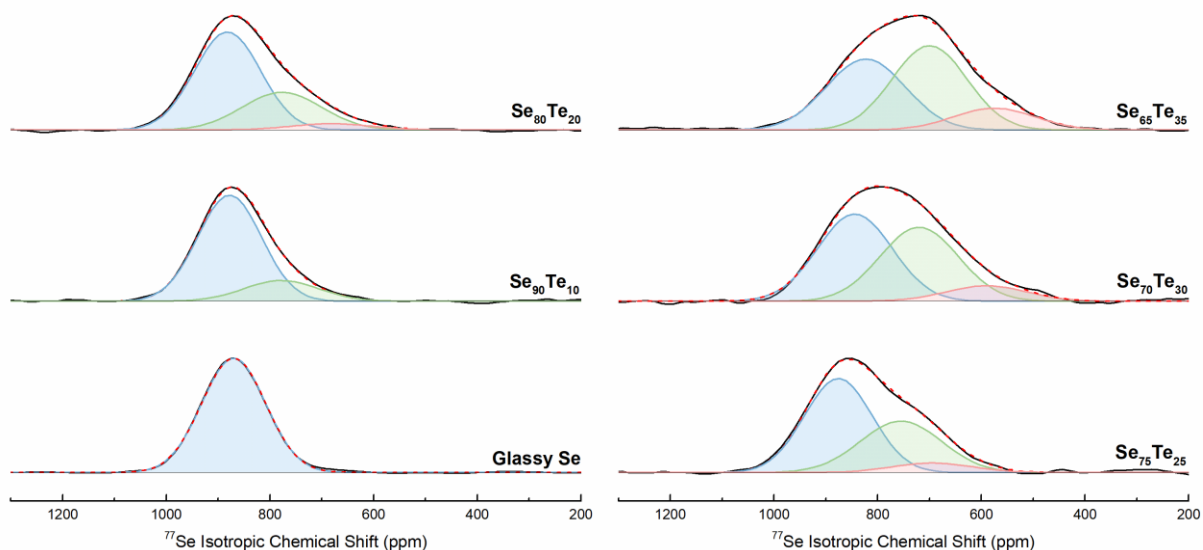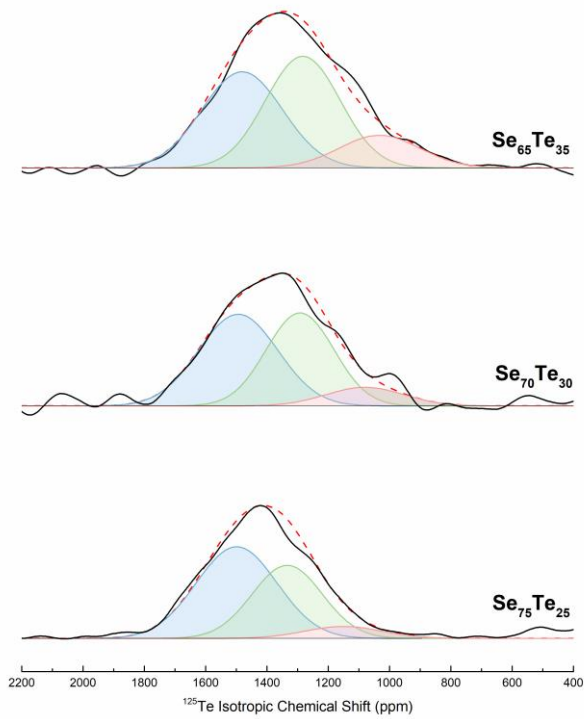
Figure 4a-3 Experimental (black solid lines) and simulated (orange dashed lines) ^{125}Te isotropic NMR spectra for Te$_x$Se$_{100-x}$ glasses. Individual simulation components for Se–**Te**–Se, Se–**Te**–Te and Te–**Te**–Te sites are denoted in blue, green and pink, respectively.
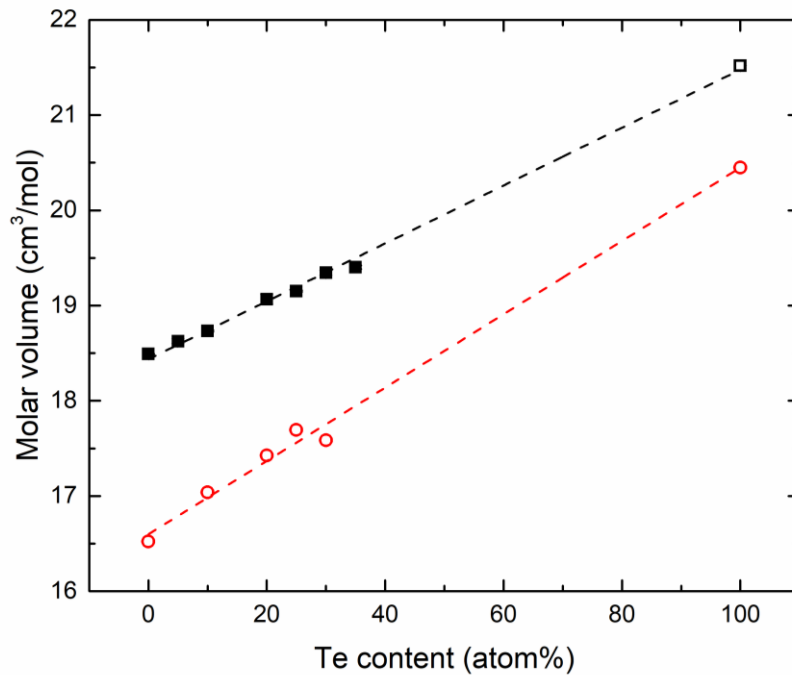
Figure 4a-4 Molar volume of Te$_x$Se$_{100-x}$ bulk glasses (filled squares) and crystals (open circles). Straight lines represent the linear least squares fit to the experimental data. The molar volume for amorphous Te film (open square) is from [21], while the data for the crystals are from [22].

The molar volume of these Te_xSe_{100-x} glasses displays a linear increase with increasing Te content (Fig. 4a-4). An extrapolation of this trend to pure Te shows good agreement with the experimental molar volume of amorphous Te film, as reported in a previous study by Ichikawa [21]. This molar volume trend of Te_xSe_{100-x} glasses is nearly parallel with that of crystalline Te_xSe_{100-x} solid solutions [22]. X-ray diffraction analysis of these crystalline alloys have been shown to be consistent with Se and Te atoms forming copolymeric $[Se,Te]_n$ chains [23]. Therefore, the similar linear compositional variation of the molar volumes of Te_xSe_{100-x} glasses in Fig. 4a-4 may be interpreted to be indicative of the presence of similar $[Se,Te]_n$ chains in the amorphous state. This structural scenario is in clear agreement with the NMR results discussed above.

Further insights into the bonding environments in these glasses can be obtained from a consideration of the CSA parameters. Unfortunately, Δ and η for the different Se and Te sites cannot be readily isolated due to substantial overlap of the isotropic resonances for the different environments, which is particularly severe for the ^{125}Te spectral line shapes (Fig. 4a-3). However, for the ^{77}Se NMR spectra, we have analyzed the anisotropic spectral slices taken at the δ_{iso} for the Se-**Se**-Te and Te-**Se**-Te sites where the overlap from the neighboring peaks is minimal. The spinning sideband intensities of these anisotropic spectra and their simulations are shown in Fig. 4a-5. The average η for the Se–**Se**–Te and Te–**Se**–Te sites do not show significant variation and vary between and 0.75 to 0.90. However, the Δ for these two sites (−180 ppm) is significantly higher than that (−150 ppm) reported in a previous study[18] for the Se-**Se**-Se site in glassy Se. Moreover, the Δ values for the Se-**Se**-Se sites decreases systematically from −150 to −170 ppm as δ_{iso} decreases from ~ 880 to 825 ppm, with increasing Te content (Fig. 4a-6). It is interesting to note that similar trends were also reported in the literature for the Ge-Se system and were ascribed to the replacement of Se with Ge as next-nearest neighbors with progressive addition of Ge [24].

Therefore, it is tempting to speculate that Te has a similar effect on the Δ and δ_{iso} of the Se nuclides in the Se–**Se**–Se sites. This hypothesis is indeed consistent with the DFT based calculations reported in a previous study that indicated a lowering of the ^{77}Se δ_{iso} of the Se-**Se**-Se site by 30 ppm as a Se next-nearest neighbor is replaced by a Te atom [19].
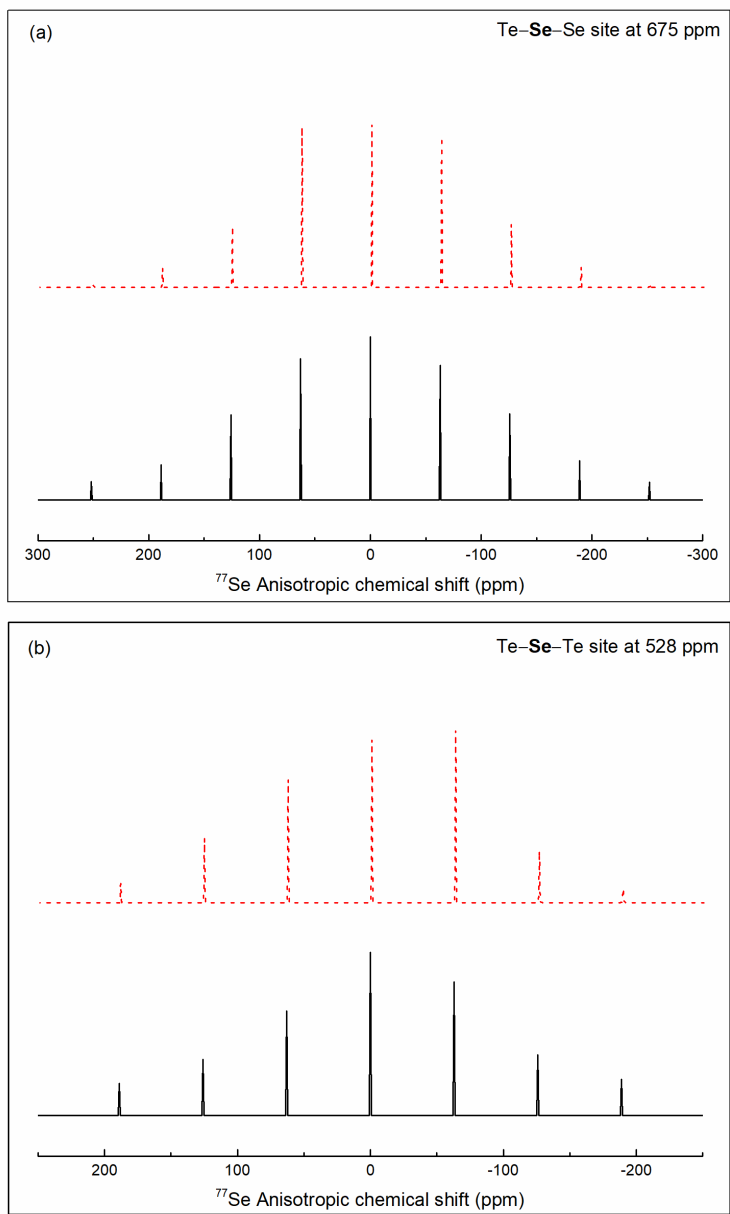
Figure 4a-5 Representative experimental ^{77}Se NMR anisotropic spinning sideband intensities (solid lines) for (a) Se–**Se**–Te and (b) Te–**Se**–Te sites in Te$_x$Se$_{100-x}$ glasses. Anisotropic slices for these three sites are taken at δ_{iso} = 675 and 528 ppm, respectively. Corresponding simulations are shown as dashed lines.
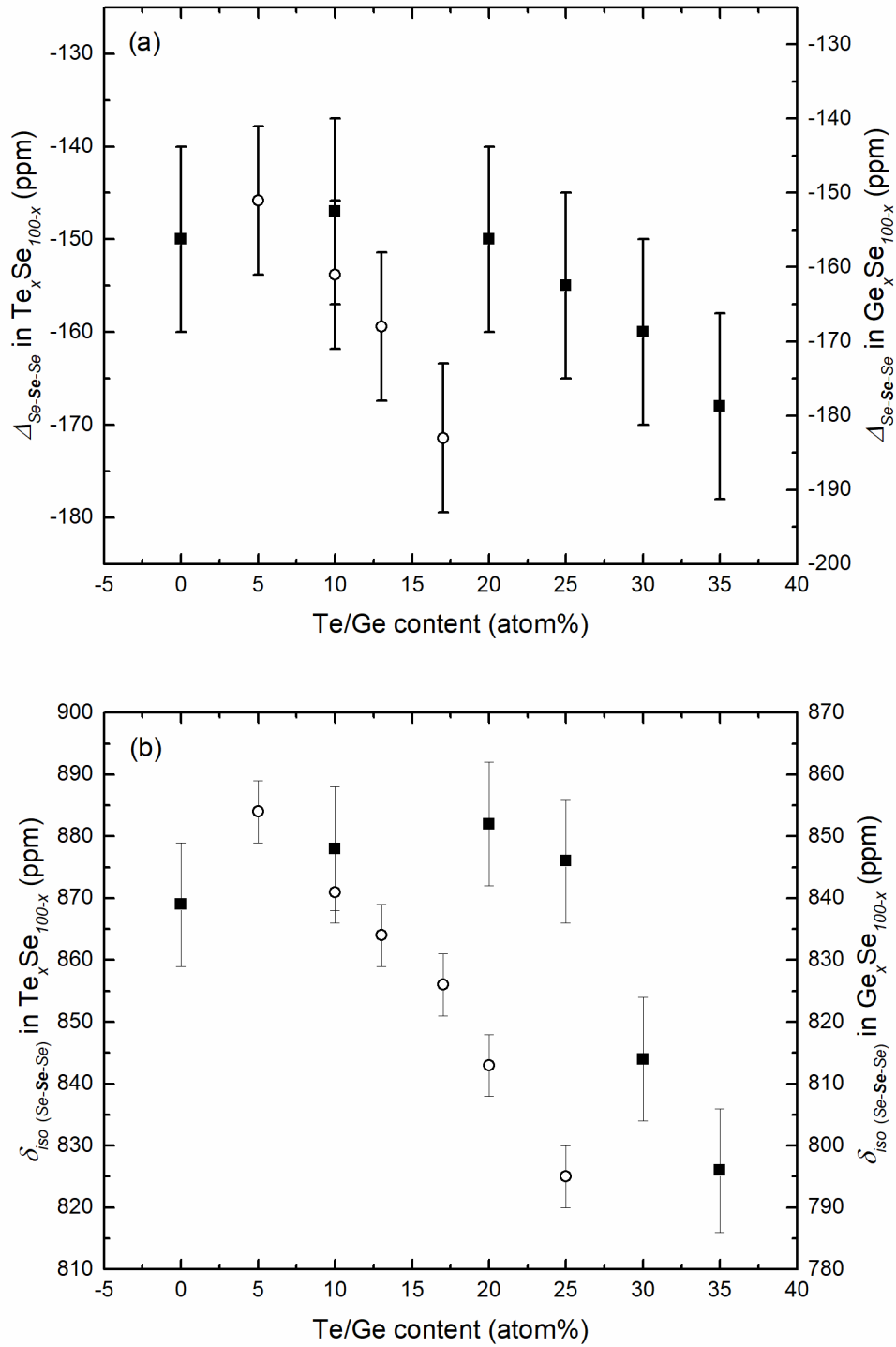
Figure 4a-6 Compositional variation of average ^{77}Se (a) Δ and (b) δ_{iso} for Se–**Se**–Se sites in Te$_x$Se$_{100-x}$ glasses (filled squares). Corresponding variation in Ge$_x$Se$_{100-x}$ glasses (open circles), taken from a previous study [24] is shown for comparison.

4a.5 Conclusion

^{77}Se and ^{125}Te 2D MATPASS/CPMG NMR spectroscopy can provide increased site resolution by separating and correlating the isotropic and the anisotropic chemical shift in two dimensions. The ^{77}Se isotropic NMR spectra allows for the identification of three different Se environments, namely Se–**Se**–Se, Se–**Se**–Te and Te–**Se**–Te sites. The compositional variation of the relative fractions of these sites suggest a completely random distribution of Se and Te atoms in [Se,Te]$_n$ copolymeric chains. Such finding is also consistent with the compositional variation of the molar volumes of these glasses. Moreover, the ^{125}Te isotropic NMR spectral line shapes can be reconstructed by three different Te sites, namely Te–**Te**–Te, Te–**Te**–Se and Se–**Te**–Se sites, with consistent δ_{iso} and peak area ratios constrained by the random distribution model, which indirectly confirms the ^{77}Se NMR results. Further insights into the local bonding environments are provided by the ^{77}Se CSA parameters of all Se sites. The ^{77}Se (^{125}Te) δ_{iso} values vary linearly with the number of nearest-neighbor Te (Se) atoms. Additionally, the ^{77}Se and ^{125}Te δ_{iso} for isostructural nearest-neighbor environments of Se and Te atoms are found to be linearly correlated. The systematic dependence of $\varDelta$ and δ_{iso} of the Se–**Se**–Se site with Te concentration can be attributed to the appearance of Te atoms as next-nearest neighbors.

Acknowledgement

References

[1]   P.A. Vermeulen, J. Momand, B.J. Kooi, Reversible amorphous-crystalline phase changes in a wide range of $Se_{1-x}Te_x$ alloys studied using ultrafast differential scanning calorimetry, J. Chem. Phys. 141 (2014) 024502.

[2]   M. Wuttig, N. Yamada, Phase-change materials for rewriteable data storage, Nat. Mater. 6 (2007) 824.

[3]   B. Bureau, X.H. Zhang, F. Smektala, J.L. Adam, J. Troles, H.L. Ma, C. Boussard-Plèdel, J. Lucas, P. Lucas, D. Le Coq, M.R. Riley, J.H. Simmons, Recent advances in chalcogenide glasses, J. Non. Cryst. Solids. 345&346 (2004) 276–283.

[4]   G. Lucovsky, A. Mooradian, W. Taylor, G.B. Wright, R.C. Keezer, Identification of the fundamental vibrational modes of trigonal, α-monoclinic and amorphous selenium, Solid State Commun. 5 (1967) 113–117.

[5]   E. Grison, Studies on tellurium-selenium alloys, J. Chem. Phys. 19 (1951) 1109–1113.

[6]   A. Zakery, S.R. Elliott, Optical properties and applications of chalcogenide glasses: a review, J. Non. Cryst. Solids. 330 (2003) 1–12.

[7]   M. Popescu, Non-Crystalline Chalcogenides, Kluwer Academic Publishers, 2002.

[8]   K. Itoh, Structure of Se-Te glasses studied using neutron, X-ray diffraction and reverse Monte Carlo modelling, J. Solid State Chem. 246 (2017) 372–378.

[9]   A. Tverjanovich, A. Cuisset, D. Fontanari, E. Bychkov, Structure of Se-Te glasses by Raman spectroscopy and DFT modeling, J. Am. Ceram. Soc. 101 (2018) 5188–5197.

[10]   B. Bureau, C. Boussard-plèdel, M. Lefloch, J. Troles, J. Lucas, D. Rennes, D. Beaulieu, Selenium-Tellurium Sequences in Binary Glasses as Depicted by ^{77}Se and [125]Te NMR, J. Phys. Chem. B. 109 (2005) 6130–6135.

[11]   I. Hung, T. Edwards, S. Sen, Z. Gan, MATPASS/CPMG: A sensitivity enhanced magic-angle spinning sideband separation experiment for disordered solids, J. Magn. Reson. 221 (2012) 103–109.

[12]   D.J. States, R.A. Haberkorn, D.J. Ruben, A 2D Nuclear Overhauser Experiment with pure absorption phase in four quadrants, J. Magn. Reson. 48 (1982) 286–292.

[13]   D.C. Kaseman, I. Hung, K. Lee, K. Kovnir, Z. Gan, B. Aitken, S. Sen, Tellurium speciation, connectivity, and chemical order in As_xTe_{100-x} glasses: Results from two-dimensional [125]Te NMR spectroscopy, J. Phys. Chem. B. 119 (2015) 2081–2088.

[14]   D. Massiot, F. Fayon, M. Capron, I. King, S. Le Calvé, B. Alonso, J.O. Durand, B. Bujoli, Z. Gan, G. Hoatson, Modelling one- and two-dimensional solid-state NMR spectra, Magn. Reson. Chem. 40 (2002) 70–76.

[15]   R.K. Harris, E.D. Becker, S.M. Cabral De Menezes, R. Goodfellow, P. Granger, NMR nomenclature: Nuclear spin properties and conventions for chemical shifts (IUPAC recommendations 2001), Pure Appl. Chem. 73 (2001) 1795–1818.

[16] U. Haeberlen, High Resolution NMR in Solids Selective Averaging: Supplement 1 Advances in Magnetic Resonance, Elsevier, 2012.

[17] B. Bureau, J. Troles, M. Le Floch, F. Smektala, J. Lucas, Medium range order studied in selenide glasses by ^{77}Se NMR, J. Non. Cryst. Solids. 326&327 (2003) 58–63.

[18] M. Marple, J. Badger, I. Hung, Z. Gan, K. Kovnir, S. Sen, Structure of Amorphous Selenium by 2D ^{77}Se NMR Spectroscopy: An End to the Dilemma of Chain versus Ring, Angew. Chemie. 129 (2017) 9909–9913.

[19] L. Bouëssel Du Bourg, C. Roiland, L. Le Pollès, M. Deschamps, C. Boussard-Plédel, B. Bureau, C.J. Pickard, E. Furet, Impact of Te on the structure and ^{77}Se NMR spectra of Se-rich Ge-Te-Se glasses: a combined experimental and computational investigation, Phys. Chem. Chem. Phys. 17 (2015) 29020–29026.

[20] M. Björgvinsson, G.J. Schrobilgen, Homo-and Heteropolychalcogenide Anions Ch^{2-} HCh^-, Ch_2^{2-}, Ch_3^{2-} and Ch_4^{2-} (Ch = Se and/or Te): Solution ^{1}H, ^{77}Se, [123]Te, and [125]Te NMR study, Inorg. Chem. 30 (1991) 2540–2547.

[21] T. Ichikawa, Electron Diffraction Study of the Local Atomic Arrangement in Amorphous Tellurium Films, Phys. Stat. Sol. (B) 56 (1973) 707-715.

[22] G.C. Das, M.B. Bever, D.R. Uhlmann, S.C. Moss, Relaxation phenomena in selenium-tellurium alloys, J. Non. Cryst. Solids. 7 (1972) 251-270.

[23] E. Grison, Studies on tellurium-selenium alloys, J. Chem. Phys. 19 (1951) 1109-1113.

[24] D.C. Kaseman, I. Hung, Z. Gan, S. Sen, Observation of a Continuous Random Network Structure in Ge_xSe_{100-x} Glasses: Results from High-Resolution ^{77}Se MATPASS/CPMG NMR Spectroscopy, J. Phys. Chem. B. 117 (2013) 949–954.

Chapter 4b

Rheology of Supercooled Se-Te Chain Liquids: Role of Te as an

Interchain Cross-linker

4b.1 Abstract

The shear relaxation behavior of supercooled Se_xTe_{100-x} ($70 \leq x \leq 95$) liquids are studied using oscillatory parallel plate rheometry. The difference in the relaxation timescales of the slow bond scission/renewal dynamics and the fast segmental chain motion that coexist in Se decreases monotonically with progressive addition of Te, until only one relaxation process can be identified in the $Se_{70}Te_{30}$ liquid. This evolution of the relaxation dynamics mimics the rheological behavior of Ge/As-Se liquids, when traditional chain crosslinkers such as Ge/As is added to Se. This finding suggests that the Te atoms serve as pseudo-crosslinkers via secondary bonding interactions between adjacent $[Se,Te]_n$ chains. This interchain interaction results in a lowering of the motional degrees of freedom of the constituent chains in Se_xTe_{100-x} liquids in the supercooled region. However, the compositional invariance of the superliquidus viscosity of these liquids suggests that the interchain interaction constraint can be lifted at high temperatures.

4b.2 Introduction

Selenium (Se) and tellurium (Te) are isoelectronic chalcogens with strong structural similarities. The structure of stable crystalline polymorphs of Se and Te consist of polymeric $[Se]_n$ or $[Te]_n$ helical chains, where Se and Te atoms are twofold coordinated and form lattices with trigonal and hexagonal symmetry, respectively [1,2]. In addition, Se can also exist as a metatstable monoclinic allotrope that consists of Se_8 rings [1]. On the other hand, recent high-resolution ^{77}Se NMR spectroscopic results have shown that amorphous Se derived via melt-quenching consists practically solely of $[Se]_n$ chains, as no Se in the ring environment could be detected [3].

However, in spite of their structural similarities, Se and Te exhibit rather different glass forming abilities [4,5]. Se forms bulk glass rather easily upon quenching of the parent melt, while Te displays a strong tendency for crystallization upon supercooling and, therefore, forms glass only in the form of thin films. This behavior of Te is believed to result from strong secondary bonding interactions (SBI) between adjacent $[Te]_n$ chains. The SBIs between the neighboring Te atoms in adjacent chains are thought to result from the overlap between the Te 5p electron lone pair in one chain and the empty antibonding σ* orbital of Te in an adjacent chain, and such interactions can become as strong as the primary covalent Te-Te bonds within a chain [6]. These interactions involving delocalization of Te 5p electrons are also believed to be responsible for its higher metallicity compared to S or Se as well as the metallic character of liquid Te [6–10]. Another possible explanation for the metallic behavior of liquid Te is the shortening of $[Te]_n$ chains resulting from bond dissociation at high temperatures. This process can lead to an increased density of unpaired electrons associated with the Te atoms at the chains terminations and electron hopping between the short chain segments [11,12].

Although the crystalline structures of Se and Te share strong similarities, the coordination number of Te in the liquid phase has been debated for a long time. Previous studies based on neutron diffraction suggested Te to be present in both twofold and threefold coordination with an average coordination number of ~ 2.5 [13–16]. On the other hand, Silva and Cutler claimed on the basis of optical spectroscopic studies that Te exists in twofold coordination in liquid Se-Te alloys with up to 80% Te [11]. The bonding environment and the electronic interaction scenario for Te is clear in its crystalline state [6]. However, such understanding is still lacking for amorphous Te and tellurides, and could be crucial in building structure-property relationships in, for example, the Ge-Sb-Te phase change materials that are utilized in optical memory technology [17]. Binary Se-Te glasses constitute an interesting model system in this regard for the investigation of the SBI associated with Te atoms as glasses in this system are characterized by relatively simple blended copolymer $[Se,Te]_n$ chains of twofold coordinated Se and Te atoms [18–20]. Here we report the results of a rheological study of supercooled binary Se-Te liquids to demonstrate that the existence of such SBIs is clearly manifested in the viscoelastic relaxation behavior of these liquids. The proposed structural rationalization is found to be consistent with the compositional variation of the viscosity and the glass transition temperature T_g.

4b.3 Experimental Methods

4b.3.1 Sample Preparation and physical characterization

Binary Se_xTe_{100-x} glasses with $x = 95$, 90, 80, and 70 were prepared in ~14 g batches from constituent elements using the conventional melt-quench method in evacuated fused quartz ampoules (6mm inner diameter). Mixtures of Se (Alfa Aesar, 99.999%) and Te (Alfa Aesar, 99.9999%) were taken in fused quartz ampoules that were evacuated (10^{-4} Torr) and flame sealed

prior to loading into a rocking furnace. The ampoules were heated to 873 K over a period of 11 hours and subsequently held at this temperature for 12 hours to ensure homogeneity. The ampoules were then quenched in ice-water to obtain the glass samples.

All Se_xTe_{100-x} glasses were chemically analyzed using a Cameca SE-100 electron microprobe equipped with wavelength dispersive spectrometers to check for possible micron-scale phase separation. All glasses were found to be chemically homogeneous at the micron-scale and their compositions were within ±0.5 at% of nominal. The glass transition temperature T_g was measured using a differential scanning calorimeter (Mettler-Toledo DSC1). Approximately 20 mg powdered glass sample was hermetically sealed in a 40 µL aluminum pan. Scans were taken in a flowing nitrogen environment with a heating rate of 20 K/min. T_g was determined to within ± 2 °C as the onset of the glass transition.

4b.3.2 Parallel Plate Rheometry

Small amplitude oscillatory shear (SAOS) rheological measurements on the Se_xTe_{100-x} supercooled liquids were carried out in a flowing Ar gas atmosphere using an Anton-Paar MCR92 parallel plate rheometer. The rheometer was operated under oscillatory mode with an 8 mm upper plate and a stationary lower plate with a gap of ~ 1 mm. Before the rheometry measurements, all samples were heated above their softening point, pressed and then trimmed to form a sandwich-like geometry between the plates. During each measurement, the samples were allowed to equilibrate at each temperature for 5 minutes, followed by the application of oscillatory strain with angular frequency ω varying between 1 and 600 rad/s within the linear viscoelastic range of the material and concomitantly the torque was measured to calculate the storage and the loss moduli G´ and G″ as a function of ω. Multiple measurements were carried out at multiple temperatures

for each sample and master curves of G′(ω) and G″(ω) were constructed using time-temperature superposition (TTS). The viscosity master curves were then calculated from the relation $\eta(\omega) = \frac{\sqrt{G'^2 + G''^2}}{\omega}$. Details of the experimental setup and procedure can be found in a previous publication [21]. The Se_xTe_{100-x} glasses become increasingly susceptible to surface crystallization as the Te content increases. Therefore, fresh samples were used for rheological measurements at each temperature to avoid thermal cycling and each measurement was repeated on multiple samples to ensure reproducibility. The physical appearance of the samples was checked immediately after the end of each measurement, which indicated the lack of any discernible surface crystallization.

4b.4 Results and Discussion

The ω dependence of the storage modulus G′ and the loss modulus G″ of the Se_xTe_{100-x} supercooled liquids is shown in Fig. 4b-1 in the form of master curves after performing TTS to the raw data at a nearly iso-viscous (~ 10^7 Pa.s) temperature. At low frequencies, in the terminal regime, all liquids display G′ < G″ and a Maxwellian viscoelastic behavior with G′ ~ ω^2 and G″~ ω. On the other hand, at the highest frequencies G′ reaches a plateau which represents the high-frequency glassy shear modulus of the liquid, which is on the order of a few GPa. At this point the glass-forming liquids display a completely elastic behavior. The corresponding frequency-dependent viscosity $\eta(\eta) = \frac{\sqrt{G'^2 + G''^2}}{\omega}$ data in Fig. 4b-1 clearly demonstrate the expected rapid frequency-dependent drop in viscosity in this regime with increasing ω. More interestingly, G′ displays another plateau region at intermediate frequencies, marking the first onset of frequency dependence of η (Fig. 4b-1). This plateau is most prominent in pure Se and $Se_{95}Te_5$ liquids and still remains observable for the $Se_{90}Te_{10}$ liquid, while it is apparently absent in liquids with ≥20%
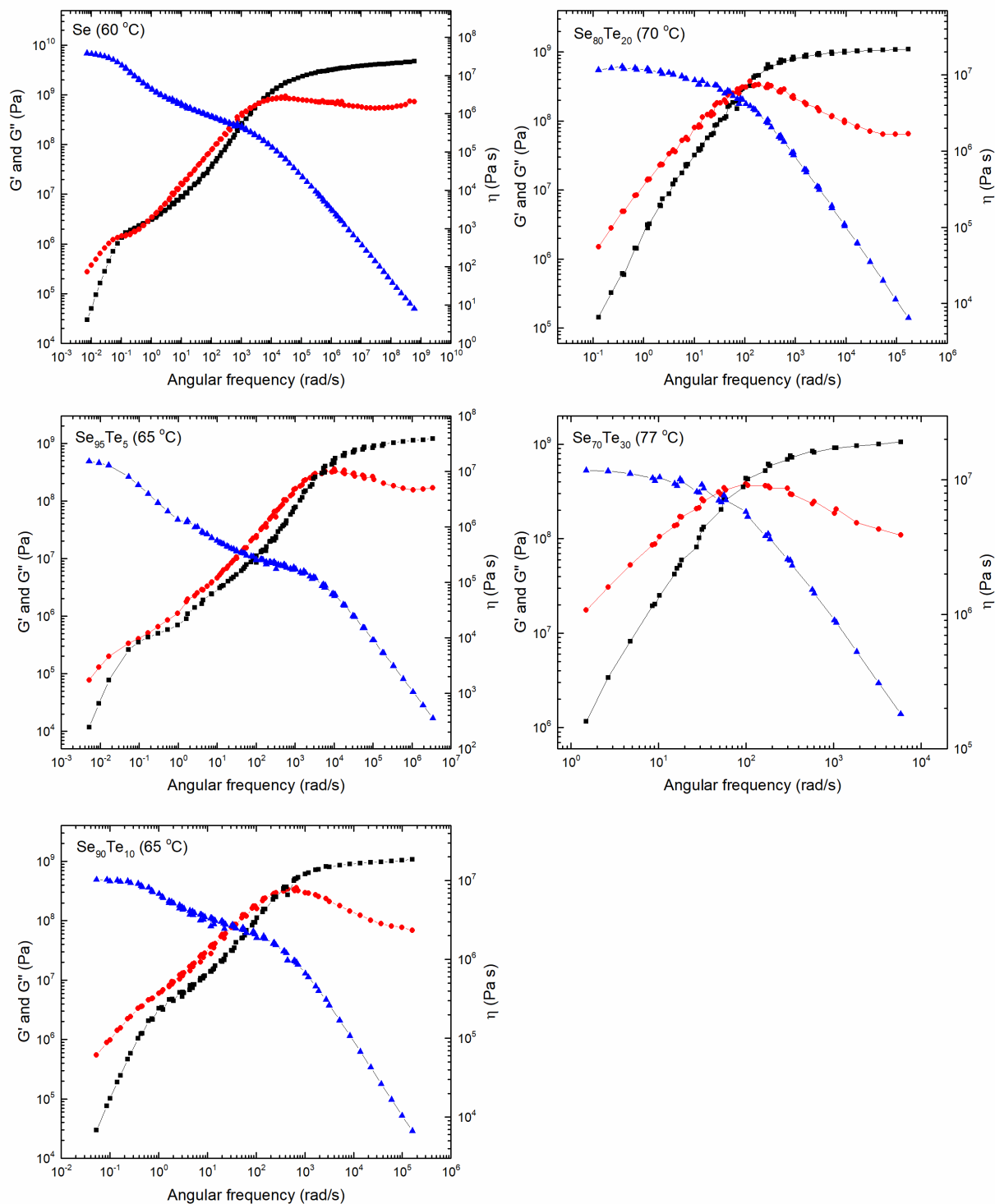
Figure 4b-1 Master curves of the frequency dependence of storage modulus G′ (black squares), loss modulus G″ (red circles), and viscosity (blue triangles) of Se_xTe_{100-x} liquids. The composition and the reference temperatures for TTS are listed in the inset of each panel. Data for pure Se are shown for comparison and are taken from Zhu *et al.* [22].

Te (Fig. 4b-1). Additionally, the low-frequency plateau modulus increases and the frequency separation between the two plateaus decreases with progressive addition of Te. Recent studies have reported a similar compositional evolution of $G'(\omega)$ and $G''(\omega)$ in As-Se and Ge-Se liquids as As or Ge is progressively added to Se. It was shown in these studies that the two plateaus in $G'(\omega)$ represent the existence of two relaxation processes with widely different timescales and relaxation moduli. The slow and the fast processes associated with the low- and high- frequency plateaus were found to correspond to Se-Se bond scission/renewal and Se chain segmental motion, respectively [22,23]. The fast process involving Se chain motion disappears on progressive addition of Ge or As to Se, due to the shortening of the chain segments as the chains are cross-linked to form a rigid three-dimensional network. It was found that Se chain segments shorter than ~ 3 to 5 Se atoms could not sustain the segmental motion as a pathway for shear relaxation [24].

Previous structural investigations using Raman and [77]Se nuclear magnetic resonance spectroscopy indicated that the Se_xTe_{100-x} binary glasses consist of $[Se,Te]_n$ chains [18–20] with nearly random distribution of Se and Te atoms in the chains. Therefore, it is reasonable to assume that, similar to Se, all Se_xTe_{100-x} liquids would also exhibit two relaxation processes: segmental chain motion and bond scission/renewal dynamics. However, as noted above, the evolution of the $G'(\omega)$ and $G''(\omega)$ spectra of these liquids with progressive addition of Te mimics that observed when known cross-linkers such as Ge or As are added to Se. The rheological data in Fig. 4b-1 suggest that, while Se-rich compositions ($90 \leqslant x \leqslant 100$) have two distinct relaxation processes, further addition of Te results in a single relaxation process characteristic of network liquids.

Additional insight regarding the timescale distribution for these two relaxation processes can be gained from the corresponding relaxation spectrum H(τ), which can be calculated following Ninomiya and Ferry's method [25]:

$$H(\tau) = \frac{G'(a\omega) - G'(\omega/a)}{2 \ln a} - \frac{a^2}{(a^2 - 1)^2} \frac{G'(a^2\omega) - G'(\omega/a^2) - 2G'(a\omega) + 2G'(\omega/a)}{2 \ln a} \Bigg|_{1/\omega = \tau}$$

where a is the frequency increment on a logarithmic scale of the measurement. The H(τ) master curves for all compositions are shown in Fig. 4b-2. The two peaks in H(τ) correspond to the most probable relaxation times for the two processes (Fig. 4b-1). The presence of two relaxation processes can now be discerned even in the case of the $Se_{80}Te_{20}$ liquid (Fig. 4b-2). It is evident from Fig. 4b-2 that the slow process displays a rather narrow and symmetric Debye-type distribution of relaxation times, as would be intuitively expected for bond breaking dynamics, while the fast process is characterized by a much broader distribution of relaxation times. The relaxation strength of the slow process is significantly weaker, as bond scission/renewal events at any instant in the structure are expected to be few and spatially far between. On the other hand, the strength of the fast process is greater, and its broad time distribution is consistent with the widespread cooperative segmental motion of the chain moieties. Moreover, the temporal coupling between the two relaxation processes increases with increasing Te content, as the two peaks move closer to each other at a similar viscosity level until only one relaxation process can be seen in the highest Te containing $Se_{70}Te_{30}$ liquid (Fig. 4b-2).

Simulation of these timescale distributions with Gaussian peaks (Fig. 4b-2) indicates that the full-width-at-half-maximum (FWHM) of the distribution for the slow bond-breaking process is compositionally invariant (FWHM ~ 0.55 log units), except for pure Se, where it is narrower (FWHM ~ 0.35 log units). This result is possibly indicative of the fact that bond scission in Se-Te
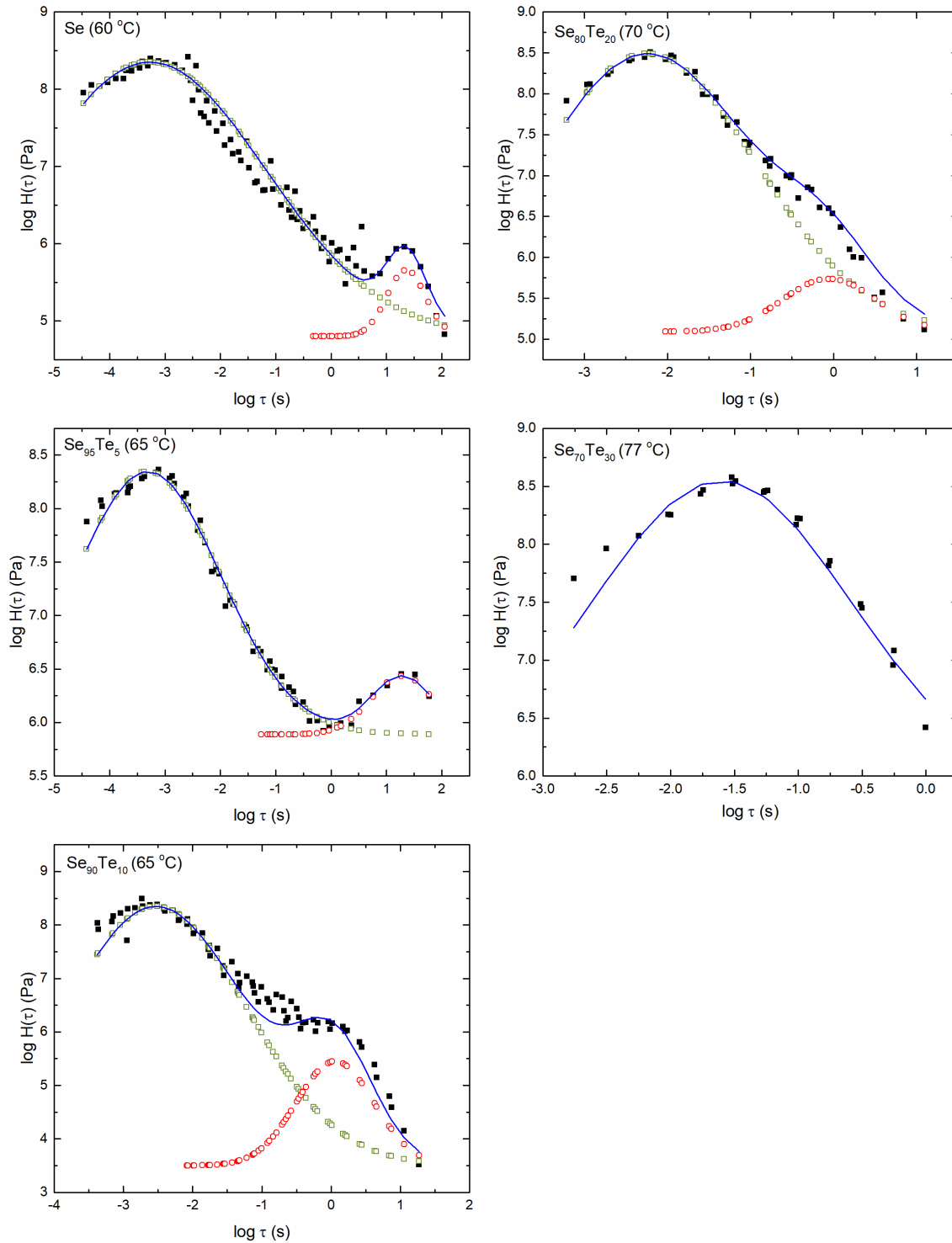
Figure 4b-2 Relaxation spectra H(τ) of Se_xTe_{100-x} liquids. Filled black squares represent the experimental data. Open green squares and red circles are Gaussian components fitted to the fast and slow process, respectively. Solid lines represent the sum of the two components, i.e., total fit to the experimental data. Data for the H(τ) spectrum of pure Se is taken from Zhu *et al.* [22].

alloys involves three different bond types, namely Se-Se, Se-Te and Te-Te, as well as the secondary bonds involving Te atoms, while pure Se has only Se-Se bonds. On the other hand, the timescale distribution for the fast process is the widest for pure Se (FWHM ~ 2 log units) and it decreases upon initial addition of Te (FWHM ~ 1.3 log units), beyond which it remains nearly constant until it decreases again in the $Se_{70}Te_{30}$ liquid, where only one relaxation process is observed (Fig. 4b-2). When taken together, these results are consistent with a scenario where addition of Te to Se results in a strong SBI between chains, which effectively acts as pseudo-crosslinking (Fig. 4b-3) with Te atoms serving as nodes that connect mobile selenium chain segments. Therefore, the SBI reduces the flexibility of the $[Se,Te]_n$ chains with progressive addition of Te atoms. Consequently, segmental chain motion becomes more difficult compared to that in pure Se and eventually culminates in bond scission. Thus, as evidenced in Figs 4b-1 and 2, the two relaxation processes become increasingly temporally coupled with addition of Te, until only a single relaxation process is observed at the highest Te content. This pseudo crosslinking effect would be expected to result in a more rigid structure in binary Se_xTe_{100-x} glasses compared to that for pure Se. This hypothesis is indeed consistent with the observation that the T_g of Se_xTe_{100-x} glasses increases nearly linearly with Te content in this composition range (Fig. 4b-4). Moreover, the increased rigidity of the structure is also evident in the temperature dependence of the viscosity of Se_xTe_{100-x} liquids determined in the present study as well as the viscosity data reported in the literature [26–29], which show a monotonic increase in isothermal viscosity with increasing Te content (Fig. 4b-5). It may be noted here that the SBI between $[Se,Te]_n$ chains introduced by Te is likely weaker than the primary bonds introduced by conventional cross-linkers such as As/Ge, but significantly stronger than, for example, van der Waals interactions. In fact, the typical interatomic distance associated with the SBI is found to be somewhere intermediate between the characteristic
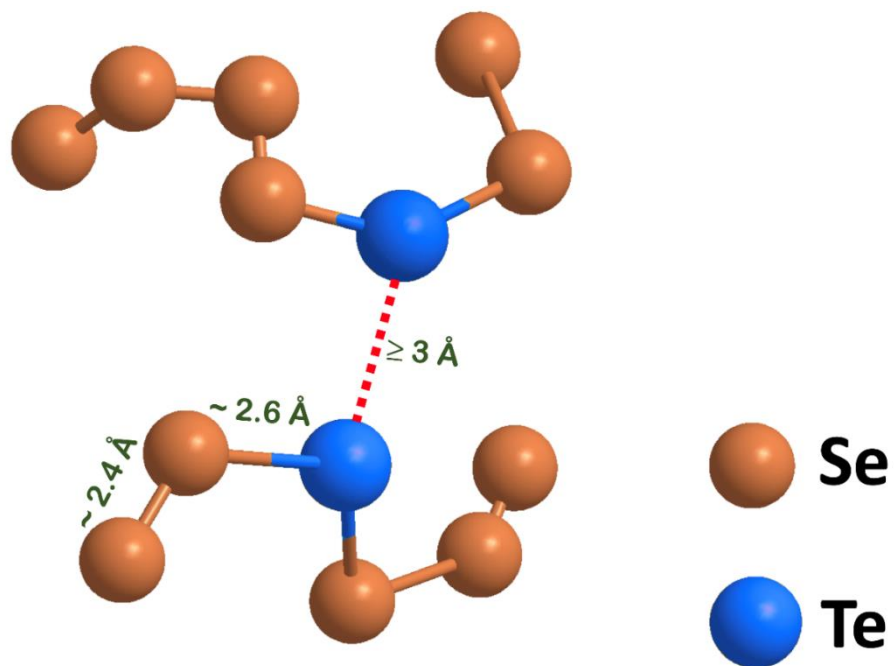
Figure 4b-3 Cartoon showing SBI (dashed red line) between Te atoms in adjacent $[Se,Te]_n$ chain segments in the binary Se-Te system.
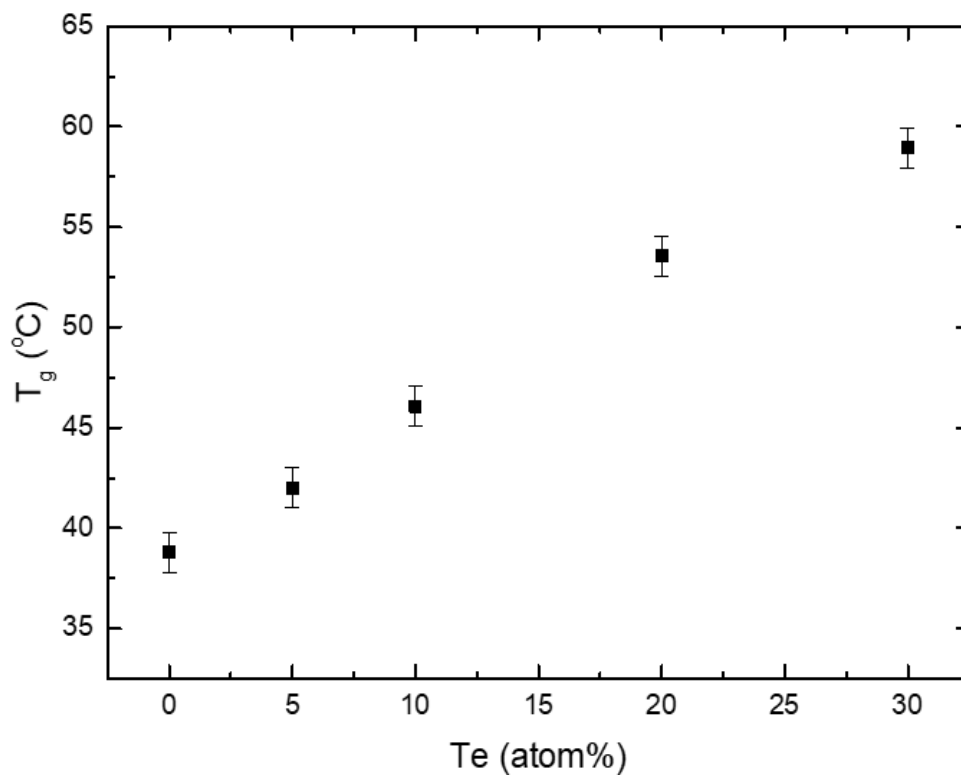
Figure 4b-4 Glass transition temperature T_g of binary Se_xTe_{100-x} glasses.

values for covalent bonding and for van der Waals interactions. For example, typical Te-Te covalent bond length is ~ 2.7-2.8 Å while, the Te-Te SBI distance is ≥3.0 Å [6]. Therefore, the presence of the SBI in Se_xTe_{100-x} glasses or liquids is not in any way indicative of an increased coordination number of Te atoms. Consequently, unlike the network formed with As/Ge-Se, the chain elements are retained in Se-Te. Therefore, the SBI-related constraints will likely be lifted at high temperature and the dynamical behavior of $[Se,Te]_n$ chains would become quite similar to those characteristic of $[Se]_n$ chains. This scenario is in agreement with the high-temperature viscosity data for Se_xTe_{100-x} liquids, which show compositional invariance over a relatively wide range of viscosity in the superliquidus region (Fig. 4b-5).
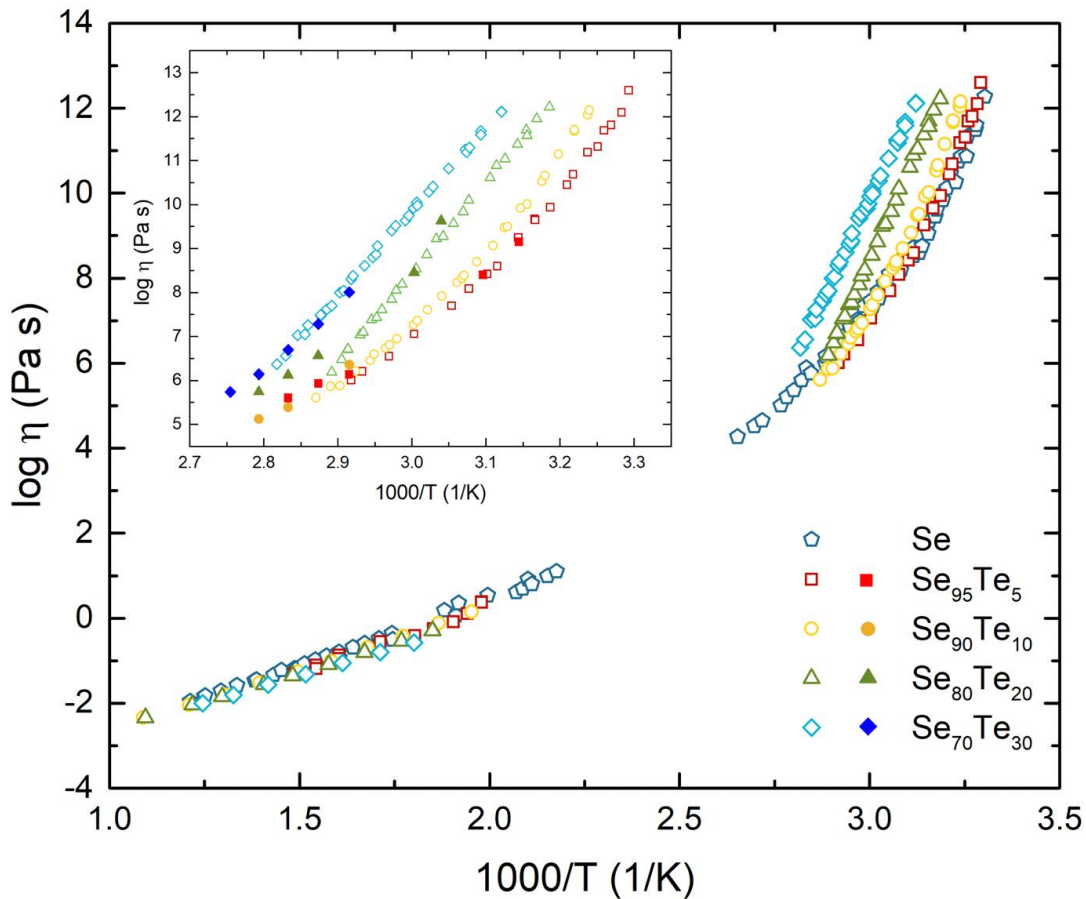
Figure 4b-5 Temperature dependence of viscosity of pure Se and binary Se-Te liquids as reported in the literature [26–29]. Inset shows the comparison between data collected in the present study (filled symbols) and literature data (open symbols) in the supercooled region.

Finally, the relative coupling of the fast segmental chain motion and the slow bond scission/renewal dynamics to viscous flow can be estimated using the Maxwell relation according to which the contribution to the viscosity η from the slow process is given by $\eta_s = G_s\tau_s$ and that from the fast process is given by $\eta_f = (G_f - G_s)\tau_f \approx G_f\tau_f$ [30]. The G and τ in these equations are the plateau shear moduli, and the relaxation time corresponding to the specific relaxation process, respectively. The $Se_{95}Te_5$ supercooled liquid is chosen for this purpose since the rheological data for this composition allow for direct determination of τ_s and τ_f at multiple temperatures from the locations of the onset of frequency dependence of $\eta(\omega)$, and G_s and G_f are estimated from Fig. 4b-1 to be ~ 10^6 Pa and 10^9 Pa, respectively. The η_s and η_f are compared to the experimental $\eta_{exp.}$ for the $Se_{95}Te_5$ supercooled liquid in Fig. 4b-6. It is clear from this comparison that both relaxation
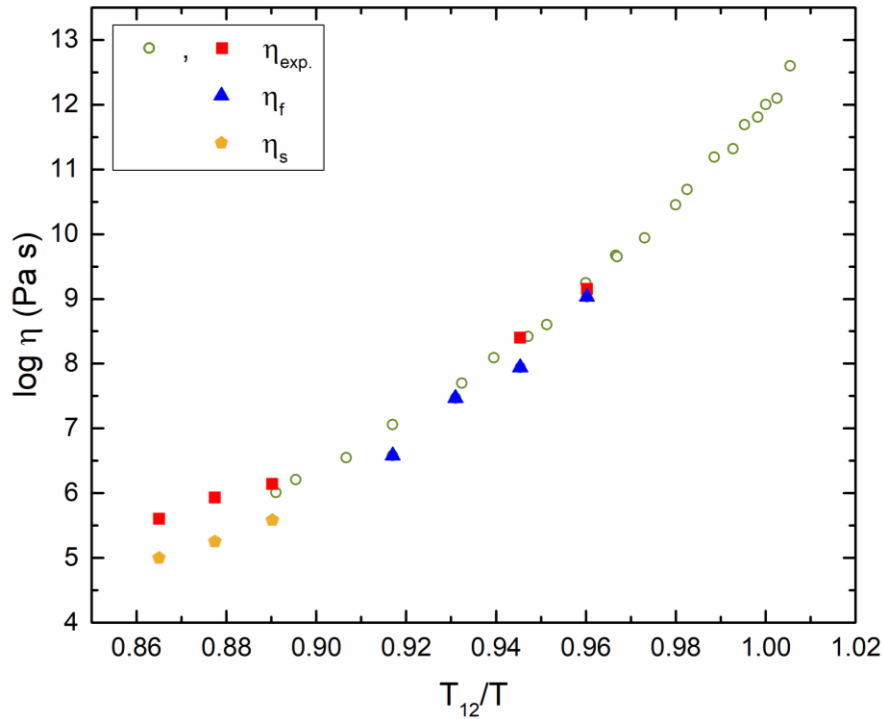
Figure 4b-6 Viscosity contributions from the slow process η_s (filled yellow pentagons) and from the fast process $\eta_f = G_f\tau_f$ (filled blue triangles) for supercooled $Se_{95}Te_5$ liquid are compared to experimentally measured viscosity from the present study (filled red squares) and from literature (open green circles) [27].

processes are coupled to viscous flow in their respective temperature ranges. This result is likely indicative of a mechanistic connection between the two dynamical processes in spite of their widely separated timescales. Although the exact nature of this connection remains unclear at this stage, it is tempting to speculate that the rapid segmental motion of the $[Se,Te]_n$ chains leads every so often to a locally highly strained state such that the chain can recover from it only via the breaking of a Se/Te-Se/Te bond. This hypothesis could be tested in future studies using molecular dynamics simulations.

4b.5 Conclusion

Chalcogens such as S and Se are typically characterized by twofold coordination in their elemental form as well as in a wide variety of crystalline and amorphous chalcogenide compounds. However, the bonding behavior of the heavier chalcogen Te remains controversial as, compared to the analogous sulfides and selenides, the increased metallicity of Te in its elemental form and in tellurides is believed to result from its strong SBI. It is shown in the present study that this SBI is manifested in the rheological behavior of Se_xTe_{100-x} supercooled liquids containing copolymeric $[Se,Te]_n$ chains. Our rheological measurements presented demonstrate that the timescales of the fast and slow relaxation processes in Se_xTe_{100-x} liquids with high Se content ($80 \leqslant x \leqslant 100$), which correspond to segmental chain motion and bond scission/renewal events, respectively, become increasingly coupled until only one relaxation process is observed for the $Se_{70}Te_{30}$ liquid. This gradual transition in the dynamical behavior is quite similar that displayed by Ge/As-Se liquids with increasing relative concentration of the conventional crosslinkers, namely Ge and As. When taken together, these results suggest that the SBI of Te results in a sufficiently strong interchain interaction in the Se_xTe_{100-x} liquids, such that Te atoms act as nodal points in the $[Se,Te]_n$ chains, imparting rigidity and, consequently, Te acts as a pseudo-crosslinker. This scenario is

shown to be consistent with the compositional variation of T_g of these liquids and their isothermal viscosity in the supercooled regime. Moreover, the compositional invariance of viscosity at superliquidus temperatures suggests that the constraints imposed by the SBI between the $[Se,Te]_n$ chains are eventually overcome with increasing temperature. Viscosity contributions of the fast and slow relaxation processes are estimated in the $Se_{95}Te_5$ supercooled liquid using the Maxwell relation. Both processes are shown to be closely related to viscosity in their respective temperature ranges, which might indicate a mechanistic coupling between them.

Acknowledgements

References

[1]   G. Lucovsky, A. Mooradian, W. Taylor, G.B. Wright, R.C. Keezer, Identification of the fundamental vibrational modes of trigonal, α-monoclinic and amorphous selenium, Solid State Commun. 5 (1967) 113–117.

[2]   E. Grison, Studies on tellurium-selenium alloys, J. Chem. Phys. 19 (1951) 1109–1113.

[3]   M. Marple, J. Badger, I. Hung, Z. Gan, K. Kovnir, S. Sen, Structure of Amorphous Selenium by 2D ^{77}Se NMR Spectroscopy: An End to the Dilemma of Chain versus Ring, Angew. Chemie. 129 (2017) 9909–9913.

[4]   A. Zakery, S.R. Elliott, Optical properties and applications of chalcogenide glasses: A review, J. Non. Cryst. Solids. 330 (2003) 1–12.

[5]   M. Popescu, Non-Crystalline Chalcogenides, Kluwer Academic Publishers, 2002.

[6]   T. Chivers, R.S. Laitinen, Tellurium: A maverick among the chalcogens, Chem. Soc. Rev. (2015) 1725–1739.

[7]   S. Yi, Z. Zhu, X. Cai, Y. Jia, J.H. Cho, The Nature of Bonding in Bulk Tellurium Composed of One-Dimensional Helical Chains, Inorg. Chem. 57 (2018) 5083–5088.

[8]   H. Endo, Structural and electronic properties of liquid tellurium, J. Non. Cryst. Solids. 156–159 (1993) 667–674.

[9]   S. Tamaki, Phase transition in liquids, Phase Transitions. 66 (1998) 167–257.

[10]   Y. Tsuchiya, The anomalous negative thermal expansion and the compressibility maximum of molten Ge-Te alloys, J. Phys. Soc. Japan. (1991) 227–234.

[11]   L.A. Silva, M. Culter, Optical properties of liquid Se-Te alloys, Phys. Rev. B. 42 (1990) 7103.

[12]   M. Misawa, A short-chain model for local structure in liquid tellurium, J. Phys. Condens. Matter. 4 (1992) 9491–9500.

[13]   B. Cabane, J. Friedel, Local order in liquid tellurium, J. Phys. 32 (1971) 73.

[14]   G. Tourand, B. Cabane, M. Breuil, Structure of liquid tellurium, J. Non. Cryst. Solids. 8–10 (1972) 676–686.

[15]   A. Menelle, R. Bellissent, A.M. Flank, Short range order in liquid Se-Te system by neutron scattering, Phys. B Condens. Matter. 157 (1989) 174–176.

[16]   M.E. Welland, M. Gay, J.E. Enderby, Physics of disordered systems, Plenum Press, New York, 1985.

[17]   M. Wuttig, N. Yamada, Phase-change materials for rewriteable data storage, Nat. Mater. 6 (2007) 824.

[18]   K. Itoh, Structure of Se-Te glasses studied using neutron, X-ray diffraction and reverse Monte Carlo modelling, J. Solid State Chem. 246 (2017) 372–378.

[19]   B. Bureau, C. Boussard-plèdel, M. Lefloch, J. Troles, J. Lucas, D. Rennes, D. Beaulieu, Selenium-Tellurium Sequences in Binary Glasses as Depicted by ^{77}Se and [125]Te NMR, 109 (2005) 6130–6135.

[20]   A. Tverjanovich, A. Cuisset, D. Fontanari, E. Bychkov, Structure of Se-Te glasses by Raman spectroscopy and DFT modeling, J. Am. Ceram. Soc. 101 (2018) 5188–5197.

[21]   S. Sen, W. Zhu, B.G. Aitken, Behavior of a supercooled chalcogenide liquid in the non-Newtonian regime under steady vs. oscillatory shear, J. Chem. Phys. 147 (2017) 034503.

[22]   W. Zhu, B.G. Aitken, S. Sen, Observation of a Dynamical Crossover in the Shear Relaxation Processes in Supercooled Selenium Near the Glass Transition, J. Chem. Phys. 150 (2019) 094502.

[23]   W. Zhu, I. Hung, Z. Gan, B. Aitken, S. Sen, Dynamical process related to viscous flow in a supercooled arsenic selenide glassforming liquid: Results from high-temperature ^{77}Se NMR Spectroscopy, J. Non. Cryst. Solids. (2019). (Accepted)

[24]   S. Sen, Y. Xia, W. Zhu, M. Lockhart, B. Aitken, Nature of the floppy-to-rigid transition in chalcogenide glass-forming liquids, J. Chem. Phys. 150 (2019) 144509.

[25]   J.D. Ferry, Viscoelastic properties of polymers, John Wiley & Sons, 1980.

[26]   P. Koštál, J. Málek, Viscosity of selenium melt, J. Non. Cryst. Solids. 356 (2010) 2803–2806.

[27]   P. Koštál, J. Málek, Viscosity of Se-Te glass-forming system, Pure Appl. Chem. 87 (2015) 239–247.

[28]   J.C. Perron, J. Rabit, J.F. Rialland, Impurity dependence of the viscosity of liquid selenium, Philos. Mag. B Phys. Condens. Matter; Stat. Mech. Electron. Opt. Magn. Prop. 46 (1982) 321–330.

[29]   J. Barták, P. Koštál, D. Valdés, J. Málek, T. Wieduwilt, J. Kobelke, M.A. Schmidt, Analysis of viscosity data in As_2Se_3, Se and $Se_{95}Te_5$ chalcogenide melts using the pressure assisted melt filling technique, J. Non. Cryst. Solids. 511 (2019) 100–108.

[30]   T. Scopigno, S.N. Yannopoulos, F. Scarponi, K.S. Andrikopoulos, D. Fioretto, G. Ruocco, Origin of the λ transition in liquid sulfur, Phys. Rev. Lett. 99 (2007) 025701.

Chapter 5a

Compositional Evolution of Structure and Connectivity in Binary P-Se Glasses: Results from 2D Multinuclear NMR and Raman Spectroscopy

5a.1 Abstract

The atomic structure of binary P_xSe_{100-x} glasses with $5 \leq x \leq 70$ is investigated using Raman spectroscopy and two-dimensional ^{77}Se and ^{31}P isotropic-anisotropic correlation nuclear magnetic resonance (NMR) spectroscopy. These spectroscopic results, when taken together, demonstrate that the structure of P_xSe_{100-x} glasses with $x \leq 50$ consists primarily of -Se-Se-Se- chain elements, pyramidal $P(Se_{1/2})_3$ units, ethylene-like $_{2/2}SeP–PSe_{2/2}$ units, and $Se=P(Se_{1/2})_3$ tetrahedral units. The chain structure of Se becomes increasingly cross-linked by P-Se polyhedral units and the degree of connectivity increases with progressive increase in P content up to $x \sim 50$, at which point the -Se-Se-Se- chain elements completely disappear, and the structure becomes highly rigid. The compositional variation of the Se-**Se**-Se environments as obtained from the ^{77}Se isotropic NMR spectra reveals that the connectivity between the Se-Se and P-Se units in glasses with $x \leq 50$ is intermediate to that of the random and the fully clustered scenarios. Further increase in P content results in the formation of P_4Se_3 molecules such that at $x = 63$ the structure becomes predominantly molecular, consisting of P_4Se_3 molecules likely held together via van der Waals forces. The structure of glasses with $x > 63$ is characterized by P_4Se_3 molecules and likely non-molecular P_4Se_3-like species, along with amorphous red phosphorus-like regions. These P_4Se_3-like moieties and the amorphous red phosphorus-like units can connect to each other via P-P bonds and their relative concentrations increase with increasing P content. This compositional evolution of structural connectivity of P_xSe_{100-x} glasses is shown to be consistent with the corresponding variation in the glass transition temperature.

5a.2 Introduction

Chalcogenide crystals and glasses have found important technological applications in the areas of infrared photonics, phase change memory and remote sensing.[1–5] More recently crystals in the P-Se system have been found to be highly efficient as an anode material for solid-state Na-ion batteries.[6,7] The unusually large composition range for bulk glass formation and the complex compositional variation of the structural building blocks make the binary P-Se system somewhat unique among glass-forming chalcogenides. Consequently, the structure of P-Se glasses has been investigated extensively in the past decades using a wide range of techniques including Raman scattering, neutron diffraction, X-ray absorption and nuclear magnetic resonance (NMR) spectroscopy.[8–15] Bulk glass formation in the P-Se binary system is reported in the composition range 0 at.% $\leq$ P $\leq$ 80 at.% with a narrow gap centered around 57 at.% P corresponding to the stoichiometry of P_4Se_3 molecules.[16] Previous Raman scattering, ^{31}P magic-angle-spinning (MAS) and two-dimensional (2D) J-resolved NMR spectroscopic studies [8–10,15] have provided a detailed picture of the identification and the composition dependent evolution of relative fractions of the constituent P-centric coordination polyhedra and short-range structure of P-Se glasses. The structure of the Se-rich glasses ($\leq$ 20 at.% P) consists of Se chains interconnected primarily by $Se=P(Se_{1/2})_3$ tetrahedra and $P(Se_{1/2})_3$ pyramids. As the P content increases beyond 30 at.%, the P atoms exist predominantly in the form of $P(Se_{1/2})_3$ pyramids and $_{2/2}SeP-PSe_{2/2}$ ethylene-like units, whereas in P-rich glasses with >50 at.% P, the P atoms are incorporated in P_4Se_3 (and possibly P_4Se_2) molecules and also form amorphous red phosphorus-like structural moieties.[9] Therefore, the structure of P-Se glasses evolves, with increasing P content, from linear chains to highly crosslinked networks all the way to zero-dimensional molecules and finally to molecules embedded in a polymeric matrix. Such structural complexity

including the violation of the 8–N rule for P coordination, strong violation of chemical order via the formation of P-P homopolar bonds even in Se-excess glasses and the formation of predominantly molecular glasses can be contrasted with the relative structural simplicity of selenide glasses containing conventional crosslinkers such as As or Ge that do not display such behavior. Although the evolution of the short-range structure of binary P-Se glasses in terms of the P speciation has been studied extensively throughout the glass formation range, little is known regarding the speciation of the Se environments and the intermediate-range order in terms of the connectivity between the constituent structural units. In this regard, the only systematic study, to the best of our knowledge, was carried out by Eckert *et al.*[17] In this study the intermediate-range order of P-Se glasses was described in terms of the connectivity between the Se–Se segments and the P containing building blocks on the basis of results from ^{31}P–^{77}Se spin echo double resonance (SEDOR) and *in situ* high-temperature ^{77}Se wideline NMR spectroscopy.[17] Their results were shown to be consistent with a model of random connectivity between these structural moieties. However, such a conclusion could not be experimentally verified without the direct knowledge of Se speciation in these binary P-Se glasses due to the lack of high-resolution ^{77}Se NMR data. High-resolution ^{77}Se NMR spectroscopy in chalcogenide glasses remains challenging owing to the low natural abundance of ^{77}Se (~7%), its long spin-lattice relaxation time, large chemical shift range and chemical shift anisotropy (CSA). The last two problems can be addressed effectively via the application of the 2D magic-angle-turning phase-adjusted spinning sidebands (MATPASS) NMR technique, which can separate the CSA from the isotropic chemical shift in a separate dimension, thereby avoiding any CSA-related broadening and consequently increasing the spectral resolution in the isotropic dimension.[18] Moreover, the separation of isotropic shift from CSA allows the

use of high magnetic fields for increased sensitivity and resolution without requiring fast spinning of samples in small-volume rotors for CSA averaging.

It may be noted here that the chemical shift δ of a nuclide is a second rank tensor that can be described using the principal components δ_{xx}, δ_{yy}, and δ_{zz}. The isotropic chemical shift δ_{iso} is the average of these three components:

$$\delta_{iso} = \frac{1}{3}\left(\delta_{xx} + \delta_{yy} + \delta_{zz}\right)$$

Following the Haeberlen convention these principal components are arranged such that:[19]

$$|\delta_{zz} - \delta_{iso}| \geq |\delta_{xx} - \delta_{iso}| \geq |\delta_{yy} - \delta_{iso}|$$

More commonly, however, the tensor is reported in terms of δ_{iso} and the CSA expressed by the reduced anisotropy Δ and the asymmetry parameter η, which are related to the principal components as:

$$\Delta = \delta_{zz} - \delta_{iso}$$

$$\eta = \frac{\delta_{xx} - \delta_{yy}}{\delta_{zz} - \delta_{iso}}$$

The CSA parameters Δ and η represent the deviation of the tensor from spherical and axial symmetry, respectively. While δ_{iso} of a nuclide is characteristic of its coordination environment, the CSA carries important complementary information related to the symmetry of its local electronic environment. Therefore, the separation of isotropic and anisotropic chemical shifts in two dimensions makes MATPASS a powerful NMR technique in the investigation of short- and intermediate- range structural order in glasses. Here we present the results of a comprehensive

structural investigation of binary P_xSe_{100-x} glasses with $5 \leq x \leq 70$ using high-resolution 2D ^{77}Se and ^{31}P MATPASS NMR spectroscopy. The composition dependent evolution of the relative fractions of different Se and P environments as obtained from the analyses of the ^{77}Se and ^{31}P NMR data are used in combination with Raman spectroscopic results to build a more complete model of intermediate-range order and structural connectivity in these glasses.

5a.3 Experimental Methods

5a.3.1 Sample preparation and physical characterization

Binary P_xSe_{100-x} glasses with $x = 5, 10, 20, 25, 30, 35, 40, 45, 50, 63, 67,$ and 70 were prepared in ~12g batches from constituent elements using the conventional melt-quench method. Mixtures of red phosphorus (Spectrum, 99.999%) and selenium (Alfa Aesar, 99.999%) were taken in 6mm inner diameter quartz ampoules that were evacuated (10^{-4} Torr) and flame-sealed prior to loading into a rocking furnace. The ampoules were slowly heated to 923 K over 13 hours and held at this temperature for 36 h to ensure melt homogeneity. The ampoules were then quenched in water to obtain the glass samples.

The glass transition temperature T_g of the P_xSe_{100-x} glasses was measured using a differential scanning calorimeter (Mettler-Toledo DSC1). Approximately 15 mg of powdered glass sample was hermetically sealed in a 40 μL aluminum crucible. Scans were performed at 10 °C/min under a continuously flowing nitrogen environment. T_g was determined to within ± 1 °C as the onset of the glass transition.

5a.3.2 Raman spectroscopy

The Raman spectra of all glasses were collected in backscattered geometry using a Renishaw 1000 Raman microscope spectrometer equipped with a He-Ne laser operating at a

wavelength of 633 nm. Each Raman spectrum was collected at 50% laser power with 1 cm^{-1} resolution. The backscattered light was detected using a charge-coupled device cooled at 200K.

5a.3.3 NMR spectroscopy

The 2D ^{77}Se MATPASS/Carr-Purcell Meiboom-Gill (CPMG)[18] and ^{31}P MATPASS[20] NMR spectra for all glasses were acquired at the National High Magnetic Field Laboratory (NHMFL) using a 31 mm bore 19.6 T magnet equipped with a Bruker Avance NEO console operating at the resonance frequency of 158.7 MHz and 336.6 MHz for ^{77}Se and ^{31}P, respectively, and a Low-E double-resonance probe. Crushed glass samples were packed into 3.2 mm ZrO$_2$ rotors and spun at 10 kHz. The ^{77}Se spectra were acquired with $\pi/2$- and π-pulses of 3.0 and 6.0 μs, respectively, and CPMG echo-train acquisition with 159 echoes was acquired for each transient to enhance sensitivity. The method of States et al.[21] for hypercomplex data acquisition was applied to the CPMG pulse phase and the receiver phase simultaneously. The 2D acquisition consisted of 16 hypercomplex t_1 increments each with 24 transients, and 110 s recycle delay, for a total experimental duration of 23.5 h per spectrum. The ^{31}P spectra were acquired with $\pi/2$- and π-pulses of 2.6 and 5.2 μs, respectively. The 2D acquisition consisted of 16 complex t_1 increments each with 12 transients and 240 s recycle delay, for a total experimental duration of 12.8 h per spectrum. The 2D spectra were sheared to an isotropic/anisotropic representation in the direct/indirect dimensions during processing, as detailed in the works of Hung et al.[18,20] Representative 2D ^{31}P and ^{77}Se MATPASS spectra of P$_x$Se$_{100-x}$ glasses obtained in this study are shown in Fig. 5a-1.

^{77}Se MAS and ^{31}P PASS NMR data were collected for the molecule-rich P$_x$Se$_{100-x}$ glasses with $x = 63$, 67 and 70. The ^{77}Se MAS spectra were collected at 19.6 T using the NHMFL system described above with a $\pi/2$-pulse of 3.0 μs, 5.0 s recycle delay, and 16 transients averaged per sample. Crushed glass samples were packed into 3.2 mm ZrO$_2$ rotors and spun at 10 kHz. The ^{31}P
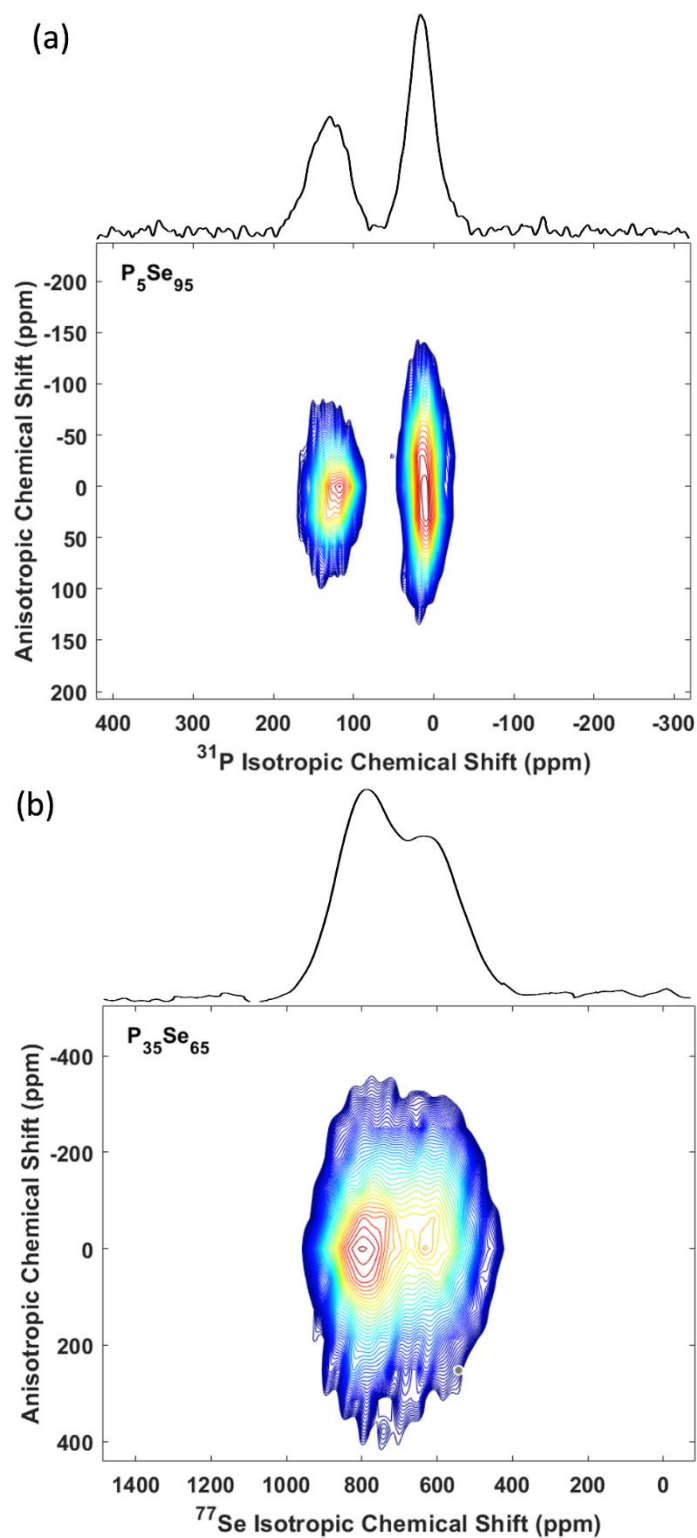
Figure 5a-1 Contour plots of representative (a) ^{31}P MATPASS and (b) ^{77}Se MATPASS/CPMG spectra of P$_x$Se$_{100-x}$ glasses. Glass compositions are indicated in the inset. Total projection along isotropic dimension is shown on top of each plot (solid black line).

PASS spectra were collected at UC Davis using a Bruker Avance spectrometer operating at 11.7 T (Larmor frequency of 202.4 MHz for ^{31}P) and a Bruker triple resonance MAS probe. Crushed samples were spun at a rate of 6 kHz in 4 mm ZrO_2 rotors. The PASS pulse sequence consisted of a $\pi/2$ pulse (1.95 μs) followed by a train of π pulses. The inter-pulse delays were rotor synchronized according to the solutions of the PASS equations given by Antzutkin *et al.*[22] All pulses were cogwheel phase cycled to eliminate the effects of pulse imperfections. The 2D acquisition consisted of 32 hypercomplex t_1 increments, each with 12 transients, and a recycle delay of 20 s was used. All ^{77}Se and ^{31}P NMR spectra were externally referenced by recording the [17]O signal of natural abundance H_2O and using the appropriate frequency ratios as reported in the IUPAC recommendations.[23] The isotropic and anisotropic spectral line shapes, as obtained from the MATPASS and PASS data, were simulated using the software program DMFit to obtain the relative fractions of the various Se and P environments and their corresponding CSA parameters.[24]

5a.4 Results and Discussion

5a.4.1 Raman Spectroscopy

The Raman spectra of all P_xSe_{100-x} glasses are shown in Fig. 5a-2. The major bands in $x \leq$ 50 glass compositions can be readily assigned on the basis of previous studies [8,10] to the Se–Se stretching mode (~ 250 cm^{-1}), the symmetric and asymmetric stretching of P–Se bonds in pyramidal $P(Se_{1/2})_3$ units (~ 330 cm^{-1} and 210 cm^{-1}, respectively), the vibrational modes of ethylene-like $_{2/2}SeP–PSe_{2/2}$ units (~ 185 cm^{-1}, 330-350 cm^{-1} and 370 cm^{-1}), and the stretching of the P=Se bonds in $Se=P(Se_{1/2})_3$ tetrahedral units (~ 500 cm^{-1}). The Se–Se stretching band at ~ 250

cm^{-1} is the most intense in Se rich glasses and its intensity decreases continuously with increasing P content, whereas the intensities of the bands corresponding to the P containing
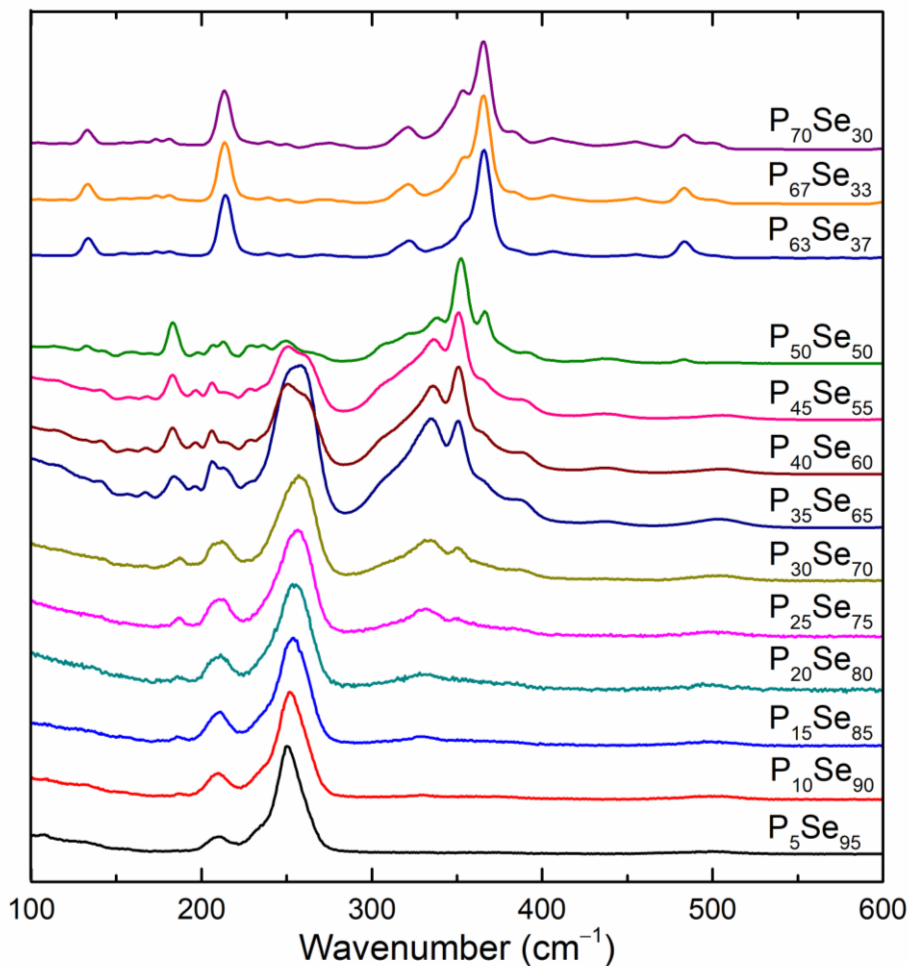
Figure 5a-2 Unpolarized Raman spectra of $P_x Se_{100-x}$ glasses. Glass compositions are listed alongside the spectra.

structural moieties concomitantly increase up to 35% P (Fig. 5a-2). Above 35 at.% P, the intensity of the 185 cm^{-1} band continues to increase, while that of the 210 cm^{-1} band decreases, suggesting the incorporation of an increasing number of P atoms into the ethylene-like $_{2/2}SeP–PSe_{2/2}$ units. When taken together, these observations indicate that the Se chains are crosslinked by the various P containing structural moieties and the average chain length is progressively shortened due to an increasing degree of connectivity of the glass structure. This compositional evolution of the

structure of P-Se glasses is in broad agreement with that reported in a previous study by Georgiev *et al.*[8] However, it may be noted here that, in the Raman spectra reported by Georgiev *et al.,* the 185 cm^{-1} band corresponding to the $_{2/2}$SeP–PSe$_{2/2}$ unit becomes barely noticeable for the first time in the P$_{20}$Se$_{80}$ glass, while in the present study a weak signature of this band can already be seen in the spectrum of the P$_{10}$Se$_{90}$ glass (Fig. 5a-2). This observation in the present study is consistent with the 2D J-resolved ^{31}P NMR spectroscopic results on P-Se glasses reported by Bytchkov *et al.,*[9] which have conclusively shown that the $_{2/2}$SeP-PSe$_{2/2}$ units definitely appear in P-Se glasses with >10% P.

Besides the abovementioned bands, new bands located at ~ 133, 213, 366, and 484 cm^{-1}, which correspond to the intramolecular modes of P$_4$Se$_3$ molecules,[15] appear in the Raman spectrum of the P$_{50}$Se$_{50}$ glass (Fig. 5a-2). These molecular bands dominate the Raman spectra of P-Se glasses with $x \geq 63$, indicating that the P$_4$Se$_3$ molecules are a major constituent of the structure of these P-rich glasses (Fig. 5a-2). Finally, the appearance of bands at ~ 353 and 500 cm^{-1} in the Raman spectra of these P-rich glasses is likely indicative of the formation of amorphous red phosphorus-like structural moieties.[15] Therefore, when taken together these results suggest that the nanostructure of the P-rich glasses consists of P$_4$Se$_3$ molecules coexisting with amorphous red phosphorus-like regions.

5a.4.2 ^{31}P NMR

The ^{31}P isotropic NMR spectra of the P$_x$Se$_{100-x}$ glasses with $x \leq 50$ display two distinct resonances centered at δ_{iso} ~ 129 ppm and 10 ppm with the relative intensity of the former increasing monotonically with increasing P content (Fig. 5a-3). Previous ^{31}P NMR studies have shown that the resonance near δ_{iso} ~ 10 ppm can be assigned to the tetrahedral Se=P(Se$_{1/2}$)$_3$ site
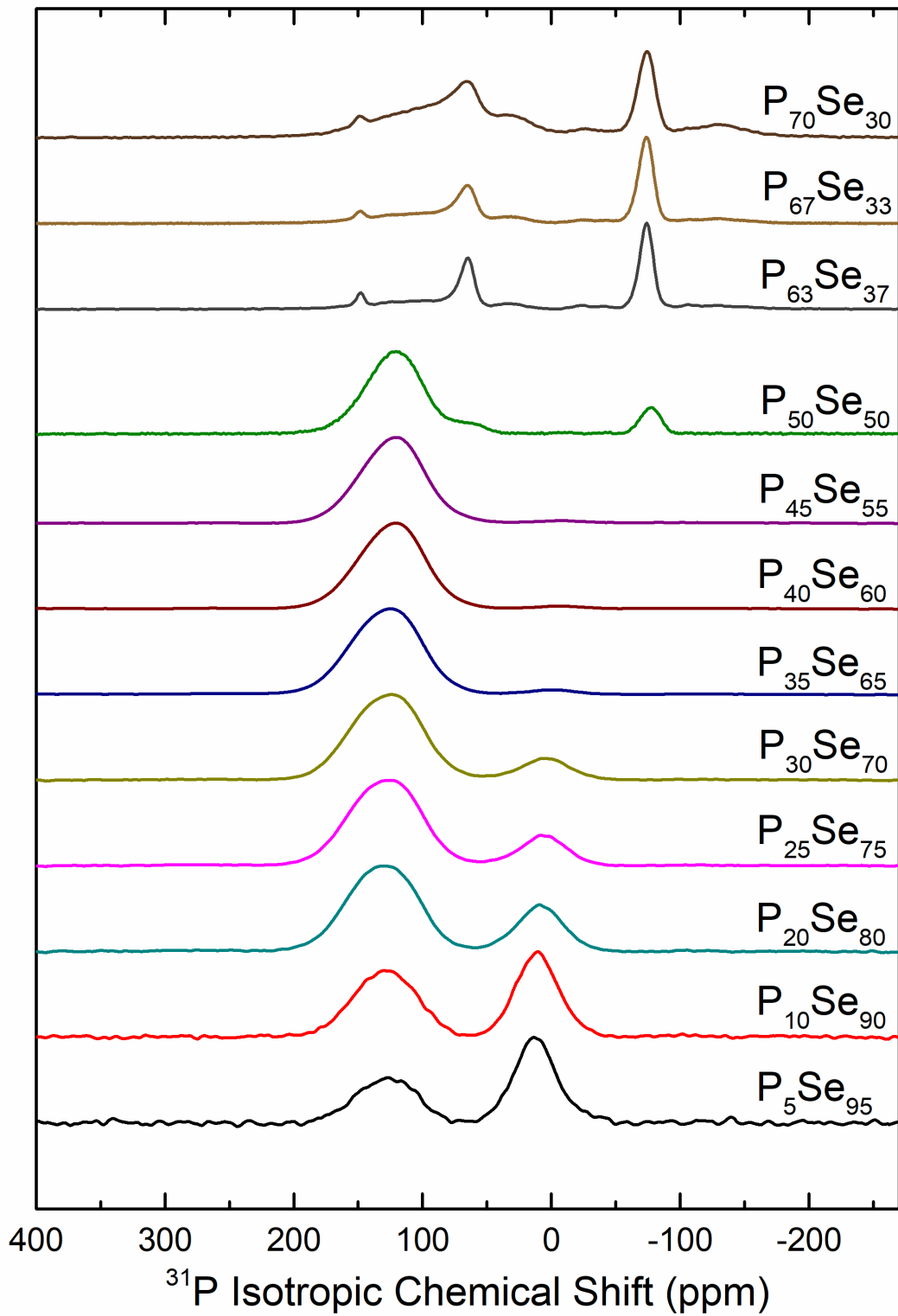
Figure 5a-3 ^{31}P isotropic NMR spectra of P_xSe_{100-x} glasses. Glass compositions are listed alongside the spectra.

while the resonance located at δ_{iso} ~ 129 ppm corresponds to P atoms in pyramidal P(Se$_{1/2}$)$_3$ units.[9,11] These studies were able to show, on the basis of ^{31}P dipolar NMR and 2D J-resolved ^{31}P NMR spectroscopic results, that this resonance also contained signal from P in $_{2/2}$SeP–PSe$_{2/2}$ units with δ_{iso} ~ 125 ppm and that, with increasing P concentration, the relative contribution of $_{2/2}$SeP–PSe$_{2/2}$ units increased compared to that from P(Se$_{1/2}$)$_3$ units. The separation of the ^{31}P isotropic and anisotropic shifts into two dimensions in the MATPASS and PASS NMR spectra obtained in the present study allows for the determination of the chemical shift tensor parameters Δ and η for the P sites from the simulations of the corresponding spinning sideband intensity pattern in the anisotropic dimension (Fig. 5a-4). These simulations performed at several δ_{iso} values yield average values of $\Delta = -127 \pm 10$ ppm and $\eta = 0.9 \pm 0.1$ for the tetrahedral Se=P(Se$_{1/2}$)$_3$ environment and $\Delta = -78 \pm 10$ ppm and $\eta = 0.8 \pm 0.1$ for the pyramidal P(Se$_{1/2}$)$_3$ and ethylene-like $_{2/2}$SeP–PSe$_{2/2}$ environments. These ^{31}P chemical shift tensor parameters for all P$_x$Se$_{100-x}$ glasses are listed in Table 5a-1 and shown in Fig. 5a-5. As shown in previous studies, the resonance at δ_{iso} ~ 129 ppm is expected to be dominated by the P(Se$_{1/2}$)$_3$ units near x=15, while the $_{2/2}$SeP–PSe$_{2/2}$ units are expected to dominate near x=50.[9,11] Therefore, if the ^{31}P chemical shift tensor parameters for these two units are significantly different than one would expect a monotonic evolution of the average values of Δ and η in the composition range $15 \le x \le 50$. However, it is apparent from Table 5a-1 and Fig. 5a-5 that within experimental error neither Δ nor η shows any significant change with glass composition, although the average absolute value of Δ does appear to increase monotonically from ~ 80 ppm to ~ 90 ppm with increasing P content in this composition range. Unfortunately, the magnitude of the change in Δ is well within the experimental error (Fig. 5a-5) and thus, the observed trend cannot be assigned unequivocally to a replacement of the P(Se$_{1/2}$)$_3$ units with the $_{2/2}$SeP–PSe$_{2/2}$ units in the structure of these glasses with increasing P content.

Although a full quantitative analysis of composition-dependent variation of the relative fractions of all three types of P environments is prohibited by the complete overlap of the signals from the $P(Se_{1/2})_3$ and $_{2/2}SeP–PSe_{2/2}$ sites in the isotropic ^{31}P NMR spectra, the ratios for three- and four-coordinated P environments in all glass compositions with $x \leq 50$ can be obtained by integrating the corresponding peak areas. This procedure yields highly accurate speciation results

Figure 5a-4 Experimental (empty red circles) and simulated (black traces) ^{31}P NMR spinning sideband intensities in the anisotropic dimension for (a) three-coordinated P sites and (b) four-coordinated P sites in P_5Se_{95} glass at δ_{iso} ~ 127 ppm and 8 ppm, respectively.

for three- and four-coordinated P environments in these glasses as the isotropic spectra correspond to MAS spectra at infinite spinning speed, which are free from CSA and dipolar coupling related broadening interactions under MAS. The resulting relative fractions of these P environments show smooth variation with composition as the relative fraction of three-coordinated P atoms increases and that of fourfold coordinated P atoms decreases with increasing P content (Fig. 5a-6). A comparison of these P-speciation data with those obtained in previous studies using regular 1D ^{31}P MAS NMR (Fig. 5a-6) show reasonable agreement within experimental error except for glasses

(a)

(b)
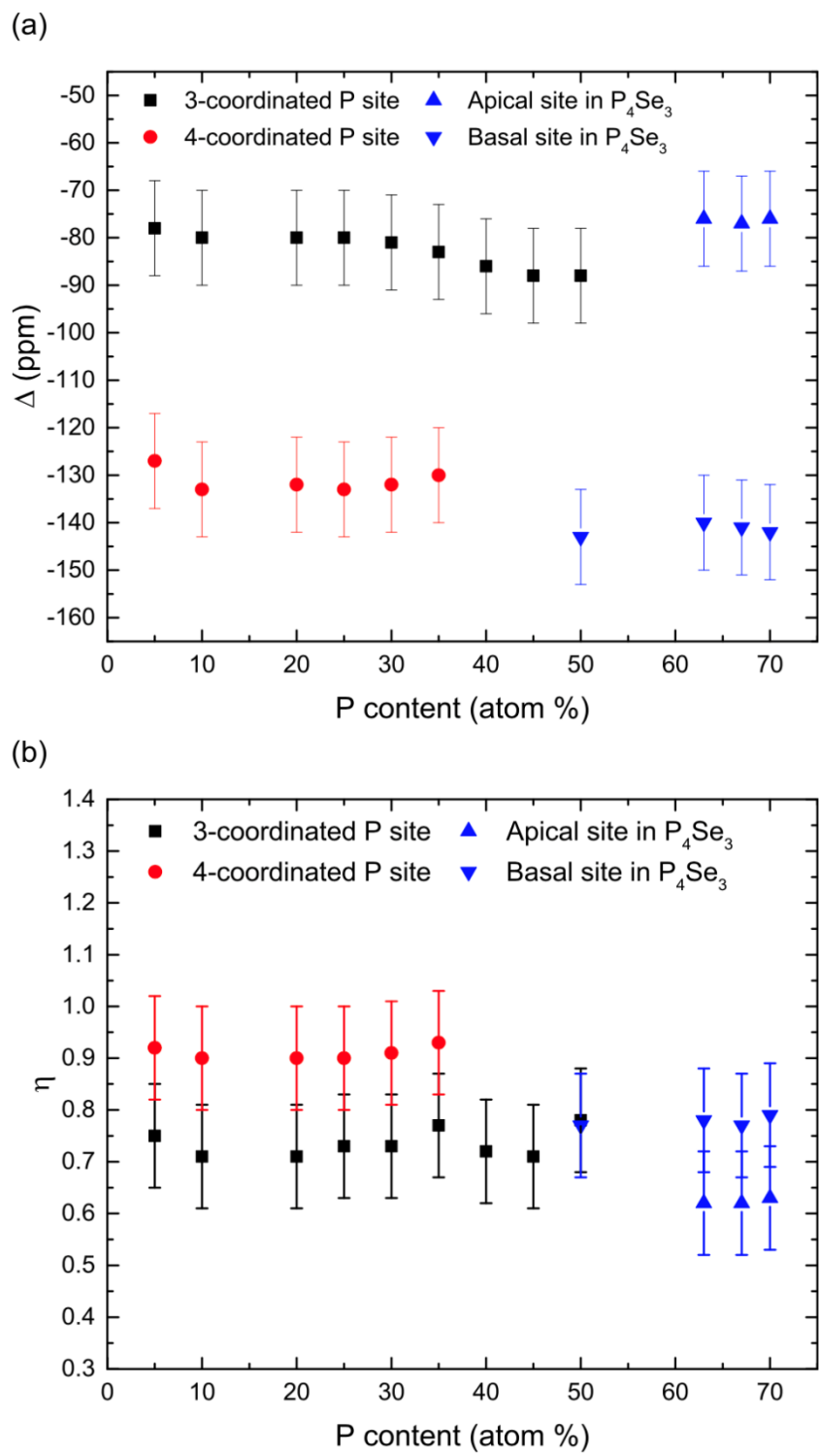
Figure 5a-5 Compositional variation of ^{31}P chemical shift tensor parameters Δ (a) and η (b) for various P sites in $P_x Se_{100-x}$ glasses.

with $x \leq 20$, where the MAS speciation data show a gentler variation with composition, albeit with a rather large scatter due to the weaker signal:noise of the corresponding spectra.[9,11]
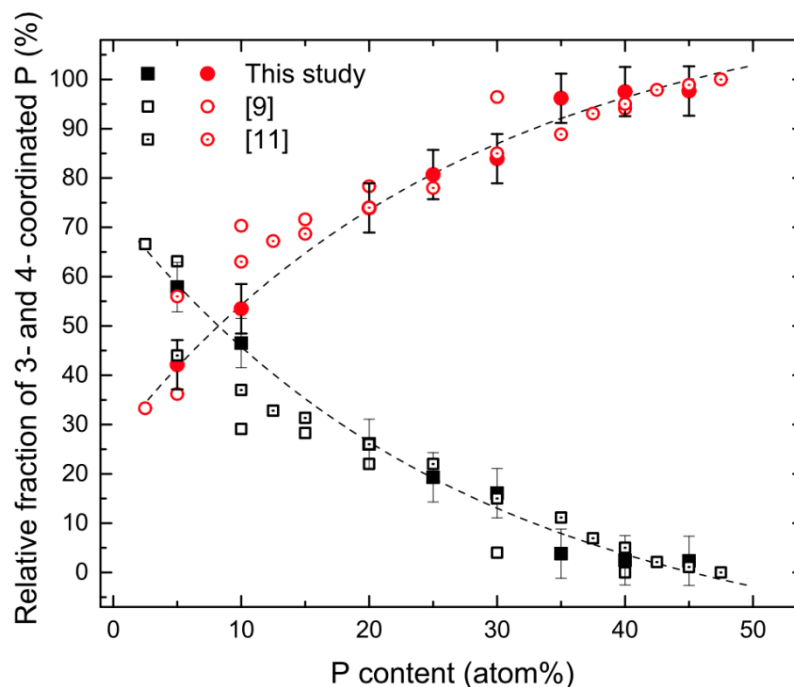
Figure 5a-6 Compositional variation of three-coordinated (filled red circles) and four-coordinated (filled black squares) P site fractions obtained from simulations of ^{31}P isotropic NMR spectra in this study and values reported in the literature from ^{31}P MAS NMR (open symbols).[9,11] Dashed lines through the filled symbols are guides to the eye.

In contrast to P_xSe_{100-x} glasses with $x \leq 50$, the ^{31}P PASS NMR spectra of glasses with $x \geq$ 63 are dominated by strong and relatively narrow resonances centered at ~ 66 and −74 ppm that can be readily assigned, on the basis of their relative area fractions of 1:3, to the apical and basal P sites, respectively, in P_4Se_3 molecules (Fig. 5a-3).[25] However, this ratio becomes closer to 1:2 in the ^{31}P PASS NMR spectrum of the $P_{70}Se_{30}$ glass. These two sites differ significantly in their CSA as simulations of the corresponding spinning sideband intensity patterns in the anisotropic dimension yield $\Delta = 140$ (−76) ± 10 ppm and $\eta = 0.8$ (0.6) ± 0.1 for the basal (apical) site (Fig. 5a-7, Table 5a-1). It may be noted that these resonances, albeit weak, are clearly detectable in the ^{31}P isotropic spectrum of the $P_{50}Se_{50}$ glass, indicating the first appearance of P_4Se_3
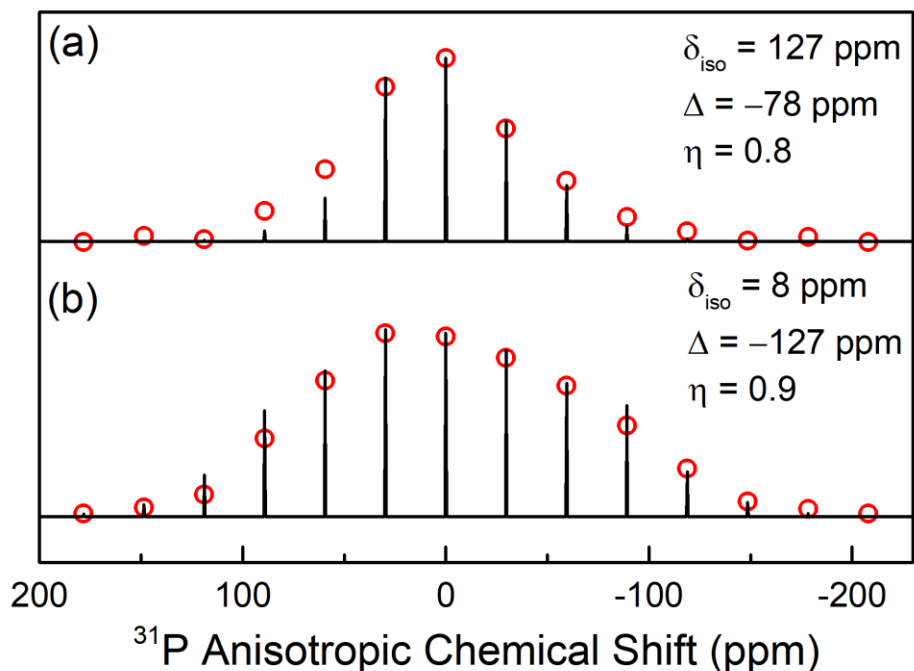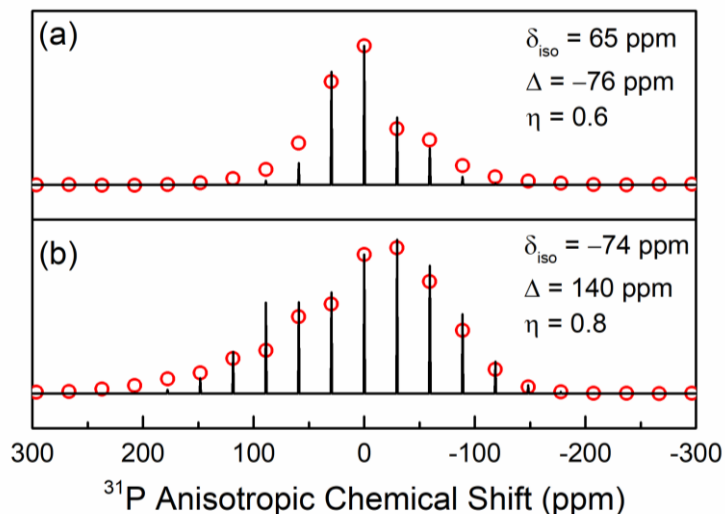
Figure 5a-7 Experimental (empty red circles) and simulated (black traces) ^{31}P NMR spinning sideband intensities in the anisotropic dimension for (a) apical and (b) basal P sites in P_4Se_3 molecules in $P_{63}Se_{37}$ glass, respectively.

Table 5a-1 ^{31}P chemical shift anisotropy parameters for P_xSe_{100-x} glasses.

	3-coordinated P site		4-coordinated P site		Apical P site in P_4Se_3		Basal P site in P_4Se_3	
	Δ (±10 ppm)	η (±0.1)	Δ (±10 ppm)	η (±0.1)	Δ (±10 ppm)	η (±0.1)	Δ (±10 ppm)	η (±0.1)
P_5Se_{95}	-78	0.8	-127	0.9	–	–	–	–
$P_{10}Se_{90}$	-80	0.7	-133	0.9	–	–	–	–
$P_{20}Se_{80}$	-80	0.7	-132	0.9	–	–	–	–
$P_{25}Se_{75}$	-80	0.7	-133	0.9	–	–	–	–
$P_{30}Se_{70}$	-81	0.7	-132	0.9	–	–	–	–
$P_{35}Se_{65}$	-83	0.8	-130	0.9	–	–	–	–
$P_{40}Se_{60}$	-86	0.7	–	–	–	–	–	–
$P_{45}Se_{55}$	-88	0.7	–	–	–	–	–	–
$P_{50}Se_{50}$	-88	0.8	–	–	–	–	-143	0.8
$P_{63}Se_{37}$	–	–	–	–	-76	0.6	-140	0.8
$P_{67}Se_{33}$	–	–	–	–	-77	0.6	-141	0.8
$P_{70}Se_{30}$	–	–	–	–	-76	0.6	-142	0.8

molecules in the structure of this glass as P content is increased in the P_xSe_{100-x} system (Fig. 5a-3). The ^{31}P NMR spectra of glasses with $x \geq 63$ glasses also contain a broad resonance centered at ~ 90 ppm that was assigned in the literature to P atoms in amorphous red phosphorus type environments and three relatively weak resonances near 150, 30 and −125 ppm, which have not yet been conclusively assigned to specific structural units. Based on a recent ^{31}P NMR study of bicyclic P-Se compounds[26] here we tentatively assign these resonances near 150, 30 and −125 ppm to the P sites in various isomeric, albeit non-molecular, P_4Se_3 moieties that are characterized by an opening of the P_3 basal ring in the original P_4Se_3 molecules (Fig. 5a-8). This ring opening enables these moieties to establish connection to the amorphous red phosphorus domains via P-P bonds (Fig. 5a-8).
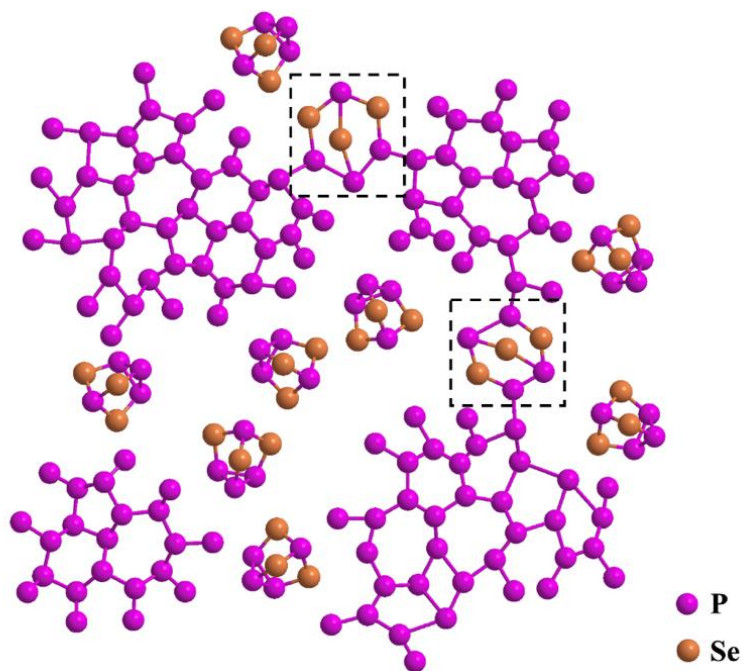
Figure 5a-8 Cartoon showing structure of P_xSe_{100-x} glasses with $x \geq 63$ consisting primarily of isolated P_4Se_3 molecules and amorphous red phosphorus-like regions with the latter being occasionally crosslinked by P-P bonds with P_4Se_3-like units denoted in dashed boxes.

This structural scenario is consistent with the observation that the ratio of the apical:basal P sites increases from 1:3 in P_xSe_{100-x} glasses with $x \leq 66.7$ to 1:2 in the $P_{70}Se_{30}$ glass. The formation of

such P_4Se_3-like moieties is also consistent with the observation that the Raman spectra of P_xSe_{100-x} glasses with $x \geq 63$ do not show significant change with composition in terms of the appearance of any new band corresponding to the appearance of other distinctly different molecular units (Fig. 5a-2). As discussed below, further corroboration of this hypothesis comes from the ^{77}Se MAS NMR spectra of these glasses with $x \geq 63$ (see below). It is interesting to note that, in these high-P glasses, the relative concentrations of the amorphous red phosphorus-like regions and these P_4Se_3-like moieties rise with increasing P content, resulting in an increase in the average structural connectivity as the P content increases from 63 to 70 at.% (Fig. 5a-3).

5a.4.3 ^{77}Se NMR

The ^{77}Se isotropic NMR spectra of these P_xSe_{100-x} glasses are shown in Fig. 5a-9. The spectra of glasses with $x \leq 50$ are dominated by two broad resonances centered at δ_{iso} of ~ 853 and ~ 700 ppm (Fig. 5a-9). However, a self-consistent simulation of these spectral line shapes over this composition range warrants the use of three Gaussian peaks centered at 830-850 ppm, 750-760 ppm and 575-630 ppm. These peaks can be assigned to Se-**Se**-Se, Se-**Se**-P and P-**Se**-P environments, respectively.[27] The corresponding simulation parameters are listed in Table 5a-2. It is clear from Table 5a- 2 that the intensity of the peak at 830-850 ppm progressively decreases and its δ_{iso} shifts to higher frequencies with increasing P content. A similar shift in [77]Se δ_{iso} for this resonance has been observed in the past in the ^{77}Se NMR spectra of Ge-Se and As-Se glasses and can be attributed to the appearance of P as next-nearest-neighbors as the Se chain length is shortened due to their progressive cross-linking by P atoms.[28,29] It is interesting to note that the δ_{iso} of the P-**Se**-P resonance shows an even larger shift to higher frequencies with increasing P
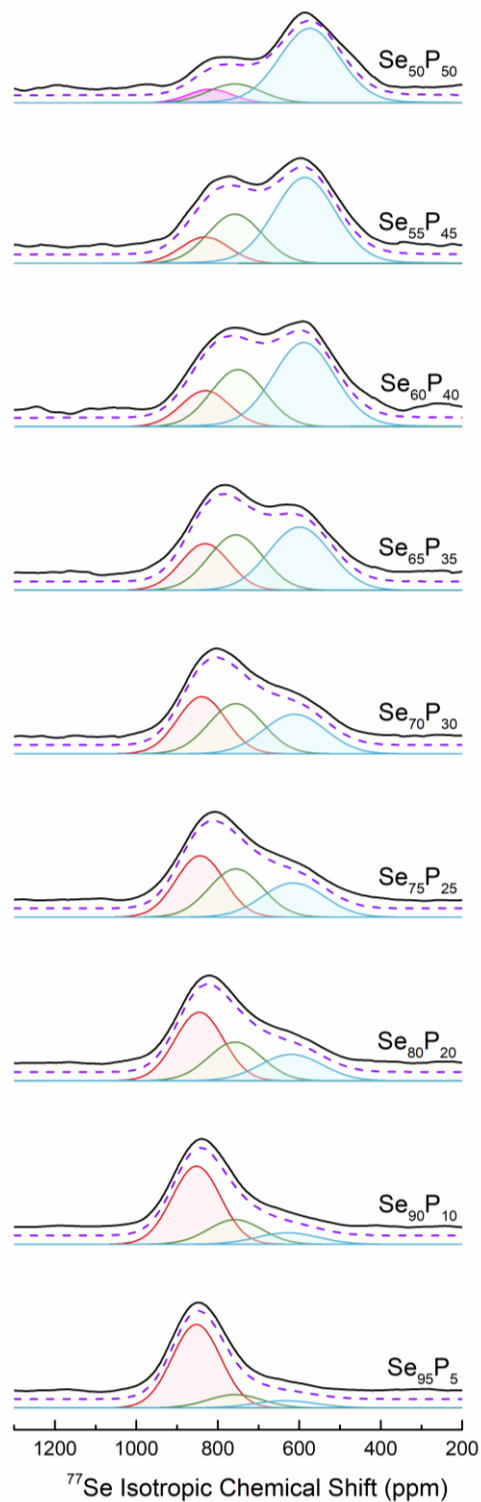
Figure 5a-9 Experimental (solid black line) and simulated (dashed purple line) ^{77}Se isotropic NMR spectra of P_xSe_{100-x} glasses with $x \leq 50$. Individual simulation components for Se–**Se**–Se, Se–**Se**–P and P–**Se**–P sites are denoted in orange, green and blue, respectively. The simulation component in pink in the spectrum of $P_{50}Se_{50}$ glass corresponds to P–**Se**–P sites in P_4Se_3 molecules.

content compared to that of the Se-**Se**-Se sites (Table 5a- 2). It may be recalled that the P speciation in these glasses changes from being predominantly a combination of Se=P(Se$_{1/2}$)$_3$ and P(Se$_{1/2}$)$_3$ sites to being dominated by the $_{2/2}$SeP–PSe$_{2/2}$ sites with increasing P content. Consequently, the P-**Se**-P environment becomes increasingly representative of the type that connects the $_{2/2}$SeP–PSe$_{2/2}$ sites forming P-P-**Se**-P-P connections. The high-frequency shift of the P-**Se**-P resonance with increasing P content can therefore be again attributed to the presence of P as next-nearest neighbors. Simulation of the spinning sideband intensity pattern in the anisotropic dimension (Fig. 5a-10) yields average CSA tensor parameters of Δ = −151 ± 10 ppm; η = 0.9 ± 0.1 for the Se-**Se**-Se environment, and Δ = 290 ± 10 ppm; η = 0.9 ± 0.1 for the P-**Se**-P environment. These ^{77}Se chemical shift tensor parameters for all P$_x$Se$_{100-x}$ glasses are listed in Table 5a-3 and shown in Fig. 5a-11.
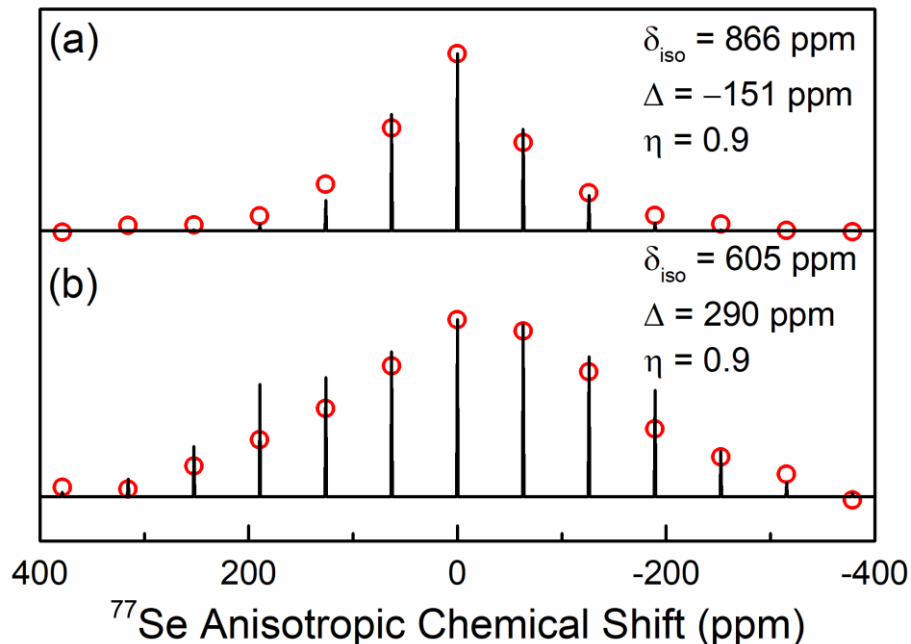
Figure 5a-10 Experimental (open red circles) and simulated (black traces) ^{77}Se NMR spinning sideband intensities in the anisotropic dimension for (a) Se–**Se**–Se sites in P$_5$Se$_{95}$ glass and (b) P–**Se**–P sites in P$_{30}$Se$_{70}$ glass, taken at δ_{iso} ~ 866 ppm and 605 ppm, respectively.

Table 5a-2 ^{77}Se NMR parameters used for simulation of ^{77}Se isotropic NMR line shapes. Asterisks denote P-**Se**-P site in P_4Se_3 molecules.

Glass composition	P_5Se_{95}	$P_{10}Se_{90}$	$P_{20}Se_{80}$	$P_{25}Se_{75}$	$P_{30}Se_{70}$	$P_{35}Se_{65}$	$P_{40}Se_{60}$	$P_{45}Se_{55}$	$P_{50}Se_{50}$	
Se–**Se**–Se										
δ_{iso} (±10 ppm)	853	853	846	844	840	832	831	827		
peak width (±10 ppm)	140	140	140	140	140	140	140	140		
relative fraction (±5%)	78	65	47	39	35	24	17	13		
Se–**Se**–P										
δ_{iso} (±10 ppm)	755	758	758	756	756	756	751	758	759	
peak width (±10 ppm)	155	155	155	155	157	157	157	157	155	
relative fraction (±5%)	14	23	30	34	34	33	30	28	16	
P–**Se**–P										
δ_{iso} (±10 ppm)	634	629	620	615	612	600	589	587	575	**819***
peak width (±10 ppm)	179	179	179	179	179	179	179	178	176	**127***
relative fraction (±5%)	8	12	23	27	31	43	53	59	75	**9***
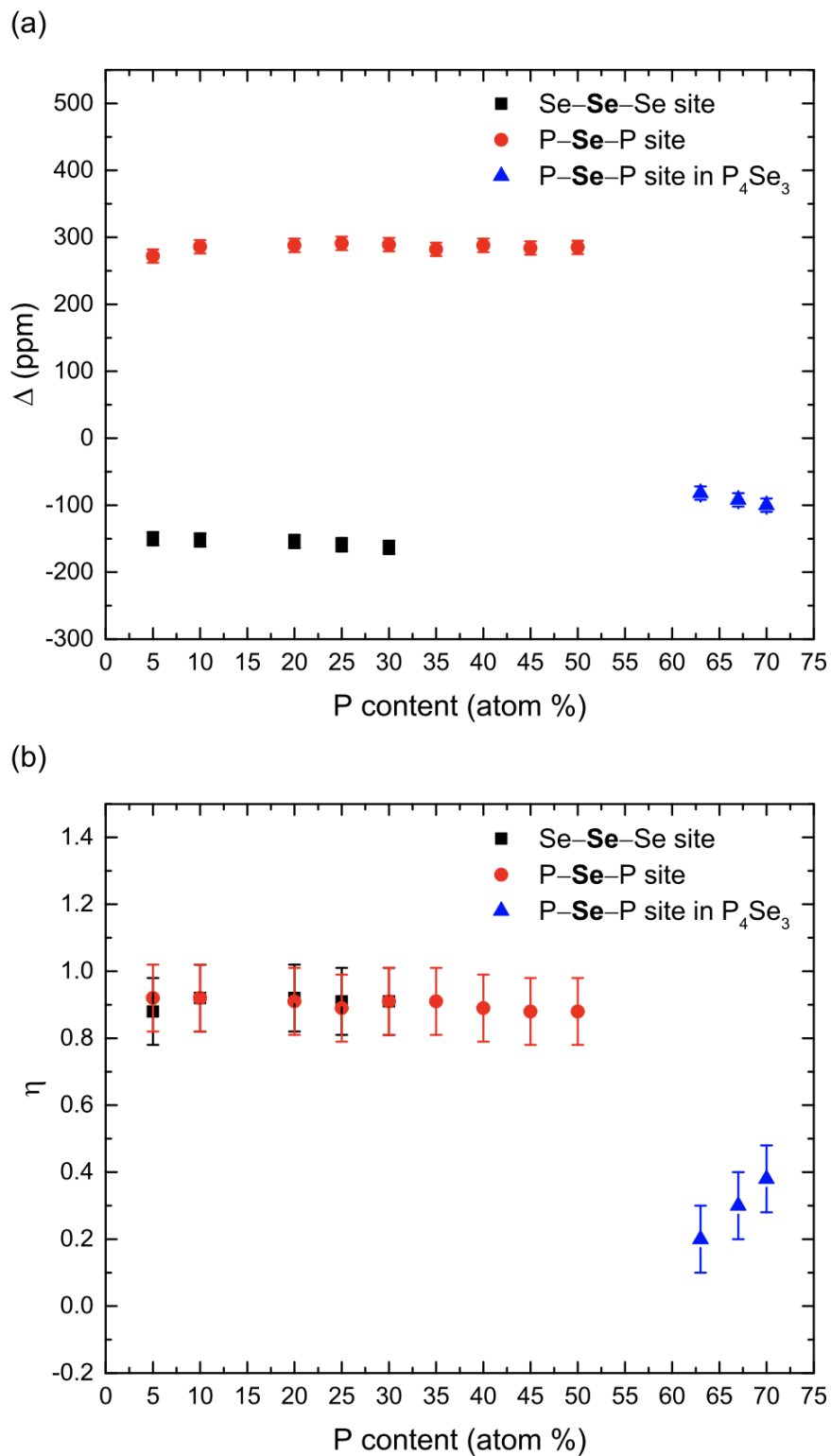
Figure 5a-11 Compositional variation of ^{77}Se chemical shift tensor parameters Δ (a) and η (b) for various Se sites in P_xSe_{100-x} glasses.

In contrast to glasses with $x \leq 50$, the ^{77}Se MAS NMR spectra of P-rich glasses with $x \geq$ 63 show only one Se resonance centered at ~ 826 ppm (Fig. 5a-12). In spite of the similarity in δ_{iso} of this resonance with that of the Se-**Se**-Se environment, the CSA tensor parameters for the former ($\Delta = -90 \pm 10$ ppm; $\eta \sim 0.3 \pm 0.1$) are found to be distinctly different from those ($\Delta = -151 \pm 10$ ppm; $\eta \sim 0.9 \pm 0.1$) characteristic of the latter (Table 5a-3, Figs. 5a-11, 13). As shown by the Raman and ^{31}P NMR spectroscopic results, P_4Se_3 molecules are a major constituent of the structure of these P-rich glasses and consequently this Se resonance centered at ~ 826 ppm can be assigned to the P–**Se**–P sites in these molecules. This structural assignment is consistent with the previously reported [77]Se δ_{iso} (~ 800 ppm) for crystalline P_4Se_3 in the literature.[30] Moreover, it is important to note that the width of the ^{77}Se MAS NMR resonance in these high-P glasses progressively increases with increasing P content from 63 at.% to 70 at.% (Fig. 5a-12). The ^{77}Se MAS NMR spectrum of $P_{63}Se_{37}$ glass displays the narrowest linewidth, which is consistent with a tight distribution of P-Se-P angles and P-Se distances, as would be expected for a molecule such as P_4Se_3. The increased ^{77}Se MAS NMR linewidth in $P_{67}Se_{33}$ and $P_{70}Se_{30}$ glasses indicates an increase in the heterogeneous broadening that can be ascribed to a wider range of P-Se-P angles and P-Se distances that is likely associated with the appearance and increasing concentration of the P_4Se_3-like structural moieties as hypothesized above.

Finally, the compositional variation of the relative fractions of Se-**Se**-Se, P-**Se**-Se and P-**Se**-P environments in glasses with $x \leq 50$, as obtained from the simulations of the ^{77}Se isotropic NMR spectral line shapes, is shown in Fig. 5a-14. The monotonic decrease in the relative fraction of Se–**Se**–Se environments provides evidence in favor of the shortening of Se chains with increasing P content. On the other hand, the P–**Se**–P fraction shows an opposite trend of monotonic increase, while the Se–**Se**–P fraction displays a local maximum at ~ 25-30 at% P (Table 5a-2). In
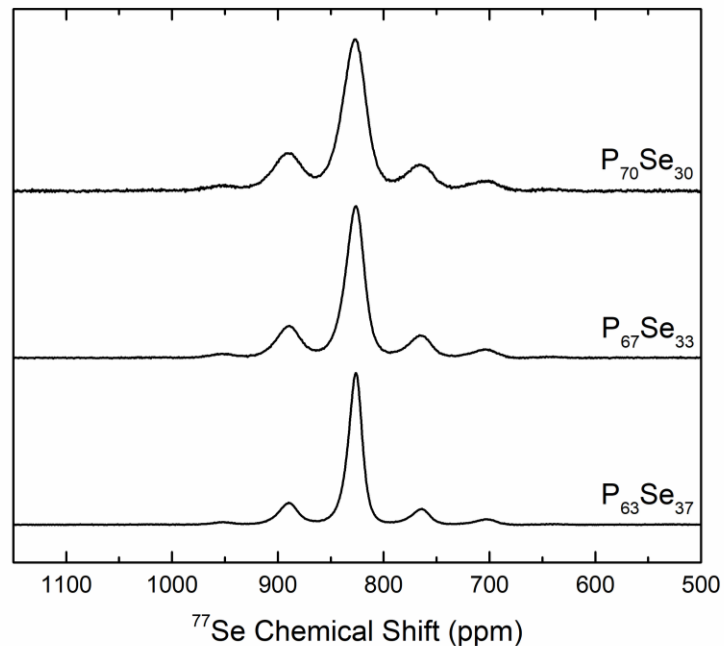
Figure 5a-12 ^{77}Se MAS NMR spectral line shapes of P_xSe_{100-x} glasses with $x \geq 63$. Glass compositions are listed alongside the spectra.

Table 5a-3 ^{77}Se chemical shift anisotropy parameters for P_xSe_{100-x} glasses.

	Se−**Se**−Se site		P−**Se**−P site		P−**Se**−P site in P_4Se_3	
	Δ (±10 ppm)	η (±0.1)	Δ (±10 ppm)	η (±0.1)	Δ (±10 ppm)	η (±0.1)
P_5Se_{95}	-150	0.9	272	0.9	−	−
$P_{10}Se_{90}$	-152	0.9	286	0.9	−	−
$P_{20}Se_{80}$	-154	0.9	288	0.9	−	−
$P_{25}Se_{75}$	-159	0.9	291	0.9	−	−
$P_{30}Se_{70}$	-163	0.9	289	0.9	−	−
$P_{35}Se_{65}$	−	−	282	0.9	−	−
$P_{40}Se_{60}$	−	−	288	0.9	−	−
$P_{45}Se_{55}$	−	−	284	0.9	−	−
$P_{50}Se_{50}$	−	−	285	0.9	−	−
$P_{63}Se_{37}$	−	−	−	−	-82	0.2
$P_{67}Se_{33}$	−	−	−	−	-92	0.3
P70Se30	−	−	−	−	-100	0.4

137
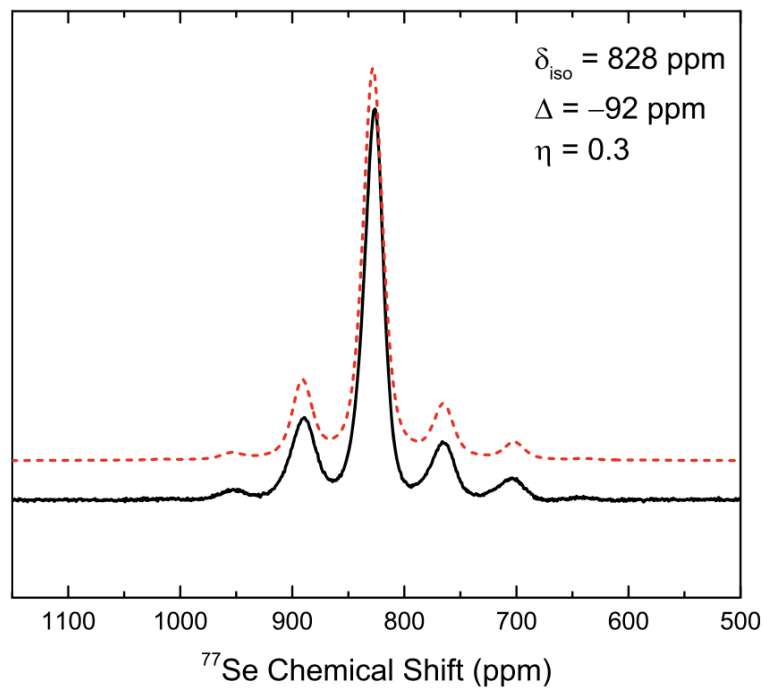
Figure 5a-13 Representative simulation (dotted line) of ^{77}Se MAS NMR spectrum (solid line) of P$_{67}$Se$_{33}$ glass.
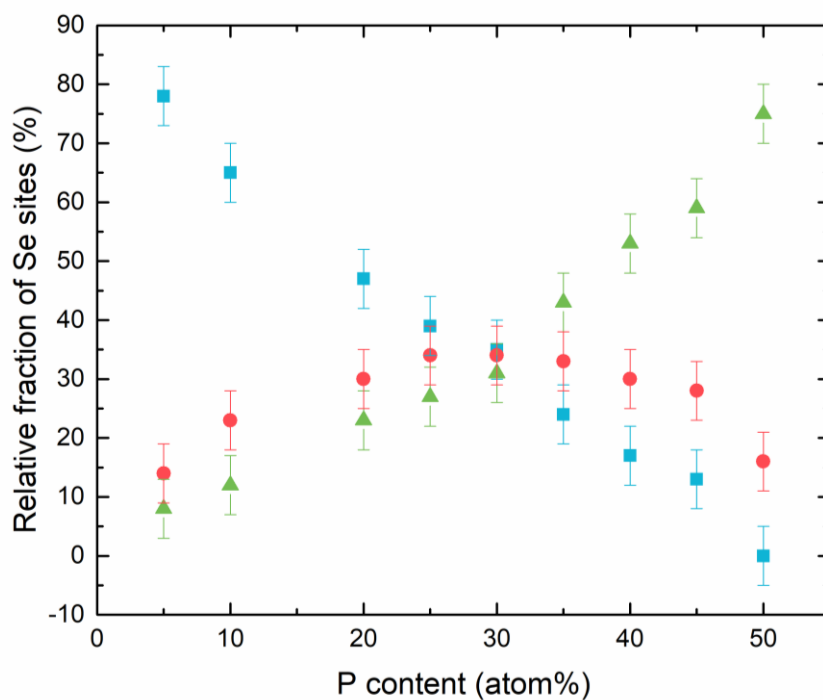
Figure 5a-14 Compositional variation of Se–**Se**–Se (blue square), Se–**Se**–P (red circle) and P–**Se**–P (green triangle) site fractions obtained from simulations of ^{77}Se isotropic NMR spectra.

order to better understand the spatial distribution and connectivity between the Se-Se and P-Se linkages in the structure, the compositional trend of the Se–**Se**–Se environments is compared with the predictions of several models (Fig. 5a-15). Among these models the chain crossing model assumes that all P-containing structural moieties are separated by at least one Se–Se unit such that no P-Se- P linkages exist, whereas the clustering model assumes that these moieties are all linked together via P–Se–P bridges to form P-rich regions. Clearly the presence of a significant fraction of Se-**Se**-P sites in these glasses indicates that the clustering model does not accurately describe the connectivity between the Se-Se and P-Se units in these glasses. The random model on the other hand simply considers a random spatial distribution of Se-Se and P-Se units in the glass structure.[17] All model calculations also take into account the presence of the terminal P=Se bond on the Se=P(Se$_{1/2}$)$_3$ units and the P-P bond on the $_{2/2}$SeP–PSe$_{2/2}$ units.[17] It is clear from Fig. 5a-15 that both random and chain crossing models describe the experimental data well for the Se-**Se**-Se site fractions at low P contents (x ~20), whereas the experimental data at higher P contents falls between the random and clustering model predictions. This result based on high-resolution ^{77}Se NMR spectra is significantly different from the findings of Maxwell *et al.,* especially for compositions with $x \geq 30$, where their data based on high-temperature ^{77}Se NMR and ^{31}P-^{77}Se SEDOR NMR suggested a random connectivity between the Se-Se and P-Se units.[17] These authors claimed that their Se-**Se**-Se speciation results as obtained from high temperature ^{77}Se NMR were more accurate than those from SEDOR NMR since the imperfections of the 180° pulse on the ^{31}P channel resulted in less than 100% ^{31}P inversion efficiency for the latter experiments, and thus in an over estimation of the Se-**Se**-Se site population. However, we argue that the ^{77}Se isotropic NMR spectra obtained in the present study using 2D ^{77}Se MATPASS/CPMG NMR provide superior resolution and accuracy of selenium speciation compared to the high-
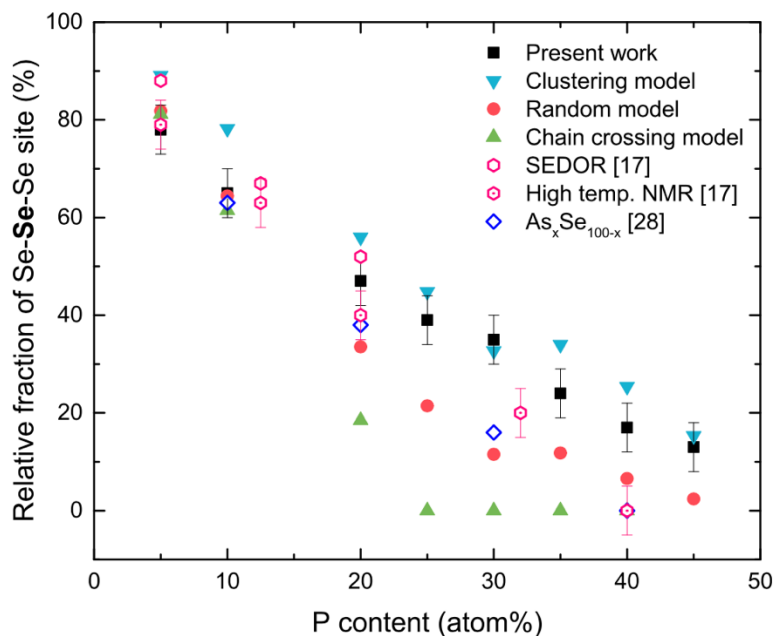
Figure 5a-15 Compositional variation of Se–**Se**–Se site fraction (black squares) compared with that predicted by the clustering (inverted blue triangles), random (pink circles), and chain crossing models (green triangles). Fractional concentration of Se-**Se**-Se environment in P-Se (open pink hexagons) and As-Se (open blue diamonds) binary glasses reported in previous studies is also included for comparison.[17,28]

temperature ^{77}Se NMR spectra reported by Eckert and coworkers in these pioneering early studies.[17] Therefore, the experimentally observed selenium speciation in these P_xSe_{100-x} glasses with $x \leq 50$ indicates that the spatial distribution of the constituent structural building blocks is best described as intermediate to that predicted by the random and the clustered scenarios. This result can be contrasted with the Se-**Se**-Se speciation in binary As_xSe_{100-x} glasses, which follows a random distribution as shown in Fig. 5a-15.[28] One of the striking features of the P_xSe_{100-x} glasses is the abundance of P-P bonds as exemplified by the ethylene-like $_{2/2}SeP–PSe_{2/2}$ units in Se-excess or stoichiometric compositions (P ≤40 at.%), whereas analogous species are not present in the corresponding As_xSe_{100-x} glasses.[9] In fact, the Raman spectroscopic results presented in this study show that P-P bonds appear for the first time in a highly Se-excess composition with only ~ 10 at.% P. On the other hand, while the structure of the stoichiometric $As_{40}Se_{60}$ glass consists

almost exclusively of AsSe$_{3/2}$ pyramids, the structure of the P$_{40}$Se$_{60}$ glass consists predominantly

of $_{2/2}$SeP–PSe$_{2/2}$ units.[9,28]

5a.4.4 Structural connectivity and glass transition behavior

The T_g of all P$_x$Se$_{100-x}$ glasses determined in this study are shown in Fig. 5a-16. The values

are in general in good agreement with those previously reported in the literature.[8,9,31–34]

However, it may be noted that, while all glasses prepared in the present study display a single glass

transition, Bytchkov *et al.* reported the observation of two T_g for the P$_{67}$Se$_{33}$ glass.[9] This

discrepancy could perhaps be related to a lack of homogenization of the sample during melting in

the latter study. The highly non-monotonic compositional variation of T_g for these glasses as seen

in Fig. 5a-16 is completely consistent with the corresponding structural evolution. When taken

together, the Raman, ^{31}P and ^{77}Se NMR spectroscopic results indicate that the structural

connectivity of the P$_x$Se$_{100-x}$ glasses increases with progressive addition of P to Se up to x ~50, at

which point the -Se-Se-Se- chain elements disappear and the structure becomes highly rigid. This

structural evolution is in accordance with the corresponding increase in T_g with P content in this

composition range (Fig. 5a-16). The T_g increases slowly up to ~ 40% P as the Se chains are

increasingly cross-linked by P atoms and the average Se chain length decreases. As P content

increases to 50 at.% the Se chain elements completely disappear and the structure becomes fully

cross-linked via P-Se-P linkages and T_g rapidly increases by ~ 100 °C (Fig. 5a-16). Beyond this

point, further addition of P results in the formation of P$_4$Se$_3$ molecules, which drastically lowers

the connectivity of the structure. The concentration of these molecules in these glasses maximizes

near x ~63 and correspondingly T_g decreases by nearly 180 °C. At higher P concentrations the

structural connectivity increases again as the amorphous red phosphorus like regions become

dominant and, consequently, T_g increases by ~ 40 °C as P content increases from 63 to 70 at.%. This compositional evolution of the structural connectivity and of T_g of P_xSe_{100-x} glasses can be contrasted with that reported in the case of As_xSe_{100-x} glasses by Yang *et al.*[35] While the P_xSe_{100-x} glasses show a maximum in T_g at $x = 50$, for the As_xSe_{100-x} glasses this maximum is located at the stoichiometric composition, i.e., at $x = 40$. This difference can be readily attributed to the early appearance of the As_4Se_4 and As_4Se_3 cage molecules in Se-deficient As_xSe_{100-x} glasses with $x > 40$ while, the appearance of the P_4Se_3 molecules is delayed in P_xSe_{100-x} glasses until $x > 50$.[35] Moreover, compared to the P_xSe_{100-x} system, near $x \sim 60$ the molecule content appears to remains significantly lower in the As_xSe_{100-x} glasses, which is consistent with a smaller drop in T_g in the latter.
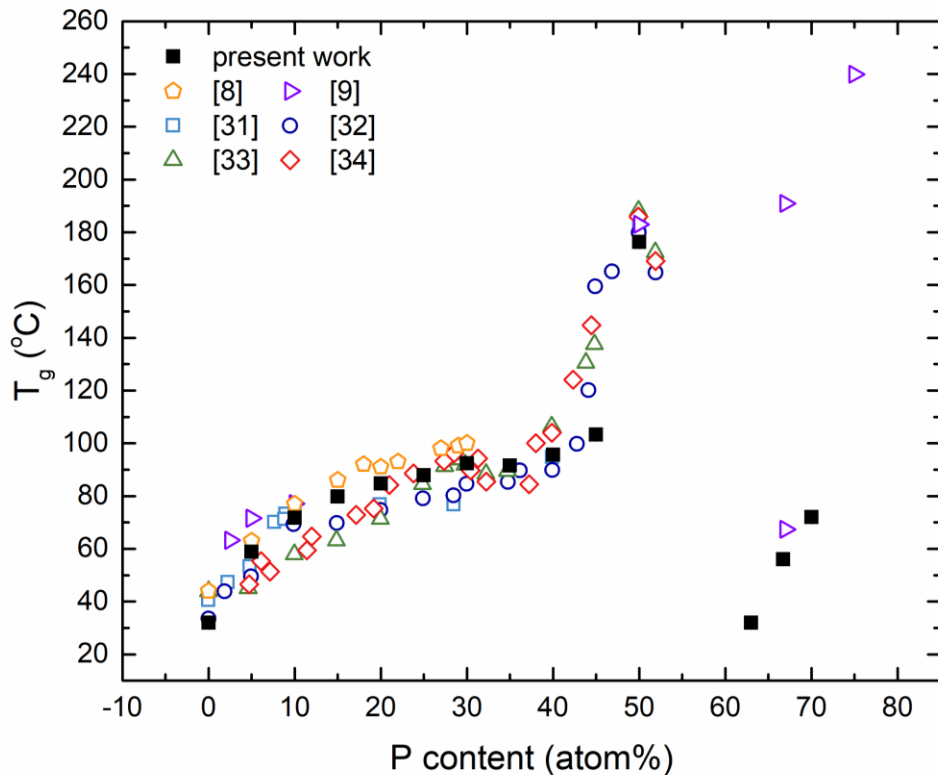
Figure 5a-16 Composition dependence of T_g of binary P_xSe_{100-x} glasses determined in the present study (filled squares) and those reported in the literature (open symbols).[8,9,31–34]

5a.5 Conclusion

The compositional evolution of structure and connectivity of $P_x Se_{100-x}$ glasses with $5 \leq x \leq 70$ is studied using a combination of Raman, ^{77}Se and ^{31}P NMR spectroscopy. Progressive addition of P to Se in glasses with $x \leq 50$ results in cross-linking of Se chains via pyramidal $P(Se_{1/2})_3$ units, ethylene-like $_{2/2}SeP-PSe_{2/2}$ units, and $Se=P(Se_{1/2})_3$ tetrahedral units, which ultimately leads to the disappearance of the chain units and the formation of a rigid network structure of corner-shared P-Se polyhedra at $x \approx 50$. Correspondingly, in this composition range the relative concentration of the Se-**Se**-Se (P-**Se**-P) sites monotonically decreases (increases) with increasing x, and that of the P-Se-Se units goes through a maximum near $x \approx 30$. Additionally, the systematic compositional variation of ^{77}Se δ_{iso} of Se-**Se**-Se and P-**Se**-P sites is found to be related to the number of P atoms as the next-nearest-neighbors. The connectivity between the P-Se and Se-Se building blocks in this composition range is best described as intermediate to that of the random and clustered scenarios. The largely connected network of P-Se polyhedra in the $P_{50}Se_{50}$ glass gives way to a structure made primarily of P_4Se_3 molecules held together by van der Waals forces in the $P_{63}Se_{37}$ glass. In fact, the first appearance of these molecules is observed in the ^{31}P NMR spectrum of the $P_{50}Se_{50}$ glass. Further increase in the P content in glasses with $x \geq 63$ results in an increasingly connected network via a decrease in the relative concentration of the P_4Se_3 molecules and the appearance and increase in the concentration of amorphous red phosphorus-like structural moieties and P_4Se_3-like groups that are likely linked via P-P bonds. The overall evolution of the structural connectivity is consistent with the pronounced nonmonotonic compositional variation in T_g.

Acknowledgements

References

[1]   A. Zakery, S.R. Elliott, Optical properties and applications of chalcogenide glasses: a review, J. Non. Cryst. Solids. 330 (2003) 1–12.

[2]   B. Bureau, X.H. Zhang, F. Smektala, J.L. Adam, J. Troles, H.L. Ma, C. Boussard-Plèdel, J. Lucas, P. Lucas, D. Le Coq, M. R. Riley, J. H. Simmons, Recent advances in chalcogenide glasses, J. Non. Cryst. Solids. 345&346 (2004) 276–283.

[3]   L. Calvez, Chalcogenide glasses and glass-ceramics: Transparent materials in the infrared for dual applications, Comptes Rendus Phys. 18 (2017) 314–322.

[4]   J.M. Harbold, F.Ö. Ilday, F.W. Wise, J.S. Sanghera, V.Q. Nguyen, L.B. Shaw, I.D. Aggarwal, Highly nonlinear As–S–Se glasses for all-optical switching, Opt. Lett. 27 (2002) 119.

[5]   C. Quémard, F. Smektala, V. Couderc, A. Barthélémy, J. Lucas, Chalcogenide glasses with high non linear optical properties for telecommunications, J. Phys. Chem. Solids. 62 (2001) 1435–1440.

[6]   J. Yu, H. Zhang, E. Olsson, T. Yu, Z. Liu, S. Zhang, X. Huang, W. Li, Q. Cai, A novel amorphous P_4SSe_2 compound as an advanced anode for sodium-ion batteries in ether-based electrolytes, J. Mater. Chem. A. 9 (2021) 12029–12040.

[7]   Y. Cao, M.K. Majeed, Y. Li, G. Ma, Z. Feng, X. Ma, W. Ma, P_4Se_3 as a new anode material for sodium-ion batteries, J. Alloys Compd. 775 (2019) 1286–1292.

[8]   D.G. Georgiev, M. Mitkova, P. Boolchand, G. Brunklaus, H. Eckert, M. Micoulaut, Molecular structure, glass transition temperature variation, agglomeration theory, and network connectivity of binary P-Se glasses, Phys. Rev. B. 64 (2001) 134204.

[9]   A. Bytchkov, F. Fayon, D. Massiot, L. Hennet, D.L. Price, ^{31}P solid-state NMR studies of the short-range order in phosphorus-selenium glasses, Phys. Chem. Chem. Phys. 12 (2010) 1535–1542.

[10]   R.T. Phillips, M.K. Ellis, Microstructure of P-Se glasses and low frequency Raman scattering, J. Non. Cryst. Solids. 164–166 (1993) 135–138.

[11]   D. Lathrop, H. Eckert, Quantitative determination of the structural units in phosphorus-selenium glasses by ^{31}P dipolar and magic-angle-spinning NMR spectroscopy, Phys. Rev. B. 43 (1991) 7279–7287.

[12]   D. Lathrop, H. Eckert, Chemical disorder in non-oxide chalcogenide glasses. Site speciation in the system phosphorus-selenium by magic angle spinning NMR at very high spinning speeds, J. Phys. Chem. 93 (1989) 7895–7902.

[13]   D. Lathrop, H. Eckert, Dipolar NMR Spectroscopy of Nonoxidic Glasses. Structural Characterization of the System Phosphorus-Selenium by [31]P-[77]Se Spin Echo Double Resonance NMR, J. Am. Chem. Soc. 112 (1990) 9017–9019.

[14]   D. Lathrop, H. Eckert, NMR studies of chalcogenide glasses: The system phosphorus-selenium, J. Non. Cryst. Solids. 106 (1988) 417–420.

[15] R.T. Phillips, D. Wolverson, M.S. Burdis, Y. Fang, Observation of discrete molecular structures in glassy P_xSe_{1-x} by Raman spectroscopy, Phys. Rev. Lett. 63 (1989) 2574–2577.

[16] Z.U. Borisova, Glassy Semiconductors, Springer US, 1981.

[17] R. Maxwell, D. Lathrop, H. Eckert, Intermediate-range order in phosphorus-selenium glasses. Constraints from ^{31}P and ^{77}Se NMR spectroscopy, J. Non. Cryst. Solids. 180 (1995) 244–250.

[18] I. Hung, T. Edwards, S. Sen, Z. Gan, MATPASS/CPMG: A sensitivity enhanced magic-angle spinning sideband separation experiment for disordered solids, J. Magn. Reson. 221 (2012) 103–109.

[19] U. Haeberlen, High Resolution NMR in Solids Selective Averaging: Supplement 1 Advances in Magnetic Resonance, Elsevier, 2012.

[20] I. Hung, Z. Gan, On the practical aspects of recording wideline QCPMG NMR spectra, J. Magn. Reson. 204 (2010) 256–265.

[21] D.J. States, R.A. Haberkorn, D.J. Ruben, A two-dimensional nuclear overhauser experiment with pure absorption phase in four quadrants, J. Magn. Reson. 48 (1982) 286–292.

[22] O.N. Antzutkin, S.C. Shekar, M.H. Levitt, Two-Dimensional Sideband Separation in Magic-Angle-Spinning NMR, J. Magn. Reson. Ser. A. 115 (1995) 7–19.

[23] R.K. Harris, E.D. Becker, S.M. Cabral De Menezes, R. Goodfellow, P. Granger, NMR nomenclature: Nuclear spin properties and conventions for chemical shifts (IUPAC recommendations 2001), Pure Appl. Chem. 73 (2001) 1795–1818.

[24] D. Massiot, F. Fayon, M. Capron, I. King, S. Le Calvé, B. Alonso, J.O. Durand, B. Bujoli, Z. Gan, G. Hoatson, Modelling one- and two-dimensional solid-state NMR spectra, Magn. Reson. Chem. 40 (2002) 70–76.

[25] D.C. Kaseman, O. Gulbiten, B.G. Aitken, S. Sen, Isotropic rotation vs. Shear relaxation in supercooled liquids with globular cage molecules, J. Chem. Phys. 144 (2016) 174501.

[26] B.W. Tattershall, E.L. Sandham, Interdependence of phosphorus-31-selenium-77 NMR coupling constants in bicyclic phosphorus selenide compounds, J. Chem. Soc. Dalt. Trans. (2001) 1834–1840.

[27] R. Maxwell, H. Eckert, Molten-state kinetics in glass-forming systems. A high-temperature NMR study of the system phosphorus-selenium, J. Phys. Chem. 99 (1995) 4768–4778.

[28] D.C. Kaseman, I. Hung, Z. Gan, B. Aitken, S. Currie, S. Sen, Structural and Topological Control on Physical Properties of Arsenic Selenide Glasses, J. Phys. Chem. B. 118 (2014) 2284–2293.

[29] D.C. Kaseman, I. Hung, Z. Gan, S. Sen, Observation of a Continuous Random Network Structure in Ge_xSe_{100-x} Glasses: Results from High-Resolution [77]Se MATPASS/ CPMG

NMR Spectroscopy, J. Phys. Chem. B. 117 (2013) 949–954.

[30] T. Pietraß, R. Seydoux, R.E. Roth, H. Eckert, A. Pines, ^{31}P to [77]Se cross polarization in β-P$_4$Se$_3$, Solid State Nucl. Magn. Reson. 8 (1997) 265–267.

[31] Z. Borisova, B. Kasatkin, E. Kim, Glaeser im Systemen Phosphor-Selen, Izv. Akad. Nauk SSSR Neorg. Mater. 9 (1973) 822.

[32] F. Heyder, D. Linke, Zur Glasbildung in den Systemen Phosphor-Schwefel und Phosphor-Selen, Z. Chem. 13 (1973) 480.

[33] R. Blachnik, A. Hoppe, Glass transition and specific heats in the systems P-S, P-Se, As-S and As-Se, J. Non. Cryst. Solids. 34 (1979) 191–201.

[34] Y. Monteil, H. Vincent, A New Phosphorus Selenide P$_4$Se$_4$, Z. Anorg. Allg. Chem. 416 (1975) 181.

[35] G. Yang, B. Bureau, T. Rouxel, Y. Gueguen, O. Gulbiten, C. Roiland, E. Soignard, J.L. Yarger, J. Troles, J.C. Sangleboeuf, P. Lucas, Correlation between structure and physical properties of chalcogenide glasses in the As$_x$Se$_{1-x}$ system, Phys. Rev. B. 82 (2010) 195206.

Chapter 5b

Structural Control on the Rheological Behavior of Binary P-Se

Supercooled Liquids

5b.1 Abstract

The link between the atomic structure and the shear relaxation behavior of P_xSe_{100-x} ($0 \leqslant x \leqslant 25$) supercooled liquids is investigated using Raman spectroscopy and parallel plate rheometry. The P atoms in these glasses form $Se=P(Se_{1/2})_3$, $P(Se_{1/2})_3$ and $_{2/2}SeP\text{-}PSe_{2/2}$ units, which serve as cross-linkers of the $[Se]_n$ chain segments. The frequency dependence of the storage and loss moduli as well as the relaxation spectra $H(\tau)$ indicate that liquids with >85% Se are characterized by the coexistence of a slow and a fast relaxation process corresponding to bond scission/renewal and Se chain segmental motion, respectively. On the other hand, liquids with ≤85% Se display only the bond scission/renewal process. The $H(\tau)$ spectra suggest that the relaxation-time τ distribution for Se chain dynamics is a sensitive function of the chain length, while that for bond scission/renewal is controlled by the variety of bond types and structural moieties involved.

5b.2 Introduction

The rheological behavior of supercooled glass-forming liquids is intimately linked to their viability for various processing techniques [1,2]. Thus, a fundamental understanding of the structural control on the rheological behavior of glass-forming liquids is of paramount importance in the optimization of the corresponding processing parameters. Comprehensive and systematic studies in this direction have recently been carried out on a variety of binary chalcogenide glass-formers in the As-Se, Ge-Se, Se-Te and As-S systems [3–7]. While the structure of glassy/liquid Se consists primarily of two coordinated Se atoms forming polymeric $[Se]_n$ chains [8], the addition of Ge or As results in progressive cross-linking of these chains and a concomitant shortening of the segmental chain length [9–11]. Rheological studies of supercooled Se-rich liquids using small angle oscillatory shear (SAOS) have shown the existence of a slow and a fast relaxation process with widely different timescales and relaxation moduli. The slow and fast processes were shown to correspond to bond scission/renewal and segmental motion of Se chains, respectively [12,13]. Progressive shortening of the Se chain length with increasing Ge/As concentration leads to an increase in the timescale of the segmental chain motion, as this dynamical process becomes increasingly dependent and thus temporally coupled to the bond scission/renewal [3,4]. Although all slow relaxation processes correlate to the bond scission/renewal event, some variations still exist in between systems because different chemical bonds/interactions are involved in different structural environments. For instance, the bond scission/renewal process in the binary Se-Te system involves not only the possible Se-Se, Se-Te, and Te-Te bonds, but also the strong secondary bonding interactions between adjacent chains, resulting in a much broader relaxation time distribution when compared with the slow relaxation process in pure Se [6]. This structural evolution of the viscoelastic relaxation ultimately results in the disappearance of the segmental

chain motion across all binary systems as the Se chain segments become too short (≤ 3 to 5 Se atoms) to sustain the segmental motion [3]. At this point the shear relaxation of these liquids is entirely controlled by the bond scission-renewal dynamics. While segmental chain motion is expected to be a function of the effective chain length, the bond scission/renewal is expected to be controlled by the bond types associated with the various structural moieties in the liquid. In fact, an analysis of the relaxation spectrum derived from the frequency dependent shear modulus data has shown that, compared to pure Se, binary Se-Te liquids with copolymeric $[Se,Te]_n$ chains display a broader distribution of the bond scission/renewal timescales [6]. This result was hypothesized to be indicative of the fact that, unlike pure Se consisting of only Se-Se bonds, bond scission in Se-Te alloys involves a variety of bond types, including Se-Se, Se-Te and Te-Te, as well as the secondary bonds involving Te atoms. Here we extend such studies to the supercooled liquids in the binary P-Se system to systematically investigate the effect of a wide variety of different bond types, structural moieties and connectivity on the viscoelastic relaxation behavior.

The P-Se system exhibits an extensive glass formation range which can be divided into two regions, the Se-rich region with $0 \leq x \leq 54$ and P-rich regions with $64 \leq x \leq 84$. The narrow composition window in between these two regions is centered on the P_4Se_3 stoichiometry, which displays high crystallization tendency [14]. The composition-dependent structural evolution in the Se-rich and P-rich glass formation regions has been extensively investigated by Raman scattering, and solid state [77]Se and ^{31}P nuclear magnetic resonance (NMR) spectroscopy [15–21]. These studies have indicated that the structure of P-Se glasses with P content below 30 at.% consists primarily of $Se=P(Se_{1/2})_3$ tetrahedral units and $P(Se_{1/2})_3$ pyramidal units linked by $[Se]_n$ chains. The relative fraction of the $[Se]_n$ chains decreases with increasing P content and the structure changes to a polymeric network consisting predominantly of $_{2/2}SeP\text{-}PSe_{2/2}$ and some $P(Se_{1/2})_3$ units

that are connected via short Se-Se segments. Finally, at P contents of ≥45 at.% a significant amount of embedded P_4Se_3 molecules appear in these glasses. Previous variable-temperature ^{31}P and ^{77}Se NMR spectroscopy studies [22–24] showed the presence of two types of dynamical processes in P-Se liquids within this composition range: at low P contents (≤25%) the dynamics involve Se site exchange between Se-bonded and P-bonded Se via reaction 1 (see below), while at higher P contents (≥30%) the process involves the interconversion between different P sites as represented by equations 2 and 3 below:

$$P(Se_{1/2})_3 + Se \leftrightarrow Se=P(Se_{1/2})_3 \qquad\qquad (1)$$

$$P_2(Se_{1/2})_4 + Se \leftrightarrow 2P(Se_{1/2})_3 \qquad\qquad (2)$$

$$3P_2(Se_{1/2})_4 \leftrightarrow 2P(Se_{1/2})_3 + P_4Se_3 \qquad\qquad (3)$$
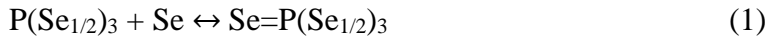
Therefore, the liquids in the P-Se system with their rich structural complexity lend themselves as ideal candidates for an exploration of the effects of the variety in bonding and structural moiety and connectivity on the shear relaxation behavior. Here we investigate such effects in a detailed rheological study of the shear relaxation behavior of binary P-Se supercooled liquids with ≤25 at.% P using small amplitude oscillatory shear (SAOS) measurements. The glass structure was characterized using Raman spectroscopy and correlations between glass structure and shear relaxation behavior are discussed in detail.

5b.3 Experimental Methods

5b.3.1 Sample preparation and characterization

Binary P_xSe_{100-x} glasses with $x = 5, 10, 15, 20,$ and 25 were synthesized in ~12 g batches using the conventional melt-quench method. Elemental red phosphorus (Spectrum, 99.999%) and selenium (Alfa Aesar, 99.999%) were mixed together in stoichiometric ratios and subsequently

flame-sealed in evacuated (10^{-4} Torr) quartz ampoules. The ampules were then sealed and placed in a rocking furnace, slowly heated to 923 K over 13 hours and held at this temperature for 36 h to ensure melt homogeneity. The melts were subsequently quenched to form glass by dipping the ampoules in water.

The glass transition temperature T_g of these $P_x Se_{100-x}$ glasses was measured using a Mettler-Toledo DSC1 differential scanning calorimeter. Approximately 15 mg of powdered glass sample was loaded in a hermetically sealed 40 μL aluminum crucible, and scans were performed at 10 °C/min under a continuously flowing nitrogen environment. T_g was determined to within ± 1 °C as the onset of the glass transition. The unpolarized Raman spectra of all glasses were collected in backscattering geometry with a resolution of 1 cm^{-1}, using a Renishaw 1000 Raman Microscope System equipped with a diode laser operating at a wavelength of 785 nm. Backscattered light was detected using a charge-coupled device cooled at 200 K.

5b.3.2 SAOS Parallel Plate Rheometry

The SAOS and steady shear rheological measurements reported here were carried out on either an MCR92 or an MCR302 parallel plate rheometer (Anton-Paar) under a constant flow of nitrogen gas, respectively. The temperature is controlled by a Peltier heater (up to 200 °C) in MCR92 and a convection oven (up to 600 °C) in MCR302. In both setups, the upper plate was used to apply strain and measure torque while the bottom plate remained stationary. During each measurement the glass sample was first rapidly heated and trimmed at its softening point to achieve a sandwich geometry between the upper oscillatory plate and lower stationary plate with plate size of 8 mm and 25 mm diameter for the SAOS and the steady shear measurements, respectively, with a gap/sample thickness of ~ 1 mm. At each desired measurement temperature, the samples were allowed to equilibrate for 5 minutes followed by the application of a sinusoidal strain with varying

153

angular frequency ω between 1 to 600 rad/s and the induced torque was recorded to calculate the storage and loss moduli G′ and G″ as a function of ω. Measurements were carried out at multiple temperatures for each sample and master curves of $G'(\omega)$ and $G''(\omega)$ were constructed using time-temperature superposition (TTS). All SAOS measurements are done within the predetermined linear viscoelastic range. The viscosity of all supercooled P_xSe_{100-x} liquids was obtained under steady shear condition with samples confined in a ~0.8 mm gap between two plates. At each temperature, the Newtonian viscosity was measured at shear rates $\dot{\gamma}$ ranging between 0.01/s to 100/s and the average viscosity is reported.

5b.4 Results and Discussion

The Raman spectra of all P_xSe_{100-x} glasses are shown in Fig. 5b-1. The compositional evolution of these spectra agrees well with those reported on similar compositions in a previous study by Georgiev *et al.* [15]. The most intense band in these spectra centered at ~ 250 cm^{-1} corresponds to Se–Se stretching mode in $[Se]_n$ [25]. The bands centered at ~ 330 cm^{-1} and 210 cm^{-1} correspond, respectively, to symmetric and asymmetric stretching of P-Se bonds in the pyramidal $P(Se_{1/2})_3$ units. On the other hand, the vibrational modes of the ethylene-like $_{2/2}SeP-PSe_{2/2}$ units give rise to the bands located at ~ 185 cm^{-1}, 330-350 cm^{-1} and 370 cm^{-1}. Finally, the broad band centered at ~ 500 cm^{-1} corresponds to the stretching of the P=Se bonds in the $Se=P(Se_{1/2})_3$ tetrahedral units [15]. It is to be noted here that the Raman spectra in Fig. 5b-1 differ from those reported by Georgiev *et al.* [15] in one important respect. In the present study the 185 cm^{-1} band corresponding to the $_{2/2}SeP-PSe_{2/2}$ units appears clearly for the first time in the Raman spectrum of the $P_{15}Se_{85}$ glass, although it can be argued that the first hint of this band can be seen even in the spectrum of the $P_{10}Se_{90}$ glass (Fig. 5b-1). In contrast, this band becomes barely visible
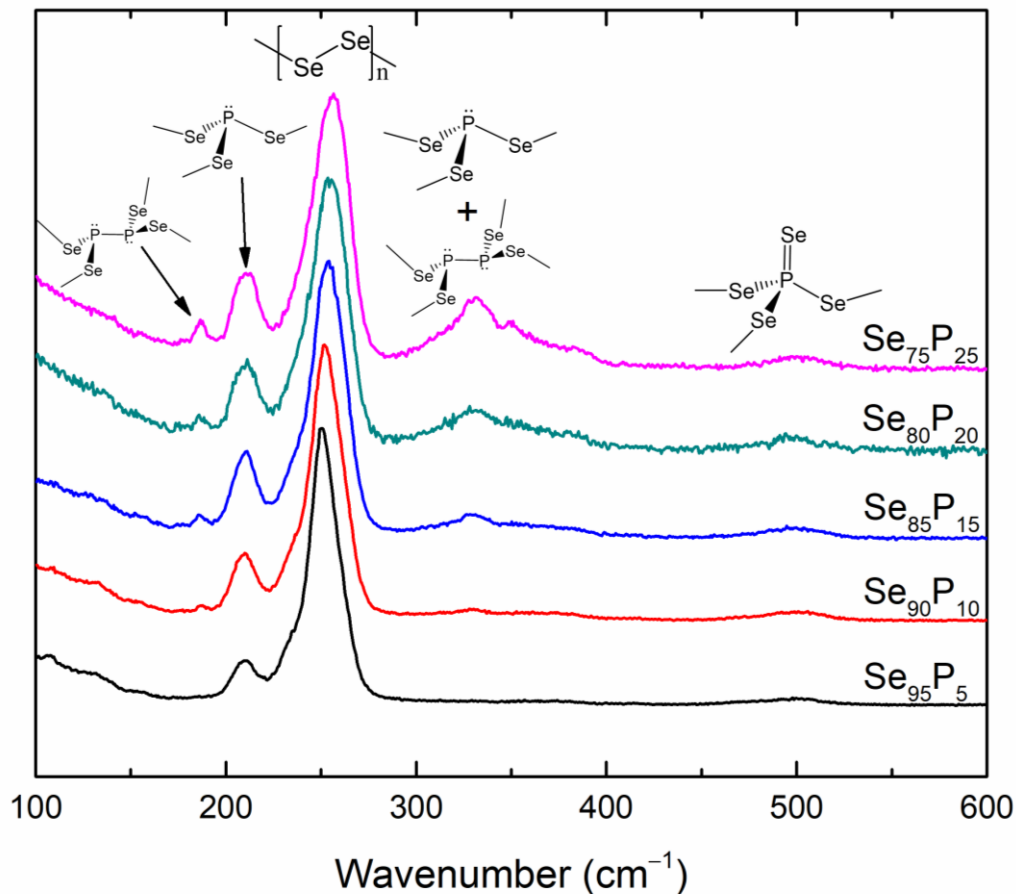
Figure 5b-1 Unpolarized Raman spectra of $P_x Se_{100-x}$ glasses showing structural assignment of various bands (see text for details). All spectra are normalized to the most intense peak at ~ 250 cm^{-1}.

for the first time in the Raman spectrum of the $P_{20}Se_{80}$ glass reported by Georgiev *et al.* [15]. It is unclear whether this difference could stem from the fact that the Raman spectra of *Georgiev et al.* were collected using a wavelength of 647 nm, which is located close to the optical band gap of amorphous Se and Se-rich chalcogenide glasses. However, a recent study by Bytchkov *et al.* [16] based on two-dimensional J-resolved ^{31}P magic-angle-spinning nuclear magnetic resonance (NMR) spectroscopy has conclusively shown that the $_{2/2}SeP$-$PSe_{2/2}$ units appear in P-Se glasses with >10% P, and a significant fraction (~ 6-7%) of P atoms resides in these units in the $P_{15}Se_{85}$ glass. Therefore, the Raman spectra of $P_x Se_{100-x}$ glasses obtained in the present study (Fig. 5b-1) are indeed consistent with the ^{31}P NMR results of Bytchkov *et al.* [16].

As expected, the intensities of all bands corresponding to the P-containing structural moieties exhibit a monotonic increase with respect to that the 250 cm^{-1} band with progressive addition of P to Se (Fig. 5b-1). This result demonstrates that addition of P to Se in this composition range results in an increasing degree of structural cross-linking and concomitant shortening of the average length of the [Se]$_n$ chain segments. The increasing structural connectivity and thus rigidity with increasing P content are also evident in the corresponding compositional variation in the T_g (Fig. 5b-2) and viscosity (Fig. 5b-3) of these liquids [15,26–30]. Besides T_g, the high-temperature viscosity determined in the present study, as well as the previously reported low-temperature viscosity data [30], show that the isothermal viscosity of these liquids monotonically increases with increasing P concentration (Figs. 5b-2,3). These viscosity data over the entire temperature range shown in Fig. 5b-3 are fitted to the MYEGA equation [31,32]:

$$log\ \eta = log_{10}\eta_{\infty} + \frac{K}{T} \cdot exp\left(\frac{C}{T}\right) \tag{4}$$

where the parameters $log_{10}\eta_{\infty}$, K, and C are all treated as fitting variables. The fragility index m, where $m = \left.\frac{d\ log_{10}\eta}{dT_g/T}\right|_{T=T_g}$, was subsequently calculated from these fitting parameters using the relation [32]:

$$m = \left(\frac{K}{T_g}\right)\left(1 + \frac{C}{T_g}\right)\exp\left(\frac{C}{T_g}\right) \tag{5}$$

The compositional variation of m thus obtained for these P-Se liquids (Fig. 5b-4) displays a sharp decrease with increasing P content up to 15% P, which is consistent with the rapid lowering of the Se chain conformational entropy upon cross linking with P atoms [3].
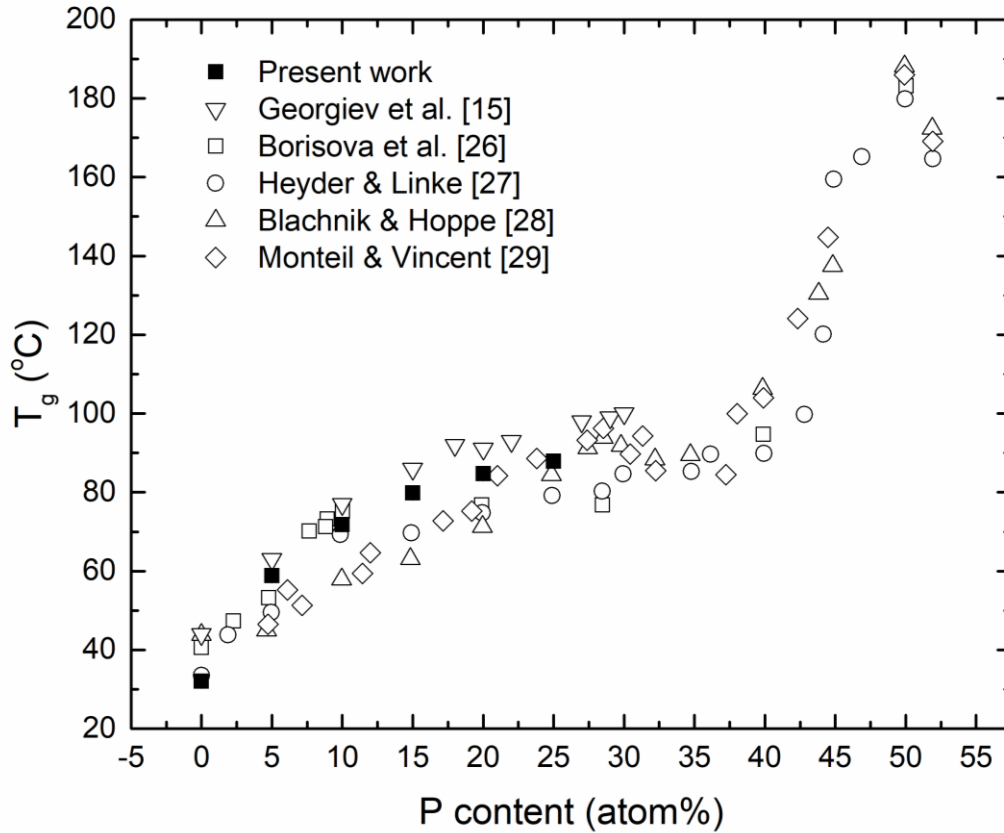
Figure 5b-2 Composition dependence of T_g of binary P_xSe_{100-x} glasses determined in the present study and reported in the literature.

The impact of this structural evolution on the rheological behavior is apparent in the experimental master curves of G′(ω) and G″(ω) constructed using TTS at nearly iso-viscous (~ 10^9 Pa.s) temperatures for all P_xSe_{100-x} supercooled liquids (Fig. 5b-5). In the low frequency regime G′(ω) < G″(ω), and both moduli approximately follow the Maxwell scaling of G′(ω) ~ ω^2 and G″(ω) ~ ω. On the other hand, in the high-frequency elastic regime G′(ω) approaches its glassy limit G_∞, while G″(ω) decreases with increasing frequency. The corresponding dynamical viscosity $\eta\,(\omega) = \frac{\sqrt{G'^2+G''^2}}{\omega}$ shows a transition from a frequency-independent to a frequency-dependent behavior with increasing ω (Fig. 5b-5). As has been shown in previous studies, the

157
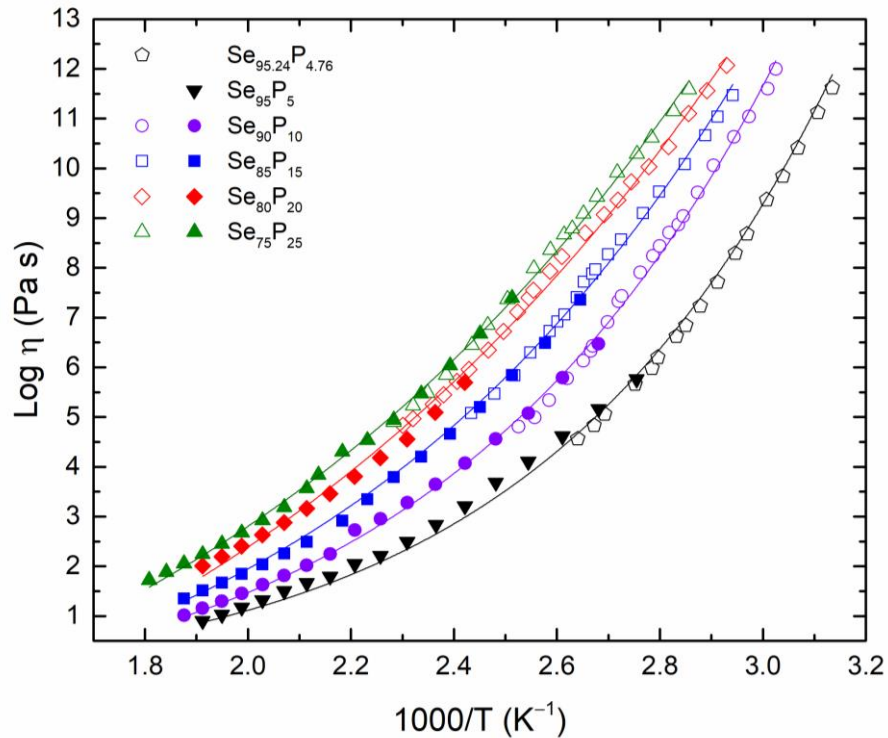
Figure 5b-3 Temperature dependence of viscosity η of binary P_xSe_{100-x} liquids. Filled symbols correspond to data obtained in the present study, while corresponding open symbols are data taken from a previous study [30]. Solid lines through the datapoints are fits to the MYEGA equation (see Eqn. 4 in text for details). Compositions corresponding to the different symbols are explained in the legend.
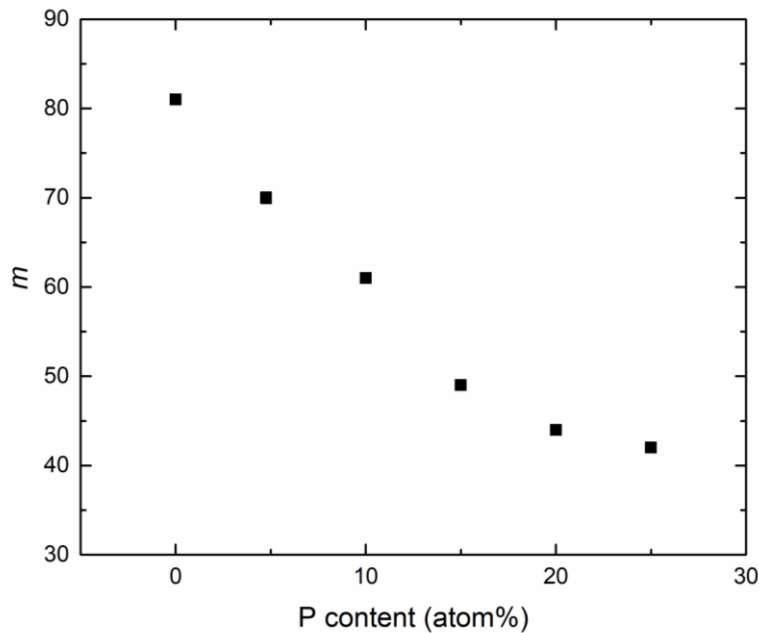
Figure 5b-4 Composition dependence of fragility index m of P_xSe_{100-x} liquids. Errors are within the size of the symbols. Fragility index for pure Se is taken from Koštál *et al.* [36].

region between the low- and high- frequency regimes for the Se liquid is marked by two crossovers between G′ and G″ and two corresponding transitions in the frequency dependence of $\eta(\omega)$ (Fig. 5b-5) [13]. Moreover, at intermediate frequencies G′(ω) displays a linear frequency dependence (Fig. 5b-5). The two crossovers between G′ and G″ clearly suggest the presence of two relaxation processes in liquid Se with characteristic frequencies marked by the locations of these crossovers, which were assigned in previous studies to the fast segmental chain motion and the slow bond scission/renewal dynamics [12,13]. The initial addition of 5 to 10 at.% P to Se appears to bring the timescales of these dynamical processes closer i.e. increases their temporal coupling to such an extent that the overlapping G″(ω) peaks for the two processes obscure the low-frequency G′-G″ crossover (Fig. 5b-5). However, the underlying existence of the two dynamical processes can be clearly observed in the two onsets of the frequency dependence of $\eta(\omega)$. Furthermore, for these liquids the linear frequency-scaling of G′(ω) at intermediate frequencies is also apparent in Fig. 5b-5. Such a scaling behavior was observed in previous studies to be a characteristic of short chains containing a few molecules in supramolecular polymeric liquids [33,34]. The increased coupling between the chain motion and bond scission/renewal in these P-Se liquids suggests that the rigidity constraints imposed on the mobility of the Se chain segments due to their cross linking with the P atoms can only be overcome successfully via breaking of the constituent P-Se and Se-Se bonds in the structure. Indeed Eqns. 1 and 2 derived from dynamical NMR studies [22–24] could be interpreted as representing the coupling between Se-Se and P-Se bond scission in the structure. Further increase in the P content ($\geqslant$ 15 at.% P) results in a single G′-G″ crossing characteristic of liquids with a single α-relaxation timescale. The disappearance of the dynamical process corresponding to the fast segmental chain motion is consistent with the cross-linking induced shortening of the
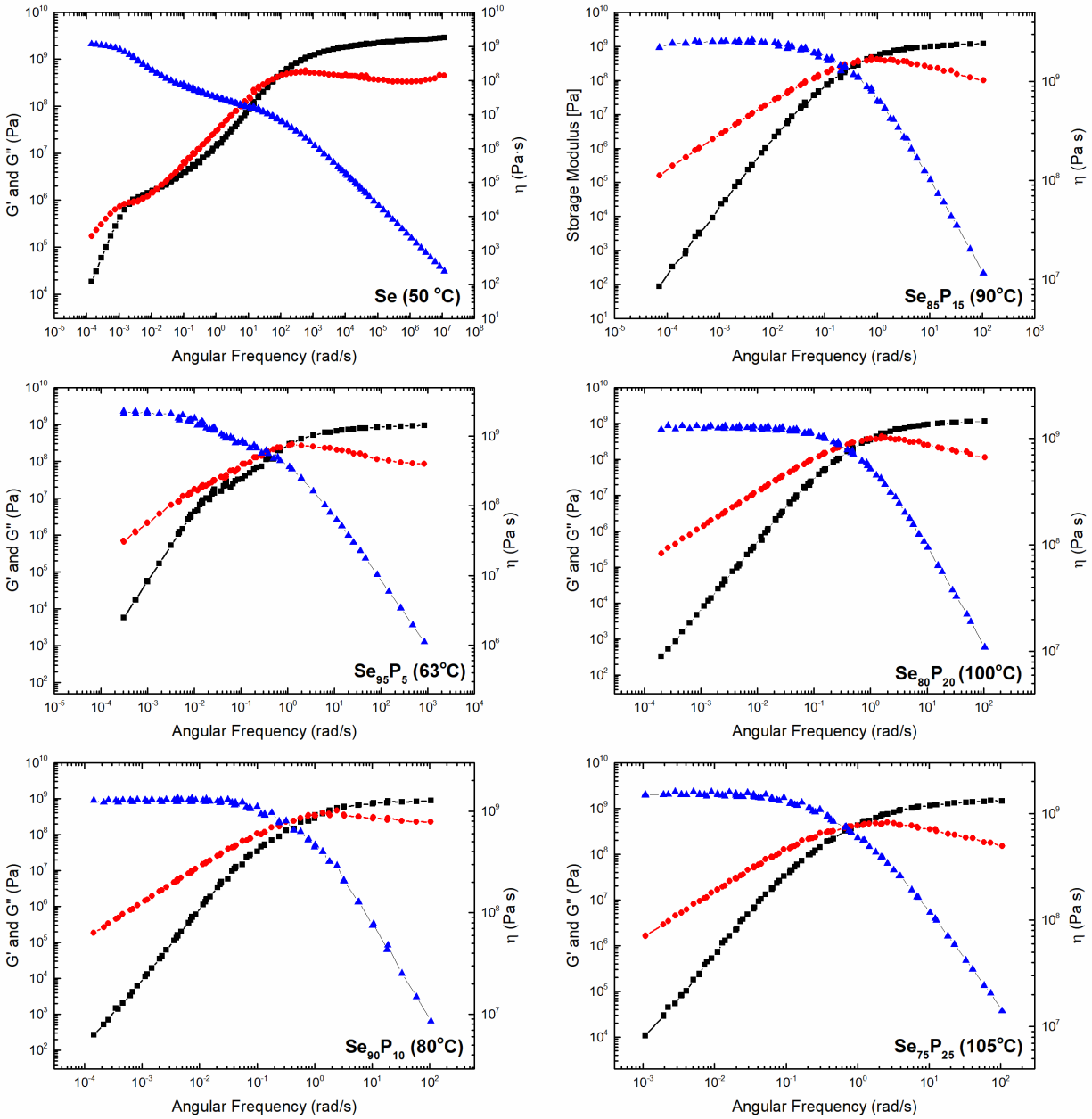
Figure 5b-5 Master curves of the frequency dependence of storage modulus G′ (squares), loss modulus G″ (circles) and viscosity η (triangles) of $P_x Se_{100-x}$ supercooled liquids with the reference temperature listed alongside the composition in each plot. Data for pure Se, included for comparison, are from Zhu *et al.* [13].

Se chain segments in these liquids with $\geqslant$ 15 at.% P to the point that they can no longer sustain the fast segmental motion.

Further insight into the structural control on the dynamics of these P_xSe_{100-x} liquids can be obtained from the relaxation spectrum, i.e., from the distribution of the relaxation times $H(\tau)$ in these supercooled liquids. The $H(\tau)$ spectrum can be calculated from the $G'(\omega)$ and $G''(\omega)$ data following Ninomiya and Ferry's method [35],

$$H(\tau) = \frac{G'(a\omega) - G'(\omega/a)}{2\ln a} - \frac{a^2}{(a^2 - 1)^2} \frac{G'(a^2\omega) - G'(\omega/a^2) - 2G'(a\omega) + 2G'(\omega/a)}{2\ln a}\Bigg|_{1/\omega=\tau}$$

where a is the frequency increment on a logarithmic scale of the measurement. The compositional evolution of the $H(\tau)$ spectra for all P-Se supercooled liquids is shown in Fig. 5b-6. Two relaxation processes with overlapping timescale distributions can be immediately recognized in the $H(\tau)$ spectra of pure Se and Se-rich compositions with $\leq$10 at.% P. Deconvolution of the $H(\tau)$ spectrum of Se shows a broad and intense peak at shorter timescales corresponding to the segmental chain motion and a weaker and narrower peak centered at longer timescales corresponding to bond scission/renewal. The relative peak intensity is determined by the probability of the relaxation mechanism, which reflects the predominance of the segmental chain motion in Se and P_5Se_{95} liquids. The peak corresponding to bond scission/renewal broadens and becomes more intense with progressive shortening of the Se chain length upon addition of P up to 10 at. %. On the other hand, only one relaxation process is evident in the $H(\tau)$ spectra of compositions with 15-25 at.% P. At this point the Se chain segments in the structure are too short to sustain the segmental dynamics and the composition-independent $H(\tau)$ spectra are dominated by bond scission/renewal.
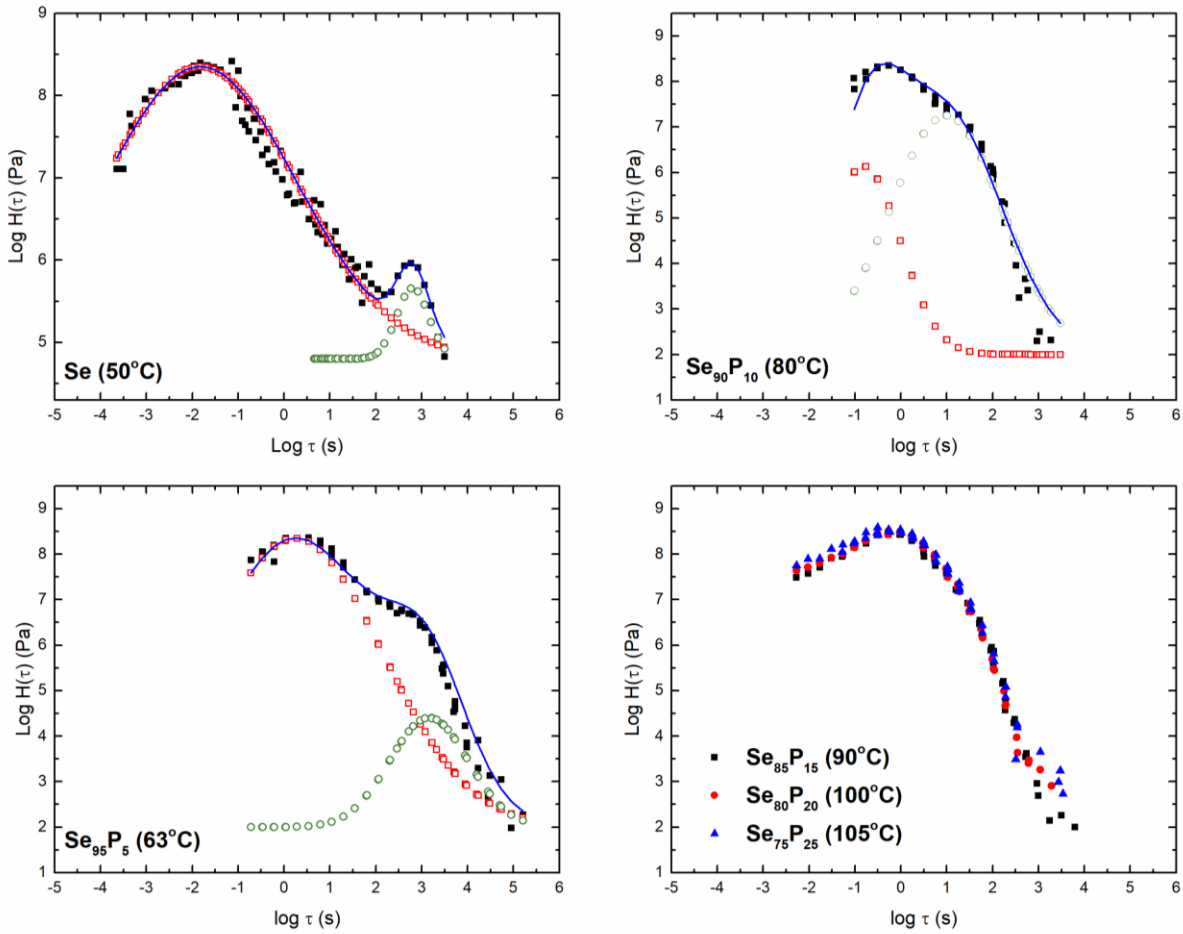
Figure 5b-6 Relaxation spectra H(τ) of P_xSe_{100-x} supercooled liquids. Filled squares are experimental data. Empty squares and circles represent the Gaussian fitting of the fast and slow processes, respectively. Solid lines represent the total fit to the experimental data. Data for pure Se is taken from Zhu *et al.* [13].

The timescale distribution for the segmental chain motion should reflect the associated conformational entropy and, thus, would be a sensitive function of the effective chain length. This idea is borne out in the composition dependence of the corresponding peak full-width-at half-maximum (FWHM) in the H(τ) spectra in Fig. 5b-6. The FWHM of this peak decreases from ~ 2.0 to ~ 0.8 log units upon increasing the P content from 0 to 10 at.%. On the other hand, the timescale distribution for the bond scission/renewal dynamics is expected to be controlled by the variety of the bond types and structural units. This hypothesis appears to be consistent with the increase in the corresponding peak FWHM from ~ 0.35 to ~ 1.23 log units in the H(τ) spectra (Fig.

162

5b-6) as the P content is increased from 0 to 10 at. % along with the diversity in the bonding and structure, including the appearance of P-Se, P-P and P=Se bonds, as well as $PSe_{3/2}$ pyramids, $Se=P(Se_{1/2})_3$ tetrahedra and ethylene-like $_{2/2}SeP-PSe_{2/2}$ units in addition to the Se-Se bonds in Se chains. The validity of these hypotheses can be further tested by comparing the rheological behavior of high-Se liquids with different cross-linkers, namely P, Ge and As. Such a comparison between the $G'(\omega)$, $G''(\omega)$ and $H(\tau)$ spectra of P_5Se_{95}, Ge_4Se_{96} and As_5Se_{95} liquids with similar Se chain length and at nearly iso-viscous ($\sim 10^9$ Pa.s) temperature is shown in Fig. 5b-7. The $G'(\omega)$ and $G''(\omega)$ data for the Ge_4Se_{96} and As_5Se_{95} liquids are taken from a previous study [3,5]. The most noteworthy feature in these spectra is the difference in the separation of the timescale between the fast segmental chain motion and the slow bond scission/renewal dynamics, which is significantly smaller in the P-Se liquid compared to its Ge or As counterparts. This result suggests that the temporal coupling between the two relaxation mechanisms is the strongest in the P-Se system. As mentioned above, such a strong coupling may originate from the presence of the unique speciation equilibria in this system, exemplified by Eqns. 1 and 2 that require the involvement and rearrangement of the Se chain segments in the interconversion between $Se=P(Se_{1/2})_3$ or $P_2(Se_{1/2})_4$ and $P(Se_{1/2})_3$ units. Moreover, while the FWHM of the fast process in the $H(\tau)$ spectra is similar in all cases, that of the slow process (~ 0.86 log units) for the P_5Se_{95} liquid is much larger than that for the Ge_4Se_{96} and As_5Se_{95} liquids (~ 0.56 log units). The similar FWHM for the chain dynamics in all three liquids is not surprising considering the fact that they all have similar Se chain lengths. On the other hand, as noted above, the P_5Se_{95} liquid is characterized by a wider variety of bonding and structural moieties compared to its As and Ge analogues, which are characterized by either Ge-Se or As-Se bonds and either $GeSe_{4/2}$ tetrahedra or $AsSe_{3/2}$ pyramids. This is consistent with the significantly larger FWHM for the bond

scission/renewal dynamics in the H(τ) spectrum of the P₅Se₉₅ liquid compared to those for the Ge₄Se₉₆ and As₅Se₉₅ liquids.
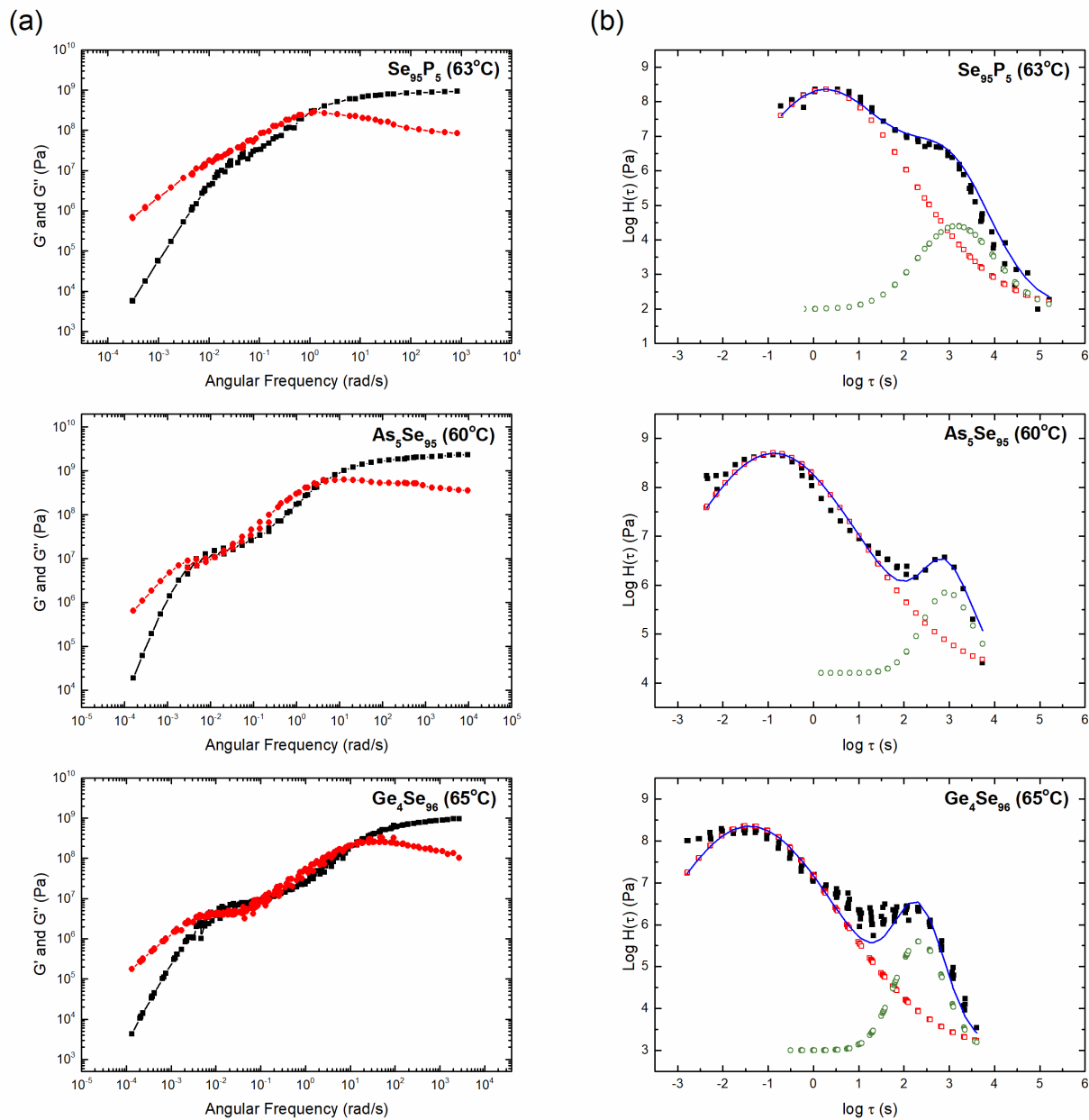
Figure 5b-7 Comparisons between binary P₅Se₉₅, Ge₄Se₉₆ [3] and As₅Se₉₅ [5] supercooled liquids with similar [Se]ₙ chain length of (a) master curves of G′ (squares), G″ (circles) and (b) relaxation spectra H(τ). The symbols in (b) have the same meaning as in Fig. 5b-6.

5b.5 Conclusion

The structure of binary P_xSe_{100-x} ($0 \leqslant x \leqslant 25$) glasses is characterized by $[Se]_n$ chain segments that are cross-linked by $PSe_{3/2}$ pyramids, $Se=P(Se_{1/2})_3$ tetrahedra and ethylene-like $_{2/2}SeP\text{-}PSe_{2/2}$ structural units. The structural evolution is consistent with the corresponding variation in isothermal viscosity, glass transition temperature T_g and fragility m. Similar to their counterparts in the As-Se and Ge-Se systems, the $G'(\omega)$ and $G''(\omega)$ data for the Se-rich P_xSe_{100-x} liquids with $x \leq 10$ display the presence of two relaxation processes, namely fast segmental Se chain motion and slow bond scission/renewal dynamics. The corresponding relaxation spectra $H(\tau)$ indicate that the distribution of the relaxation timescale for chain dynamics is closely related to the Se chain length, whereas that for bond scission/renewal is controlled by the variety of the bond types and structural moieties involved in the process. Inspection of the $H(\tau)$ spectra indicate that these two dynamical processes are more strongly coupled in P-Se liquids, compared to their As-Se and Ge-Se counterparts with similar Se chain lengths. This unique behavior of P-Se liquids is likely due to the causal relationship between the chemical exchange between the $Se=P(Se_{1/2})_3$ or $P_2(Se_{1/2})_4$ and $P(Se_{1/2})_3$ units and the segmental motion of the Se chains. Finally, the segmental chain dynamics disappears in liquids with $x \geq 15$ as the Se chain length becomes too short to sustain such motion.

Acknowledgements

References

[1]   B.G. Aitken, S.C. Currie, B.C. Monahan, L.-M. Wu, E.W. Coonan, Chalcogenide glass for low viscosity extrusion and injection molding, US 7116888 B1, 2006.

[2]   Q. Zheng, J.C. Mauro, Viscosity of glass-forming systems, J. Am. Ceram. Soc. 100 (2017) 6–25.

[3]   S. Sen, Y. Xia, W. Zhu, M. Lockhart, B. Aitken, Nature of the floppy-to-rigid transition in chalcogenide glass-forming liquids, J. Chem. Phys. 150 (2019) 144509.

[4]   W. Zhu, B.G. Aitken, S. Sen, Communication: Observation of ultra-slow relaxation in supercooled selenium and related glass-forming liquids, J. Chem. Phys. 148 (2018) 111101.

[5]   W. Zhu, B. Aitken, S. Sen, Investigation of the shear relaxation behavior of As-Se liquids within the framework of entropic and elastic models of viscous flow, J. Non. Cryst. Solids. 534 (2020) 119959.

[6]   B. Yuan, B. Aitken, S. Sen, Rheology of supercooled Se-Te chain liquids: Role of Te as an interchain cross-linker, J. Non. Cryst. Solids. 529 (2020) 119764.

[7]   W. Zhu, M.J. Lockhart, B.G. Aitken, S. Sen, Rheology of the λ transition in liquid sulfur: Insights from arsenic sulfide liquids, J. Chem. Phys. 148 (2018) 244506.

[8]   M. Marple, J. Badger, I. Hung, Z. Gan, K. Kovnir, S. Sen, Structure of Amorphous Selenium by 2D ^{77}Se NMR Spectroscopy: An End to the Dilemma of Chain versus Ring, Angew. Chemie. 129 (2017) 9909–9913.

[9]   G. Yang, B. Bureau, T. Rouxel, Y. Gueguen, O. Gulbiten, C. Roiland, E. Soignard, J.L. Yarger, J. Troles, J.C. Sangleboeuf, P. Lucas, Correlation between structure and physical properties of chalcogenide glasses in the As_xSe_{1-x} system, Phys. Rev. B. 82 (2010) 195206.

[10] T.G. Edwards, S. Sen, E.L. Gjersing, A combined ^{77}Se NMR and Raman spectroscopic study of the structure of Ge_xSe_{1-x} glasses: Towards a self consistent structural model, J. Non. Cryst. Solids. 358 (2012) 609–614.

[11] E.L. Gjersing, S. Sen, Structure, Connectivity, and Configurational Entropy of Ge_xSe_{100-x} Glasses: Results from ^{77}Se MAS NMR Spectroscopy, J. Phys. Chem. C. 114 (2010) 8601–8608.

[12] W. Zhu, I. Hung, Z. Gan, B. Aitken, S. Sen, Dynamical processes related to viscous flow in a supercooled arsenic selenide glass-forming liquid: Results from high-temperature ^{77}Se NMR spectroscopy, J. Non. Cryst. Solids. 526 (2019) 119698.

[13] W. Zhu, B.G. Aitken, S. Sen, Observation of a dynamical crossover in the shear relaxation processes in supercooled selenium near the glass transition, J. Chem. Phys. 150 (2019) 094502.

[14] Z.U. Borisova, Glassy Semiconductors, Springer US, 1981.

[15] D.G. Georgiev, M. Mitkova, P. Boolchand, G. Brunklaus, H. Eckert, M. Micoulaut, Molecular structure, glass transition temperature variation, agglomeration theory, and network connectivity of binary P-Se glasses, Phys. Rev. B. 64 (2001) 134204.

[16] A. Bytchkov, F. Fayon, D. Massiot, L. Hennet, D.L. Price, ^{31}P solid-state NMR studies of the short-range order in phosphorus-selenium glasses, Phys. Chem. Chem. Phys. 12 (2010) 1535–1542.

[17] R.T. Phillips, M.K. Ellis, Microstructure of P-Se glasses and low frequency Raman scattering, J. Non. Cryst. Solids. 164–166 (1993) 135–138.

[18] D. Lathrop, H. Eckert, Quantitative determination of the structural units in phosphorus-selenium glasses by ^{31}P dipolar and magic-angle-spinning NMR spectroscopy, Phys. Rev. B. 43 (1991) 7279–7287.

[19] D. Lathrop, H. Eckert, Dipolar NMR Spectroscopy of Nonoxidic Glasses. Structural Characterization of the System Phosphorus-Selenium by [31]P-[77]Se Spin Echo Double Resonance NMR, J. Am. Chem. Soc. 112 (1990) 9017–9019.

[20] D. Lathrop, H. Eckert, Chemical disorder in non-oxide chalcogenide glasses. Site speciation in the system phosphorus-selenium by magic angle spinning NMR at very high spinning speeds, J. Phys. Chem. 93 (1989) 7895–7902.

[21] D. Lathrop, H. Eckert, NMR studies of chalcogenide glasses: The system phosphorus-selenium, J. Non. Cryst. Solids. 106 (1988) 417–420.

[22] R. Maxwell, H. Eckert, Molten-state kinetics in glass-forming systems. A high-temperature NMR study of the system phosphorus-selenium, J. Phys. Chem. 99 (1995) 4768–4778.

[23] R. Maxwell, H. Eckert, Speciation Equilibria, Clustering, and Chemical-Exchange Kinetics in Non-Oxide Glasses and Melts. High-Temperature ^{31}P NMR Study of the System Phosphorus-Selenium, J. Am. Chem. Soc. 115 (1993) 4747–4753.

[24] R. Maxwell, H. Eckert, Chemical Equilibria in Glass-Forming Melts: High-Temperature ^{31}P and ^{77}Se NMR of the Phosphorus-Selenium System, J. Am. Chem. Soc. 116 (1994) 682–689.

[25] S.N. Yannopoulos, K.S. Andrikopoulos, Raman scattering study on structural and dynamical features of noncrystalline selenium, J. Chem. Phys. 121 (2004) 4747–4758.

[26] Z. Borisova, B. Kasatkin, E. Kim, Izv. Akad. Nauk SSSR Neorg. Mater. 9 (1973) 822.

[27] F. Heyder, D. Linke, Z. Chem. 13 (1973) 480.

[28] R. Blachnik, A. Hoppe, Glass transition and specific heats in the systems P-S, P-Se, As-S and As-Se, J. Non. Cryst. Solids. 34 (1979) 191–201.

[29] Y. Monteil, H. Vincent, Z. Anorg. Allg. Chem. 416 (1975) 181.

[30] E.I. Kim, G.M. Orlova, Viscosity of glasses in the P-Se system, J. Appl. Chem. USSR. 47 (1974) 1081–1021.

[31] J.C. Mauro, Y. Yue, A.J. Ellison, P.K. Gupta, D.C. Allan, Viscosity of glass-forming liquids, Proc. Natl. Acad. Sci. 106 (2009) 19780–19784.

[32] C. Zhang, L. Hu, Y. Yue, J.C. Mauro, Fragile-to-strong transition in metallic glass-forming liquids, J. Chem. Phys. 133 (2010) 014508.

[33] C. Gainaru, R. Figuli, T. Hecksher, B. Jakobsen, J.C. Dyre, M. Wilhelm, R. Böhmer, Shear-Modulus Investigations of Monohydroxy Alcohols: Evidence for a Short-Chain-Polymer Rheological Response, Phys. Rev. Lett. 112 (2014) 098301.

[34] N. Lou, Y. Wang, X. Li, H. Li, P. Wang, C. Wesdemiotis, A.P. Sokolov, H. Xiong, Dielectric relaxation and rheological behavior of supramolecular polymeric liquid, Macromolecules. 46 (2013) 3160–3166.

[35] J.D. Ferry, Viscoelastic properties of polymers, John Wiley & Sons, 1980.

[36] P. Koštál, J. Málek, Viscosity of Se-Te glass-forming system, Pure Appl. Chem. 87 (2015) 239–247.

Chapter 5c

Rheological Behavior of Supercooled P-Se Glass-forming Liquids:

From Networks to Molecules and the Emergence of Power-Law

Behavior

5c.1 Abstract

The effect of the network-to-molecular structural transformation with increasing phosphorus content in $P_x Se_{100-x}$ $(30 \leq x \leq 67)$ supercooled liquids on their shear-mechanical response is investigated using oscillatory shear rheometry. While network liquids with $30 \leq x \leq 40$ are characterized by shear relaxation via a network bond scission/renewal process, a Maxwell scaling of the storage (G′) and loss (G″) shear moduli and a frequency-independent viscosity at low frequencies, a new relaxation process emerges in liquids with intermediate compositions $(45 \leq x \leq 50)$. This process is attributed to an interconversion between network and molecular structural moieties. Predominantly molecular liquids with $x \geq 63$, on the other hand, are characterized by a departure from the Maxwell behavior as the storage modulus shows a linear frequency scaling $G′(\omega) \sim \omega$ over nearly the entire frequency range below the G′-G″ crossover and a nearly constant ratio of G″/G′ in the terminal region. Moreover, the dynamic viscosity of these rather fragile molecular liquids shows significant enhancement over that of network liquids at frequencies below the dynamical onset and does not reach a frequency-independent regime even at frequencies that are four orders of magnitude lower than that of the onset. Such power-law relaxation behavior of the molecular liquids is ascribed to an extremely broad distribution of relaxation timescales with the coexistence of rapid rotational motion of individual molecules and cooperative dynamics of transient molecular clusters, with the latter being significantly slower than the shear relaxation timescale.

5c.2 Introduction

The processing of glasses from their parent supercooled liquids is critically dependent on the rheological behavior of the latter. Moreover, the frequency ω dependence of the shear mechanical response, including the storage and loss shear moduli (G′ and G″, respectively) and viscosity η, of glass-forming liquids sheds light on the atomistic details of the relaxation processes associated with the glass transition and related phenomena. The shear mechanical response and modes of structural relaxation of a supercooled liquid critically depends on the nature of the structural moieties and the resulting dimensionality and connectivity of the network (e.g. isolated vs. associated molecules, 1-D chains or 3-D polyhedral network).[1,2] For example, the primary or α-relaxation of polymeric chain liquids is controlled by the segmental motion of the constituent chains, while the motion of the covalently bonded backbone structure gives rise to the slowest relaxation mode in these systems.[3] In contrast, a significantly simple rheological behavior is displayed by the archetypal 3D network oxide liquids such as silicates and borates, where the structural relaxation is controlled by the bond scission/renewal based reconfiguration of the network. Correspondingly the shear mechanical response of these liquids shows a "normal liquid" behavior with a single G′-G″ crossover at high frequency and a Maxwell scaling of $G(\omega) \sim \omega^n$ at low frequencies in the terminal regime, with $n = 2$ and 1 for G′ and G″, respectively.[4,5] Such simple behavior is also displayed by the non-associated organic molecular glass-forming liquids such as tris-naphthylbenzene, where the viscosity and structural relaxation of the supercooled liquid involve local flow processes of the constituent molecules that redistribute the free volume.[6,7] On the other hand, seemingly simple molecular liquids such as monohydroxy alcohols and various other low-molecular-weight hydrogen bonded liquids have shown intense Debye relaxation modes in their rheological spectra that are slower than the structural relaxation,

which lead to significant viscosity enhancement.[7,8] Nuclear magnetic resonance (NMR) spectroscopic studies indicated that these modes in monohydroxy alcohols were related to the restructuring of transient chains via hydrogen bonding between molecules.[9]

The compositional evolution of the shear mechanical response of glass-forming chalcogenide liquids is particularly interesting since the structure of these liquids can be tuned, as a function of composition, from being predominantly molecular, all the way to a 3D network. Previous systematic small-amplitude oscillatory shear (SAOS) rheometry studies on binary selenide liquids in the As-Se, Ge-Se and P-Se systems[10–13] have shown that the structural relaxation of Se-rich liquids consisting of $[\text{-Se-}]_n$ chain-like structural moieties is characterized by the coexistence of a slow Debye-like process and a fast process. ^{77}Se dynamical nuclear magnetic resonance (NMR) spectroscopic studies[14] have indicated that the slow process corresponds to the bond scission/renewal induced $[\text{-Se-}]_n$ chain restructuring in the structure, while the fast process is associated with the segmental dynamics of these chains. The addition of Ge, As or P to Se leads to cross-linking of these chains and their effective shortening. Consequently, the segmental dynamics disappear at a Ge/As/P concentration where the chain length becomes too short to sustain the segmental dynamics and the structural network becomes sufficiently cross-linked and rigid. At this stage the structural relaxation is controlled by the bond scission/renewal induced restructuring of the emerging network, and correspondingly, the shear mechanical response shows a behavior similar to that characteristic of the archetypal network oxide liquids mentioned above.

A significant departure from this evolutionary scheme of rheological behavior has recently been reported in Ge-As sulfide glass-forming liquids where a progressive increase of the molecule : network ratio in the structure resulted in a monotonic lowering of n from 2 for to 1 for the scaling

of $G'(\omega) \sim \omega^n$ in the entire low frequency regime below the G'-G'' crossover.[15] Moreover, at the highest molecule content the ratio G''/G' reached a nearly constant value and the liquid did not display a purely viscous response even at the lowest frequencies. It may be noted that, while such power-law rheological behavior has not been observed in non-associated organic molecular glass-forming liquids such as tris-naphthylbenzene, it has been extensively reported in widely different classes of soft matter including gels, elastomers, biomaterials and composites.[16] Although the phenomenological soft glassy rheology model captures the range of this behavior well, an atomistic explanation remains missing in the literature to date.[17]   Moreover, the generality of this power-law relaxation behavior in non-associated molecular inorganic glass forming liquids remains to be explored. Here we report the results of a rheological study of $P_x Se_{100-x}$ supercooled liquids with $30 \leq x \leq 67$ to investigate the effects of network-to-molecular transformation on their shear-mechanical response and to explore the generality of the power-law shear mechanical response in non-associated molecular chalcogenides. The corresponding compositional evolution of the structural relaxation mechanisms and their effect on viscous flow are discussed.

5c.3 Experimental Methods

5c.3.1 Sample Synthesis

The $P_x Se_{100-x}$ glasses ($30 \leq x \leq 67$) were synthesized in ~12g batches using the conventional melt-quench method. For $30 \leq x \leq 50$, constituent elements, red phosphorus (Spectrum, 99.999%) and selenium (Alfa Aesar, 99.999%), were loaded in evacuated (10^{-4} Torr) quartz ampoules and then placed in a rocking furnace, slowly heated to 873K over 13 hours and held at this temperature for 36 h to ensure melt homogeneity. The melts were finally quenched to form glass by dipping the ampoules in water. The predominantly molecular glasses $P_{63}Se_{37}$ and $P_{67}Se_{33}$ were prepared in

similar fashion but the ampoules were cooled to 623K and held at this temperature for 30 minutes prior to quenching.

5c.3.2 Parallel Plate Rheometry

The rheological measurements of all compositions were carried out on an Anton-Paar MCR 92 parallel plate rheometer equipped with a Peltier heater (up to 200 °C) under constant nitrogen gas flow. The samples were prepared by first rapidly heating them inside the rheometer to the softening point and then pressing between the upper oscillatory plate (8mm diameter) and the lower stationary plate and trimming to a disk-like shape with a thickness of ~ 1 mm. For SAOS measurements the samples were allowed to equilibrate at each desired measurement temperature followed by the determination of the linear viscoelastic region. During the SAOS measurement, a sinusoidal strain was applied with varying angular frequency ω between 1 to 600 rad/s and the induced torque was recorded to calculate the storage and loss moduli G′ and G″ as a function of ω. Measurements were carried out at multiple temperatures for each sample and master curves of G′(ω) and G″(ω) were constructed using time-temperature superposition (TTS). The dynamic viscosity was calculated from the relation $\eta' = \frac{G''}{\omega}$.

The Newtonian viscosity η of two compositions with $x = 63$ and 67 was measured using steady shear for $\eta \leq 10^9$ Pa.s and using creep for $\eta \geq 10^{10}$ Pa.s. The Newtonian viscosity was determined in the steady shear measurements as the ratio of stress to strain rate at various strain rates $\dot{\gamma}$ ranging between 0.01 s^{-1} and 1 s^{-1} at each temperature. For creep measurements, a constant shear stress τ was applied to the thermally equilibrated sample while the strain response was constantly monitored as a function of time. The viscosity is obtained from the relation $\eta = \frac{\tau}{\dot{\gamma}}$ in the steady-state region where the strain rate $\dot{\gamma}$ no longer changes with time.

5c.4 Results and Discussion

Previous structural studies of $P_x Se_{100-x}$ glasses based on Raman and multi-nuclear (^{31}P and [77]Se) NMR spectroscopy[18–25] have conclusively shown that the structure of the Se-rich liquids in this system consists predominantly of $[-Se-]_n$ chains. Progressive addition of P results in cross-linking and shortening of the Se chain segments to form a 3D network. Such a compositional evolution of structure continues up to $x \sim 50$ and is broadly similar to those observed in As-Se and Ge-Se systems. However, further increase in P content results in the formation of P_4Se_3 molecules and the structure becomes predominantly molecular for $x \geq 63$. The temperature-dependent G′ and G″ spectra of all $P_x Se_{100-x}$ supercooled liquids in the composition range $30 \leq x \leq 67$ are shown in Fig. 5c-1a. At each temperature, only a portion of the whole spectrum is revealed within the observation window of the rheometer. As expected, these spectra gradually shift from low to high frequency with increasing temperature, which enables a sequential observation of a wide frequency range. The experimental master curves of G′(ω) and G″(ω) constructed using time-temperature superposition (TTS) for all $P_x Se_{100-x}$ supercooled liquids, at temperatures corresponding to the isokom of approximately $\sim 10^9$ Pa.s, are shown in Figure 5c-1b. At high frequencies, G′(ω) in these master curves reaches a plateau corresponding to the glassy modulus G_∞ , which is ~ 1.3 to 1.5 GPa for the network liquids with $30 \leq x \leq 40$, while it drops by 50% (0.7 – 0.8 GPa) for the molecular $P_{63}Se_{37}$ and $P_{67}Se_{33}$ liquids. This change in G_∞ is consistent with a drastic lowering of the structural connectivity in the latter liquids resulting from the formation of P_4Se_3 molecules, which are held together in the structure via weak intermolecular Van der Waals bonding.[18] It is
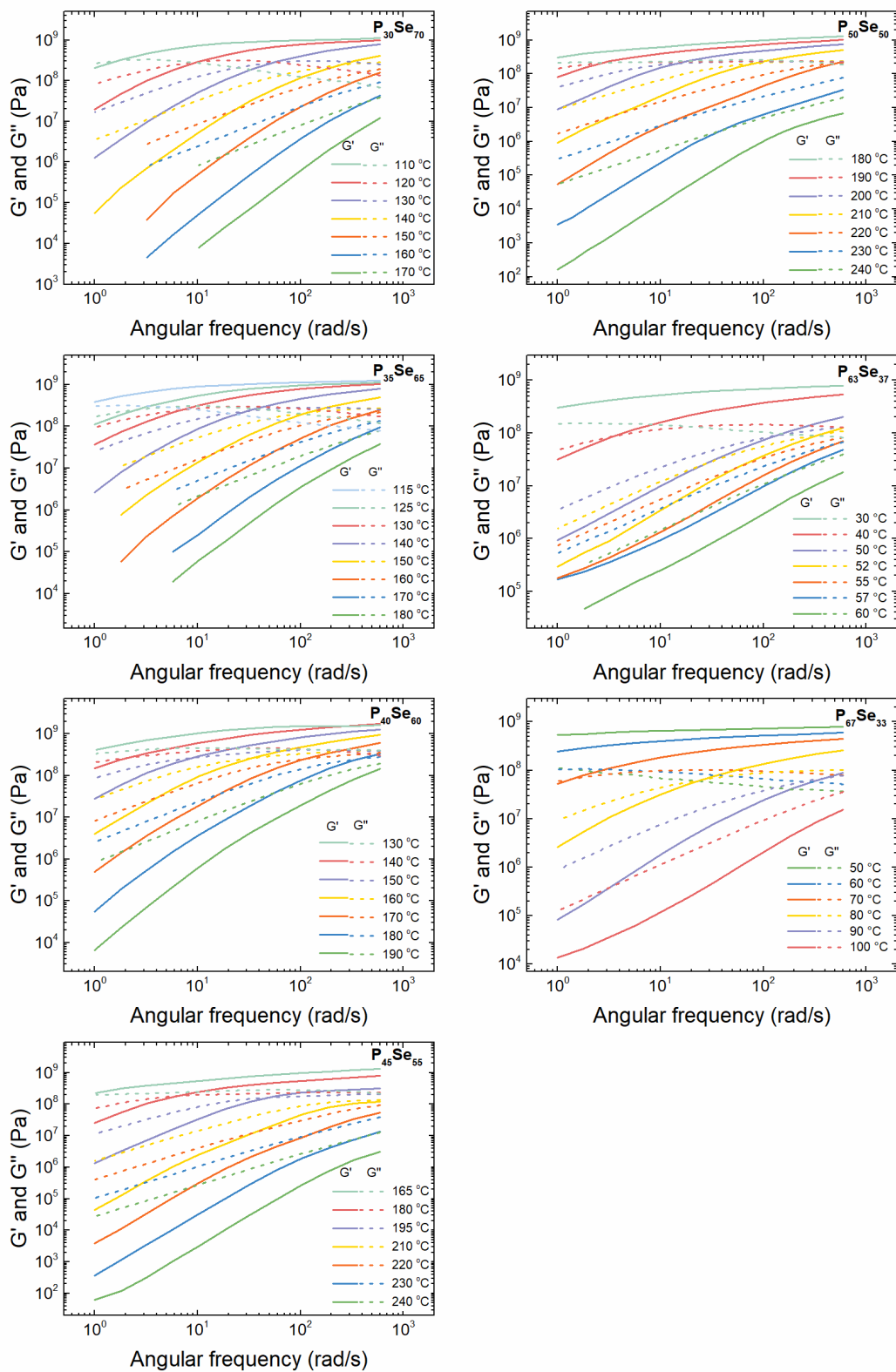
Figure 5c-1 (a) Frequency dependence of G′ (solid lines) and G″ (dashed lines) at different temperatures for P$_x$Se$_{100-x}$ supercooled liquids.
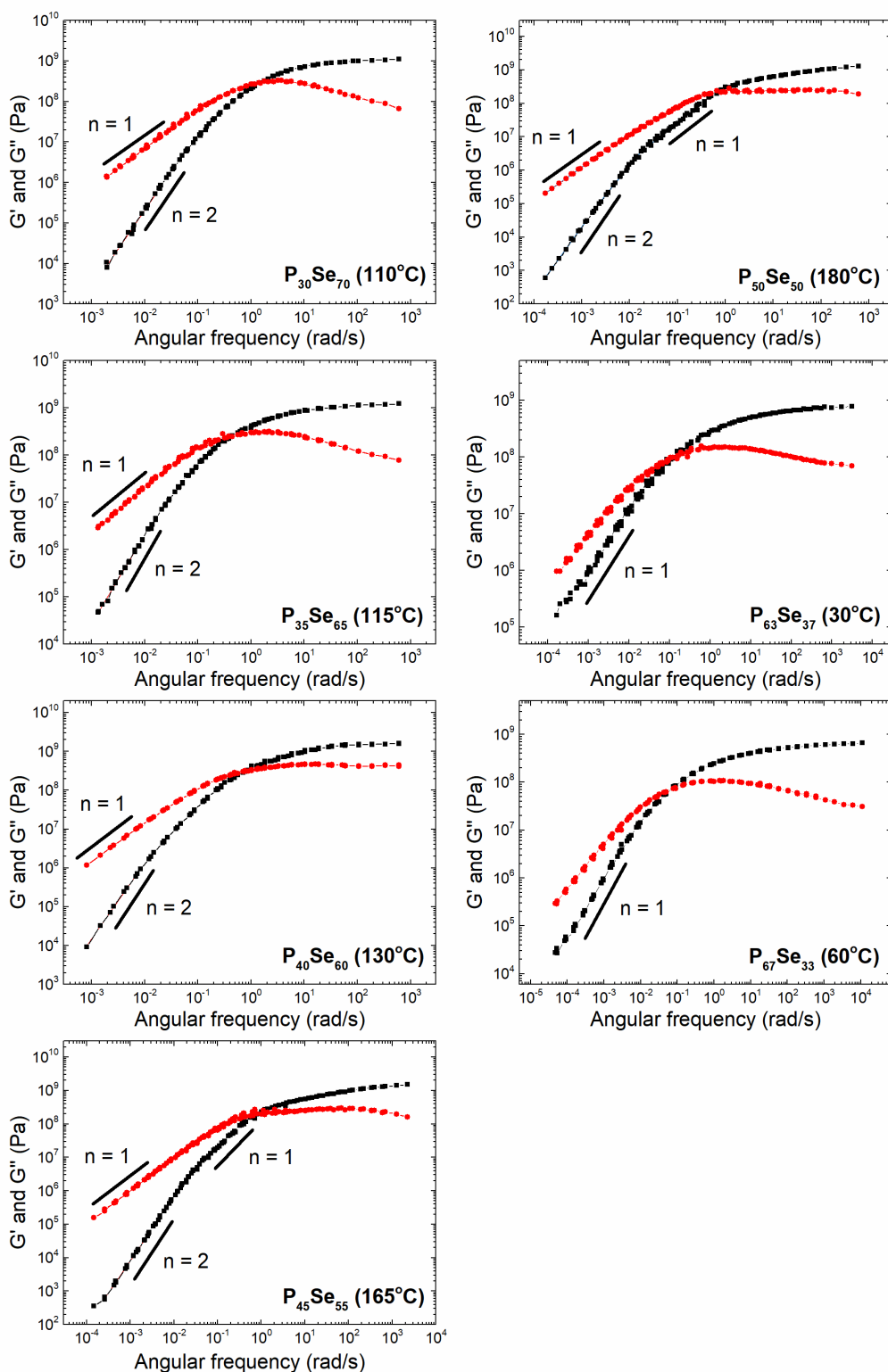
Figure 5c-1 (b) Master curves of G′(ω) (black squares) and G″(ω) (red circles) of P_xSe_{100-x} supercooled liquids with the reference temperatures for TTS listed alongside the compositions in each panel. Solid straight-line segments mark the slopes n in different frequency regions.

apparent that the network liquids with composition $30 \leq x \leq 40$ display a normal behavior with a single relaxation process and Maxwell scaling of G′ and G″ in the terminal regime. This primary relaxation process in liquids with compositions ranging between $15 \leq x \leq 25$ was assigned in a previous study to P-Se and Se-Se bond scission/renewal.[13] Such a process is likely to remain active and responsible for structural relaxation in liquids with $30 \leq x \leq 40$. However, the viscoelastic spectra for the $P_{45}Se_{55}$ and $P_{50}Se_{50}$ liquids show a clear and relatively abrupt change in the frequency dependence of G′ from $n = 2$ in the terminal regime to $n \sim 1$ for G′ values above a few MPa (Fig. 5c-1b). Therefore, these liquids are characterized by two relaxation processes and the change in slope with increasing frequency to $n \sim 1$ suggests the emergence of a new relaxation mode. Previous studies have demonstrated that the network structure of P_xSe_{100-x} glasses with $45 \leq x \leq 50$ consists primarily of ethylene-like $_{2/2}SeP–PSe_{2/2}$ units that are expected to form 2D corrugated sheet-like superstructural moieties.[18,19] Moreover, ^{31}P and ^{77}Se dynamical NMR studies[26–28] in the literature have shown that the bond scission/renewal dynamics in these liquids are associated with interconversion between different P sites that can be represented in the form of the reaction: $3P_2(Se_{1/2})_4 \leftrightarrow 2P(Se_{1/2})_3 + P_4Se_3$. Such an interconversion between the network and molecular (P_4Se_3) topological elements would result in a change in the intermediate-range structure and is expected to appear as a separate relaxation mode in the viscoelastic spectrum, consistent with the experimental observation.

In contrast to these predominantly network P_xSe_{100-x} liquids, the viscoelastic spectra of the P_4Se_3 molecule-rich $P_{63}Se_{37}$ and $P_{67}Se_{33}$ liquids display a rather different behavior where the ω dependences of G′ and G″ are parallel and both follow a slope of $n = 1$ in the terminal region. As noted earlier, this frequency dependence of G′ and G″ and the nearly constant ratio of G″/G′ in the terminal region are the signatures of a power-law relaxation behavior of a wide variety of soft

matter, including and most notably gels near their critical point, which are characterized by a broad distribution of structural length scales and relaxation timescales.[29]   The validity of this hypothesis is tested here by comparing the relaxation time spectra of the normally behaving $P_{30}Se_{70}$ network liquid with that of the molecular $P_{63}Se_{37}$ liquid (Fig. 5c-2). The $H(\tau)$ spectrum can be derived, in principle, from the corresponding $G'(\omega)$ or $G''(\omega)$ data using one of the following relations with G_0 being the equilibrium modulus:

$$G'(\omega) = G_0 + \int_{-\infty}^{\infty} \frac{\omega^2\tau^2}{1 + \omega^2\tau^2} H\, dln\tau,$$

$$G''(\omega) = G_0 + \int_{-\infty}^{\infty} \frac{\omega\tau}{1 + \omega^2\tau^2} H\, dln\tau.$$

Therefore, the determination of $H(\tau)$ requires inversion of these relations and calculation of derivatives of $G'(\omega)$ or $G''(\omega)$ with respect to $\ln \omega$. Instead, here the $H(\tau)$ spectra are calculated without taking these derivatives, following Ninomiya and Ferry's approximate method that employs a numerical differencing procedure.[30] This method requires values of $G'(\omega)$ spaced at equal intervals on a log frequency scale above and below the frequency $\omega = 1/\tau$ at which $H(\tau)$ is calculated, e.g., $G'(\omega)$ values can be taken at frequencies $\omega/a^2,\ \omega/a,\ \omega,\ a\omega,\ and\ a^2\omega$, where a is a constant multiplier. Then $H(\tau)$ can be approximated as:

$$H(\tau) = \frac{G'(a\omega) - G'(\omega/a)}{2\ln a} - \frac{a^2}{(a^2 - 1)^2} \frac{G'(a^2\omega) - G'(\omega/a^2) - 2G'(a\omega) + 2G'(\omega/a)}{2\ln a}\Bigg|_{1/\omega=\tau}$$

$$(1)$$

A value of $\log a = 0.25$ is used in the present calculations, as a careful evaluation of this numerical method has shown that $\log a$ needs to be in the range 0.2-0.4 for an accurate

approximation of H(τ), as larger values lead to poor approximation and smaller values lead to large fluctuations in the differencing result.[30] It is clear from Fig. 5c-2 that the H(τ) spectrum of the $P_{63}Se_{37}$ liquid is significantly broader than that of the $P_{30}Se_{70}$ liquid, with the former displaying an extended long-time tail and a plateau on the short-time side (Fig. 5c-2). This behavior of the $P_{63}Se_{37}$ liquid is remarkably similar to that observed in a previous study for the molecular $Ge_3As_{52}S_{45}$ liquid (Fig. 5c-2).[15] The broadening of H(τ) at short times or high frequencies is consistent with the results of a previous two-dimensional ^{31}P NMR study[31] that has shown that the constituent P_4Se_3 molecules in the $P_{63}Se_{37}$ liquid perform rapid isotropic rotational reorientation at timescales that are orders of magnitude faster than the shear relaxation time scale in the supercooled region. This strongly temporally decoupled rotation of individual molecules is reminiscent of the situation in plastic crystals where the constituent molecules perform rapid rotation at the lattice sites.[31–33] On the other hand, the long-time tail of H(τ) characteristic of this liquid may be attributed to correlated reorientation dynamics in transient molecular clusters.

Further insights into the relaxation time distribution can be obtained by simulating the viscoelastic spectra of the $P_{30}Se_{70}$ network and $P_{63}Se_{37}$ molecular liquids using the Havriliak-Negami (H-N) function for the frequency dependence of the complex modulus $G^*(\omega)$:[34]

$$G^*(\omega) = G_\infty + (G_0 - G_\infty)\frac{1}{[1+(i\omega\tau_H)^\alpha]^\beta}; \ \ 0 < \alpha, \ \alpha\beta < 1 \qquad (2)$$

where G_∞ and G_0 are the infinite frequency glassy shear modulus and the zero-frequency modulus, and τ_H, α and β represent the characteristic H-N relaxation time, broadness, and asymmetry of the corresponding relaxation time distribution, respectively. The H-N equation reduces to the Cole-Davidson distribution for $\alpha = 1$ and the Cole-Cole distribution for $\beta = 1$. It may be noted that
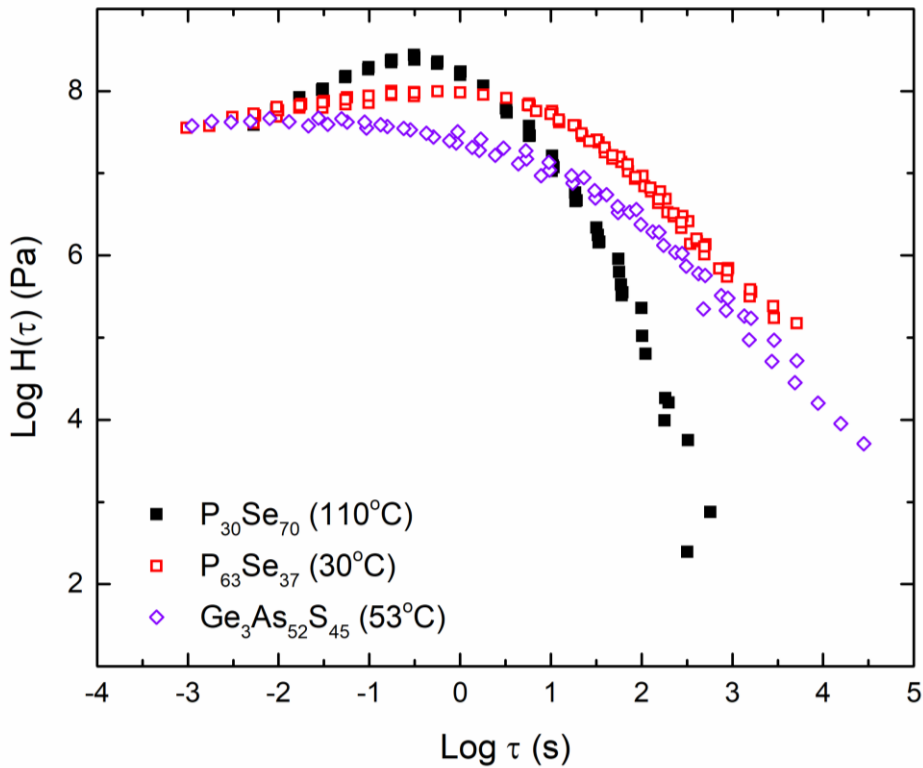
Figure 5c-2 Relaxation spectra H(τ) of supercooled $P_{30}Se_{70}$ network liquid (filled black squares) and molecular $P_{63}Se_{37}$ liquid (empty red squares) at 110°C and 30°C, respectively. H(τ) of supercooled molecular $Ge_3As_{52}S_{45}$ liquid (open purple diamonds) from a previous study is shown for comparison.[15]

although the H-N function takes the limiting values of the dynamic shear modulus to zero at low frequencies and to a plateau at G_∞ for high frequencies as required for an α-relaxation process, the viscosity does not reach a frequency-independent regime at a finite low-frequency limit. The latter outcome is indeed characteristic of gels.[16,29] The simulations of the viscoelastic spectra of the $P_{30}Se_{70}$ and $P_{63}Se_{37}$ liquids with the H-N function are shown in Fig. 5c-3. Both the Maxwell scaling in the terminal regime, characteristic of the network liquid, and the "anomalous" scaling of G´~ ω exhibited by the molecular liquids are captured well using the H-N function. While the viscoelastic spectrum of the network $P_{30}Se_{70}$ liquid can be fitted with α =1.0 and β = 0.32, i.e., the Cole-Davidson model, that of the molecular $P_{63}Se_{37}$ liquid can only be simulated with considerably smaller α (= 0.82) and β (= 0.13) values, suggesting that the relaxation time spectrum of the latter

is significantly broader and more asymmetric compared to that of the former liquid. The

corresponding probability density function of the log-relaxation time $h_{HN}(\log \tau)$ for these two

liquids can be obtained using the following relations:

$$h_{HN}(\log \tau) = \frac{1}{A\pi} \frac{\sin(\beta\Psi)}{((\tau\omega_H)^{-2\alpha} + 2(\tau\omega_H)^{-\alpha}\cos(\pi\alpha) + 1)^{\frac{\beta}{2}}},$$

$$\Psi = \frac{\pi}{2} - \arctan\left(\frac{(\tau\omega_H)^{\alpha} + \cos(\pi\alpha)}{\sin(\pi\alpha)}\right) \tag{3}$$

where $A = (\ln 10)^{-1}$ and $\omega_H = 1/\tau_H$ is the characteristic H-N relaxation frequency. The calculated

$h_{HN}(\log \tau)$ spectra show that the relaxation time distribution of the $P_{30}Se_{70}$ liquid indeed exhibits

a less skewed and narrower peak whereas that of the $P_{63}Se_{37}$ molecular liquid show displays a

rather broad and highly skewed distribution with an extended short-time tail (Fig. 5c-4). The broad

distribution of relaxation times for the molecular liquids is indicative of the presence of a

correspondingly complex potential energy landscape (PEL) with a wide range of barrier heights

separating the metabasins. Such a PEL is characteristic of liquids with high fragility index m,

where $m = \frac{d\log_{10}\eta}{d(T_g/T)}\Big|_{T=T_g}$, and T_g is the glass transition temperature.[35]

The fragility index of the two molecular liquids $P_{63}Se_{37}$ and $P_{67}Se_{33}$ is obtained by fitting

the temperature dependence of their viscosity as determined in this study (Fig. 5c-5) with the

MYEGA equation:[36,37]

$$\log \eta = \log_{10}\eta_\infty + \frac{K}{T} \cdot exp\left(\frac{C}{T}\right) \tag{4}$$

where $\log_{10}\eta_\infty$, K, and C are all fitting parameters. The corresponding fragility index m is

calculated from these fitting parameters using the following relation:

$$m = \left(\frac{K}{T_g}\right)\left(1 + \frac{C}{T_g}\right)\exp\left(\frac{C}{T_g}\right) \qquad (5)$$

where the T_g of the binary P-Se glasses were obtained from previous reports in the literature.[18,38]
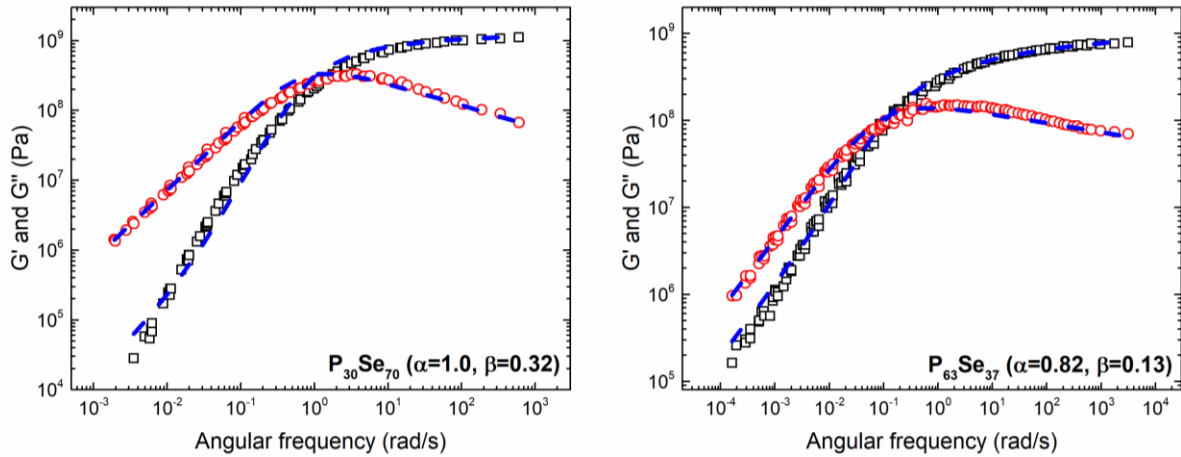
Figure 5c-3 Viscoelastic spectra G′(ω) (empty black squares) and G″(ω) (empty red circles) of $P_{30}Se_{70}$ network (left panel) and $P_{63}Se_{37}$ molecular (right panel) liquids fitted with the H-N function (Eq. 2, dashed line). The fitting parameters α and β are listed in each plot.
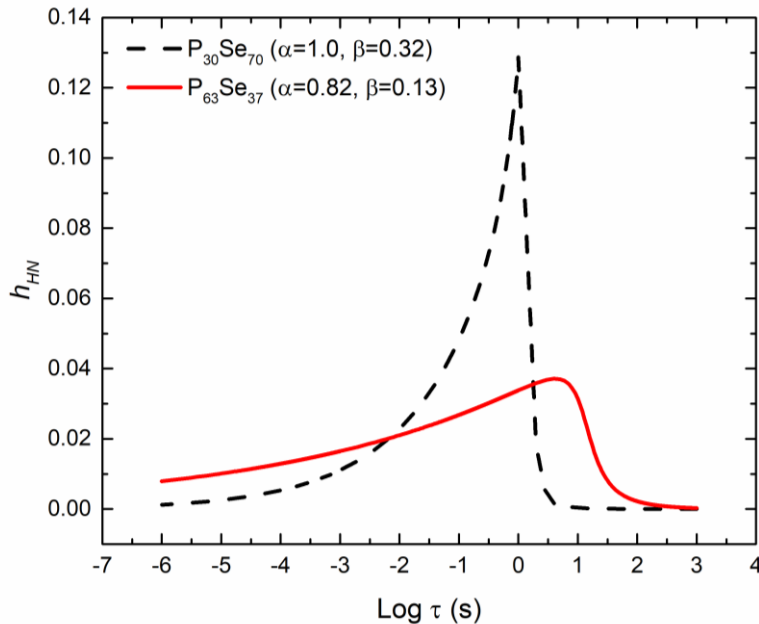
Figure 5c-4 The probability density function of H-N log-relaxation time $h_{HN}(\log\tau)$ for $P_{30}Se_{70}$ network (dashed line) and $P_{63}Se_{37}$ molecular liquids (solid line) calculated using Eq. 3 (see text for details).

It may be noted that the T_g of the molecular P-Se glasses are much lower than their network counterparts, consistent with the formation of P_4Se_3 molecules that drastically lowers the connectivity of the structure.[18] These calculations yield quite high values of m ranging between 65 and 75 for these molecular liquids, indicating that these liquids are indeed significantly more fragile than their network counterparts with $25 \leq x \leq 50$, that are characterized by $m \sim 35 \pm 5$.[13]
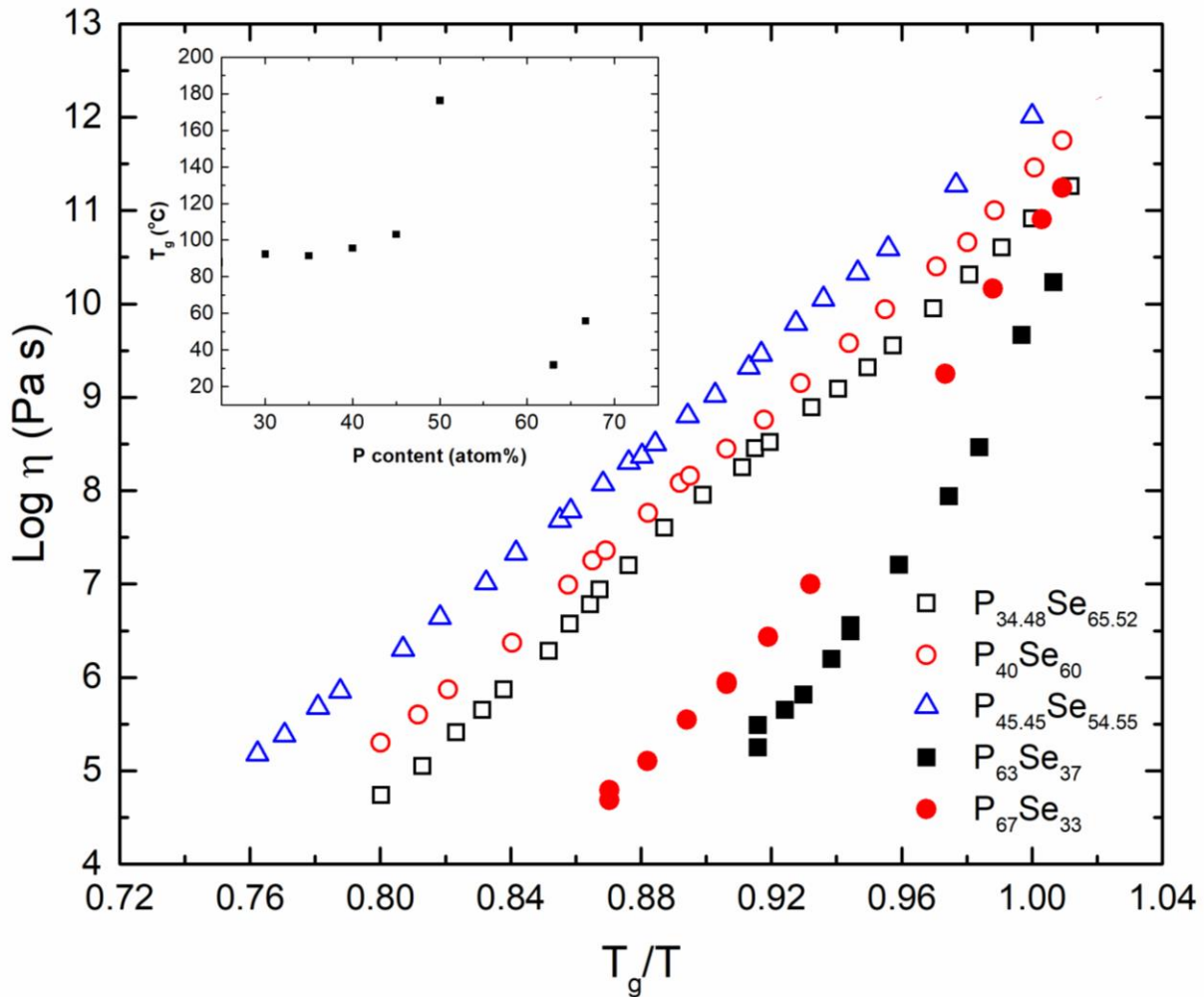
Figure 5c-5 Temperature dependence of viscosity η of binary P_xSe_{100-x} liquids. Filled symbols are experimental data obtained in present study and the open symbols are data taken from a previous study.[38] Inset shows compositional variation of T_g of these glasses from previous reports in the literature.[18,38]

The unusual shear-mechanical response of the molecular P-Se liquids is further explored in their dynamic viscosity $\eta'(\omega)$ behavior in a scaled viscosity $Z(\omega)$ vs. normalized frequency ω/ω_{max} plot (Fig. 5c-6). Here ω_{max} is the frequency corresponding to the maximum in G'' and $Z(\omega)$ is defined as:

$$Z(\omega) = \frac{\eta'(\omega)}{(G_\infty/\omega_{max})} \qquad (6)$$

It may be noted that (G_∞/ω_{max}) is equal to $\eta'(\omega \sim \omega_{max})$, which corresponds to the stress relaxation process. It is evident from Fig. 5c-6 that $Z(\omega)$ for the network P_xSe_{100-x} liquids with $30 \leq x \leq 50$ reaches the frequency independent region below $\omega/\omega_{max} \sim 0.1$. Such behavior is characteristic of a wide range of network and unassociated molecular glass-forming liquids.[7,15] In contrast, the molecular P_xSe_{100-x} liquids with $x = 63$ and 67 show clear viscosity enhancement over the normal network liquids in the low-frequency region below $\omega/\omega_{max} \sim 1$ with a frequency scaling of $Z(\omega) \sim (\omega/\omega_{max})^{-0.12}$ (Fig.5c-6). Moreover, like gels, the dynamic viscosity of these molecular liquids does not reach a frequency independent regime even at the lowest frequencies of measurement ($\omega/\omega_{max} \sim 10^{-4}$) accessed in the present study, consistent with the presence of ultraslow relaxation processes in these liquids with timescales significantly longer than that of shear relaxation.

185
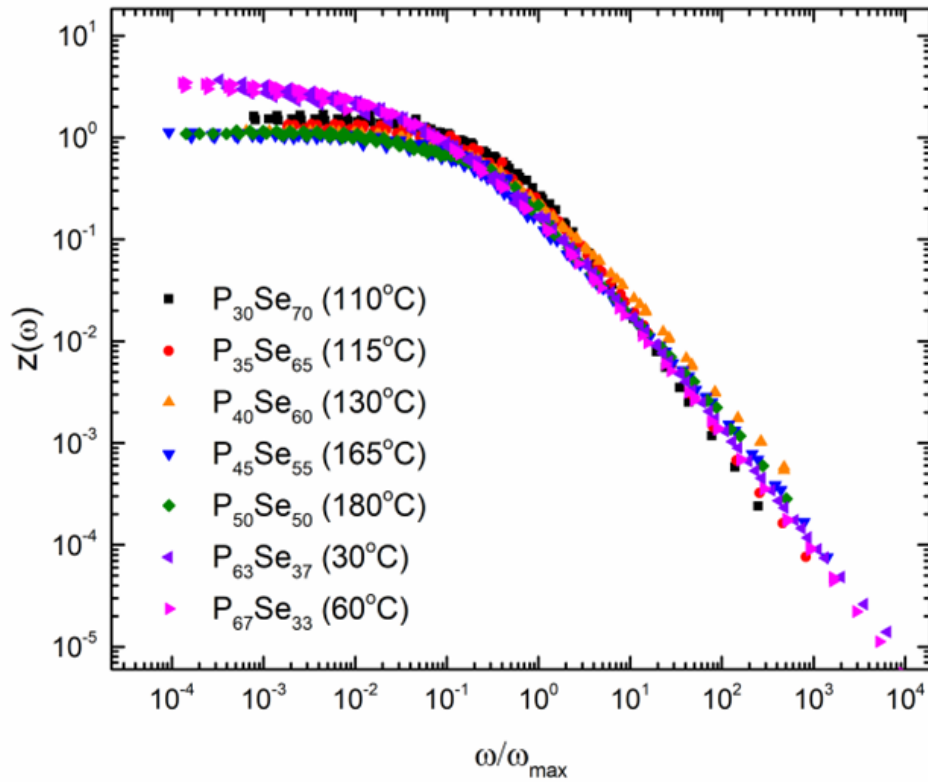
Figure 5c-6 Scaled dynamic viscosity $Z(\omega)$ as a function of normalized frequency ω/ω_{max} of P_xSe_{100-x} liquids. Corresponding temperatures are shown in parentheses alongside each composition.

Indications for the existence of ultraslow relaxation processes are also apparent when one compares the van Gurp – Palmen (vGP) plot of the phase angle δ vs. Mod(G^*) of the $P_{30}Se_{70}$ network liquid with that of the $P_{63}Se_{37}$ molecular liquid (Fig. 5c-7). Here, by definition, $\tan\delta = G''/G'$ and $G^* = \sqrt{G'^2 + G''^2}$. It is clear from Fig. 5c-7 that, while δ of the $P_{30}Se_{70}$ liquid reaches a value of ~90° at low frequencies characteristic of a purely viscous response in the terminal regime, that of the $P_{63}Se_{37}$ liquid plateaus out at ~80°, implying that a purely viscous response is not obtained even at the lowest frequencies of measurement. As noted earlier and shown in Fig. 5c-7, a similar viscoelastic behavior was recently reported in another molecular liquid of composition $Ge_3As_{52}S_{45}$.[15] Therefore, similar to gels at their critical point, a small

elastic component of the shear-mechanical response remains present at these frequencies in these molecular liquids, which, therefore, persist in a state intermediate between a liquid and a solid.
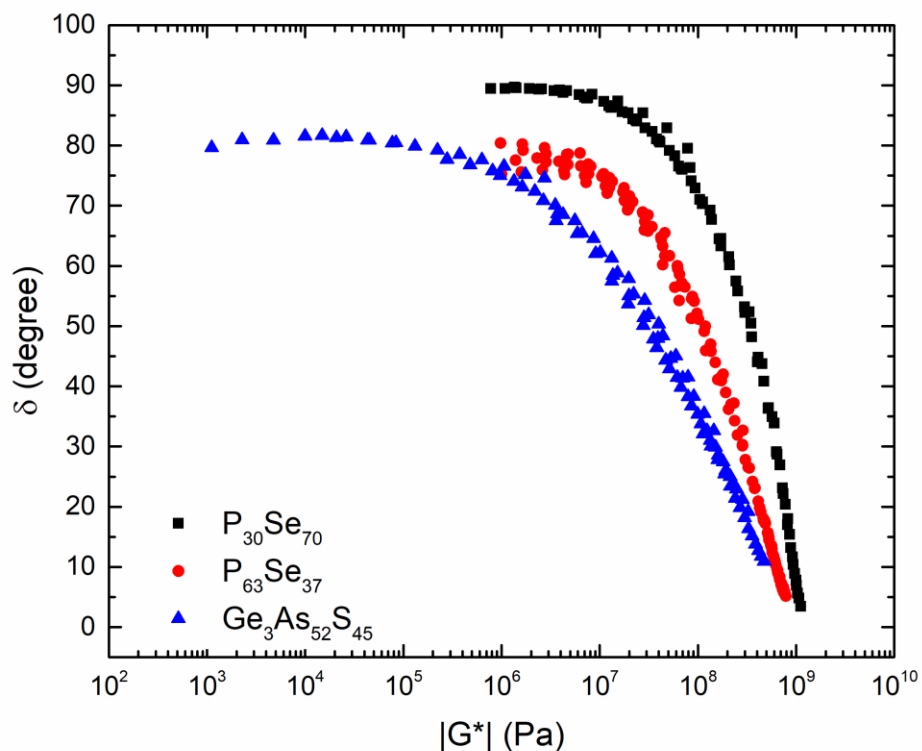
Figure 5c-7 vGP plot of phase angle δ vs. |G*| of $P_{30}Se_{70}$ network liquid (black squares) and molecular $P_{63}Se_{37}$ liquid (red squares). Data for molecular $Ge_3As_{52}S_{45}$ liquid (blue triangles) from a previous study is shown for comparison.[15]

5c.5 Conclusion

The compositional evolution of the viscoelastic response of P_xSe_{100-x} ($30 \leq x \leq 67$) supercooled liquids is found to be correlated with the accompanying network-to-molecular structural transformation. The rheological behavior of these liquids is found to progressively deviate from that of a "normal" network liquid with increasing x in this composition range. While the liquids with compositions $30 \leq x \leq 40$ behave as simple liquids with a single bond scission/renewal relaxation process, the supercooled $P_{45}Se_{55}$ and $P_{50}Se_{50}$ liquids display an

additional relaxation mode, which likely corresponds to a structural interconversion between ethylene-like $_{2/2}$SeP–PSe$_{2/2}$ units and P$_4$Se$_3$ molecules. In contrast to these normal network liquids that display a Maxwell frequency scaling of G$'\sim \omega^2$ and G$'' \sim \omega$ in the terminal region, the molecular liquids with $x \geq 63$ display an apparently anomalous scaling of G$'\sim \omega$ at frequencies below the G$'$-G$''$ crossover. These viscoelastic spectra are simulated with the H-N function to obtain the distribution of the relaxation timescales in these liquids. This analysis indicates that the molecular liquids are characterized by rather broad relaxation time distributions compared to those characteristic of their network counterparts. These results are corroborated by the phase angle variation and the viscosity enhancement observed in low frequency region below the dynamical onset all the way down to $\omega/\omega_{max} \sim 10^{-4}$. These results, when taken together, suggest the presence of ultraslow relaxation processes in these highly fragile molecular liquids and the lack of a purely viscous response similar to that displayed by gels at their critical point.

Acknowledgements

References

[1]   C.M. Roland, Viscoleastic Behavior of Rubbery Materials, Oxford University Press, Oxford, 2011.

[2]   J.D. Ferry, Viscoelastic properties of polymers, John Wiley & Sons, 1980.

[3]   M. Doi, S.F. Edwards, The Theory of Polymer Dynamics, Oxford University Press, Oxford, 1986.

[4]   J.J. Mills, Low frequency storage and loss moduli of soda-silica glasses in the transfoilmation range, J. Non. Cryst. Solids. 14 (1974) 255–268.

[5]   J. Tauke, T.A. Litovitz, P.B. Macedo, Viscous relaxation and non-Arrhenius behavior in B2O3, J. Am. Ceram. Soc. 51 (1968) 158–163.

[6]   B. Mei, B. Zhuang, Y. Lu, L. An, Z. Wang, Local-Average Free Volume Correlates with Dynamics in Glass Formers, J. Phys. Chem. Lett. 13 (2022) 3957–3964.

[7]   S.P. Bierwirth, C. Gainaru, R. Böhmer, Communication: Correlation of terminal relaxation rate and viscosity enhancement in supramolecular small-molecule liquids, J. Chem. Phys. 148 (2018) 221102.

[8]   R. Böhmer, C. Gainaru, R. Richert, Structure and dynamics of monohydroxy alcohols-Milestones towards their microscopic understanding, 100 years after Debye, Phys. Rep. 545 (2014) 125–195.

[9]   C. Gainaru, R. Meier, S. Schildmann, C. Lederle, W. Hiller, E.A. Rössler, R. Böhmer, Nuclear-magnetic-resonance measurements reveal the origin of the debye process in monohydroxy alcohols, Phys. Rev. Lett. 105 (2010) 258303.

[10]   W. Zhu, B.G. Aitken, S. Sen, Communication: Observation of ultra-slow relaxation in supercooled selenium and related glass-forming liquids, J. Chem. Phys. 148 (2018) 111101.

[11]   W. Zhu, B. Aitken, S. Sen, Investigation of the shear relaxation behavior of As-Se liquids within the framework of entropic and elastic models of viscous flow, J. Non. Cryst. Solids. 534 (2020) 119959.

[12]   S. Sen, Y. Xia, W. Zhu, M. Lockhart, B. Aitken, Nature of the floppy-to-rigid transition in chalcogenide glass-forming liquids, J. Chem. Phys. 150 (2019) 144509.

[13]   B. Yuan, B. Aitken, S. Sen, Structural control on the rheological behavior of binary P-Se supercooled liquids, J. Non. Cryst. Solids. 559 (2021) 120669.

[14]   W. Zhu, I. Hung, Z. Gan, B. Aitken, S. Sen, Dynamical processes related to viscous flow in a supercooled arsenic selenide glass-forming liquid: Results from high-temperature ^{77}Se NMR spectroscopy, J. Non. Cryst. Solids. 526 (2019) 119698.

[15]   S. Sen, W. Zhu, B. Yuan, B.G. Aitken, Rheological behavior of molecular vs network chalcogenide supercooled liquids, J. Chem. Phys. 153 (2020) 134504.

[16]   S. Aime, L. Cipelletti, L. Ramos, Power law viscoelasticity of a fractal colloidal gel, J.

Rheol. (N. Y. N. Y). 62 (2018) 1429–1441.

[17] P. Sollich, F. Lequeux, P. Hébraud, M.E. Cates, Rheology of soft glassy materials, Phys. Rev. Lett. 78 (1997) 2020–2023.

[18] B. Yuan, B. Aitken, I. Hung, Z. Gan, S. Sen, Compositional Evolution of the Structure and Connectivity in Binary P-Se Glasses: Results from 2D Multinuclear NMR and Raman Spectroscopy, J. Phys. Chem. B. 125 (2021) 13057–13067.

[19] A. Bytchkov, F. Fayon, D. Massiot, L. Hennet, D.L. Price, ^{31}P solid-state NMR studies of the short-range order in phosphorus-selenium glasses, Phys. Chem. Chem. Phys. 12 (2010) 1535–1542.

[20] D.G. Georgiev, M. Mitkova, P. Boolchand, G. Brunklaus, H. Eckert, M. Micoulaut, Molecular structure, glass transition temperature variation, agglomeration theory, and network connectivity of binary P-Se glasses, Phys. Rev. B. 64 (2001) 134204.

[21] R.T. Phillips, M.K. Ellis, Microstructure of P-Se glasses and low frequency Raman scattering, J. Non. Cryst. Solids. 164–166 (1993) 135–138.

[22] D. Lathrop, H. Eckert, Quantitative determination of the structural units in phosphorus-selenium glasses by ^{31}P dipolar and magic-angle-spinning NMR spectroscopy, Phys. Rev. B. 43 (1991) 7279–7287.

[23] D. Lathrop, H. Eckert, Dipolar NMR Spectroscopy of Nonoxidic Glasses. Structural Characterization of the System Phosphorus-Selenium by 31P-77Se Spin Echo Double Resonance NMR, J. Am. Chem. Soc. 112 (1990) 9017–9019. https://doi.org/10.1021/ja00180a078.

[24] D. Lathrop, H. Eckert, Chemical disorder in non-oxide chalcogenide glasses. Site speciation in the system phosphorus-selenium by magic angle spinning NMR at very high spinning speeds, J. Phys. Chem. 93 (1989) 7895–7902.

[25] D. Lathrop, H. Eckert, NMR studies of chalcogenide glasses: The system phosphorus-selenium, J. Non. Cryst. Solids. 106 (1988) 417–420.

[26] R. Maxwell, H. Eckert, Molten-State Kinetics in Glass-Forming Systems. A High-Temperature NMR Study of the System Phosphorus-Selenium, J. Phys. Chem. 99 (1995) 4768–4778.

[27] R. Maxwell, H. Eckert, Chemical Equilibria in Glass-Forming Melts: High-Temperature ^{31}P and ^{77}Se NMR of the Phosphorus-Selenium System, J. Am. Chem. Soc. 116 (1994) 682–689.

[28] R. Maxwell, H. Eckert, Speciation Equilibria, Clustering, and Chemical-Exchange Kinetics in Non-Oxide Glasses and Melts. High-Temperature ^{31}P NMR Study of the System Phosphorus-Selenium, J. Am. Chem. Soc. 115 (1993) 4747–4753.

[29] J.E. Martin, D. Adolf, The Sol-Gel Transition in Chemical Gels, Annu. Rev. Phys. Chem. 42 (1991) 311–339.

[30] K. Ninomiya, J. Ferry, Some Approximation Equatinos Useful in the Phenomenological

Treatment of Linear Viscoelastic Data, J. Colloid Sci. 14 (1959) 36–48.

[31] D.C. Kaseman, O. Gulbiten, B.G. Aitken, S. Sen, Isotropic rotation vs. Shear relaxation in supercooled liquids with globular cage molecules, J. Chem. Phys. 144 (2016) 174501.

[32] P. Mondal, P. Lunkenheimer, R. Böhmer, A. Loidl, F. Gugenberger, P. Adelmann, C. Meingast, Dielectric relaxation dynamics in C60 and C70, J. Non. Cryst. Solids. 172–174 (1994) 468–471.

[33] T. Chattopadhyay, C. Carlone, A. Jayaraman, H.G. V. Schnering, Effect of temperature and pressure on the Raman spectrum of As_4S_3, J. Phys. Chem. Solids. 43 (1982) 277–284.

[34] S. Havriliak, S. Negami, A complex plane representation of dielectric and mechanical relaxation processes in some polymers, Polymer. 8 (1967) 161–210.

[35] P.G. Debenedetti, F.H. Stillinger, Supercooled Liquids and the Glass Transition, Nature. 410 (2001) 259–267.

[36] J.C. Mauro, Y. Yue, A.J. Ellison, P.K. Gupta, D.C. Allan, Viscosity of glass-forming liquids, Proc. Natl. Acad. Sci. 106 (2009) 19780–19784.

[37] C. Zhang, L. Hu, Y. Yue, J.C. Mauro, Fragile-to-strong transition in metallic glass-forming liquids, J. Chem. Phys. 133 (2010) 14508.

[38] E.I. Kim, G.M. Orlova, Viscosity of glasses in the P-Se system, J. Appl. Chem. USSR. 47 (1974) 1018–1021.

Chapter 6

Conclusions and Future Work

When taken together, the findings reported in this dissertation lead to an atomistic understanding of the relationship between structure, dynamical processes and relaxation phenomena in model binary chalcogenide systems, which sheds light on the fundamentals of viscous flow in the supercooled region. The structure of S_xSe_{100-x} glasses consists of copolymeric $[S,Se]_n$ chains and heterocyclic S_ySe_{8-y} rings. Se and S atoms show strong preference to form the chain and the ring elements, respectively, which prevents a random or homogeneous mixing between these two elements. It is the total chain vs. ring content in the structure that controls both the atomic packing and the mobility of the constituent structural units. As the total chain content increases with increasing Se concentration in these glasses, the stronger interaction between the chain elements compared to rings, results in less efficient atomic packing and lower mobility, which are manifested in the decreasing molar volume and increasing T_g, respectively. On the other hand, the timescale of the S/Se – S/Se bond scission/renewal dynamics in these supercooled liquids rapidly increases with S concentration, owing to a lowering of conformational entropy of the chain elements due to steric hindrance from the ring elements. Consequently, the S_xSe_{100-x} liquids become progressively less fragile with increasing S concentration. A similar behavior is also displayed by liquid elemental S, where the ring:chain ratio abruptly decreases above the λ-transition, resulting in a concomitant fragile-to-strong transition.

In contrast to the S-Se binary system, where the glass structure shows significant violation of chemical order, glasses in the Se-Te binary system display strong chemical ordering. Se and Te are isoelectronic and the structure of the stable crystalline polymorphs of both elements consists of polymeric $[Se]_n$ or $[Te]_n$ helical chains, where Se and Te atoms are twofold coordinated. Consequently, the structure of Se-Te binary glasses is characterized by random connectivity between Se and Te and formation $[Se,Te]_n$ copolymeric chains. The increased metallicity of Te is

hypothesized to result in strong secondary bonding interaction between these chains, where Te acts as a pseudo-crosslinker. This scenario is found to be consistent with the compositional variation of T_g of these liquids and their isothermal viscosity in the supercooled regime. This constraint on the chain motion in Se_xTe_{100-x} liquids imposed by the cross-linking via the SBI of Te atoms is overcome at superliquidus temperatures where the isothermal viscosity becomes independent of the Te content. On the other hand, unlike the pseudo-crosslinking role of Te, halogens such as I, when incorporated into amorphous Se, act as chain terminators. Therefore, progressive addition of I into Se results in a shortening of Se chains, which results in an expected decrease in isothermal viscosity and T_g as well as an increase in molar volume and fragility. The average chain length in liquids could be tuned by varying the I content, which allows the determination of the scaling of isothermal viscosity with chain length.

Finally, the widest composition range for alloying is displayed by the P_xSe_{100-x} glasses with $5 \leq x \leq 70$. Initial addition of P to Se results in progressive cross-linking of Se chains via pyramidal $P(Se_{1/2})_3$ units, ethylene-like $_{2/2}SeP–PSe_{2/2}$ units, and $Se=P(Se_{1/2})_3$ tetrahedral units in glasses with $x \leq 50$. Ultimately, the chain units completely disappear, and the structure becomes a rigid network of corner-shared P-Se polyhedra at $x \approx 50$. Further increase in the P content results in a collapse of the network, and a complete loss in connectivity due to the formation of P_4Se_3 molecules held together by van der Waals forces in the $P_{63}Se_{37}$ glass. Beyond this point increase in the P content results in a patchy network as the relative concentration of the P_4Se_3 molecules decreases and that of amorphous red phosphorus-like structural moieties and P-P bonded P_4Se_3-like groups increases. The compositional variation in isothermal viscosity, T_g, and fragility index m is shown to be completely consistent with this scenario of a complex and highly nonmonotonic structural evolution of these glasses.

The viscoelastic spectra G′(ω) and G″(ω) for the Se-rich P_xSe_{100-x} liquids with $x \leq 10$ display the presence of two relaxation processes, namely a fast segmental Se chain motion and a slow bond scission/renewal dynamics. This behavior of the Se-rich P_xSe_{100-x} compositions is rather similar to their counterparts in the As-Se and Ge-Se systems. The segmental chain dynamics disappears in liquids with $x \geq 15$ as the Se chain length becomes too short to sustain such motion. The network-to-molecular structural transformation in P_xSe_{100-x} supercooled liquids with higher P content such that $30 \leq x \leq 67$ is manifested in their viscoelastic response. While the liquids with compositions $30 \leq x \leq 40$ behave as network liquids with a single bond scission/renewal relaxation process, the molecule-rich $P_{45}Se_{55}$ and $P_{50}Se_{50}$ liquids display an additional relaxation mode, which likely corresponds to a structural interconversion between ethylene-like $_{2/2}SeP–PSe_{2/2}$ units and P_4Se_3 molecules. Predominantly molecular liquids with $x \geq 63$, on the other hand, are characterized by a power-law relaxation behavior which is ascribed to an extremely broad distribution of relaxation timescales with the coexistence of rapid rotational motion of individual molecules and cooperative dynamics of transient molecular clusters, with the latter being significantly slower than the shear relaxation timescale. These highly fragile molecular liquids display a rather unique gel-like lack of a purely viscous response and the presence of ultraslow relaxation processes in these.

It may be noted here that while these studies are the first of their kind for supercooled chalcogenide liquids, they provide a tremendous wealth of structural and dynamical information that may enable one to establish predictive atomistic models of relaxation phenomena in these liquids. For example, the results presented here demonstrate that in pure Se the primary structural building blocks are polymeric $[Se]_n$ chains formed by two coordinated Se atoms and the corresponding rheological behavior is shown to be characterized by two coexisting dynamical

processes, the fast segmental chain motion, and the slow Se-Se bond scission/renewal process. Addition of elements such as P (and also, Ge or As) cross-link the $[Se]_n$ chains and the average chain length decreases.[1–3] This structural evolution results in a progressive decrease in the difference between the fast and slow dynamical processes in their timescale and eventually the fast relaxation process vanishes when the average length of the $[Se]_n$ chains becomes shorter than ~ 3 to 5 Se atoms.[4] Further increase in the cross-linker content results in a rigid three-dimensional network consisting corner-shared polyhedra with only minor violation in the chemical order.[1,2] At this point, the rheological behavior is shown to be consistent with the structural relaxation being entirely controlled by the As-Se bond scission/renewal process.[5] Previous structural studies have indicated that in contrast to Se-rich and stoichiometric compositions, the structure of Se-deficient compositions consists of metal-metal homopolar bonds.[1,2] As expected, the relative concentration of these homopolar bonds increases progressively with increasing cross-linker metal content and results in the formation of various low-dimensional structural moieties. However, the role of homopolar bonding and of the various associated low-dimensional structural moieties in controlling the rheological behavior of chalcogen-deficient liquids has never been investigated in the past, in a systematic fashion.

On the other hand, little is known regarding the mechanistic connections between structure, dynamics, and relaxation mechanisms in amorphous oxide networks that are key materials for a rather wide range of technological applications. The coexistence of bridging and non-bridging oxygen atoms in these networks may in fact give rise to complex relaxation behavior with the coexistence of multiple dynamical processes such as those observed in S or Se -rich liquids in the present study, where the structure is characterized by the coexistence of 3D network and low-dimensional molecular or chain element.[6–8] The slow bond scission/renewal and the fast

segmental dynamics of Se chains are found to couple very differently with shear and structural relaxation. Such complex dynamical phenomena disappear in the chalcogenide liquids that are characterized by a fully cross-linked network.[9–11] It is tempting to speculate that similar coexistence of multiple dynamical processes in fragile oxide liquids with moderately and highly modified networks may hold the clue to deciphering the observed difference in the relaxation kinetics of different physical variables such as enthalpy, volume and stress. Future systematic studies of glass-forming oxide liquids are needed to test the validity of such conjectures.

Reference

[1]   D.C. Kaseman, I. Hung, Z. Gan, B. Aitken, S. Currie, S. Sen, Structural and Topological Control on Physical Properties of Arsenic Selenide Glasses, J. Phys. Chem. B. 118 (2014) 2284–2293.

[2]   G. Yang, B. Bureau, T. Rouxel, Y. Gueguen, O. Gulbiten, C. Roiland, E. Soignard, J.L. Yarger, J. Troles, J.C. Sangleboeuf, P. Lucas, Correlation between structure and physical properties of chalcogenide glasses in the As_xSe_{1-x} system, Phys. Rev. B. 82 (2010) 195206.

[3]   D.C. Kaseman, I. Hung, Z. Gan, S. Sen, Observation of a continuous random network structure in Ge_xSe_{100-x} glasses: Results from high-resolution ^{77}Se MATPASS/CPMG NMR spectroscopy, J. Phys. Chem. B. 117 (2013) 949–954.

[4]   S. Sen, Y. Xia, W. Zhu, M. Lockhart, B. Aitken, Nature of the floppy-to-rigid transition in chalcogenide glass-forming liquids, J. Chem. Phys. 150 (2019) 144509.

[5]   W. Zhu, I. Hung, Z. Gan, B. Aitken, S. Sen, Dynamical process related to viscous flow in a supercooled arsenic selenide glassforming liquid: Results from high-temperature ^{77}Se NMR Spectroscopy, J. Non. Cryst. Solids. 526 (2019) 119698.

[6]   Y. Xia, W. Zhu, M. Lockhart, B. Aitken, S. Sen, Fragility and Rheological Behavior of Metaphosphate Liquids: Insights Into Their Chain vs. Network Characters, J. Non. Cryst. Solids. 514 (2019) 77–82.

[7]   Y. Xia, W. Zhu, J. Sen, S. Sen, Observation of polymer-like flow mechanism in a short-chain phosphate glass-forming liquid, J. Chem. Phys. 152 (2020) 044502.

[8]   Y. Xia, H. Chen, B. Aitken, S. Sen, Rheological characterization of complex dynamics in Na-Zn metaphosphate glass-forming liquids, J. Chem. Phys. 155 (2021) 054503.

[9]   W. Zhu, B.G. Aitken, S. Sen, Observation of a Dynamical Crossover in the Shear Relaxation Processes in Supercooled Selenium Near the Glass Transition, J. Chem. Phys. 150 (2019) 94502.

[10]   W. Zhu, B. Aitken, S. Sen, Investigation of the shear relaxation behavior of As-Se liquids within the framework of entropic and elastic models of viscous flow, J. Non. Cryst. Solids. 534 (2020) 119959.

[11]   Y. Xia, B. Yuan, O. Gulbiten, B. Aitken, S. Sen, Kinetic and calorimetric fragility of chalcogenide glass-forming liquids: Role of shear vs enthalpy relaxation, J. Phys. Chem. B. 125 (2021) 2754–2760.